UNIVERSITÉ DE NICE-SOPHIA ANTIPOLIS – UFR Sciences
École Doctorale de « Sciences Fondamentales et Appliquées »

THÈSE

POUR OBTENIR LE TITRE DE

DOCTEUR EN SCIENCES
DE L'UNIVERSITÉ DE NICE-SOPHIA ANTIPOLIS

SPÉCIALITÉ : PHYSIQUE

PRÉSENTÉE ET SOUTENUE PAR

WALTER PAULS

SINGULARITÉS COMPLEXES DES ÉCOULEMENTS INCOMPRESSIBLES PARFAITS

THÈSE DIRIGÉE PAR URIEL FRISCH

Soutenue le 3 octobre 2007

JURY:

M. CLAUDE BARDOS	Professeur émérite	*Rapporteur*
M. PHILIPPE BLANCHARD	Professeur	*Examinateur*
M. YANN BRENIER	Directeur de recherche	*Examinateur*
M. JEAN-DANIEL FOURNIER	Directeur de recherche	*Examinateur*
M. URIEL FRISCH	Directeur de recherche émérite	*Directeur*
M. JORIS VAN DER HOEVEN	Chargé de recherche	*Examinateur*
M. KOJI OHKITANI	Professeur	*Rapporteur*
M. GEORGE PAPANICOLAOU	Professeur	*Examinateur*

An meine Eltern, vor allem meine Mutter.

ਇਕ ਨੁੱਕਤੇ ਵਿਚ ਗੱਲ ਮੁੱਕਦੀ ਏ
ਬੁੱਲ੍ਹੇ ਸ਼ਾਹ

اک نقطے وِچ گلّ مُکّدی ہے
بلھے شاہ

It's all in One contained

Bulleh Shah, English transl. by K. S. Duggal

А для низкой жизни были числа
Как домашний, подъяремный скот,
Потому что все оттенки смысла
Умное число передает.

Н.С. Гумилев

But on earth the numbers were created,
Like the cattle yokèd and confined,
For the numbers always clearly stated
Every shade of meaning they defined.

N. S. Gumilev, English transl. by A. Shaumyan

Remerciements

Tout d'abord je tiens à remercier Uriel Frisch, mon directeur de thèse, qui m'a guidé au cours des quatre dernières années. Son soutien, son aide et ses encouragements m'ont beaucoup apporté. Il m'a beaucoup appris non seulement dans le domaine de la mécanique des fluides, mais aussi dans des domaines très divers, comme la linguistique, l'histoire, la langue et la cuisine françaises et le ski. Malgré ses nombreux efforts, si je n'ai pas réussi à devenir « un bon Allemand »; j'en suis le seul responsable.

Ensuite je remercie George Papanicolaou pour son soutien et son hospitalité, grâce auxquels j'ai pu faire un séjour à l'Université de Stanford et aussi pour avoir accepté d'être membre du jury.

Ma reconnaissance va à Claude Bardos et Koji Ohkitani qui ont accepté d'être les rapporteurs de cette thèse. Je les remercie chaleureusement pour leur remarques et suggestions.

Tout un volet du travail de thèse a bénéficié de très fructueuses interactions avec Joris van der Hoeven. Qu'il en soit vivement remercié, ainsi que pour avoir accepté d'être membre du jury.

Je remercie également Yann Brenier, Philippe Blanchard et Jean-Daniel Fournier pour avoir accepté d'être membres du jury.

Une partie notable des travaux de cette thèse a été faite en collaboration étroite avec mes amis Takeshi Matsumoto et Jérémie Bec. Je les remercie vigoureusement. Je remercie Hélène Frisch qui m'a souvent aidé et réconforté et avec laquelle j'ai eu beaucoup de discussions intéressantes.

Je remercie Dhrubaditya Mitra : nous n'avons pas seulement travaillé ensemble mais on s'est bien amusés, scientifiquement et autrement. J'ai eu beaucoup d'interactions fructueuses avec Andrei Sobolevskii; je le remercie pour son aide.

Pendant ma thèse j'ai pu effectuer un séjour à l'Université de Stokholm, où j'ai eu beaucoup de discussions stimulantes avec August Tsikh and Mikael Passare. Je les remercie pour leur hospitalité. À cette ocasion je remercie aussi le « Dom Knigi » à Saint-Petersburg.

En 2005 j'ai pu participé à l'École d'été de Woods Hole, organisée par Charles Doering et Oliver Bühler que je remercie beaucoup. Je remercie aussi Eric Vanden-Eijnden pour son aide et son soutien qui m'ont permis d'effectuer une partie des travaux présentés dans la thèse. Je tiens aussi à remercier Joseph Keller, William Young, Jean-Luc Thiffeault, Onno Bokhove et les autres participants de l'École d'été.

Durant les années de thèse j'ai pu effectuer un séjour étendu à l'Indian Institute of Science à Bengaluru, grâce à l'hospitalité de Rahul Pandit, avec qui j'ai eu beaucoup d'interactions et qui m'a beaucoup fait profiter de son expérience. Je l'en remercie chaleureusement.

Mes remerciements vont aussi à Alain Pumir de nombreuses discussions et de son intêret constant pour mon travail.

Je dois beaucoup à Andreas Degenhard, qui par son soutien et son encouragement a beaucoup contribué à ce que je puisse m'engager dans ce travail de thèse. Je l'en remercie chaleureusement.

Je remercie Konrad Bajer pour son hospitalité qui m'a permis d'effectuer un séjour á l'Institut de Géophysique à Varsovie. Rudolf Friedrich et Rafaela Hillerbrand m'ont accueilli à l'Institut de Physique Théorique à Münster où j'ai fait un séjour très profitable dont je les remercie.

Je remercie Ernst Joachim Weniger pour son hospitalité, des discussions fructueuses et l'intêret porté à mon travail.

Durant ma thèse je beaucoup apprecié le cadre de travail et l'environnement agréable

qu'offrent l'Observatoire de la Côte d'Azur et le Laboratoire Cassiopée. J'y ai eu des interactions fructueuses, en particulier avec Michel Hénon, Hans Scholl, Yannik Ponty, Alexandros Alexakis, Sanjit Mitra et Alain Noullez. Parmi les visiteurs de l'Observatoire je tiens particulièrement à remercier Mikhail Blank, Konstantin Khanin, Vlad Zheligosvky, Olga Podvigina et Evgenii Kuznetsov avec qui j'ai eu de nombreuses discussions.

Je remercie tout le personnel adminstratif et technique du laboratoire pour son constant soutien. Je remercie tout particulièrement Fabrice Ubaldi pour son aide avec des problèmes informatiques. Je suis très reconnaissant à toute l'équipe du restaurant et spécialement à Khaled pour ses excellents repas dans une atmosphère si conviviale.

Finalement, je tiens à exprimer ma gratitude à mes amis et à ma famille, sans lesquels ce travail n'aurait pas été possible.

Table des matières

Liste des publications afférentes à la thèse

- A Borel transform method for locating singularities of Taylor and Fourier series p. 35

  W. Pauls and U. Frisch, J. Stat. Phys. 127, pp. 1095–11119 (2007)

- Nature of complex singularities for the 2D Euler equation . . . . . p. 83

  W. Pauls, T. Matsumoto, U. Frisch and J. Bec, Physica D 219, pp. 40–59 (2006).

- Lagrangian singularities of steady two-dimensional flow . . . . . p. 119

  W. Pauls and T. Matsumoto, Geophys. Astrophys. Fluid Dyn. 99, pp. 61–75 (2005).

- Lagrangian singularities of steady two-dimensional flow . . . . . p. 134

  W. Pauls and T. Matsumoto, Proceed. Frontiers of Nonlinear Phys. II, pp. 236-242 (2005).

- Transport in cellular flows from the viewpoint of stochastic differential equations p. 143

  W. Pauls, Proceedings Woods Hole Gephysical Fluid Dynamics Summer School (2005).

Chapter 1

Introduction générale

L'équation[1] d'Euler – l'objet central d'étude de cette thèse – peut à première vue paraître plutôt simple, voire élémentaire. C'est dû partiellement à la façon très directe et optimisée dont elle est obtenue dans les cours de physique modernes, mais c'est dû aussi aux notations qui remontent en fait à Euler lui-même [Eul57], ce qui tend à dissimuler ses aspects non triviaux. De plus, l'équation d'Euler est fréquemment considerée comme non physique, car elle ne prend pas en compte la friction interne dans le fluide, décrivant ainsi, selon les termes de Feynman [Fey64], « de l'eau sèche ».

En regardant de plus près, on se rend compte que ce point de vue contient quelques conceptions fausses. Prenons par exemple la dérivation de l'équation décrivant la dynamique des écoulements parfaits c'est-à-dire précisément de l'équation d'Euler. Pendant deux décennies (1734-1755) elle occupait les meilleurs physiciens et mathématiciens du XVIII^e siècle; cela a commencé par le travail du jeune D. Bernoulli (la loi de pression dite de Bernoulli) et a culminé avec Euler établissant sa fameuse équation [Tru54, Cal96, Dar05, DF07]. Et cette histoire est loin d'être terminée ! Environ deux cents ans plus tard, Arnold [Arn66], s'inspirant de la dérivation variationnelle de l'équation d'Euler par Lagrange, a montré que le mouvement des écoulements inviscides peut être décrit comme un mouvement géodésique sur le groupe des difféomorphismes conservant le volume.

Concernant l'objection d'être non physique, l'opinion est de plus en plus répandue que l'équation d'Euler reste importante au moins pour deux raisons majeures. Premièrement, elle correspond, du moins formellement, à la limite des nombres de Reynolds infinis $Re \to \infty$. Deuxièmement, il existe des phénomènes qui sont partiellement cachés par la présence du terme visqueux et qui peuvent être étudiés plus facilement dans la forme «nue» du cas inviscide. Un de ces phénomènes est la *déplétion* – la tendance d'un écoulement à supprimer les non linéarités et à approcher, au moins localement, une des nombreuses solutions de l'équation d'Euler stationnaire.

Les aspects mathématiques de l'équation d'Euler ont étés intensivement étudiés durant les cent dernières années, voir, par exemple, [MB02, MP94] et [BT07, Cha07, Con07] pour des articles de revue récents. Pourtant, quelques questions mathématiques essentielles restent complêtement ouvertes. Par exemple, on ne sait pas si l'équation d'Euler tri-dimensionelle est bien posée pour des données initiales suffisamment lisses : un écoulement intialement, disons, analytique développe-t-il une singularité réelle en un temps fini ?

Pour des données initiales analytiques, les solutions de l'équation d'Euler peuvent être prolongées dans le domaine complexe : les variables d'espace ainsi que la vitesse, la vorticité et la pression sont étendues à des valeurs complexes. Il est connnu depuis les travaux de [BBZ76, Ben76a, Ben76b] que pour de telles données, d'hypothétiques singu-

[1] For English translation see page 11.

larités réelles sont précédées par des singularités complexes qui atteignent le domaine réel après un temps fini. Ces dernières peuvent être extraites du comportement à hauts nombres d'onde du spectre d'énergie de la solution.

Il a été proposé dans [FMB03] d'essayer d'obtenir des renseignements sur la géometrie et la nature des singularités complexes des solutions de l'équation d'Euler lesquelles, en dimension supérieure à un, ne sont pas des points. C'est un objectif important de la présente thèse, car on peut espérer qu'une meilleure compréhension des singularités éclaircira le problème de la déplétion (et la possibilité d'avoir des singularités en temps fini).

En pratique, il est très difficile d'obtenir des renseignement sur les singularités complexes des solutions de l'équation d'Euler par voie analytique. De ce fait on est naturellement amené à étudier de telles problèmes avec des outils numériques. Toutefois, l'étude numérique de problèmes aussi délicats que celui des singularités est extrêmement difficile; souvent il n'est pas possible de donner une estimation objective du rôle que jouent les erreurs numériques.

Analyse numérique des singularités complexes

Supposons qu'on nous donne une solution de l'équation d'Euler calculée par voie numérique, par exemple, sous la forme d'un développement en série de Fourier. Si nous voulons étudier ses singularités complexes, la première question qui se pose est : quelle information sur les singularités complexes de cette solution peut être extraite des données numériques ? La réponse à cette question, discutée dans Partie I, a deux aspects. Le premier aspect est essentiellement mathématique et est traité au Chapitre I. Le second, discuté au Chapitre II, est plustôt operationnelle et concerne les choix d'algorithmes nécessaires pour traiter les données numériques.

Géometrie de singularités complexes

Tout d'abord nous avons besoin d'une compréhension détaillée de la relation entre les propriétés des coefficients de Taylor et les singularités des fonction analytiques correspondantes. Dans le cas des fonctions d'une variable complexe cette relation a été établie déjà au XIX^e siècle par Darboux. En simplifiant, on peut dire qu'asymptotiquement les coefficients de Taylor d'une fonction dont la singularité la plus proche de l'origine est en $Z^\star$ se comportent comme $(Z^\star)^{-n}$. Pour des fonctions de plusieurs variables complexes la première contribution remonte aussi au XIX^e siècle. Dans [Poi92] Poincaré a regardé comment les singularités d'une fonction de deux variables complexes déterminent le comportement de ses coefficients de Fourier à hauts nombres d'onde, en utilisant un argument de pincement qui plus tard a été repris par Hadamard pour étudier les singularités de la composition de Hadamard de deux séries.

La relation géométrique entre les singularités d'une fonction rationnelle de deux variables complexes et les propriétés asymptotiques de ses coefficients de Taylor a été étudiée d'une façon mathématiquement rigoureuse dans les travaux de Tsikh et de l'école d'analyse complexe de Krasnoyarsk. Comme nous allons l'expliquer au Chapitre 4, dans ce contexte, quelques notions récemment introduites en géométrie algébrique, telles que les *amibes*, les *coamibes* et les *contours*, deviennent très utiles, voir 3.2. Il s'avère que le comportement asymptotique des coefficients de Taylor est déterminé par une courbe de dimension réelle un formant un sous-ensemble de la variété singulière qui est étroitement liée à ce que l'on appelle le contour. Par exemple, le terme dominant dans le développement asymptotique du module des coefficients de Taylor est donné par $\mathrm{e}^{-\delta(\theta)k}$, où $k(\cos\theta, \sin\theta) = (k_1, k_2)$ est

la représentation en coordonnées polaires et $\delta(\theta)$ et la fonction de support du domaine de convergence de la série correspondante.

Détermination numérique des développements asymptotiques

L'analyse numérique du comportement asymptotique des coefficients de Taylor peut être placée dans un cadre plus général que celui que nous avons discuté jusqu'ici. Supposons qu'on nous donne une suite monotone $g(n)$ et que cette suite ait un développement asymptotique que nous souhaitons déterminer. Si nous ne disposons que d'un nombre fini de termes (jusqu'à $N_{\max}$), combien de termes du développement asymptotique de $g(n)$ pouvons nous déterminer? Il se trouve que ce problème peut être traité par la méthode d'interpolation asymptotique de van der Hoeven qui a étée développée récemment [Hoe06] et qui est brièvement décrite dans [PF07]).

Avec Uriel Frisch j'ai testé cette méthode dans divers cas, tels que la détermination numérique des développements asymptotiques des coefficients de Fourier des solutions de l'équation de Burgers et du nombre de polygones autoévitants sur un réseau carré et en nid d'abeille.

La méthode d'interpolation asymptotique de van der Hoeven ne s'applique pas aux cas où les singularités les plus proches viennent par exemple par paires à la même distance de l'origine. Le comportement asymptotique des coefficients de Taylor est alors donné par $(Z_1^\star)^{-n} + (Z_2^\star)^{-n}$, et donc la suite $g(n)$ est oscillante. Or la méthode d'interpolation asymptotique ne s'applique qu'à des suite monotones.

Pour traiter de tels cas on peut utiliser la tranformation de Borel numérique avec un thèoreme dû à Pólya. Ce dernier affirme que la transformée de Borel d'une fonction analytique $f(z)$ avec des singularités qui sont à une distance finie de l'origine est une fonction entière $F(\zeta)$. Asymptotiquement cette fonction entière se comporte comme $\mathrm{e}^{h(\mathtt{Arg}(\zeta))|\zeta|}$ pour $|\zeta| \to \infty$, où l'*indicatrice*, c'est-à-dire la fonction $h(\cdot)$ est déterminée par les singularités de $f(z)$. Une fois l'indicatrice connue, par exemple par voie numérique, on peut obtenir des renseignements sur les singularités des la fonction $f(z)$. Avec Uriel Frisch j'ai testé la méthode BPH sur les singularités des solutions de l'équation d'Euler uni-dimensionelle, voir [PF07].

Le pas suivant consiste à généraliser la méthod BPH à plusieurs dimensions. Ici, pour des raisons de simplicité nous nous limitons au cas bi-dimensionel. Une approche directe utilisée dans cette thèse est d'analyser les asymptotiques des coefficients $\hat{F}(k_1, k_2)$ le long des *directions rationnelles* : on fixe deux nombres premiers entr'eux p et q, et on considère la suite $g(n) = \hat{F}(np, nq)$. La suite $g(n)$ peut alors être analysée de la même façon que dans le cas uni-dimensionel.

Dans la Section 4.2 nous proposons de tester cette généralisation sur un exemple de fonction rationnelle. Le développement en série de Taylor de telles fonctions est calculé à très haute précision en utilisant l'équation aux différences linéaire associée à ces fonctions rationnelles, voir 4.2.2. Ensuite, nous appliquons la méthode à la détermination du contour, variété de dimension réelle un, située sur la variété singuliére, qui est elle de dimension complexe un.

Singularités complexes de diverses équations hydrodynamiques

Les outils pour l'étude numérique des singularités complexes, décrites dans la Partie I, tels que la méthode d'interpolation asymptotique et la méthode BPH, nécessitent des données ayant à la fois une haute résolution et une très haute précision. Il s'avère qu'il est assez

difficile d'obtenir des telles données à partir de calculs numériques, surtout en raison des erreurs de troncature et de discrétisation.

Ici, pour réduire ces erreurs, nous utilisons des développements de Taylor en temps et des développements de Fourier en espace et nous nous limitons à des écoulements périodiques. Nous restreignons aussi les données initiales à être des polynômes trigonométriques[2]. Dans ce cas les équations hydrodynamiques se ramènent à des relations de réccurence non linéaires avec des convolutions, en sorte que les coefficients de Fourier spatiaux et les coefficients de Taylor temporels peuvent être calculés en précision arbitraire. Notons toutefois, que de cette façon nous déplaçons le problème en quelque sorte dans le domaine de la théorie de nombres, perdant l'intuition analytique et géométrique.

Cette approche a été introduite par Taylor et Green dans l'article clef [TG37] et dévéloppée ultérieurement dans [BMONMF83, PG97]. Notons qu'en utilisant des conditions initiales complexes très simples dont le nombre d'harmoniques est égal au nombre des dimensions spatiales, la complexité combinatoire se trouve grandement simplifiée. En fait, de telles conditions initiales donnent la description des singularités complexes dans le régime asymptotique des temps courts pour des écoulements à conditions initiales du type polynômes trigonométriques, voir [PMFB06].

Plus précisement nous étudierons les équations du type

$$\partial_t \boldsymbol{w} = B(\boldsymbol{w}, \boldsymbol{w}), \tag{1.1}$$

dans un domaine d-dimensionel périodique. Ici, $\boldsymbol{w}$ désigne un champs vectoriel hydrodynamique, $B(\cdot,\cdot)$ est un opérateur quadratique homogène, et la condition initiale est la somme de d ondes planes

$$\boldsymbol{w}_0 = \sum_{i=1}^{d} \hat{\boldsymbol{w}}(\mathfrak{p}_i) e^{-i\boldsymbol{z}\cdot\mathfrak{p}_i}, \tag{1.2}$$

où $\mathfrak{p}_i$ désigne les modes intiaux. En observant que l'équation (1.1) admet des solutions auto-similaires complexes

$$\boldsymbol{w} = (1/t)\tilde{\boldsymbol{w}}(\tilde{\boldsymbol{z}}), \qquad \tilde{\boldsymbol{z}} = \boldsymbol{z} + i\boldsymbol{\lambda}\ln t, \tag{1.3}$$

nous pouvons la réduire à un problème indépendant du temps

$$(-1 + i\boldsymbol{\lambda}\cdot\tilde{\nabla})\tilde{\boldsymbol{w}} = \tilde{B}(\tilde{\boldsymbol{w}}, \tilde{\boldsymbol{w}}). \tag{1.4}$$

Ici, $\boldsymbol{\lambda}$ est un vecteur complexe convenablement choisi et dépendant de $\mathfrak{p}_i$. Dans [FMB03] l'équation ci-dessus est appelée équation de similarité. Enfin, sous certaines restrictions[3] sur la forme de l'operateur $B(\cdot,\cdot)$ l'équation (1.4) peut être écrite sous la forme d'une relation de récurence.

Au Chapitre 4, Section 4.1 cette approche est testée dans le cas analytiquement soluble de l'équation de Burgers uni-dimensionelle avec la condition initiale $u_0 = (-1/2)\sin x$; nous déterminons en particulier, le développement de Taylor–Fourier complet de la solution.

Pour des équations qui ne sont pas complètement académiques, comme par exemple les équations d'Euler bi- et tri-dimensionelles et les équations de la MHD bi-dimensionelle, il y a très peu de chances d'obtenir des solutions analytiques. C'est pourquoi, j'ai calculé leurs solutions numériquement à très haute précision (à l'exception du cas tri-dimensionel,

[2] A noter que récemment Sinai et Li [LS06] ont prouvé l'existence de singularités complexes pour des solutions des équations de Navier–Stokes tri-dimensionnelles pour des conditions initiales à valeurs complexes convenablement choisies.

[3] Essentiellement, $B(\cdot,\cdot)$ ne devrait inclure que des multiplications et des dérivées. Les cas que nous avons étudiés satisfont clairement cette condition.

où les calculs à précision élevée ne sont pas faisables pour l'instant). Une fois les coefficients de Taylor/Fourier déterminés, leur comportement asymptotique est étudié numériquement avec les outils des Chapitre I et II.

L'équation d'Euler bi-dimensionelle

Le Chapitre 5 contient les résultats centraux de cette thèse. Je commence par la formulation générale du problème des asymptotiques aux temps courts pour l'équation d'Euler bi-dimensionelle. Ici, il importe de noter que pour la condition initiale $\hat{F}(\mathbf{p})\mathrm{e}^{-\mathrm{i}\,\mathbf{p}\cdot\mathbf{z}} + \hat{F}(\mathbf{q})\mathrm{e}^{-\mathrm{i}\,\mathbf{q}\cdot\mathbf{z}}$ la solution peut être rendue indépendante des amplitudes initiales $\hat{F}(\mathbf{p})$ et $\hat{F}(\mathbf{q})$, voir la Section 5.1. Ensuite, la solution dépendante du temps de l'équation d'Euler est ramenée à la solution d'une équation indépendante du temps, avec deux paramètres: le rapport des modules $\eta = |\mathbf{q}|/|\mathbf{p}|$ des deux modes de base et leur angle ϕ. Comme il a été remarqué dans [PMFB06], cette équation de similarité a la forme d'une équation d'Euler stationnaire avec un terme de résistance de Rayleigh.

Comme je n'ai pas pu trouver des solutions non triviales exactes de l'équation de similarité, j'ai essayé un développement perturbatif. Pour celà je note que lorsque $|\mathbf{q}| = |\mathbf{p}|$ on obtient une solution exacte de l'équation de similarité qui correspond à une solution stationnaire de l'équation d'Euler (dans laquelle la non linéarité est complètement "dépletée"). Utilisant alors $\varepsilon = |\mathbf{q}|/|\mathbf{p}| - 1$ comme petit paramètre, je fais un développement de la solution en puisance de ε. Au premier ordre j'obtiens une équation linéaire aux dérivées partielles qui est en gros l'équation d'Euler linéarisée avec un terme source convenable. En supprimant le terme non local dans cette équation (celui qui comporte un laplacien inverse) on obtient un modèle dans lequel la vorticité est traitée comme un scalaire passif, voir [PMFB06]. La solution correspondante est conjecturée être une fonction méromorphe, avec une singularité qui est un pôle simple. La variété singularière peut être décrite explicitement, voir [PMFB06] et le Chapitre 5, Section 5.2. Les deux premiers termes du développement asymptotique ont la forme $k^{-5/2}\mathrm{e}^{-\delta(\theta)}$, où la fonction $\delta(\theta)$ est la solution d'une équation différentielle ordinaire convenable.

Contrairement aux solutions du modèle de scalaire passif, les solutions de l'équation qui s'obtient au premier ordre du développement en ε ne sont pas méromorphes, en raison de la présence du laplacien inverse qui introduit des corrections logarithmiques. Toutefois, le terme dominant et le premier terme sous-dominant du développement asymptotique de la fonction de courant en espace de Fourier sont les mêmes que pour le modèle du scalaire passif. Les différences émergent seulement à des ordres plus élevés du développement.

Pour l'étude numérique de l'équation de similarité on utilise sa représentation sous la forme d'une relation de récurrence (équation aux différences partielles) pour calculer les solutions en espace de Fourier pour divers choix des vecteurs de base $\mathbf{p}$ et $\mathbf{q}$ avec une très haute précision. Ensuite ces solutions peuvent être analysées en utilisant la méthode d'interpolation asymptotique. Le terme dominant et le premier terme sous-dominant du développement asymptotique sont de la forme usuelle $k^{-\alpha}\mathrm{e}^{-\delta(\theta)k}$. Il n'est pas surprenant que la fonction $\delta(\theta)$, qui détermine la géométrie de la variété singulière des solitions, dépende des vecteurs de base $\mathbf{p}$ et $\mathbf{q}$. Ce qui est surprenant, ce que l'exposant α du préfacteur algébrique dépend aussi en partie des paramètres qui définissent les données initiales. Plus précisement, l'exposant α dépend de l'angle ϕ entre les modes de base, mais ne dépend pas du rapport η de leur modules, voir [PMFB06]. Cela rend les singularités *non universelles*, ce qui est une situation assez exceptionelle dans le domaine de la dynamique non linéaire et qui pourrait être lié à la dépletion susmentionnée.

Dans le domaine de paramètres $\phi \in [0, \pi]$ deux cas sont d'un intérêt particulier: $\phi = 0$ et $\phi = \pi$. Bien évidemment, pour des modes de base aussi bien parallèles ($\phi =$

0) qu'anti-parallèles, les conditions initiales sont également des solutions stationnaires de l'équation d'Euler, pour lesquelles les coefficients de Fourier de tous les modes s'annulent, sauf les modes initiaux. Ce qui est alors intéressant c'est d'étudier les limites $\phi \to 0$ et $\phi \to \pi$ accompagnées de remises à l'échelle convenables.

Dans la pratique, le cas $\phi = 0$ est étudié en utilisant les solutions qui sont renormalisée en fonction de l'angle entre les deux modes de base. Il se trouve que dans ce cas spécial le développement asymptotique de la solution peut être étudié de façon très précise : j'ai déterminé l'exposant $\alpha(0) = 5/2$ avec une précision absolue entre 10^{-8} et 10^{-10}. En outre, j'ai déterminé la structure du développement asymptotique avec deux termes de plus par rapport aux cas $\phi \neq 0$. La théorie de ce resultat extrêmement précis est toujours mal comprise. A ce propos il est important de mentionner que la structure de la solution dans le cas $\phi = 0$ est identique à celle des solutions de l'équation d'Euler linéarisée.

Contrairement au cas $\phi = 0$, il n'est pas possible d'étudier le cas des modes antiparallèles $\phi = \pi$ directement, et cela en raison de la présence de résonances. En fait, un nombre infini de coefficients deviennent infini dans ce cas[4].

Toutefois, l'étude numérique des solutions quand ϕ s'approche de π indique que $\alpha(\pi) = 3$. Notons ici que la même valeur de l'exposant est obtenue pour les solutions de l'équation de Burgers bi-dimensionelle. Pour des valeurs de ϕ entre 0 et π l'exposant $\alpha(\phi)$ semble être une fonction monotone croissante de ϕ. Cela confirme que la nature des singularités de l'équation d'Euler bi-dimensionnelle est non universelle, étant fortement dépendant des conditions initiales, du moins dans le régime asymptotique des temps courts.

Dans la Section 4.4 quelques commentaires sur la non universalité de l'exposant du préfacteur algébrique sont présentés. Je note d'une part, à propos des conditions initiales avec $\phi \to 0$, que (i) la variété singulière est presque plate, et (ii) la non linéarité est fortement réduite et l'écoulement se comporte presque comme un scalaire passif. D'autre part, pour les écoulements avec $\phi \to \pi$ la variété singulière n'est pas loin d'être complêtement repliée et les interactions non linéaires dans l'écoulement sont très fortes (ce qui se reflète dans la valeur $\alpha = 3$). Il est tentant de lier la géometrie de la variété singulière (par exemple sa courbure) à la déplétion du terme non linéaire dans l'équation d'Euler. Je note aussi que la non universalité de l'exposant α ne semble pas être une particularité des écoulements bi-dimensionnels inviscides.

Nous discutons aussi dans la Section 4.4 la pertinence des résultats obtenus dans le régime asymptotique des temps courts quand on passe aux temps intermédiaires. Aux temps courts les singularités d'une solution de l'équation d'Euler bi-dimensionnelle s'obtiennent en superposant les différentes parties de la variété singulière qui correspondent aux diverses *directions asymptotiques* alors que les interactions non linéaires entr'elles peuvent être étudiées par un développement en t. Bien évidemement, aux temps intermédiaires et bien plus encore aux temps longs, l'interaction entre les singularités devient très forte ; on ne peut plus alors parler des diverses parties de la variété singulière en interaction entre elles.

Équations de la MHD bi-dimensionnelle

Au Chapitre 5 nous donnons une formulation générale de l'approche asymptotique aux temps courts pour les équations de la MHD bi-dimensionnelle. Puisque nous avons deux champs hydrodynamiques – la fonction de courant Ψ et le potentiel magnétique A – au lieu d'un (ce qui était le cas pour l'équation d'Euler) et deux modes de base, la solution dépend de quatre paramètres : le rapport des modules $\eta = |\mathbf{q}|/|\mathbf{p}|$ des deux modes de base, leur angle ϕ et les deux paramètres complexes qui fixent les amplitudes des conditions initiales,

[4]Nous conjecturons que ces résonances sont dues à l'incompressibilité.

voir la Section 7.1. De ce fait, une étude systématique des solutions exige plus d'efforts mais reste faisable.

Jusqu'à maintenant j'ai étudié plusieures conditions initiales en utilisant des calculs numériques à haute précision. J'ai constaté que la positivité des coefficients de Fourier que j'avais observée dans le cas de l'équation d'Euler bi-dimensionnelle, est perdue pour certaines conditions intiales. Cela indique que la « division » de la variété singulière, qui dans le cas eulerien n'a lieu qu'au-delà du régime des temps temps courts, dans le cas MHD est déjà présente aux temps courts. Ainsi, pour étudier des telles solutions en détail avons-nous besoin de la généralisation bi-dimensionnelle de la méthode BPH décrite au Chaptitre 2.

Toutefois, pour quelques conditions initiales spéciales la positivité des coefficients de Fourier persiste. Ces cas spéciaux peuvent être étudiés avec la même méthode d'interpolation asymptotique que celle utilisée pour l'équation d'Euler bi-dimensionnelle. Il s'avère aussi que les coefficients de Fourier ont la forme asymptotique $k^{-\alpha}\mathrm{e}^{-\delta(\theta)k}$. Au moins dans deux cas je trouve l'exposant du préfacteur algébrique $\alpha \approx 3/2$ aussi bien pour la fonction de courant que pour le potentiel magnétique. Cependant, les contributions des termes sous-dominants suivants sont assez fort, si bien que la précision avec laquelle on peut déterminer α est beaucoup plus basse que dans le cas eulérien.

L'équation d'Euler tri-dimensionnelle

Au Chapitre 6 nous discutons l'approche asymptotique aux temps courts pour l'équation d'Euler tri-dimensionnelle. Une condition initiale générique en trois dimensions possède trois modes initiaux et neuf amplitudes initiales qui doivent satisfaire la condition d'incompressibilité. Par conséquent, il y a quatre paramètres réels qui décrivent la dépéndance de la solution dans les modes de base et neuf paramètre réels (trois paramètres complexes plus trois paramètres réels) qui sont déterminés par les amplitudes initiales.

L'exploration numérique de cet espace de paramètres d'une dimension aussi élevée ne me semble pas être faisable actuellement. De ce fait, je me suis décidé à ne considérer que quelques conditions intiales simples, comme celle de Kida–Pelz, ou la condition initiale

$$\begin{aligned} u_1 &= \sin x_2 + \sin x_3, \\ u_2 &= \sin x_1 + \sin x_3, \\ u_3 &= \sin x_1 + \sin x_2, \end{aligned} \tag{1.5}$$

introduite par Pelz et Ohkitani, voir [PO05]. Un autre obstacle est le fait que je fais les calculs en utilisant directement les relations de récurence obtenues à partir de l'équation d'Euler en régime asymptotique à temps courts, ce qui n'est pas très efficace numériquement. Même en se contentant de calculer les coefficients de Fourier en double précision, on n'est pas capable d'atteindre des hautes résolutions.

Néanmoins, j'ai obtenu quelques résultats préliminaires qui sont présentés dans la Section 6.2.

Singularités complexes en coordonnées lagrangiennes

Une approche prometteuse pour améliorer notre compréhension de la dynamique des singularités complexes des solutions de l'équation d'Euler, en deux aussi bien qu'en trois dimensions, consiste à étudier leur comportement en coordonnées lagrangiennes. Cette approche a été initiée par Takeshi Matsumoto, Jérémie Bec et Uriel Frisch in 2002, qui ont étudié les singularités complexes numériquement pour la condition initiale $\Psi(z_1, z_2) = \cos z_1 + \cos 2z_2$, see [MBF07].

Il y a au moins deux raisons pour étudier les singularités complexes en coordonnées lagrangiennes : (i) comprendre le mécanisme par lequel un champ hydrodynamique, par exemple la vorticité, peut devenir singulier dans le domaine complexe et (ii) analyser le rôle de la déplétion dans un cadre lagrangien plutôt qu'eulérien.

Concernant le premier point, on peut remarquer que, la vorticité étant conservée le long des trajectoires, la seul façon d'obtenir une singularité est d'avoir une singularité dans l'application lagrangienne inverse. Il existe un simple mécanisme – d'ailleurs purement cinématique – pour créer des singularités complexes : l'application lagrangienne inverse peut envoyer des points qui sont à distance finie du domaine réel à l'infini en un temps fini. Un exemple particulièrement simple est donné par les solutions stationnaires de l'équation d'Euler. En effet, dans les cas les plus simples le champ de vitesse est intégrable, c'est à dire que l'application lagrangienne peut être calculée explicitement. Ainsi, dans [PM05a, PM05b], mon premier travail sur les singularités complexes fait avec Takeshi Matsumoto, j'ai donné une représentation explicite de l'ensemble des points singulier de l'application lagrangienne pour un cas intégrable de l'écoulement ABC.

Transport stochastique en écoulements cellulaires dans la limite des nombres de Péclet infinis

Avec Eric Vanden-Eijnden et George Papanicolaou j'ai travaillé sur le problème du transport stochastique dans des écoulements cellulaires dans la limite de diffusivité nulle. Ce travail est présenté au Chapitre 8. Avec George Papanicolaou j'ai donné une description asymptotique du transport stochastique qui s'applique à des écoulements cellulaires bornés arbitraires et à des écoulements cellulaires non bornés dans lesquels les cellules sont connectées par une seule ligne de niveau de la fonction de courant. Le processus asymptotique correspondant est une marche aléatoire à temps continu sur le graphe associé à l'écoulement. Pour cette marche aléatoire nous avons déterminé les probabilités de transition et les temps de transition.

Avec Eric Vanden-Eijnden j'ai analysé la diffusion stochastique dans des écoulements avec une structure topologique differente, à savoir dans les écoulements dans lesquels chaque ligne de niveau de la fonction de courant est bornée. Dans ce cas le processus asymptotique est construit en utilisant les resultats de Wentzell et Freidlin [FW93, FW98] sur des petites perturbations stochastiques des systèmes intégrables. L'espace des états est dans ce cas le graphe de Reeb de la fonction de courant, la diffusion ayant lieu le long les arêtes du graphe. Les équations de Fokker– Planck correspondantes sont alors obtenues par une procédure qui ressemble aux méthodes de perturbations en mécanique classique.

Goulot d'étranglement et « thermalisation avortée »

Enfin, je mentionne un travail que j'ai décidé de ne pas inclure dans cette thèse car il n'est que faiblement relié au reste des matériaux et n'a été commencé qu'il y a quelques mois. En turbulence développée, ce que l'on appelle habituellement un goulot d'étranglement (bottleneck) c'est un comportement non monotone du spectre d'énergie compensé $k^{5/3}E(k)$ dans la région de transition entre le domaine inertiel et le domaine dissipatif (essentiellement une bosse dans le spectre compensé).

Le travail concerne les équations du type hydrodynamique (incluant l'équation de Navier–Stokes, l'équation de Burgers et des modèles de turbulence divers, comme par exemple la fermeture EDQNM) avec « hyperviscosité », c'est-à-dire avec un taux de dissipation $\mu(|k|/k_d)^{2\alpha}$ et $\alpha > 1$. Il est conjecturé que pour $\alpha \to \infty$ et μ, k_d fixés, les solutions

tendent vers celles obtenues en imposant une troncature de Galerkin avec dissipation nulle et suppression des modes de Fourier au-delà du la coupure k_d. On sait depuis le travail récent de Cichowlas et al. [CBDB05] que pour des valeurs de k_d suffisamment grandes, la solution de l'équation avec troncature de Galerkin développe un domaine thermalisé à hauts nombres d'ondes (avec un spectre qui se comporte comme k^2 en trois dimensions). Il est proposé d'interpréter le phenomème de goulot d'étranglement (qui devient plus prononcé pour des valeurs de α croissantes) comme une thermalisation avortée. Cela implique en outre une réduction forte de l'intermittence aux échelles du goulot d'étranglement.

Un rapport d'avancement sur ces questions (écrit avec Uriel Frisch) se trouve à `www.obs-nice.fr/etc7/bottle.pdf`.

En fait, ce travail avait été commencé il y a longtemps (par Uriel Frisch et Achim Wirth) et était resté en sommeil jusqu'à l'article récent de Chichowlas et al. Maintenant nous collaborons sur divers aspects de ces questions avec Jian-Zhou Zhu, Susan Kurien, Rahul Pandit, Samriddhi Ray, Konstantin Khanin, Mikhail Blank et Achim Wirth.

Chapter 2

General introduction

The Euler equation – the central subject of study in this thesis – at first sight may seem to be quite simple, almost elementary. This is partially because of the straightforward way in which it is derived in the modern physics courses, but it is also due to the notations which actually go back to Euler himself [Eul57] and which hide some of its nontrivial aspects. Furthermore, the Euler equation is sometimes viewed as unphysical, because it is not taking into account the internal friction of the fluid and thus, in Feynman's words [Fey64], describes "dry water".

Looking more closely, we see that this point of view holds some misconceptions. Take for example the derivation of the Euler equation. It took two decades (1734-1755) of efforts by the best physicists and mathematicians of the XVIIIth century, beginning with the D. Bernoulli's early work (Bernoulli's pressure law) and culminating with Euler establishing his celebrated equation [Tru54, Cal96, Dar05, DF07]. And it was not yet the end of the story! Approximately two hundred years later Arnold [Arn66] showed, very much in the spirit of Lagrange's variational derivation of the Euler equation, that the motion of inviscid fluids can be understood as geodesic motion on the group of volume preserving diffeomorphisms.

As to the unphysical objection, there is a growing consensus that the Euler equation (and not just the Navier–Stokes equation) remains of interest for at least two major reasons. Firstly, it corresponds, at least formally, to the high Reynolds number limit $Re \to \infty$. Secondly, there exist certain phenomena which may be partially obscured by the presence of the viscous term and which are more easily and effectively studied in the "bare" form in the inviscid case. One of these phenomena is *depletion*, i.e. the tendency of the flow to suppress nonlinearities and to approach – at least locally – one of the numerous steady-state solutions of the Euler equation.

Mathematical aspects of the Euler equation have been intensively studied in the course of the last hundred years, see, for instance, [MB02, MP94] and [BT07, Cha07, Con07] for recent reviews. Nevertheless, some essential mathematical questions remain open. For example, it is not known whether the three-dimensional Euler equation is well-posed for sufficiently smooth initial data: do solutions starting from, say real analytic initial conditions, develop a real singularity in a finite time?

For analytic initial data, the solutions of the Euler equation can be extended to the complex domain: the space variables, together with the velocity, the vorticity and the pressure are then extended to complex values. It is known since the work of [BBZ76, Ben76a, Ben76b] that, for such data, hypothetical real singularities are necessarily preceeded by complex ones, hitting the real domain after a finite time. It was pointed out in [SSF83] that this can be used to detect such real singularities by monitoring numerically the approach to the real domain of complex singularities. The latter can be inferred from the

high-wavenumber behavior of the energy spectrum of the solution.

It was suggested in [FMB03] that we should try to obtain information about the geometry and type of complex singularities of solutions of the Euler equation which in more than one spatial dimension are definitely not point-like. This is an important goal of the present thesis, since we can expect that better understanding of singularities will shed light on the issue of depletion (and the possibility of a finite-time blow-up).

In practice, information on complex singularities of solutions of the Euler equation is very hard to obtain analytically. Therefore, we are naturally lead to exploring such issues by numerical means. However, numerical investigation of such delicate problems as singularities is tremendously difficult and it is often impossible to give an objective estimation of the role played by numerical errors.

Numerical analysis of complex singularities

Suppose that we are given a numerically calculated solution of the Euler equation, for example in the form of an expansion into a Fourier series. If we want to study its complex singularities, the first problem which arises is: what information on complex singularities of this solution can be extracted from the numerical data? The answer to this question, which is discussed in Part I, has two aspects. The first aspect is mostly mathematical and is treated in Chapter 4. The second aspect is operational and concerns the choice of algorithms which we need to process the data, see Chapter 5.

Geometry of complex singularities

First of all, we need to have sufficient understanding of the connections between the properties of Taylor coefficients and the singularities of the corresponding analytical functions. In the case of function of one-complex variable this relation has been established already in the 19th century by Darboux [Dar78]. Simplifying, one can say that asymptotically Taylor coefficients of a function whose singularity closest to zero is $Z^\star$ behave like $(Z^\star)^{-n}$. For functions of several complex variables the first contribution also goes back to the 19th century. In [Poi92] Poincaré has analyzed how singularities of a function of two compex variables determine the high wavenumber behaviour of its Fourier coefficients, using a pinching argument which has been later applied by Hadamard to studying singularities of Hadamard's composition of two series.

The geometrical connection between singularities of a rational function of two complex variables and the properties of its Taylor coefficients has been studied rigorously in the works of Tsikh and the Krasnoyarsk school of complex analysis. As we shall explain in Chapter 4, in this context notions recently introduced in the algebraic geometry, such as *amoeba*, *coamoeba* and *contour* become very useful, see 3.2. It turns out that the asymptotic behavior of Taylor coefficients is determined by a curve of real dimension one on the singular set which is closely related to the contour. For example, the leading order term in the asymptotic expansion of the modulus of Taylor coefficients is of the form $\mathrm{e}^{-\delta(\theta)k}$, where $k(\cos\theta, \sin\theta) = (k_1, k_2)$ is the representation of the wavevector in polar coordinates and $\delta(\theta)$ is the *support function* of the domain of convergence of the corresponding series.

Numerical determination of asymptotic expansions

Let us remark that the numerical analysis of the asymptotical behavior of Taylor coefficients can be put into a more general setting which is the following. Suppose that we are given (numerically, but with a very high precision) a monotonic sequence $g(n)$. We assume that

this sequence has an asymptotic expansion which we need to determine. Given only a finite number of terms (say up to $N_{\max}$) how many terms can we determine in the asymptotic expansion of $g(n)$? This problem can be handled by a recently developped asymptotic interpolation method of van der Hoeven [Hoe06] (which is briefly described in [PF07]).

Together with Uriel Frisch I have tested this method in various cases, such as the determination of asymptotic expansion of Fourier coefficients of solutions of the one-dimensional Burgers equation and of the number of self-avoiding polygons on square and honeycomb lattices, see [PF07].

The asymptotic interpolation method of van der Hoeven is not applicable in the case when there is a pair of singularities, both at the same distance from the origin. The asymptotics of the Taylor coefficients are then given by the sum $(Z_1^\star)^{-n} + (Z_2^\star)^{-n}$ and are oscillatory, whereas the asymptotic interpolation applies only to monotonic sequences.

To handle this case, numerical Borel transformation in combination with a theorem due to Pólya can be used. Namely, the Borel transformation of an analytical function $f(z)$ with sigularities which are at finite distance from the origin is an entire function $F(\zeta)$. Asymptotically it behaves like $\mathrm{e}^{h(\mathrm{Arg}(\zeta))|\zeta|}$ for $|\zeta| \to \infty$, where function $h(\cdot)$, called *indicatrix*, is determined by the singularities of $f(z)$. Once the indicatrix is known, for example calculated numerically, we can obtain information on the singularities of the function $f(z)$. We will refer to this method as the BPH (Borel–Pólya–Hoeven) method. Together with Uriel Frisch I have tested the BPH method on the singularities of solutions of the one-dimensional Burgers equation, see [PF07].

The next step consists in generalizing the BPH method to several dimensions. Here we find it convenient to concentrate only on the two-dimensional case. A straightforward aproach which is used in this thesis consists in analyzing the asymptotics of the coefficients $\hat{F}(k_1, k_2)$ along *rational directions*, that is, fixing two relatively prime numbers p and q we consider the sequence $\hat{F}(np, nq)$. This sequence can be analyzed in the same way as in the ordinary one-dimensional case.

In Section 4.2 we propose to test this generalization on the example of rational functions. The Taylor series expansion of such functions can be calculated with high precision using the linear difference equation associated to this rational function, see 4.2.2. Then we can apply the method described above to determine numerically a curve of real dimension one on the singular set, the latter having complex dimension one.

In Section 4.2.3 we describe a multi-dimensional generalization of Pólya's theorem due to Ivanov and Stavsky and propose to use it for the numerical analysis of Taylor/Fourier coefficients.

Complex singularities of various hydrodynamic equations

The tools for numerical analysis of complex singularities which we describe in Part I, such as the asymptotic interpolation method and the BPH method, require data obtained with both high resolution and high precision. However, getting such data from numerical simulations turns out sometimes to be quite hard, most notably because of truncation errors and errors introduced through time discretization.

Here, to reduce such errors, we use Taylor expansions in time and Fourier expansions in space and limit ourselves to periodic flows. We also restrict the initial conditions to those given by trigonometric polynomials.[1] Then our hydrodynamic equations are reduced to nonlinear recursion relations involving convolutions and the spatial Fourier coefficients and

[1] Note, that recently Sinai and Li [LS06] have proved the existence of complex singularities for solutions of the three-dimensional Navier–Stokes equations for specially chosen complex-valued initial conditions.

Taylor coefficients in time can be calculated with arbitrary precision. Note, that in this way we in some sense shifted the problem into the domain of number theory, losing geometrical and analytical intuition.

This approach has been pioneered by Taylor and Green in the seminal paper [TG37] and further developed in [BMONMF83, PG97]. Note that if we use very simple complex valued initial conditions in which the number of harmonics is equal to the number of space dimensions, the combinatorial complexity is greatly reduced. Actually, such initial conditions give an asymptotic description of complex singularities in the asymptotic régime of $t \to 0_+$ for flows with intial conditions of trigonometric polynomial type, see [PMFB06].

More precisely, we will study equations of the type

$$\partial_t \boldsymbol{w} = B(\boldsymbol{w}, \boldsymbol{w}), \tag{2.1}$$

on a d-dimensional periodic domain. In Equation (2.1) $\boldsymbol{w}$ denotes some vector-valued hydrodynamic field, $B(\cdot,\cdot)$ is a homogeneous quadratic operator, and the initial condition is a sum of d plane waves

$$\boldsymbol{w}_0 = \sum_{i=1}^{d} \hat{\boldsymbol{w}}(\mathfrak{p}_i) e^{-i\boldsymbol{z}\cdot\mathfrak{p}_i}, \tag{2.2}$$

where $\mathfrak{p}_i$ denote the initial modes. Observing that Equation (2.1) admits self-similar complex solutions

$$\boldsymbol{w} = (1/t)\tilde{\boldsymbol{w}}(\tilde{\boldsymbol{z}}), \qquad \tilde{\boldsymbol{z}} = \boldsymbol{z} + i\boldsymbol{\lambda}\ln t, \tag{2.3}$$

where $\boldsymbol{\lambda}$ is a suitably chosen complex vector depending on $\mathfrak{p}_i$, we can reduce it to a time independent problem

$$(-1 + i\boldsymbol{\lambda}\cdot\tilde{\nabla})\tilde{\boldsymbol{w}} = \tilde{B}(\tilde{\boldsymbol{w}}, \tilde{\boldsymbol{w}}). \tag{2.4}$$

Following [FMB03] the above equation is referred to as the *similarity equation*. Finally, under some restrictions[2] on the form of the operator $B(\cdot,\cdot)$, Equation (2.4) can be converted to a recursion relation.

In Chapter 4, Section 4.1 this approach is tested in the analytically solvable case of the one-dimensional Burgers equation with initial condition $u_0 = (-1/2)\sin x$, in particular determining the complete Taylor–Fourier expansion of the solution. In Section 4.2 remarks are made on the extension of this approach to the two-dimensional Burgers equation.

For equations which are not completely academic, such as the two-dimensional Euler and MHD equations and three-dimensional Euler equations, the chances of obtaining analytical solutions are slim. Therefore, I calculated their solutions numerically with very high precision (except for the three-dimensional case, where high precision calculations are not feasible at the moment). Once the Taylor/Fourier coefficients are determined, their asymptotic behavior is determined numerically, using the tools presented in Part I.

Two-dimensional Euler equation

Chapter 5 contains the central results of this thesis. I start by giving a general formulation of the short-time asymptotic problem for the two-dimensional Euler equation. Here, it is important to note that for the initial condition $\hat{F}(\mathfrak{p})\mathrm{e}^{-\mathrm{i}\,\mathfrak{p}\cdot\boldsymbol{z}} + \hat{F}(\mathfrak{q})\mathrm{e}^{-\mathrm{i}\,\mathfrak{q}\cdot\boldsymbol{z}}$, the solutions can be made independent of the initial amplitudes $\hat{F}(\mathfrak{p})$ and $\hat{F}(\mathfrak{q})$, see Section 5.1. The time-dependent Euler equation is then reduced to a two-dimensional time-independent equation with two parameters: the aspect ratio $\eta = |\mathfrak{q}|/|\mathfrak{p}|$ and the angle ϕ between the basic modes

[2] Essentially, $B(\cdot,\cdot)$ should involve only mutiplications and derivatives. The cases which we have studied clearly satisfy this condition.

$\mathfrak{p}$ and $\mathfrak{q}$. As has been observed in [PMFB06], this similarity equation has the form of a stationary Euler equation with a Rayleigh drag term.

Since I have not been able to find any nontrivial exact solutions of the similarity equation, I have tried to use a perturbation expansion. For this I note that for $|\mathfrak{q}| = |\mathfrak{p}|$ an exact solution of the similarity equation is obtained which corresponds to a stationary solution of the Euler equation (in which the nonlinearity is completely depleted). Using $\varepsilon = |\mathfrak{q}|/|\mathfrak{p}| - 1$ as a small parameter I make an expansion of the solution in powers of ε. At first order in ε I obtain a linear partial differential equation which is basically a linearized Euler equation with a suitable source term. Omitting the nonlocal term in the linearized Euler equation (the one which involves the inverse Laplacian) yields a model in which the vorticity is treated as a passive scalar, see [PMFB06]. The corresponding solution is a conjectured meromorphic function, with a simple pole singularity. Its singular set can be described explicitly, see [PMFB06] and Chapter 5, Section 5.2. The first two terms in the asymptotic expansion of the solution in the Fourier space have the form $k^{-5/2}\mathrm{e}^{-\delta(\theta)}$, where the function $\delta(\theta)$ is determined as a solution of a suitable ordinary differential equation.

Contrary to the solutions of the passive scalar model, solutions of the linearized Euler equation are not meromorphic, due to the presence of the inverse Laplacian which introduces logarithmic corrections. Still, the leading and the first subleading order terms in the asymptotic expansion of the stream function in the Fourier space are the same as for the passive scalar model. The differences appear only at higher orders of the expansion.

The numerical study of the similarity equation makes use of its representation in the form of a recursion relation (partial difference equation) to calculate the solutions in the Fourier space for various choices of the basic vectors $\mathfrak{p}$ and $\mathfrak{q}$ with very high precision. The solutions can then be analyzed using the asymptotic interpolation method. The leading and the first subleading order terms in the asymptotic expansion of the stream function are of the standard form $k^{-\alpha}\mathrm{e}^{-\delta(\theta)k}$. It is not surprising that the function $\delta(\theta)$ which determines the geometry of the singular set of the solutions depends on the basic vectors $\mathfrak{p}$ and $\mathfrak{q}$. What is surprising, is that the exponent α of the algebraic prefactor also depends on some of the parameters characterizing the initial data. More precisely, the scaling exponent α depends on the angle ϕ between the basic modes, but not on the ratio η of their moduli, see [PMFB06]. This makes the singularities *nonuniversal*, a most unusual situation in the field of nonlinear dynamics that can be related to the aforementioned depletion.

In the whole parameter range of $\phi \in [0, \pi]$ two cases are of particular interest: $\phi = 0$ and $\phi = \pi$. Of course, both for parallel ($\phi = 0$) and antiparallel ($\phi = \pi$) basic modes the initial conditions are stationary solutions of the Euler equation for which the Fourier coefficients at all modes except the initial ones are zero. It is interesting to study the limits $\phi \to 0$ ($\phi \to \pi$ respectively) accompanied by suitable rescalings.

Practically, the case $\phi = 0$ is studied using solutions which are renormalized with respect to the angle between the two basic modes. It turns out that in this special case the asymptotic expansion of the solution can be found very accurately: the exponent $\alpha(0) = 5/2$ can be determined with absolute precision between 10^{-8} and 10^{-10}. Furthermore, I identified the structure of the asymptotic expansion with two more subleading terms than in the case $\phi \neq 0$. The theory of this exquisitely precise result is still poorly understood. In this respect it is worth noting that the structure of the solution in the case $\phi = 0$ is similar to the structure of solutions of the linearized Euler equation.

Contrary to the case $\phi = 0$, the case of antiparallel basic modes $\phi = \pi$ cannot be studied directly due, to resonances. In fact, infinitely many coefficients become infinite.[3] However, numerical study of solutions for ϕ close to π indicates that $\alpha(\pi) = 3$. Note,

[3] We conjecture that these resonances are due to incompressibility.

that the same exponent is obtained for solutions of the two-dimensional Burgers equation. For values of ϕ between 0 and π the exponent $\alpha(\phi)$ seems to be a monotonically increasing function of ϕ. This confirms that the nature of the singularities of the two-dimensional Euler equation is nonuniversal – at least in the short-time asymptotic régime – being strongly dependent on the initial conditions.

In Section 6.4 some commments on the nonuniversality of the scaling exponent are made. On the one hand, considering initial conditions with $\phi \to 0$ I observe that (i) the singular manifold is almost flat, and (ii) the nonlinearity is strongly depleted with the flow behaving almost like a passive scalar. On the other hand, for $\phi \to \pi$ the singular manifold is almost completely folded back and nonlinear interactions in the flow are strong (which is reflected in the value $\alpha = 3$). It is tempting to relate the geometry of the singular manifold (e.g. its curvature) to the depletion of the nonlinear term in the Euler equation. I also note that the observed nonuniversality of the scaling exponent α does not seem to be a particular feature of two-dimensional inviscid flows, as we shall see later.

In Section 6.4 we also discusss the relevance of the results obtained in the short-time asymptotic régime for intermediate times. At short times the singularities of a solution of the 2D Euler equation are obtained by superimposing the pieces of the singular manifold corresponding to different *asymptotic directions* whereas the nonlinear interactions between them can be analyzed by an expansion in t. Of course, at intermediate times and even more so at longer times the interaction between the singularities becomes very strong and it does not make sense anymore to speak about different parts of the singular manifold interacting with each other.

Two-dimensional MHD equations

In Chapter 7 we give a general formulation of the short-time asymptotic approach to the two-dimensional magnetohydrodynamic (MHD) equations. Since we have two hydrodynamic fields (the stream function Ψ and the magnetic potential A) instead of one in the Euler case, and two basic modes, the solution depends on four parameters: the aspect ratio η of moduli of the basic modes, the angle ϕ between the basic modes, and two complex-valued parameters depending on the amplitudes of the initial conditions, see Section 7.1. A systematic numerical study of the solutions is therefore more laborious than in the Euler case, but still feasible.

Until now I have studied several initial conditions using high-precision arithmetics. I observed that the positivity of the Fourier coefficients found for the two-dimensional Euler equation is lost in the MHD case for some initial conditions. This indicates that the "splitting" of the singular manifold which for the Euler equation occurs beyond the short-time régime is already present in the short-time régime of the MHD equations. Thus, to study such solutions in detail we need the two-dimensional generalization of the BPH method described in Chapter 5.

Surprisingly, for some special initial conditions the positivity of the Fourier coefficients persists. These special cases can then be analyzed by the asymptotic interpolation procedure which has been applied to the two-dimensional Euler equation. It turns out that the Fourier coefficients still have the asymptotic form $k^{-\alpha}\mathrm{e}^{-\delta(\theta)k}$. In at least two cases we found the algebraic prefactor exponent $\alpha \approx 3/2$, both for the stream function and the magnetic potential. However, the contributions from the next following subleading order terms are quite strong, so that the precision in determining α is much lower than in the Euler case.

Three-dimensional Euler equations

In Chapter 8 we discuss the short-time asymptotic approach to the three-dimensional Euler equation. The generic initial condition in three dimensions has three initial modes ($\mathfrak{p}$, $\mathfrak{q}$ and $\mathfrak{r}$) and nine initial amplitudes which have to satisfy the incompressibility condition. Thus, there are four real-valued parameters which describe the dependence on the basic modes and nine real-valued parameters (three complex ones and three real ones) determined by the amplitudes of the initial conditions.

Exploring this large parameter space numerically does not seem feasible for the moment. Therefore, we have restricted ourselves to some simple initial conditions, such as the Kida–Pelz flow or the flow

$$u_1 = \sin x_2 + \sin x_3, \qquad u_2 = \sin x_1 + \sin x_3 \qquad u_3 = \sin x_1 + \sin x_2, \tag{2.5}$$

which has been introduced by Pelz and Ohkitani in [PO05].

A further obstacle is that a direct use of the recursion relations obtained from the Euler equation in the short-time régime is not very efficient numerically. Even when calculating the Fourier coefficients in double precision we are not able to reach high resolutions.

Nevertheless, some preliminary results can be obtained which are presented in Section 8.2.

Complex singularities in Lagrangian coordinates

One possible way to improve our understanding of the dynamics of the complex singularities of solutions of the Euler equation, both two and three-dimensional, is to study their behavior in Lagrangian coordinates. This approach has been initiated by T. Matsumoto, J. Bec and U. Frisch in 2002, who have investigated this numerically for the initial condition $\Psi(z_1, z_2) = \cos z_1 + \cos 2z_2$, see [MBF07].

There are at least two reasons for studying complex singularities in Lagrangian coordinates: (i) understanding the mechanism by which a hydrodynamic field, e.g. the vorticity, can become singular in the complex domain and (ii) analyze the role of depletion in the Lagrangian frame as opposed to the Eulerian one.

Concerning the first point, one can note that, since the vorticity is conserved along particle trajectories, the only way by which it can become singular is to have a singular inverse Lagrangian mapping. There is a simple mechanism – which is purely kinematical, by the way – for the creation of complex singularities: Lagrangian locations at finite distances can be mapped to infinity by the inverse Lagrangian map in a finite time. A particularly simple example are flows given by stationary solutions of the Euler equation. In fact, when the dynamical systems associated to their velocity fields are integrable the Lagrangian map can be calculated explicitly. Thus, in [PM05a, PM05b], which was my first work carried out on complex singularities together with Takeshi Matsumoto, I have given an explicit representation of the set of complex Lagrangian singularities for the velocity field corresponding to an integrable instance of the ABC flow.

Stochastic transport in cellular flows in the high Péclet number limit

Together with Eric Vanden-Eijnden and George Papaicolaou I have worked on the problem of stochastic transport in cellular flows in the small diffusivity limit, see Chapter 10. With George Papanicolaou I have given an asymptotic description of stochastic transport which applies to arbitrary bounded cellular flows or to unbounded cellular flows connnected by a

single unbounded level line. The asymptotic process is a continuous time random walk on the graph associated to the flow for which we have determined the transition probabilities and transition times.

With Eric Vanden-Eijnden I have analyzed stochastic diffusion in flows with a different topological structure, namely the flows in which every level line of the stream function is bounded. In this case the asymptotic process is constructed using the results of Wentzell and Freidlin [FW93, FW98] on small stochastic perturbations of integrable systems. The state space in this case is the Reeb graph of the stream function, with particles diffusing along the edges of the graph. The corresponding Fokker–Planck equations are obtained using a procedure reminiscent of the perturbation method in clasical mechanics.

Bottleneck and "aborted thermalization"

I mention finally some work which I decided not to include in this thesis because it is only weakly related to the rest of the material and it has started but a few months ago. In fully developed turbulence what is usually called the bottleneck effect is a non-monotonic behavior of the compensated energy spectrum $k^{5/3}E(k)$ in the transition between the inertial range and the dissipation range (basically a bump in the plot).

The work concerns equations of hydrodynamical type (including the 3D Navier–Stokes equations, the Burgers equation and various models of turbulence, such as the EDQNM closure) with "hyperviscosity", i.e. having a dissipation rate $\mu(|k|/k_d)^{2\alpha}$ with $\alpha > 1$. It is conjectured that when $\alpha \to \infty$ at fixed μ and k_d, the solutions tend to those obtained by a Galerkin truncation with zero dissipation and suppression of all Fourier modes whose wavenumber exceeds the cutoff k_d. From recent work of Cichowlas et al. [CBDB05] it is known that when k_d is large enough the solution of Galerkin-truncated equations develop a thermalized range at high wavenumbers (with a k^2 spectrum in 3D). It is proposed to interpret the phenomenon of bottleneck (which becomes stronger when increasing α) as an aborted thermalization. This implies among other things a strong reduction of intermittency at bottleneck scales.

A progress report on these matters (written with U. Frisch) may be found at `www.obs-nice.fr/etc7/bottle.pdf`.

Such work was actually started a long time ago (by U. Frisch and A. Wirth) and remained dormant until the recent paper of Cichowlas et al. We are now collaborating on various aspects of these questions with Jian-Zhou Zhu, Susan Kurien, Rahul Pandit and Samriddhi Ray, Konstantin Khanin, Mikhail Blank and Achim Wirth.

Part I

Numerical reconstruction of complex singularities

Chapter 3

Amoebae, algae and all that

In this chapter we explain some elementary notions of the analysis in several complex variables and algebraic geometry which are useful for the numerical study of the complex singularities of functions of several complex variables. In physical applications, for example in hydrodynamics and statistical physics, information on complex singularities is obtained from data calculated (mostly numerically) in the form of Taylor (or Laurent) series expansions. A complete mathematical characterization of the domains of convergence of such series can be established by rather elementary means. In some cases, for example when all the coefficients are positive, the numerical determination of these domains of convergence can be done using the multi-dimensional analogue of the ratio test (cf. Section 3.1).

Actually, we can get hold of more than just the domain of convergence of the series, since the high-wavenumber asymptotical behavior of Taylor (Fourier) coefficients is determined by a subset of the singular manifold of real dimension one, usually called *contour*. To explain the relation between the asymptotics of the Taylor coefficients and the geometry of the singular set we start with the simple case of rational functions. In this context the recently developed notions of amoebae, coamoebae and contours become useful, Section 3.2. It turns out (see the following chapter) that our main object of interest in this case will be what is called the diagonal of a double Taylor series, Section 3.3.

In Section 3.2.4 we give several concrete examples of singular manifolds and the corresponding amoebae, coamoebae and contour.

3.1 Domains of convergence of double power series

In this section we restrict ourselves to functions of two complex variables, essentially to keep our notation simple. Note that all notions introduced below are easily generalized to an arbitrary number of dimensions, see [Sha92].

We use the following notation: (ξ_1, ξ_2) is a vector in $\mathbb{C}^2$, $(r_1, r_2) = (|\xi_1|, |\xi_2|) \in \mathbb{R}_{>0} \times \mathbb{R}_{>0}$ are the componentwise moduli. We also use the coordinatewise logarithmic mapping (the principal branch) defined via $(\xi_1, \xi_2) = (e^{z_1}, e^{z_2})$, where $(z_1, z_2) = (x_1 + iy_1, x_2 + iy_2)$, $(x_1, x_2) \in \mathbb{R}^2$, and $(y_1, y_2) \in [0, 2\pi) \times [0, 2\pi) = \mathbb{T}^2$ is 2π periodic.

3.1.1 Some elementary notions

Let us consider a function $F(\xi_1, \xi_2)$ which is given by the power series

$$F(\xi_1, \xi_2) = \sum_{n_1=0}^{\infty} \sum_{n_2=0}^{\infty} \hat{F}(n_1, n_2)\, \xi_1^{n_1} \xi_2^{n_2} \tag{3.1}$$

on its domain of convergence $D_{\hat{F}} \subset \mathbb{C}^2$. To characterize the domains of convergence of the power series (3.1) we will need the notions of a complete Reinhardt domain and logarithmic convexity.

Definition 3.1.1 *A Reinhardt domain D with center at a point $(\xi_1^*, \xi_2^*) \in \mathbb{C}^2$ is a domain such that for any point (ξ_1', ξ_2') in D it also contains any point*

$$(\xi_1, \xi_2) = \left\{ \left(\xi_1^* + (\xi_1' - \xi_1^*)\, \mathrm{e}^{\mathrm{i}\,\theta_1},\ \xi_2^* + (\xi_2' - \xi_2^*) \mathrm{e}^{\mathrm{i}\,\theta_2} \right) \right\} \tag{3.2}$$

for $0 < \theta_1,\ \theta_2 < 2\pi$. A Reinhardt domain is said to be complete if along with each point (ξ_1', ξ_2') it contains all points (ξ_1, ξ_2) for which $|\xi_1 - \xi_1^*| \leq |\xi_1' - \xi_1^*|$, $|\xi_2 - \xi_2^*| \leq |\xi_2' - \xi_2^*|$.

In what follows we use the complexified torus $\mathbb{C}\backslash\{0\} \times \mathbb{C}\backslash\{0\} = \mathbb{T}^2_{\mathbb{C}}$ where $\mathbb{C}\backslash\{0\}$ is the punctured complex plane. We define the mapping $\mathrm{Log} :\ \mathbb{T}^2_{\mathbb{C}} \longrightarrow \mathbb{R}^2$ by

$$\mathrm{Log}\,(\xi_1, \xi_2) = (\log|\xi_1|, \log|\xi_2|) = (x_1, x_2). \tag{3.3}$$

Definition 3.1.2 *A set $M \subset \mathbb{C}^2$ is called logarithmically convex if $\mathrm{Log}\,(M) \subset \mathbb{R}^2$ is convex.*

Domains of convergence can be characterized as follows: any logarithmically convex Reinhardt domain is the domain of convergence of a power series [Sha92]. Thus, $D_{\hat{F}}$ is a logarithmically convex Reihardt domain. Furthermore, to calculate $D_{\hat{F}}$, we use the fact that the Cauchy–Hadamard formula which in one dimension gives the radius of convergence of a power series can be generalized to several dimensions. To state this formula we need the following definition.

Definition 3.1.3 *A polydisk*

$$D(r_1, r_2) = \left\{ (\xi_1, \xi_2) \in \mathbb{C}^2 :\ |\xi_1| < r_1\,,\ |\xi_2| < r_2 \right\}$$

is called a polydisk of convergence of the series (3.1) *if $D(r_1, r_2) \subset D_{\hat{F}}$ and, furthermore, in any polydisk*

$$D(r_1', r_2') = \left\{ (\xi_1, \xi_2) \in \mathbb{C}^2 :\ |\xi_1| < r_1'\,,\ |\xi_2| < r_2' \right\},$$

where $r_1' \geq r_1$, $r_2' \geq r_2$ and at least one of these two inequalities is strict, there are points at which the series (3.1) *diverges. The radii r_1, r_2 are called conjugate radii of convergence.*

The following theorem [Sha92] is the generalization of the Cauchy–Hadamard formula.

Theorem 3.1.4 *The conjugate radii of convergence of the series* (3.1) *satisfy the relation*

$$\varlimsup_{|(n_1,n_2)|\to\infty} \sqrt[n_1+n_2]{|\hat{F}(n_1, n_2)| r_1^{n_1} r_2^{n_2}} = 1. \tag{3.4}$$

The boundary of the convex set $\mathrm{Log}\,(D_{\hat{F}})$ is then given by

$$\phi_{\hat{F}}(x_1, x_2) = 0,$$

where $\phi_{\hat{F}}(x_1, x_2)$ is a suitable function which can in principle be determined by (3.4).

3.1.2 Ratio tests for double power series

Formula (3.4) is not very convenient for numerical application. Actually, for concrete implementations a less general but simpler multi-dimensional version of the well-known ratio test has turned out to be quite usefull. The following material is a slight modification of the results of [Dan40].

In what follows we will use the notion of the support function of convex sets.

Definition 3.1.5 *The support function of a convex set K is a real-valued function $h_K(\mathbf{x})$ on $\mathbb{R}^2$ defined by*

$$h_K(\mathbf{k}) = \max\{\langle \mathbf{k}, \mathbf{x}\rangle : \mathbf{x} \in K\}. \tag{3.5}$$

For all $\mathbf{x}, \mathbf{x}' \in \mathbb{R}^2$ and $\lambda \geq 0$ the support functions are characterized by two properties:

$$h_K(\lambda \mathbf{x}) = \lambda h_K(\mathbf{x}) \qquad \text{and} \qquad h_K(\mathbf{x} + \mathbf{x}') \leq h_K(\mathbf{x}) + h_K(\mathbf{x}'). \tag{3.6}$$

The hyperplane

$$H_K(\mathbf{x}) = \{\mathbf{x}' \in \mathbb{R}^2 : \langle \mathbf{x}, \mathbf{x}'\rangle = h_K(\mathbf{x})\}, \tag{3.7}$$

where $\mathbf{x} \in \mathbb{R}^2 \backslash \{0\}$, is called the support hyperplane of K with outer normal vector $\mathbf{x}$, see [Sch93] We denote the support function of $\mathtt{Log}(D_{\hat{F}})$ by $h_{\hat{F}}(\boldsymbol{k})$. We will also use the rescaled support function which is defined by

$$h_{\hat{F}}(\boldsymbol{k}) = |\mathbf{k}|\, \delta_{\hat{F}}(\theta). \tag{3.8}$$

One possible way to calculate $\delta_{\hat{F}}(\theta)$ is to analyze the behaviour of the Taylor coefficients $\hat{F}(n_1, n_2)$ along half-lines in the (n_1, n_2)-space corresponding to *rational directions* $(p, q) = |(p, q)|(\cos\theta_{(p,q)}, \sin\theta_{(p,q)})$, that is for $(n_1, n_2) = n(p, q)$ (sometimes we may refer to (p, q) as to the rational direction with slope $q/p = \tan\theta_{(p,q)}$). Under suitable conditions, it can be shown that

$$\delta_{\hat{F}}(\theta_{(p,q)}) = \lim_{n\to\infty} \frac{1}{|(p, q)|n} \ln|\hat{F}(np, nq)|. \tag{3.9}$$

Note, that this formula is not very convenient for numerical applications, because of slow convergence. A more effective numerical approach to calculating $\delta_{\hat{F}}(\theta)$ is explained in the following chapter.

Reconstructing $\delta_{\hat{F}}(x_1, x_2)$

A priori the function $\delta_{\hat{F}}(\cdot)$ is known only for a discrete set of value $\theta_{(p,q)}$. However, assuming that $\delta_{\hat{F}}(\cdot)$ is regular enough we can actually calculate $\delta_{\hat{F}}(\theta)$ as a function of θ by taking limits. Obviously, to every direction θ corresponds a point $(x_1(\theta), x_2(\theta))$ on the boundary $\partial\mathtt{Log}\,(D_{\hat{F}})$. To establish the correspondence between $(x_1(\theta), x_2(\theta))$ and $\delta_{\hat{F}}(\cdot)$ we use some elementary notions of contact geometry, see [Arn95].

It is then natural to describe it using the manifold $S^1T^*\mathbb{R}^2$ of cooriented contact elements of the plane $\mathbb{R}^2$ with coordinates $(x_1, x_2, \theta) \in \mathbb{R}^2 \times S^1$. The contact structure is given by the condition $\alpha = 0$, where

$$\alpha = \cos\theta\, dx_1 + \sin\theta\, dx_2 \tag{3.10}$$

The standard (Darboux) form of the contact structure $\alpha = d\delta - \phi\, d\theta$ is obtained by introducing the Darboux coordinates

$$(\delta, \phi, \theta) = (\cos\theta\, x_1 + \sin\theta\, x_2, -\sin\theta\, x_1 + \cos\theta\, x_2, \theta). \tag{3.11}$$

The submanifold $(x_1(\theta), x_2(\theta), \theta)$ can be determined from the fibration $(\delta(\theta), \theta)$ using the condition $\alpha = 0$ and (3.11). We get

$$\begin{aligned} x_1(\theta) &= \cos\theta\, \delta(\theta) - \sin\theta\, \frac{d\delta}{d\theta}(\theta), \\ x_2(\theta) &= \sin\theta\, \delta(\theta) + \cos\theta\, \frac{d\delta}{d\theta}(\theta). \end{aligned} \tag{3.12}$$

Note that the correspondence between $\delta_{\hat{F}}(\cdot)$ and the curve $(x_1(\theta), x_2(\theta), \theta)$ is well-defined because of the convexity of the domain $\mathrm{Log}(D_{\hat{F}})$.

Series with positive coefficients

Assume now that the coefficients of the series are positive $\hat{F}(n_1, n_2)$. In this case we can work directly in the variables $(r_1, r_2) = (|\xi_1|, |\xi_2|)$. We obtain

$$\lim_{n\to\infty} \left(\frac{\hat{F}(np+1, nq)}{\hat{F}(np, nq)}, \frac{\hat{F}(np, nq+1)}{F(np, nq)} \right) = (r_1(\theta_{(p,q)}), r_2(\theta_{(p,q)})), \tag{3.13}$$

assuming that the limit exists. The points $(r_1(\theta_{(p,q)}), r_2(\theta_{(p,q)}))$ belong to the boundary of the domain of convergence $\partial\mathrm{Log}(D)$. Again taking limits we can obtain the whole curve $(r_1(\theta), r_2(\theta)) = (\mathrm{e}^{x_1(\theta)}, \mathrm{e}^{x_2(\theta)})$. This result is much easier to implement numerically than the two-dimensional generalization of the Cauchy–Hadamard theorem.

3.1.3 A simple example

Consider the polynomial

$$P(\xi_1, \xi_2) = 1 + \xi_1 + \xi_2. \tag{3.14}$$

The simplest function such that its singularities coincide with the set

$$\Sigma(P) = \{(\xi_1, \xi_2) : \, P(\xi_1, \xi_2) = 0\}, \tag{3.15}$$

is $F(\xi_1, \xi_2) = 1/P(\xi_1, \xi_2)$. Its Taylor expansion at $(0, 0)$ is given by

$$F(\xi_1, \xi_2) = \sum_{k_1=0}^{\infty} \sum_{k_2=0}^{\infty} \hat{F}(k_1, k_2) \xi_1^{k_1} \xi_2^{k_2} = \sum_{k_1=0}^{\infty} \sum_{k_2=0}^{\infty} (-1)^{k_1+k_2} \frac{(k_1+k_2)!}{k_1! k_2!} \xi_1^{k_1} \xi_2^{k_2}. \tag{3.16}$$

To determine the asymptotic behaviour of the Taylor coefficients for $|\mathbf{k}| \to \infty$ we use the Stirling approximation, obtaining

$$\hat{F}(k_1, k_2) = (-1)^{k_1+k_2} \frac{(k_1+k_2)!}{k_1! k_2!} \sim (-1)^{k_1+k_2} \frac{1}{\sqrt{2\pi}} \sqrt{\frac{k_1+k_2}{k_1 k_2}} \frac{(k_1+k_2)^{k_1+k_2}}{k_1^{k_1} k_2^{k_2}}. \tag{3.17}$$

Writing $k_1 = k\cos\theta$, $k_2 = k\sin\theta$ we get

$$\begin{aligned} &|\hat{F}(k_1, k_2)| \sim \\ &\frac{1}{\sqrt{k}} \exp\left\{ - \left[\cos\theta \log\left(\frac{\cos\theta}{\cos\theta + \sin\theta} \right) + \sin\theta \log\left(\frac{\sin\theta}{\cos\theta + \sin\theta} \right) \right] k \right\}, \end{aligned} \tag{3.18}$$

up to a numerical prefactor. Therefore, we have an explicit expression for $\delta_{\hat{F}}(\theta)$ which is equal to

$$\delta_{\hat{F}}(\theta) = \cos\theta \log\left(\frac{\cos\theta}{\cos\theta + \sin\theta} \right) + \sin\theta \log\left(\frac{\sin\theta}{\cos\theta + \sin\theta} \right). \tag{3.19}$$

Alternatively, using (3.14) we see that the boundary of $\mathrm{Log}(D_{\hat{F}})$ is given explicitly by the function

$$x_2(x_1) = \log\left(1 - e^{x_1}\right), \tag{3.20}$$

where $-\infty < x_1 < 0$. Now the direction of the normal to the contour at the point $(x_1, x_2(x_1))$ (taken as direction outward of the considered component) is determined by the equation

$$\frac{dx_2(x_1)}{dx_1} = -\frac{1}{\tan\theta}, \tag{3.21}$$

which in our case gives

$$x_1 = \log\left(\frac{1}{1+\tan\theta}\right), \tag{3.22}$$

Thus, the parametrization of points on the curve in terms of θ is given by

$$(x_1(\theta), x_2(\theta)) = \left(\log\left[\frac{\cos\theta}{\cos\theta+\sin\theta}\right], \log\left[\frac{\sin\theta}{\cos\theta+\sin\theta}\right]\right), \tag{3.23}$$

from which and from (3.11) we immmediately obtain the support function (3.19).

3.1.4 Domains of convergence of Laurent series

In more general cases we will deal with Laurent series

$$F(\xi_1, \xi_2) = \sum_{n_1=-\infty}^{+\infty} \sum_{n_2=-\infty}^{+\infty} \hat{F}(n_1, n_2)\, \xi_1^{n_1} \xi_2^{n_2}. \tag{3.24}$$

To describe the domain of convergence of such series we need the following definition

Definition 3.1.6 *A Reinhardt domain D with center at a point $(\xi_1^*, \xi_2^*) \in \mathbb{C}^2$ is said to be relatively complete if it does not intersect the plane $\{\xi_1 = \xi_1^*\}$ ($\{\xi_2 = \xi_2^*\}$, respectively), or, along with each point (ξ_1', ξ_2') it also contains all points (ξ_1, ξ_2'), where $|\xi_1 - \xi_1^*| \le |\xi_1' - \xi_1^*|$ ((ξ_1, ξ_2'), where $|\xi_1 - \xi_1^*| \le |\xi_1' - \xi_1^*|$, respectively).*

Thus, domains of convergence of Laurent series are characterized as relatively complete Reinhardt domains. Just as for the domains of convergence of Taylor series it can be shown that the domain of convergence of a Laurent series is logarithmically convex.

3.2 Amoebae, coamoebae and contours

Unfortunately, the methods explained in the previous section work only in few cases. Indeed, in the generic situations the limits such as (3.9) or (3.13) do not exist. Furthermore, we are above all interested in the geometry of the set of singular points, that is, we need much more information than just the knowledge of the domain of convergence.

For simplicity we start by analyzing the asymptotic behavior of the Taylor coefficients of rational functions such as $F(\xi_1, \xi_2) = P(\xi_1, \xi_2)/Q(\xi_1, \xi_2)$, where $P(\xi_1, \xi_2)$ and $Q(\xi_1, \xi_2)$ are polynomials in ξ_1, ξ_2. Obviously, the singularities of $F(\xi_1, \xi_2)$ coincide with the zero set of the polynomial $Q(\xi_1, \xi_2)$ which we denote as

$$\Sigma(Q) = \{(\xi_1, \xi_2) \in \mathbb{C}^2 : \; Q(\xi_1, \xi_2) = 0\}. \tag{3.25}$$

Therefore in this section we consider the properties of $\Sigma(Q)$ and its several geometrical representations.

3.2.1 Amoebae

The following notion is closely related to what has been introduced in Section 3.1.

Definition 3.2.1 *The amoeba $\mathcal{A}_Q$ of the polynomial Q is the image* $\mathtt{Log}(\Sigma) \subset \mathbb{R}^2$ *of the zero set* $\Sigma_Q = \big\{(\xi_1, \xi_2) \in \mathbb{T}^2_{\mathbb{C}} : \ Q(\xi_1, \xi_2) = 0\big\}$.

The restriction $\mathtt{Log}\,|_\Sigma : \Sigma(Q) \longrightarrow \mathbb{R}^2$ is called *amoeba mapping*.

The rational function $F = 1/Q$ can be expanded in a Laurent series

$$\sum_{k_1 \in \mathbb{Z}} \sum_{k_2 \in \mathbb{Z}} \hat{F}(k_1, k_2) \xi_1^{k_1} \xi_2^{k_2}$$

where the coefficients are given by

$$\hat{F}(n_1, n_2) = \frac{1}{(2\pi \mathrm{i})^2} \int_{\mathtt{Log}^{-1}(x_1^*, x_2^*)} \frac{1}{Q(\xi_1, \xi_2)} \frac{d\xi_1 \wedge d\xi_2}{\xi_1^{k_1+1} \xi_2^{k_2+1}}. \tag{3.26}$$

Here (x_1^*, x_2^*) is a point in the amoeba complement of $\mathcal{A}_Q^C$ and $\mathtt{Log}^{-1}(x_1^*, x_2^*)$ is the corresponding oriented cycle in $\mathbb{T}^2_{\mathbb{C}} \backslash \Sigma_Q$ (The orientation is chosen to be such that $d\arg(\xi_1) \wedge d\arg(\xi_2) > 0$ on $\mathtt{Log}(x_1, x_2)$.). The following holds [GKZ94]

Theorem 3.2.2 *The connected components of the amoeba complement $\mathbb{R}^2 \backslash \mathcal{A}_Q$ are convex, and they are in bijective correspondence with the different Laurent expansions (centered at the origin) of the rational function $1/Q$.*

Obviously, the second part of this theorem also applies to rational functions of the type P/Q.

To establish a connection to the material presented in the previous section, we note that the boundary a component of the amoeba complement $\mathbb{R}^2 \backslash \mathcal{A}_Q$ coincides with the boundary of the domain of convergence of the corresponding Taylor series.

3.2.2 Coamoebae

The following notion which complements the notion of the amoeba has been introduced by A.K. Tsikh and M. Passare (2002) and later reinvented in [FHKV05] under the name of alga.

Definition 3.2.3 *The coamoeba $\mathcal{A}'_Q$ of the polynomial Q is the image* $\mathtt{Arg}(\Sigma) \subset \mathbb{T}^2_{\mathbb{R}}$ *of the zero set* $\Sigma_Q = \big\{(\xi_1, \xi_2) \in \mathbb{T}^2_{\mathbb{C}} : \ Q(\xi_1, \xi_2) = 0\big\}$. *Here* $\mathtt{Arg} : \ \mathbb{C}^2 \longrightarrow \mathbb{T}^2_{\mathbb{R}}$ *is the given by*

$$\mathtt{Arg}(\xi_1, \xi_2) = (\arg \xi_1, \ \arg x_2) = (y_1, y_2). \tag{3.27}$$

Note that the properties of the coamoebae are much less nice than those of the amoebae. In particlular, as has been pointed out by A. Tsikh, an amoeba is always a closed subset of $\mathbb{R}^2$ due to the compactness of the preimage $\mathtt{Log}^{-1}(x_1, x_2)$ for all $(x_1, x_2) \in \mathbb{R}^2$, whereas a coamoeba can have quite arbitrary topological properties.

3.2.3 Contours

Consider the set $\Sigma(Q)$ of zeros of Q and a $(\xi_1, \xi_2) \in \Sigma(Q)$. In the following we assume that all points of $\Sigma(Q)$ are nonsingular, that is $(\partial_1 Q, \partial_2 Q)|_{\Sigma(Q)} \neq 0$.

Choose a neighbourhood U of (ξ_1, ξ_2) and fix a branch of the logarithm function so that $\log(U \cap \Sigma(Q))$ defines a one-dimensional complex manifold in $\mathbb{C}^2$. The amoeba mapping is obtained by projecting it onto $\mathbb{R}^2$. The set of critical points $\mathtt{crit}_{\mathtt{Log}}(Q)$ of $\mathtt{Log}\,|_\Sigma$ plays an essential role in analyzing this mapping.

Definition 3.2.4 *The set of critical values of amoeba mapping* $\mathtt{Log}|_\Sigma$ *is called the contour* $\mathcal{C}(Q)$ *of the amoeba* $\mathcal{A}$.

Now consider the complex normal direction to the curve $\log(U \cap \Sigma(Q))$ given by the *logarithmic Gauss mapping* $\gamma : \Sigma(Q) \longrightarrow \mathbb{CP}^1$

$$\gamma(\xi_1, \xi_2) = (\xi_1 \, \partial_1 Q : \xi_2 \, \partial_2 Q). \tag{3.28}$$

The following holds [Mik00]

Theorem 3.2.5 *Let* $\Sigma(Q)$ *be nowhere singular. The critical points of the amoeba mapping are given by* $\gamma^{-1}(\mathbb{RP}^1)$.

Thus, the contour can be characterized as $\mathtt{Log}(\gamma^{-1}(\mathbb{RP}^1))$. It is important to note that the boundary $\partial\mathcal{A}_Q$ of the amoeba $\mathcal{A}_Q$ is a subset of the contour $\mathcal{C}_Q$, but some parts of the contour may well be in the interior of the amoeba. Thus, we can determine the boundary of an amoeba by calculating its contour.

It is also of interst for our following considerations to consider the image of the set of critical points under the Arg mapping, i.e. $\mathtt{Arg}\left(\gamma^{-1}(\mathbb{RP}^1)\right)$, which we propose to call the *cocontour* $\mathcal{C}'_Q$.

3.2.4 Examples

In this section we illustrate the algebro-geometric notions such as amoeba, contour etc. which have been introduced previously. After the particularly simple example of singularities of a polynomial in two complex variable, we describe space-time singularities of the one-dimensional Burgers equation for a simple initial condition.

"Dimer model"

Here we analyze the geometry of the set of zeros of the polynomial

$$P(\xi_1, \xi_2) = 1 + \xi_1 + \xi_2 + \frac{e^t}{\xi_1 \xi_2} \tag{3.29}$$

corresponding to the dimer model $\mathbb{C}^3/\mathbb{Z}_3$ in [FHKV05]. As can be easily checked, $\Sigma(P)$ is nowhere singular. Therefore, Theorem 3.2.5 can be applied. Here we study the case $e^t \neq 0$ (the case $e^t = 0$, that is $t = -\infty$ having been treated before). According to Equation (3.28) and Theorem 3.2.5 the set of the critical values of $\mathtt{Log}|_{\Sigma(P)}$ is determined by the solution of equations

$$P(\xi_1, \xi_2) = 0, \tag{3.30}$$

and

$$\xi_1 \frac{\partial}{\partial \xi_1} P - s \xi_2 \frac{\partial}{\partial \xi_2} P = 0, \tag{3.31}$$

where $s \in \mathbb{R}$ (see also [The02]). For P given by (3.29) the second equation becomes

$$\left[\frac{s-2}{1-2s} + \left(\frac{s-2}{1-2s}\right)^2\right] z_1^3 + \left[\frac{2s-3}{1-2s} + \frac{2(s-1)(s-2)}{(1-2s)^2}\right] z_1^2 + \left[\frac{s-1}{1-2s} + \left(\frac{s-1}{1-2s}\right)^2\right] z_1 + e^t = 0. \tag{3.32}$$

For simplicity we denote

$$f_1(s) = \frac{s-2}{1-2s} + \left(\frac{s-2}{1-2s}\right)^2, \tag{3.33}$$

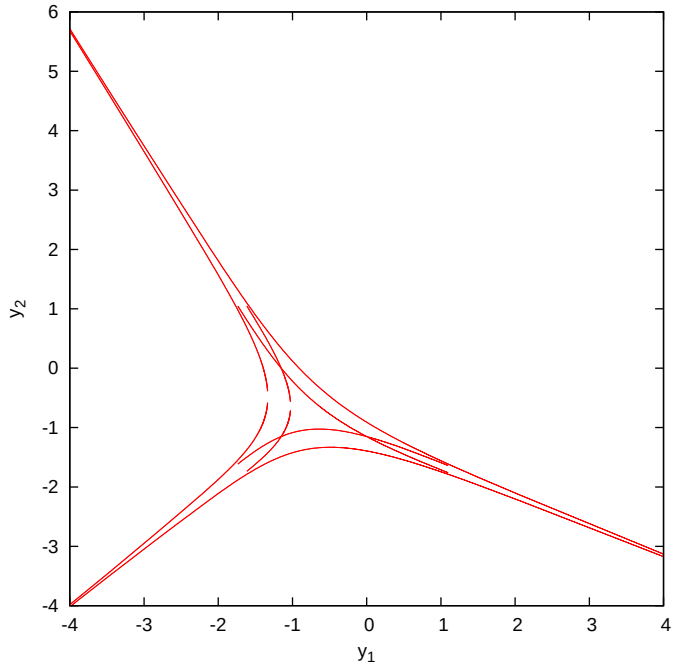

Figure 3.1: $P(z_1, z_2) = 1 + z_1 + z_2 + \frac{e^t}{z_1 z_2}$ for $e^t = 10$. Note that the exterior lines of the contour constitute the amoeba boundary.

$$f_2(s) = \frac{2s-3}{1-2s} + \frac{2(s-1)(s-2)}{(1-2s)^2}, \tag{3.34}$$

and

$$f_3(s) = \frac{s-1}{1-2s} + \left(\frac{s-1}{1-2s}\right)^2. \tag{3.35}$$

Furthermore we set $f_4 = e^t$. The solutions $z_1^{(1)}(s)$, $z_1^{(2)}(s)$ and $z_1^{(3)}(s)$ of the cubic equation are obtained using Cardan's formula. This gives for $z_2(s)$ six solutions via

$$z_2^{(i)\pm}(s) = -\frac{1+z_1^{(i)}}{2} \pm \sqrt{\frac{(1+z_1^{(i)})^2}{4} - \frac{f_4}{z_1^{(i)}}}. \tag{3.36}$$

The y-contour is represented on Fig. 3.1 for $f_4 = e^t = 10$. Note that it also defines the boundary of the amoeba of $P(z_1, z_2)$. On Fig. 3.2 are represented the parts of the contour and of the cocontour corresponding to the boundary of the amoeba of $P(z_1, z_2)$. The parts of the contour $\mathcal{C}_P$ which lie in the interior of the amoeba correspond to degenerate parts of the cocontour. These degenerate parts are just points $(x_1, x_2) = (0, \pi)$, $(-\pi, 0)$, $(-\pi, \pi)$. The coamoeba $\mathcal{A}'_P$ of $P(\xi_1, \xi_2)$ is represented on Fig. 3.3.

Space-time singularities of the one-dimensional Burgers equation

We consider solutions of the Burgers equation

$$\partial_t u + u\,\partial_z u = 0, \tag{3.37}$$

on the complexified torus $\mathbb{T}_{\mathbb{C}} = \mathbb{T}_{\mathbb{R}} + \mathrm{i}\,\mathbb{R}$, $z = x + \mathrm{i}\,y$, $x \in \mathbb{T}_{\mathbb{R}} = [0, 2\pi)$, $y \in \mathbb{R}$ with initial conditions which are triginometric polynomials. Note that t is in general complex

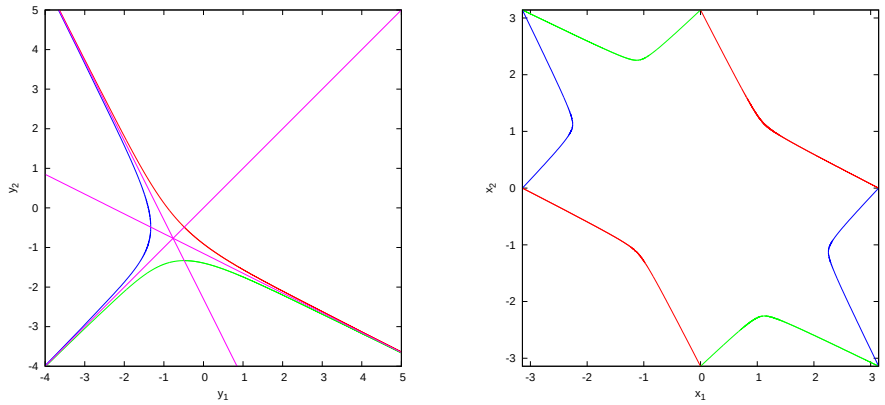

Figure 3.2: A part of the contour of the polynomial $P(z_1, z_2) = 1 + z_1 + z_2 + \frac{e^t}{z_1 z_2}$ (again $e^t = 10$) constituting the boundary of the amoeba. To each curve correspond two pieces of the cocontour.

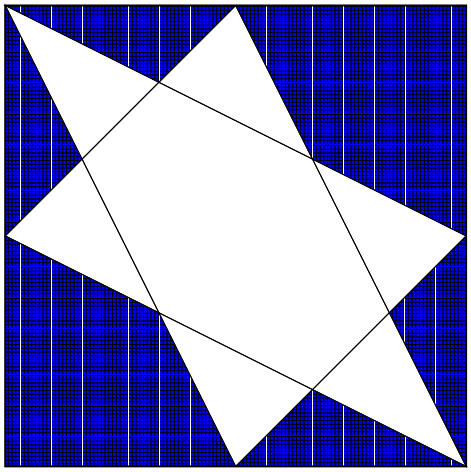

Figure 3.3: Coamoeba of the polynomial $P(\xi_1, \xi_2) = 1 + \xi_1 + \xi_2 + \frac{e^t}{\xi_1 \xi_2}$. Note that the coamoeba is independent of e^t.

valued. Since the velocity of particles is conserved along particle trajectories $u(z,t) = u_0(c)$, equation (3.37) can be solved by using Lagrangian coordinates $c = a + \mathrm{i}\, b$

$$z(c) = c + t u_0(c). \tag{3.38}$$

The Lagrangian singularities are located at zeros of the Jacobian of $z(c)$

$$1 + t\partial_c u_0(c) = 0. \tag{3.39}$$

Since u_0 is a Laurent polynomial in $\zeta = \mathrm{e}^{-\mathrm{i}\, c}$ and t, the Lagrangian singular set is a complex one-dimensional algebraic curve in $\mathbb{C}^2$. The geometry of the Lagrangian space-time singularities is naturally described in terms of amoebae, contours, etc.

Consider first the standard initial condition $u_0 = -(1/2)\sin z$. The singular set Σ is given by

$$\Sigma = \left\{ (\tau, \xi) \in (\mathbb{C}\backslash\{0\})^2 \,:\, \tau^{-1} - \frac{1}{4}\xi - \frac{1}{4}\xi^{-1} = 0 \right\}. \tag{3.40}$$

The contour is easily calculated and coincides with the boundary of the amoeba[1]

$$\ln|t| = \ln \frac{1}{|\frac{1}{4}e^{b} + \frac{1}{4}e^{-b}|}, \qquad \ln|t| = \ln \frac{1}{|\frac{1}{4}e^{b} - \frac{1}{4}e^{-b}|}. \tag{3.41}$$

Consider now the initial condition $u_0 = -(1/2)\sin z + \lambda \sin 2z$. The corresponding Lagrangian singularities are given by

$$\Sigma = \left\{ (\tau, \xi) \in (\mathbb{C}\backslash\{0\})^2 \,:\, \tau^{-1} - \frac{1}{4}\xi - \frac{1}{4}\xi^{-1} + \lambda\xi^2 + \lambda\xi^{-2} = 0 \right\}. \tag{3.42}$$

The additional relation determining the contour is

$$s\tau^{-1} = \frac{1}{4}\xi - \frac{1}{4}\xi^{-1} - 2\lambda_2\xi^2 + 2\lambda_2\xi^{-2}. \tag{3.43}$$

It is possible to calculate an explicit formula for the contour which involves solving a quartic algebraic equation. Since it is to cumbersome to write down the solution, we just give in Fig. 3.4 a graphical representation of the contour in coordinates $(b, \ln|t|)$ for the case $\lambda = (4 - \sqrt{14})/16$.

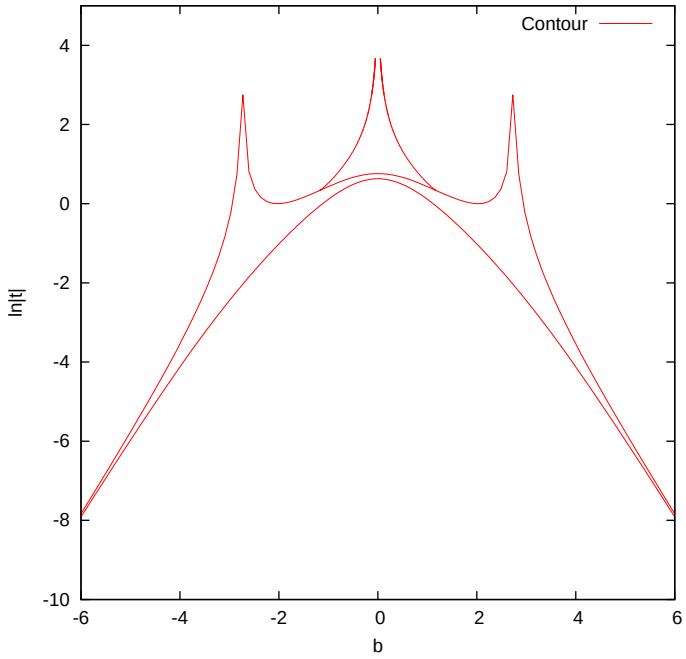

Figure 3.4: Contour of the solution of the Burgers equation with initial condition $u_0(z) = -1/2\sin z + (4 - \sqrt{14})/16 \sin 2z$. Note that a part of the contour is now located inside the amoeba.

3.3 Asympotics of Taylor coefficients along rational directions and geometry of the set of singularities

In this section we describe the relation between the geometric notions introduced in the previous section and the asymptotic behavior of the Taylor coefficients of a rational function when $|\boldsymbol{k}| \to \infty$. The results which are due to [STs84] and which we explain only briefly, can be used to develop a numerical procedure to analyze complex singularities in the cases in which the approach described in Section 3.1 does not apply, see Chapter 5.

[1] In this case the amoeba is called *solid*.

3.3.1 Diagonal of a power series and its singularities

Let us again consider the double Taylor series

$$F(\xi_1, \xi_2) = \sum_{n_1=0}^{\infty} \sum_{n_2=0}^{\infty} \hat{F}(n_1, n_2)\, \xi_1^{n_1} \xi_2^{n_2}.$$

As we have seen before, one of the possibilities to determine the domain of convergence of this series consists in determining the rate of exponential decay of the modulus of the two-dimensional Taylor coefficients along "rational directions", see Section 3.1. However, this simple result gives us only partial information about the singularities of the function $F(\xi_1, \xi_2)$ and does not hold in generic cases.

To improve it we observe that for a fixed rational direction (p, q) the asymptotic behavior of $\hat{F}(np, nq)$ is determined by the singularities of the following function of one complex variable

$$d_{(p,q)}(\zeta) = \sum_{n=0}^{\infty} \hat{F}(pn, qn)\zeta^n, \tag{3.44}$$

usually called (p, q)-*diagonal* of the series (3.3.1)[2]. The relation between the singularities of $F(\xi_1, \xi_2)$ and those of $d_{(p,q)}(\zeta)$ has been detemined completely in [STs84] for the case of rational functions of the type $P(\xi_1, \xi_2)/Q(\xi_1, \xi_2)$. Very roughly, it can be stated as follows: the set of singularities of $d_{(\cdot,\cdot)}(\zeta)$ coincides with the set of the critical points of the amoeba mapping corresponding to a suitable modification of polynomial $Q(\xi_1, \xi_2)$. That is, for a given rational direction (p, q) the singularities of $d_{(p,q)}(\zeta)$ are, with a few exceptions, given by solutions $(\xi_1(\theta_{(p,q)}), \xi_2(\theta_{(p,q)}))$ of

$$\begin{gathered} \check{Q}(\xi_1(\theta_{(p,q)}), \xi_2(\theta_{(p,q)})) = 0, \\ \sin\theta_{(p,q)} \tfrac{\partial}{\partial \xi_1} \check{Q}(\xi_1(\theta_{(p,q)}), \xi_2(\theta_{(p,q)})) - \cos\theta_{(p,q)} \tfrac{\partial}{\partial \xi_2} \check{Q}(\xi_1(\theta_{(p,q)}), \xi_2(\theta_{(p,q)})) = 0. \end{gathered} \tag{3.45}$$

Here $\check{Q}$ is the irreducible part of Q, defined as follows: if $Q = Q_1^{r_1} ... Q_\nu^{r_{nu}}$ is a factorization of Q into irreducible components, the irreducible part of Q is given by $\check{Q} = Q_1 ... Q_\nu$.

We now give a more precise formulation of this result. Fix a rational direction (p, q). Let σ_1, σ_2 be integral points of the Newton polytope Δ_Q lying on the supporting lines to Δ_Q with direction vectors (p, q). Define

$$\sigma_l(\xi_1, \xi_2) = \sum_{(k_1,k_2)\in\sigma_l} a(k_1, k_2)\xi_1^{k_1}\xi_2^{k_2}, \tag{3.46}$$

where $l = 1, 2$. After a division by a suitable monomial σ_l becomes a polynomial depending only on the variable $\zeta = \xi_1^p \xi_2^q$. Define the following sets:

$$\tilde{\Sigma}_{(p,q)} = \{\zeta \in \mathbb{C};\ \sigma_1(\zeta)\sigma_2(\zeta) = 0\} \tag{3.47}$$

and

$$\check{\Sigma}_{(p,q)} = \{\zeta = \xi_1^p \xi_2^q \in \mathbb{C} :\ \check{Q}(\xi_1, \xi_2) = 0,\ q\xi_1 \frac{\partial}{\partial \xi_1}\check{Q} - p\xi_2 \frac{\partial}{\partial \xi_2}\check{Q} = 0,\ \xi_1, \xi_2 \neq 0\}. \tag{3.48}$$

The following proposition has been proven in [STs84]:

[2] It has many applications in combinatorics [Ego77, Djo78], theory of difference equations [HK71] and even elementary particle physics [Par62, GH65].

Theorem 3.3.1 *If $F(\xi_1,\xi_2) = P(\xi_1,\xi_2)/Q(\xi_1,\xi_2)$ is a rational function, $Q(0,0) \neq 0$, then the (p,q)-diagonal $d_{(p,q)}(\zeta)$ of the corresponding Taylor series is holomorphically continued from the point $\zeta = 0$ along each arc not passing through points of the set $\Sigma_{(p,q)} = \tilde{\Sigma}_{(p,q)} \bigcup \check{\Sigma}_{(p,q)}$.*

The proof is based on the integral representation of the diagonal obtained in [HK71]

$$d_{(p,q)}(\zeta) = \frac{1}{(2\pi i)^2} \int_\Gamma \frac{F(\xi_1,\xi_2)\xi_1^{p-1}\xi_2^{q-1}}{\xi_1^p\xi_2^q - \zeta} d\xi_1 \wedge d\xi_2. \tag{3.49}$$

3.3.2 Asymptotics of the Taylor coefficients

Once the singularities of the (p,q)-diagonal $d_{(p,q)}(\zeta)$ are known, the asymptotic behavior of $\hat{F}(k_1,k_2)$ along the rational direction (p,q) can be determined by the usual techniques.

Let us first introduce some notation. We denote by $\zeta_\nu^\star(p,q)$, $\nu = 1,...,l$ the singularities of the (p,q)-diagonal $d_{(p,q)}(\zeta)$. They can be also represented as

$$\zeta_\nu^\star(p,q) = \exp\left[\tilde{x}_\nu^\star(p,q) + i\tilde{y}_\nu^\star(p,q))\right]. \tag{3.50}$$

The asymptotic behavior of the Taylor coefficients along the rational direction (p,q) is then given by

$$\hat{F}(np,nq) \sim \sum_{\nu=1}^{l} \exp\left[-n(\tilde{x}_\nu^\star(p,q) + i\tilde{y}_\nu^\star(p,q))\right]. \tag{3.51}$$

Note that since $\tilde{y}_\nu^\star(p,q)$ is 2π-periodic, it is determined up to an additive constant $2\pi m$, $m = 0, \pm1, \pm2, ...$

The leading order asymptotics of $\hat{F}(k_1,k_2)$ can thus be written as

$$\hat{F}(k_1,k_2) = \hat{F}(|\boldsymbol{k}|,\theta) \sim \sum_{\nu=1}^{l} \exp\left[-|\boldsymbol{k}|\delta_\nu(\theta) + i|\boldsymbol{k}|\phi_\nu(\theta,m)\right], \tag{3.52}$$

where

$$\delta_\nu(\theta) = \frac{1}{\sqrt{p^2+q^2}}\tilde{x}_\nu^\star(p,q), \qquad \phi_\nu(\theta;m) = -\frac{1}{\sqrt{p^2+q^2}}\left(\tilde{y}_\nu^\star(p,q) + 2\pi m\right). \tag{3.53}$$

We note that the dominant contribution to the asymptotics of $\hat{F}(k_1,k_2)$ comes from the singularities which are closest to the origin.

A very important observation is that given the functions $\delta_\nu(\theta)$ and $\phi_\nu(\theta;m)$ we can reconstruct from them the contour and the cocontour of the irreducible part $\check{Q}$ of the polynomial Q, basically by the same method as in Section 3.1.2.

Actually, it is possible to perform the asymptotic expansion of $\hat{F}(k_1,k_2)$ beyond the leading order. As has been shown in [Tsi93, Orl93, Orl94], it has the form[3]

$$\hat{F}(k_1,k_2) \sim \sum_{\nu=1}^{l} |\boldsymbol{k}|^{-\alpha_\nu} \exp\left[-|\boldsymbol{k}|\delta_\nu(\theta) + i|\boldsymbol{k}|\phi_\nu(\theta,m)\right]. \tag{3.54}$$

The values of the algebraic prefactor exponents depend on the polynomials $P(\xi_1,\xi_2)$ and $Q(x_1,\xi_2)$ (we remind the reader that $F(\xi_1,\xi_2) = P(\xi_1,\xi_2)/Q(\xi_1,\xi_2)$ is here a rational function). For details we refer to the original articles.

[3] Actually, in [Orl94] the author studied the case of asymptotics of Taylor coefficients for algebraic functions.

Chapter 4

BPH method and numerical analysis of Fourier/Taylor-coefficients

In this Chapter we show how the mathematical results relating the asymptotic behavior of Taylor coefficients and the geometry of the set of singularities can be applied numerically. We begin by explaining and testing an algorithm for numerical determination of asymptotic expansion of sequences of real numbers, introduced recently by van der Hoeven [Hoe06]. This asymptotic interpolation method applies only to monotonic sequences (descreasing or increasing) and, therefore, cannot be used in generic cases with oscillating data. To handle such data in [PF07] it is proposed to use a combination of the asymptotic interpolation method, the Borel transform and a theorem from the complex analysis due to Pólya. This Borel–Pólya–Hoeven method has been tested in [PF07] on the one-dimensional Burgers equation.

The two-dimensional extension of the BPH method consists in studying the singularities of the diagonal for a fixed rational direction. We illustrate this on the example of the "dimer model" introduced in the previous chapter. The Taylor coefficients in the corresponding expansion are calculated by the means of the linear difference equation with constant coefficients associated to the original polynomial.

4.1 Locating singularities of Fourier and Taylor series in one dimension

Before we turn to the discussion of the asymptotic interpolation method and the BPH method, we would like to point out one aspect of numerical reconstruction of asymptotic expansions which is discussed neither in [PF07] nor in [Hoe06] and which has been brought to our attention by M. Blank.

Namely, let a sequence $g(n)$ be given. Let us assume that it admits a unique transseries expansion. Then it is natural to ask, whether an algorithm for the reconstruction of transseries expansions, such as the asymptotic interpolation algorithm in [Hoe06] allows one to prove the uniqueness of the expansion. In so far as the asymptotic interpolation is concerned, it has been noticed in [Hoe06] that it cannot handle exponentially small terms. However, one may still ask wether "not too small", say logarithmic, corrections can be identified uniquely. We believe that such a rigorous identification is possible, but this question remains to be studied.

Journal of Statistical Physics, Vol. 127, No. 6, June 2007 (© 2007)
DOI: 10.1007/s10955-007-9307-z

A Borel Transform Method for Locating Singularities of Taylor and Fourier Series

W. Pauls[1,2,3] and U. Frisch[1,2]

Received September 11, 2006; accepted February 15, 2007
Published Online: March 23, 2007

Given a Taylor series with a finite radius of convergence, its Borel transform defines an entire function. A theorem of Pólya relates the large distance behavior of the Borel transform in different directions to singularities of the original function. With the help of the new asymptotic interpolation method of van der Hoeven, we show that from the knowledge of a large number of Taylor coefficients we can identify precisely the location of such singularities, as well as their type when they are isolated. There is no risk of getting artefacts with this method, which also gives us access to some of the singularities beyond the convergence disk. The method can also be applied to Fourier series of analytic periodic functions and is here tested on various instances constructed from solutions to the Burgers equation. Large precision on scaling exponents (up to twenty accurate digits) can be achieved.

KEY WORDS: complex singularities, series analyis, nonlinear dynamics

1. INTRODUCTION

In the late nineteenth Century, Pincherle[1] and then Borel[2,3] introduced what is now known as the Borel transformation: given a formal series in powers of the complex variable Z

$$f(Z) = \sum_{n=0}^{\infty} a_n Z^n, \tag{1}$$

[1] CNRS UMR 6202, Observatoire de la Côte d'Azur, BP 4229, 06304 Nice Cedex 4, France.
[2] Université de Nice–Sophia–Antipolis, Nice, France; e-mail: uriel@obs-nice.fr.
[3] Fakultät für Physik, Universität Bielefeld, Universitätsstraße 25, 33615 Bielefeld, Germany.

0022-4715/07/0600-1095/0 © 2007 Springer Science+Business Media, LLC

one introduces the Borel transformed series

$$F(\zeta) \equiv \sum_{n=0}^{\infty} \frac{a_n}{n!} \zeta^n. \tag{2}$$

Since, for Re $Z > 0$,

$$\int_0^{\infty} \zeta^n \mathrm{e}^{-Z\zeta}\, d\zeta = \frac{n!}{Z^{n+1}}, \tag{3}$$

it is useful to introduce the function

$$f^{\mathrm{BL}}(Z) \equiv \frac{1}{Z} f\left(\frac{1}{Z}\right) = \sum_{n=0}^{\infty} \frac{a_n}{Z^{n+1}}, \tag{4}$$

which is formally the Laplace transform of $F(\zeta)$ and which in this context is sometimes called the Borel–Laplace transform of F.

Borel's motivation was predominantly to give a meaning to divergent series such as $\sum n! Z^n$ and the Borel transformation has been extensively used to resum divergent series appearing in physics (see e.g. Refs. 4–6).

In 1929 Pólya[7] observed that the Borel transformation can also be used to obtain information about singularities of a Taylor series (in powers of $1/Z$) with a finite radius of convergence, in which case the function $F(\zeta)$ is entire. He proved a theorem relating the convex hull of singularities of $f^{\mathrm{BL}}(Z)$ (the smallest convex set outside of which the function is analytic) to a function called the indicatrix of $F(\zeta)$, roughly the rate of exponential growth at infinity of $F(\zeta)$ as a function of the direction (for precise definitions see Sec. 4).

Here we show that this theorem can be used in conjunction with high-accuracy numerical methods to obtain very precise information on singularities of Taylor and Fourier series. Singularities play an important role in fluid dynamics and condensed matter physics (see Refs. 8–10 and references therein). Using Pólya's theorem to devise a practical numerical method would not have been possible without recent progress in high-precision numerical algorithms and, foremost, the new technique for asymptotic interpolation of van der Hoeven[11] which can sometimes give remarkable precision (close to twenty digits) on scaling exponents.

The paper is organized as follows. In Sec. 2 we recall some known facts about Taylor and Fourier series and their singularities. In Sec. 3 we give a presentation of van der Hoeven's method from an applied mathematics point of view and show how it works in practice, using known results for the Burgers equation. In Sec. 4 we give an elementary introduction to Pólya's theorem. In Sec. 5 we present our new method, which we propose to call BPH (Borel–Pólya–Hoeven), for determining the convex hull of singularities and, for the case of isolated singularities on this hull, their positions and type. In Sec. 6 we test BPH using again the Burgers equation. In Sec. 7 we discuss open problems and make concluding remarks.

2. FROM TAYLOR AND FOURIER COEFFICIENTS TO SINGULARITIES

We first recall the close relation between Fourier and Taylor series for analytic functions. Let $u(x)$ be a 2π-periodic function which is analytic in some neighborhood of the real axis in which it can be extended to a function $u(z)$, where $z = x + \mathrm{i}\, y$. After subtraction of a suitable constant we can assume that $\int_0^{2\pi} u(x)dx = 0$. The Fourier-series representation of u reads

$$u(x) = \sum_{k=\pm 1,\, \pm 2, \ldots} \mathrm{e}^{\mathrm{i}\, kx} \hat{u}_k, \tag{5}$$

$$\hat{u}_k = \frac{1}{2\pi} \int_0^{2\pi} \mathrm{e}^{-\mathrm{i}\, kx} u(x)\, dx. \tag{6}$$

We denote by $u^+(x)$ (resp. $u^-(x)$) the partial sum of the Fourier series (5) with $k > 0$ (resp. $k < 0$), which is analytic in the upper (resp. lower) half plane $y \geq 0$ (resp. $y \leq 0$). Each of these two functions can be written as a Taylor series by an exponential change of variable:

$$u^+(z) = \sum_{k>0} \hat{u}_k Z^k, \qquad Z \equiv \mathrm{e}^{\mathrm{i}\, z}, \tag{7}$$

$$u^-(z) = \sum_{k>0} \hat{u}_{-k} \tilde{Z}^k, \qquad \tilde{Z} \equiv \mathrm{e}^{-\mathrm{i}\, z}. \tag{8}$$

Obtaining the singularities of an analytic periodic function from its Fourier coefficients is just basically the same problem as obtaining the singularities of an analytic function $f(Z) = \sum_{n=0}^{\infty} a_n Z^n$ from its Taylor coefficients a_n. Hadamard's formula gives us the radius of convergence of the Taylor series, namely the distance to the origin of the nearest singularity(ies). If we happen to know that this is an isolated singularity at $Z_\star$, we can relate the singular behavior near $Z_\star$ to the asymptotic behavior of the a_n by the Darboux theorem.[12–14] For this one assumes that, in a neighborhood of $Z_\star$, the function $f(Z)$ is given by

$$f(Z) = (1 - Z/Z_\star)^{-\nu}\, r(Z) + a(Z), \quad \nu \neq 0, -1, -2 \ldots, \tag{9}$$

$$r(Z) = \sum_{k=0}^{\infty} b_k \,(1 - Z/Z_\star)^k\,, \tag{10}$$

where the functions $r(Z)$ and $a(Z)$ are analytic in some disk centered at the origin with a radius exceeding $|Z_\star|$. It then follows that, for large n,

$$a_n \simeq \sum_{k=0}^{\infty} \frac{(-1)^k b_k Z_\star^{k-n} \Gamma(n + \nu - k)}{n! \Gamma(\nu - k)}. \tag{11}$$

The leading term is simply $a_n \simeq b_0 n^{\nu-1}/(Z_\star^n)\Gamma(\nu)$. Applied to the Fourier series (5), the leading-order Darboux formula can be recast as follows: a branch-point singularity with exponent $-\nu$ of $u(z)$ at a location $z_\star$ in the lower complex plane implies that for $k \to +\infty$ the Fourier coefficient $\hat{u}_k$ is asymptotically proportional to $k^{\nu-1}\mathrm{e}^{-\mathrm{i}kz_\star}$. This can be shown directly by applying standard steepest descent asymptotics to the integral (6).[18]

When the radius of convergence of a Taylor series is determined by a single singularity of the type assumed by Darboux, the knowledge of a sufficiently large number of Taylor coefficients with enough accuracy permits an accurate determination of the position and type of the singularity. This can be done by an iterative algorithm developed by Hunter and Guerrieri[14] or by the asymptotic interpolation method discussed in Sec. 3.

Sometimes there are two Darboux-type singularities on the convergence circle or, equivalently, the periodic function $u^+(z)$ has two singularities with the same imaginary part. The interference of the two singularities produces then a sinusoidal modulation of the Taylor coefficients. This can still be handled by an iterative algorithm,[14] but not directly by the asymptotic interpolation method, for reasons explained in Sec. 3.2. The BPH method of Sec. 5 can handle not only the case of two or more isolated singularities on the convergence circle but also "hidden" singularities located beyond this circle (or within this circle if the series is in inverse powers of Z), whose contributions to the Taylor coefficients are exponentially smaller than any term in (11). From an asymptotic point of view these contribution are "beyond all orders."

3. THE ASYMPTOTIC INTERPOLATION METHOD

Suppose that we have a function $G(r)$ of a scalar positive variable r for which we suspect that it has, for large r, an asymptotic expansion with a leading term $Cr^{-\alpha}\mathrm{e}^{-\delta r}$, as in the Darboux theorem (11), but that we only know its values numerically with high accuracy (tens to hundreds of known digits) on a regular grid $r_0,\ 2r_0, \ldots, Nr_0$ with a large number N of points (from fifty to thousands, depending on the problem). We set

$$G_n \equiv G(nr_0), \quad n = 1, 2, \ldots, N. \tag{12}$$

Can we determine parameters such as C, α and δ with high accuracy? One way is of course just to ignore the subleading corrections and to try a least square fit of the data to the functional form $Cr^{-\alpha}\mathrm{e}^{-\delta r}$, after taking a logarithm. One then has the awkward problem of having to pick a fitting interval of values of n; the procedure usually gives poor accuracy and the determination of subleading corrections is almost impossible.

A better way, used for example in Refs. 15–17, is to notice that, if we take the second ratio, defined as

$$R_n \equiv \frac{G_n G_{n-2}}{G_{n-1}^2} = \left(1 - \frac{1}{(n-1)^2}\right)^{-\alpha}, \tag{13}$$

then both the constant C and the exponential drop out. Assuming then n to be sufficiently large that we can ignore subleading corrections, we obtain

$$\alpha = -\frac{\ln R_n}{\ln(1 - 1/(n-1)^2)}. \tag{14}$$

The other two parameters C and δ appearing in (40) are then easily determined. If the remainder, that is the discrepancy between the value of α predicted by (14), which we denote α_n, and its limit α_∞ for $n \to \infty$, tends to zero in a known functional way, e.g., exponentially or algebraically, then we can extrapolate the α_n's to infinite values of n using, e.g., one of Wynn's algorithms[19,20] (see Ref. 21 for a review of extrapolation methods). We shall come back briefly to such issues in Sec. 3.2. Without knowing something about the functional form of the subleading corrections which control the remainder, extrapolation may not work very well because the choice of the appropriate algorithm depends on the functional form of the remainder.

Recently, van der Hoeven introduced the *asymptotic interpolation* method[11] which allows in principle the determination of the asymptotic expansion of G_n beyond leading-order terms. When the function G_n is known with very high precision and up to sufficiently large values of n, parameters such as the scaling exponent α can sometimes be determined with extreme accuracy, as we shall see in Sec. 3.1. An important feature of the asymptotic interpolation method is that it uses the determination of subleading terms to improve the accuracy on leading-order terms.

Here we shall just give a short elementary introduction to the asymptotic interpolation method for the case when the data G_n are real numbers. There are several variants of the asymptotic interpolation method; ours differs occasionally from that of Ref. 11. The basic idea of the asymptotic interpolation method is to perform simple "down" transformations on the data G_n which successively strip off leading and subleading terms. After a number of such down steps which depends on the quality of the data, the transformed data become sufficiently simple to allow a straightforward interpolation step. The list of down transformations which are needed is given hereafter.

I Inverse: $G_n \longrightarrow \frac{1}{G_n}$
R Ratio: $G_n \longrightarrow \frac{G_n}{G_{n-1}}$
SR Second ratio: $G_n \longrightarrow \frac{G_n G_{n-2}}{G_{n-1}^2}$
D Difference: $G_n \longrightarrow G_n - G_{n-1}$

At each stage, tests are applied to decide which of the four transformations should be applied in order to favor the stripping process as much as possible. If $|G_n| < 1$ for large n, apply **I**; otherwise proceed. If $|G_n|$ grows "slowly" at large n (we found that a useful operational definition is to see if the growth can be identified as algebraic with a rather well defined exponent), apply **D**; otherwise ("fast" growth), apply **R**. In addition, if $|G_n|$ grows or decreases exponentially at large n, we found that it saves time to apply **SR**; also, if $|G_n|$ is a slowly decreasing function, it is more convenient to apply $-\mathbf{D}$. Note that the differences or ratios involved in **R**, **SR** and **D** are backward; this conveniently keeps the maximum index N fixed.

When the procedure is iterated, after a while, an "interpolation stage" is reached where the data can be asymptotically interpolated in a simple fashion, typically by a constant plus a small remainder tending to zero at large n. Basically this means that we have successfully stripped off a certain number of terms in the asymptotic expansion. For the kind of data which we are considering here, the most useful interpolation stages usually arise at the sixth and thirteenth stages (counting the original data as stage zero).

There are two effects which limit the number of stages which can be applied to a given set of data. First, whenever a ratio or a difference are taken, the precision of the data (i.e., the relative rounding error) deteriorates; as the number of transformations applied increases, rounding errors make the data increasingly noisy, beginning usually with the highest values of n. Second, the interpolation stages require sufficiently large values of N, since the constant asymptotic behavior at large n may be preceded by non-trivial transients. For a given resolution N and a given precision, the procedure must be stopped at the latest interpolation stage not significantly affected by the two effects just mentioned. In practice we should have a significant range of values of n over which the data are almost constant and not affected by rounding noise (if the rounding noise is very low this range may extend all the way to N). When the down process is stopped the data are interpolated and the process is reversed, by applying "up" transformations which are the inverses of the down transformation in the reverse order. The inverses of the **D**, **R** and **SR** transformations involve one or two unknown additive or multiplicative constants which are determined using the highest known values of the G_n and of their down transforms.

When the process is completed, the data are asymptotically expressed as a truncated transseries. Roughly, a transseries is a formal asymptotic series involving integer or fractional powers, logarithms, exponentials and combinations thereof.[26–28]

A worked example will now give the reader a more concrete feeling.

3.1. Testing the Asymptotic Interpolation Method on the Burgers Equation with a Single-Mode Initial Condition

Here and in Sec. 6 we shall perform tests using the one-dimensional inviscid Burgers equation

$$\partial_t u(t,x) + u(t,x)\partial_x u(t,x) = 0, \tag{15}$$

with a 2π-periodic real initial condition $u_0(x)$ having a finite number of Fourier harmonics. We begin by recalling some well-known facts about the solution and the singularities of the inviscid Burgers equation. Equation (15) has an implicit solution in Lagrangian coordinates

$$u(t,x) = u_0(a); \quad x = a + tu_0(a). \tag{16}$$

Up to the time $t_\star$ of the appearance of the first shock, the Lagrangian map $a \mapsto x$ has a Jacobian

$$J(t,a) \equiv 1 + t\partial_a u_0(a) \tag{17}$$

which does not vanish in the real space domain and (16) defines a unique real solution. This solution has singularities in the complex domain (with the real part defined modulo 2π) at locations which are the images by the Lagrangian map of the zeros of the Jacobian J. Generically these are simple zeros. The singularities in Eulerian coordinates are then square-root branch points. The solution can also be written explicitly using the Fourier–Lagrangian representation,[29,30] which in a special case was actually discovered earlier by Platzman.[31] In the periodic case, the simplest representation, called the third Fourier–Lagrangian representation, valid for $k \neq 0$, is

$$u(t,x) = \sum_{k=-\infty}^{\infty} \mathrm{e}^{\mathrm{i}kx}\hat{u}_k(t), \tag{18}$$

$$\hat{u}_k(t) = -\frac{1}{2\mathrm{i}\pi kt}\int_0^{2\pi} \mathrm{e}^{-\mathrm{i}k(a+tu_0(a))}da. \tag{19}$$

In this section we take the "single-mode" initial condition

$$u_0(a) = -\frac{1}{2}\sin a, \tag{20}$$

for which the first real singularity is at $t_\star = 2$. Using (19) and the integral representation of the Bessel function J_n of integer order n (see, e.g., Ref. 32 p. 360), one finds[31]

$$\hat{u}_k(t) = \frac{\mathrm{i}}{kt}J_k(kt/2). \tag{21}$$

For convenience, we shall consider the solution at $t = 1$. This single-mode solution has only one pair of complex conjugate singularities on the imaginary axis at

$$z_\star^\pm = \pm \mathrm{i}\,\delta, \qquad \delta = \ln(2+\sqrt{3}) - \frac{\sqrt{3}}{2}. \tag{22}$$

Bessel functions of large order and arguments have an asymptotic expansion (in the sense of Poincaré), obtained through the method of steepest descent by Debye.[33] (The matter is also discussed in Chap. VIII of Ref. 34). Debye identified various asymptotic regimes which, in our notation, depend on whether t is less or larger than $t_\star$ and is or is not very close to $t_\star$; his classification is in one-to-one correspondence with that of the various regimes relating to preshocks, as discussed, for example, in Refs. 29–30. When $t = 1$, well before $t_\star$, the relevant Debye expansion for $k \to +\infty$ is:

$$\hat{u}_k(1) \simeq \frac{\mathrm{i}}{\sqrt{\pi\sqrt{3}}} k^{-\frac{3}{2}} \mathrm{e}^{-\delta k} \left(1 + \sum_{n=1}^{\infty} \frac{\gamma_n(2/\sqrt{3})}{k^n} \right), \tag{23}$$

where δ is given by (22),

$$\begin{aligned} \gamma_1(\xi) &= \frac{3\xi - 5\xi^3}{24}, \\ \gamma_2(\xi) &= \frac{81\xi^2 - 462\xi^4 + 385\xi^6}{1152}, \\ \gamma_3(\xi) &= \frac{30375\xi^3 - 369603\xi^5 + 765765\xi^7 - 425425\xi^9}{414720}, \end{aligned} \tag{24}$$

and the higher-order polynomials $\gamma_n(\xi)$ satisfy recurrence relations given, e.g., in Ref. 32. The leading term of this expansion follows also from the Darboux theorem (11).

Let us now show that the asymptotic interpolation method, as outlined in Sec. 3, when applied to the Fourier coefficients of the single-mode solution (21) can recover a suitably truncated version of the Debye expansion (23). We use all the Fourier coefficients with $k = 1, \ldots, N$, where $N = 1000$ and define our initial data set as $G_n \equiv \hat{u}_n(1)/\mathrm{i}$.

Each coefficient is calculated with an 80-digit precision (using Mathematica® and 120-digit working precision). The basic transformations and their inverses are implemented numerically in 80-digit precision, using the high-precision packages GMP and MPFR available from `http://www.swox.com/gmp/` and `http://www.mpfr.org/`.

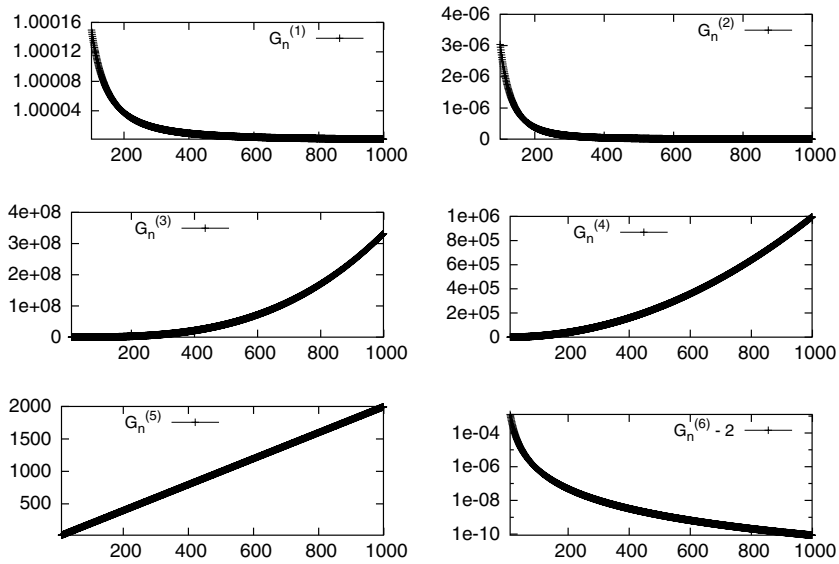

Fig. 1. Numerical output from asymptotic interpolation at stages 1–6. Stages 1–5 are represented in linear coordinates. For stage 6 we represent the difference between $G_6(n)$ and its asymptotic value 2 in lin-log coordinates.

With these data we are able to reach stage 13. The list of successively applied transformations, resulting from the tests given in Sec. 3, is

$$\textbf{SR, -D, I, D, D, D, D, I, D, D, D, D, D} \tag{25}$$

Figure 1 shows the first six stages. It is mostly intended to bring out overall features and to make clear which of the four transformations is to be selected at the next stage

It is very easy to understand why the first six stages are as listed above. Indeed, let us suppose that, to leading order, $G_n = Cn^{-\alpha}\mathrm{e}^{-\delta n}$. We can work out analytically the various transforms and we list hereafter the result up to the sixth stage, displaying only the leading and when needed the first subleading term in the large-n expansion:

$$Cn^{-\alpha}\mathrm{e}^{-\delta n} \xrightarrow{\mathbf{SR}} 1 + \frac{\alpha}{n^2} \xrightarrow{\mathbf{-D}} \frac{2\alpha}{n^3} \xrightarrow{\mathbf{I}} \frac{n^3}{2\alpha} \xrightarrow{\mathbf{D}} \frac{3n^2}{2\alpha} \xrightarrow{\mathbf{D}} \frac{3n}{\alpha} \xrightarrow{\mathbf{D}} \frac{3}{\alpha} \tag{26}$$

It is seen that stages 1 and 6 are interpolation stages at which the data are asymptotically flat. Stage 6 is particularly important since the asymptotic value $3/\alpha$ gives the scaling exponent α. According to (23), for the Burgers single-mode solution, the asymptotic value should be 2.

Let us now show in some detail how the asymptotic interpolation technique works to give us the asymptotic expansion of G_n. We begin by limiting ourselves to a six-stage procedure. The successively transformed data will be denoted

$G^{(1)}, \ldots, G^{(6)}$. Following Ref. 11, we interpolate $G^{(6)}$ by $3/\alpha$. How cleanly this can be done is visible in the last of the graphs in Fig. 1, where we show the discrepancy between $G_n^{(6)}$ and its asymptotic value 2. This discrepancy falls to about 10^{-10} at the upper end of the range. Then we determine $G^{(5)}$ by inverting the relation $G^{(6)} = \mathbf{D}G.^{(5)}$ This involves an unknown additive constant which is determined from the last data point $G_N^{(5)}$. Then we continue inverting the **D** operators appearing at stages 4 and 5, each time using the last point to obtain the additive constant. In this way we obtain a cubic polynomial for $G.^{(3)}$ We then invert the operator **I** and obtain the inverse of the aforementioned cubic polynomial, which can be written $-2\alpha n^{-3}(1 + d_1/n + d_2/n^2 + d_3/n^3 + \cdots)$ with in principle well defined constants d_1, d_2, etc. Then we invert the operator **SR**; this can be done by taking a logarithm which will transform second ratios into second increments. At the end of the process we obtain the asymptotic expansion

$$G_n \simeq Cn^{-\alpha}\mathrm{e}^{-\delta n}\left[1 + \frac{\gamma_1}{n} + \frac{\gamma_2}{n^2} + \frac{\gamma_3}{n^3} + O\left(\frac{1}{n^4}\right)\right]. \tag{27}$$

It is actually simpler to start with (27) and to apply successively the first six transformations listed in (25) to identify the parameters. With the six-stage procedure we obtain $C, \alpha, \delta, \gamma_1, \gamma_2, \gamma_3$. Their values are given in Table 1.

It is seen that the coefficients C, α and δ appearing in the leading term have a precision of at least 10^{-10}. The precision of the coefficients γ_i for the subleading terms deteriorates with the order.

We now turn to the analysis using a 13-stage procedure. This allows a much more precise determination of the aforementionned coefficients and, in principle, the determination of six additional terms in the expansion (27). After stage 6, the

Table I. Solution to the Burgers equation with single-mode initial condition: Comparison of theoretical values with 6-stage and 13-stage asymptotic interpolation values for the first six coefficients in Debye's solution (23).

	α	δ	C
6 stages	1.49999999993	0.4509324931404	0.4286913791
13 stages	1.49999999999999995	0.450932493140378061868	0.4286913790524959
Theor. value	3/2	0.450932493140378061861	0.42869137905249585643
	γ_1	γ_2	γ_3
6 stages	−0.17641252	0.17295	−0.401
13 stages	−0.17641258225238	0.172968106990	−0.406446182
Theor. value	−0.176412582252385	0.1729681069958	−0.4064461802
	γ_4	γ_5	γ_6
13 stages	1.384160933	−6.192505762	34.5269751
Theor. value	1.3841609326	−6.1925057618568063655	34.526975286449930956

Note. For 13-stage asymptotic interpolation we also give some of the higher order coefficients.

next interpolation stage is stage 13. This is easily shown by observing that the discrepancy between $G_n^{(6)}$ and its asymptotic value $3/\alpha = 2$ is $O(1/n^4)$, because all the lower-order terms have been stripped off by the first six transformations. More specifically, we have

$$G_n^{(6)} = 2 + \frac{c_1}{n^4} + \frac{c_2}{n^5} + \frac{c_3}{n^6} + \frac{c_4}{n^7} + \frac{c_5}{n^8} + \frac{c_6}{n^9} + \ell_n, \tag{28}$$

$$\ell_n = O\left(\frac{1}{n^{10}}\right). \tag{29}$$

Stages 7–13 gives us the coefficients $c_1, \ldots, c_6$ and allow us to find the remainder r_n, as defined in (28). We found that r_n, determined by this 13-stage procedure, falls to about 5×10^{-17} at the end of the range. As shown in Table 1, the precision on the first six coefficients in the asymptotic expansion has improved very much and is now of a few 10^{-17} for the exponent α.

3.2. Further Remarks on Asymptotic Interpolation

The method of asymptotic interpolation is still in the development stage; improvements and new features are thus to be expected. Some are already suggested in the initial publication.[11] One rather straightforward extension is from real to complex data. For rapidly growing data, one can use logarithms instead of ratios. In Ref. 11 it is recommended to take ratios or logarithms as often as possible and to define "slow growth" as slower than, say, $n^{5/2}$. This helps in identifying the functional form of the transseries expansion. Once this is known, we found that the values of the coefficients can be generated more efficiently by using a rather broad definition of slow growth, namely well-identifiable polynomial behavior.

A very important issue is to determine how many stages are feasible with a given resolution N and a given precision. We have found that the successive interpolation stages, at which the data are asymptotically flat, have this flat regime preceded by longer and longer transients. To make this more concrete we have investigated how far it is necessary to go to be within five per cent of the asymptotic value for the Burgers single-mode problem. For stage 6 the asymptotic value is 2 and the data are within five per cent everywhere. For stage 13, the asymptotic value is about 0.33836513 and less than five per cent discrepancy holds for $n > 25$. The next interpolation stage has number 20. The asymptotic value is $2/7$ but less than five per discrepancy holds only beyond $n = 1620$. In Fig. 2 we have represented the data at stage 20. It is seen that the discrepancy is enormous until we reach well beyond $n = 1000$. Obviously, if N is not large enough the stripping of subleading terms performed by the successive stages must be stopped *however high the precision of the data may be*. A related issue is discussed at the end of Sec. 7 of Ref. 11.

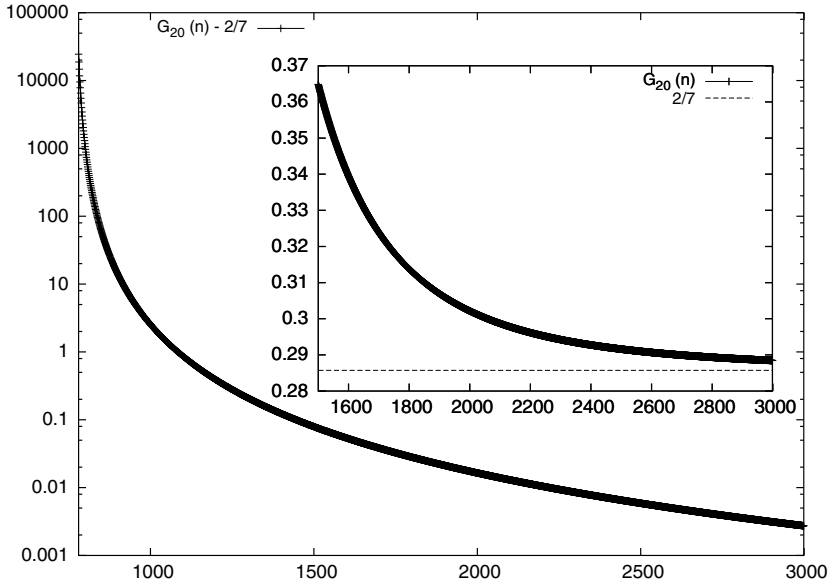

Fig. 2. Interpolation stage 20 has the asymptotic value $2/7$ as shown in the inset. The main figure shows the discrepancy $G_{20}(n) - 2/7$.

Since rounding errors increase with the stage number, a certain balance must be kept between resolution and precision. To investigate this quantitatively on the Burgers single-mode problem, we have artificially degraded our precision by adding random noise of various strengths. It appears that we need at least 16 significant digits at stage 6 and 27–35 significant digits at stage 13.

If we are only interested in obtaining an accurate determination of a few terms in the expansion (27), we may be able to retrieve them using asymptotic interpolation stopped at the sixth stage and continuing with a different strategy. Indeed we observe that, at the sixth stage, the data given by (29) have the form

$$G_n^{(6)} = s + r_n, \tag{30}$$

where the remainder r_n decays to zero as $n \to \infty$. This is a well studied situation in the theory of convergence acceleration by sequence transformations, whose goal is to replace the sequence (30) by a transformed sequence having the same limit s but a much faster decaying remainder (see, e.g., Refs. 21, 22). A simple and very popular acceleration method appropriate for (29) is Wynn's rho-algorithm,[19] although more sophisticated methods are known.[21] In our case it gives the correct value 2 with a 20-digits precision. This is even better than the 13-stage asymptotic interpolation. Note that the choice of a particular convergence acceleration method depends crucially on the functional form of the remainder. With asymptotic interpolation this form can be determined rather than having to be assumed. Here a caveat is in order: if the data are not sufficiently asymptotic the mixed

procedure just described will not work, for example because the remainder has not yet settled down to algebraic decrease. A situation of this type seems to be present in the work on short-time asymptotics discussed in Ref. 17: the rho-algorithm does not improve the quality of the scaling exponent controlling the divergence of the vorticity at the singular manifold and much higher resolutions are probably needed for that problem.

E.J. Weniger (private communication) has pointed out that asymptotic interpolation and sequence transformations have technical features in common. In asymptotic interpolation one tries to annihilate leading terms in the asymptotic expansion, whereas in sequence transformation one tries to shrink the remainder by annihilating its largest contributions, but the transformations used in both instance are often the same, for example, finite difference operators.

A powerful method of asymptotic series analysis, widely applied in statistical physics, is the method of differential approximants, which can be viewed as a generalization of the Dlog Padé method.[9] In particular it has been used to analyze self-avoiding walks (SAWs) and polygons (SAPs). We have applied the asymptotic interpolation method to data available at `http://www.ms.unimelb.edu.au/~iwan/polygons/Polygons_ser.html`. The goal was to see how well we can reproduce the asymptotics of the number of self-avoiding polygons with $2n$ steps on square and honeycomb lattices.[23–25] When analyzing the square lattice data for the largest available range, that is n up to 55, we found that asymptotic interpolation gives the value of the critical point correct to 9 decimal places, whereas differential approximants give about 3 additional digits. We observe that (i) the actual implementation with asymptotic interpolation is somewhat simpler and (ii) asymptotic interpolation is not limited to problems which can be well approximated by solutions of low-order linear differential equations.

The method of asymptotic interpolation is, in our opinion, very useful but is of course not the *panacea*. One disease it cannot directly cure is the presence of sinusoidal oscillations. For example if the analytic function $f(Z)$ has two complex conjugate singularities at $R\mathrm{e}^{\pm \mathrm{i}\phi_\star}$ on its circle of convergence, large-order Taylor coefficients will present a sinusoidal oscillation with a wavelength proportional to $\phi_\star$. After any number of stages, this oscillation is still present and the data cannot be interpolated by a constant. As we shall see now, a Borel transformation takes care of this problem and can also bring hidden singularities to the foreground.

4. PÓLYA'S THEOREM

Here we just want to give the reader a good feeling of what the theorem states and a heuristic derivation. We begin with examples discussed in Sec. 32 of Ref. 7.

Let $c = |c|e^{-i\gamma}$ be a complex number and consider the function

$$F(\zeta) = e^{c\,\zeta} = 1 + \frac{c\,\zeta}{1!} + \frac{c^2\zeta^2}{2!} + \cdots, \tag{31}$$

which corresponds to the choice $a_n = c^n$ in (2). The Borel–Laplace transform, given by (4), is

$$f^{\mathrm{BL}}(Z) = \frac{1}{Z} + \frac{c}{Z^2} + \frac{c^2}{Z^3} + \cdots = \frac{1}{Z-c}. \tag{32}$$

It has a pole at $Z = c$, whereas $F(\zeta)$ is an entire function (analytic in the whole complex domain). We set $\zeta = re^{i\phi}$ and let $r \to \infty$, holding the direction ϕ fixed; the modulus of $F(\zeta) = e^{|c|re^{\phi-\gamma}}$, in the direction ϕ, varies exponentially at the rate $h(\phi) = |c|\cos(\phi - \gamma)$, called the *indicatrix* of F. We define $k(\phi) \equiv \mathrm{Re}\,(c\,e^{-i\phi}) = |c|\cos(\phi + \gamma)$. This is the (signed) distance of the origin to the line normal to the direction ϕ passing through the pole c and is called the *supporting function* of the (single) singularity. We observe that

$$h(\phi) = k(-\phi). \tag{33}$$

This relation is the simplest instance of Pólya's theorem.

Next, following again Pólya's Sec. 32, we want to have n distinct poles at the complex locations $c_1,\ c_2,\ \ldots,\ c_p$. For this we take complex linear combinations with non-vanishing coefficients $C_1,\ C_2,\ \ldots,\ C_p$:

$$F(\zeta) = C_1 e^{c_1\zeta} + C_2 e^{c_2\zeta} + \cdots + C_p e^{c_p\zeta}. \tag{34}$$

The Borel–Laplace transform is

$$f^{\mathrm{BL}}(Z) = \frac{C_1}{Z-c_1} + \frac{C_2}{Z-c_2} + \cdots + \frac{C_p}{Z-c_p}. \tag{35}$$

For any $\phi \in [0, 2\pi]$, we define now the indicatrix and the support function, a little more formally, as

$$h(\phi) \equiv \limsup_{r\to\infty} r^{-1} \ln |F(re^{i\phi})|, \tag{36}$$

(in the present example, the lim sup is just an ordinary limit) and

$$k(\phi) \equiv \sup_{z\in K}(X\cos\phi + Y\sin\phi) = \sup_{Z\in K}\{\mathrm{Re}\,(Ze^{-i\phi})\}, \tag{37}$$

where $Z = X + iY$ and $K \equiv \{c_1,\ c_2,\ \ldots,\ c_p\}$ is the singular set. Since there is a finite number of singularities, the sup operation is just the same as the maximum. We define a *supporting line* of K as a line which has at least one point in common with K and such that all the points of K are in the same half space with respect to the line. The intersection of all these half spaces is the *convex*

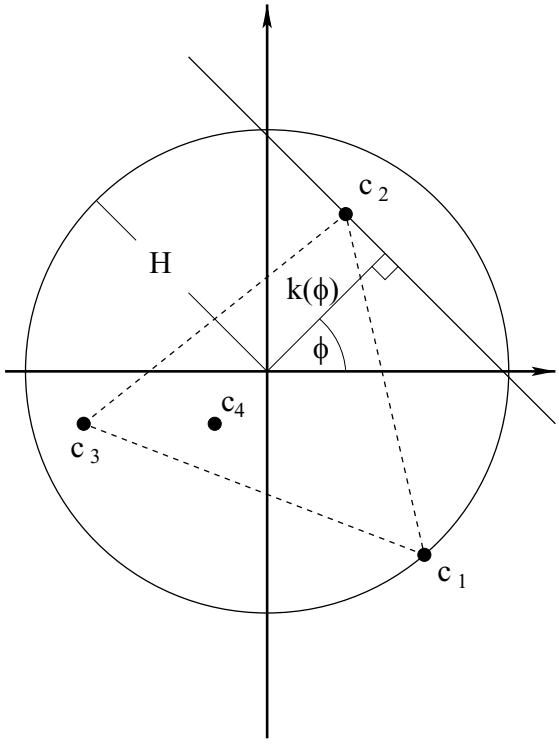

Fig. 3. Construction of the supporting function $k(\phi)$ of the set K of singularities of $f^{\mathrm{BL}}(Z)$. The singularity c_1 is on the convergence circle; the convex hull of K is defined by c_1, c_2 and c_3. The singularity c_4 is inside the convex hull.

hull of K. In the present case this is just the smallest convex polygon containing all the poles. It is readily seen that $k(\phi)$ is the (signed) distance of the origin to the supporting line normal to the direction ϕ (see Fig. 3.) The rate of growth of $F(\zeta)$ in the direction ϕ is obviously that of the fastest growing of the p exponentials in (34), which is precisely $k(-\phi)$, so that Pólya's relation (33) holds.

He proved a much more general theorem: *Let $f^{\mathrm{BL}}(Z)$ be an analytic function defined by the Taylor series (4) in powers of $1/Z$ which has a finite non-vanishing radius of convergence H, and let K be the smallest convex compact set containing its singularities, then (i) the Borel transformed series (2) defines an entire function of exponential type, and (ii) the indicatrix $h(\phi)$ of $F(\zeta)$, defined by (36), and the supporting function $k(\phi)$ of K, defined by (37), are related by $h(\phi) = k(-\phi)$ and $H = \sup_\phi h(\phi)$.*

(An entire function $F(\zeta)$ is said to be of exponential type if its modulus is bounded by $A\mathrm{e}^{a|\zeta|}$, where A and a are suitable positive constants.)

Pólya's proof (not given here) makes use of the fact that f^{BL} and F are Laplace transformed of each other, specifically,

$$f^{\mathrm{BL}}(Z) = \int_0^\infty F(\zeta)\mathrm{e}^{-Z\zeta}\, d\zeta, \tag{38}$$

$$F(\zeta) = \frac{1}{2\pi\mathrm{i}} \int_{a-\mathrm{i}\infty}^{a+\mathrm{i}\infty} f^{\mathrm{BL}}(Z)\mathrm{e}^{Z\zeta}\, dZ, \tag{39}$$

where a is any real number such that the singular set K is entirely contained in $\mathrm{Re}\, Z < a$.

Observe that no particular assumption is made regarding the type of the singularities which can be isolated (e.g. poles or branch points) or continuously distributed (natural boundary). Inside the circle of convergence $|Z| = H$, the series (4) is divergent. However if the whole circle is not a natural boundary, the function $f^{\mathrm{BL}}(Z)$ can be analytically continued to suitable Z's inside this circle and the pair of integrals (38) and (39)can be viewed as a way of resumming the divergent series (4).

In applications it frequently happens that all the "edge singularities," that is, those determining the border of the convex set K are isolated. This border is then piecewise linear, as in the case of n poles discussed above. The angular dependence of the supporting function is then given by $k(\phi) = |c_j| \cos(\phi + \gamma_j)$ in the angular interval $\phi_{j-1} < \phi < \phi_j$ for which the supporting line normal to ϕ touches K at $c_j = |c_j|\mathrm{e}^{-\mathrm{i}\gamma_j}$ (see Fig. 3). If $k(\phi)$ is known with high accuracy, then the positions of the edge singularities c_js can also be determined accurately.

Moreover we can then determine the type of an isolated singularity at c_j by studying the asymptotic behavior of $F(\zeta)$ along rays $\zeta = r\mathrm{e}^{\mathrm{i}\phi}$ with large r, in a suitable angular interval. For example, let us assume that, near c_j the function $f(z)$ has an algebraic singularity and is to leading order proportional to $(Z - c_j)^{\alpha-1}$, where the exponent α is real and not a positive integer. (If $\alpha - 1 > 0$, this behavior is assumed for a suitable first- or higher-order increment of f.) After shifting the contour of integration to follow the boundary of K near c_j (cf. Fig. 4), application of steepest descent[37] to (39) with $\zeta = r\mathrm{e}^{\mathrm{i}\phi}$ taken in the angular sector $\phi_{j-1} < -\phi < \phi_j$ and $r \to \infty$ yields

$$G(r) = \left|F(r\mathrm{e}^{\mathrm{i}\phi})\right| = Cr^{-\alpha}\mathrm{e}^{h(\phi)r}[1 + \varepsilon(r)], \tag{40}$$

$$h(\phi) = |c_j| \cos(\phi - \gamma_j). \tag{41}$$

Here C is a positive constant and $\varepsilon(r)$ tends to zero for $r \to \infty$ at a rate which depends on what is assumed for subleading corrections to the $(z - c_j)^{\alpha-1}$ singular behavior. If we are able to identify the algebraic prefactor to the exponential in (40), we can find the exponent α of the algebraic singularity.

Non-algebraic singularities can be handled similarly. For example, if near c_j the function $f(z)$ behaves as $\mathrm{e}^{1/(Z-c_j)}$, application of steepest descent shows that instead of the algebraic prefactor proportional to $r^{-\alpha}$ which appears in (40), we

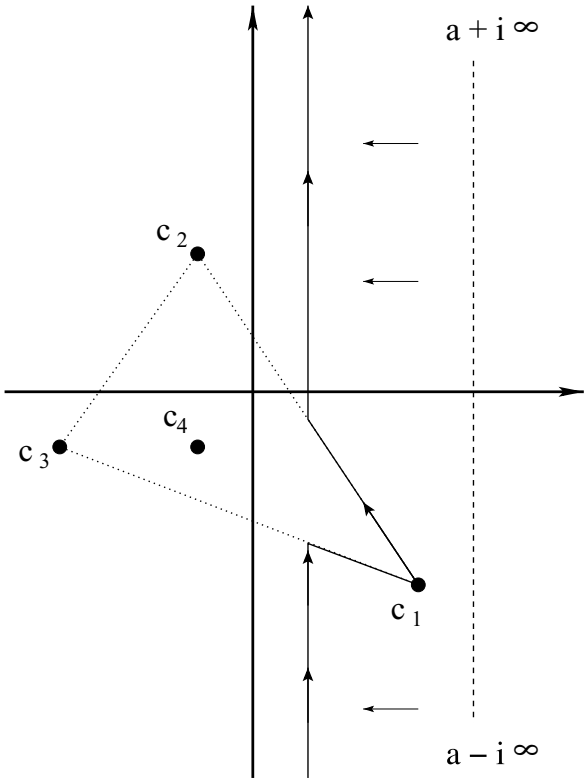

Fig. 4. Contour of integration for computing the inverse Laplace transform of $f^{\mathrm{BL}}(Z)$ (*dashed line*) and its deformation to obtain the asymptotic contribution from the singularity at c_1 (*continuous line with arrows*).

obtain an exponential prefactor proportional to $e^{\pm 2\cos(\phi/2)\sqrt{r}}$. Furthermore, if all the singularities on the convex hull of K are isolated, then (37) remains valid: the indicatrix is piecewise a cosine function.

How this is done in practice will be discussed in the next section.

5. THE BOREL–PÓLYA–HOEVEN METHOD

As we have seen in Sec. 3, the asymptotic interpolation method, applied to the Taylor coefficient of an analytic function with a finite radius of convergence determined by a single isolated singularity allows one to identify its location and type. This is not the case if there is more than one singularity on the convergence circle. Furthermore "hidden" singularities are not directly retrievable from the asymptotics of Taylor coefficients.

We can however take advantage of Pólya's theorem (Sec. 4) to replace the analysis of large-order Taylor coefficients of an analytic function by the analysis of the behavior of its Borel transform at large distances in the complex ζ plane

along various rays. This behavior can be found by asymptotic interpolation, from which we can then construct the convex hull K of the singularities and obtain their type when they are isolated. This is the BPH strategy which we now describe in a more detailed way.

We start from a truncated Taylor series in inverse powers of Z

$$f_{\mathrm{T}}^{\mathrm{BL}}(Z) = \sum_{n=0}^{N} \frac{a_n}{Z^{n+1}}, \tag{42}$$

with N terms, each of the coefficients being known with a precision ε. We construct the associated truncated Borel series

$$F_{\mathrm{T}}(\zeta) \equiv \sum_{n=0}^{N} \frac{a_n}{n!}\zeta^n. \tag{43}$$

We choose a certain number of discrete angular directions characterized by their angle ϕ. Along each ray $\zeta = r\mathrm{e}^{\mathrm{i}\phi}$, we evaluate the modulus of the Borel series at M points spaced by a constant distance (mesh) r_0:

$$G_m \equiv |F_{\mathrm{T}}(mr_0\mathrm{e}^{\mathrm{i}\phi})|, \quad m = 1,\ 2,\ \ldots,\ M. \tag{44}$$

Then we apply the asymptotic interpolation method of Sec. 3 to identify a large-m leading-order behavior. For example, for algebraic singularities we have

$$G_m \simeq C(\phi)(mr_0)^{-\alpha(\phi)}\mathrm{e}^{h(\phi)mr_0}. \tag{45}$$

This gives us the constant $C(\phi)$, the prefactor exponent $-\alpha(\phi)$ and the indicatrix $h(\phi)$ for the discrete set of directions. Pólya's theorem then gives us the supporting function $k(\phi) = h(-\phi)$ of the set K of singularities of the Taylor series. As we have seen in Sec. 4, if the singularities on the convex hull of K are isolated and are located at $|c_j|\mathrm{e}^{-\mathrm{i}\gamma_j}$, then the supporting function is piecewise a cosine function, given by $|c_j|\cos(\phi + \gamma_j)$. The exponent α gives us the type of the singularity: a branch point (or a pole) of exponent $\alpha - 1$. Other types of singularities, for example of the exponential type discussed near the end of Sec. 5, are handled similarly after identification of the appropriate asymptotic behavior.

In practice, we have to choose the set of discrete directions, the mesh r_0 and the maximum number of points M on each ray. If we happen to know the number p of isolated singularities and, at least approximately, their positions we can pinpoint the latter by taking $2p$ suitable ϕ directions. This is however rarely the case. We recommend taking a fairly large set of directions (for example 500 uniformly spaced directions) in order to reduce the risk of missing one or several of the cosine functions. The natural choice for the mesh r_0 is H^{-1} where H is the radius of convergence of the Taylor series. An approximate value is $H_{\mathrm{approx}} = (1/n)\ln|a_n|$ for large n, which is roughly constant. For the determination of the largest distance $r_{\max} = Mr_0$ we limit ourselves to the case where the function $F(r\mathrm{e}^{\mathrm{i}\phi})$ grows at

large distances, that is $h(\phi) > 0$ (otherwise there are severe numerical problems). $r_{\max}$ is then determined by the condition that the last term $a_N \zeta^N / N!$ of the (truncated) Borel series (43) should introduce a relative error in the determination of $F(r e^{i\phi})$ which does not exceed the precision ε with which the Taylor coefficients are known. A rough estimate for $|a_N|$ is H^N and for $|F(r_{\max} e^{i\phi})$ is $e^{r_{\max} H}$. Using the Stirling formula, we find that, to leading order $M \simeq N$ (the dependence on ε appears only in subleading logarithmic corrections).

We mention that an improvement would be to replace a mere polynomial truncation of the Borel series by a suitable resummation/acceleration method for computing entire functions.[38] This could be crucial for determining negative indicatrix values, that is, when $F(\zeta)$ is exponentially decreasing at large ζ.

It is of interest to know how well we can separate two discrete singularities. By Pólya's theory, each singularity contributes an exponential term to the large-r behavior of the modulus of the Borel transform. If r becomes sufficiently large compared to the difference in the two e-folding rates, only one of the two singularities will be seen. By suitably changing the direction of the ray in the ζ-plane we can then focus separately on each singularity. The worst case for discrimination is when we have two singularities which are at the same distance of the origin. Assuming that this common distance is comparable to the radius of convergence H and denoting by Δ the distance of the two singularities, we find that the largest discrepancy in e-folding rate is roughly Δ^2/H. Denoting, as above, by M the maximum number of point on a ray, we find that good separation requires the separation parameter $M\Delta^2/H^2$ to be large. Since discrepancies are amplified exponentially, a separation parameter of 10 may suffice.

We shall not here discuss issues of algorithmic complexity, such as the reduction of the number of operations to evaluate the truncated Borel series. In applications the complexity of the numerical calculations needed to accurately determine the Taylor coefficients will usually exceed very much what is needed for the BPH analysis.

6. TESTING BPH ON THE BURGERS EQUATION WITH MULTIMODE INITIAL CONDITIONS

To test the BPH method we need a Taylor series having either a pair of singularities on the convergence circle or "hidden singularities." As in Sec. 3.1, this can be done using 2π-periodic solutions of the inviscid Burgers equation. The 2-mode initial condition

$$\begin{aligned} u_0(a) &= \lambda_1 \sin a + \lambda_2 \sin(2a), \\ \lambda_1 &= -1/2, \quad \lambda_2 = (1/16)(4 - \sqrt{(14)}) + \epsilon, \\ \epsilon &= 1/150, \end{aligned} \tag{46}$$

produces at $t = 1$ a solution $u(1, z)$ having, in Eulerian coordinates, singularities at

$$z_\star^\pm = \pm 0.1103542160016972443 \pm \mathrm{i}\ 0.737097018253664793. \tag{47}$$

Henceforth we shall concentrate on the singularities of $u(1, z)$ in the lower half plane, which are also the singularities of the function $u^+(1, z)$, the sum of Fourier harmonics with $k > 0$. Note that there are two singularities with the same imaginary part and opposite real parts (this is a consequence of the symmetry $a \mapsto -a$, $u_0 \mapsto -u_0$ of the initial condition and of the complex conjugate symmetry). When the Fourier series for $u^+(1, z)$ is transformed into a Taylor series in inverse powers of Z by setting $Z = \mathrm{e}^{-\mathrm{i}z}$, the z singularities get mapped onto two complex conjugate Z singularities

$$Z_\star^\pm = 0.4755903313336372343 \pm \mathrm{i}\ 0.0526974896343733942. \tag{48}$$

The 3-mode initial condition

$$u_0(x) = \lambda_1 \sin x + \lambda_2 \sin 2x + \lambda_3 \sin 3x \tag{49}$$

$$\lambda_1 = -\frac{1}{2}, \quad \lambda_2 = \frac{4 - \sqrt{14}}{16} + \frac{1}{50}, \quad \lambda_3 = -\frac{1}{100}, \tag{50}$$

produces at $t = 1$ a solution $u(1, z)$ having, in Eulerian coordinates, in the lower complex half plane singularities at

$$z_{1\star} = -\mathrm{i}\ 0.4608974136239120258 \tag{51}$$

$$z_{2\star}^\pm = \pm 0.8575677577466957833 - \mathrm{i}\ 1.1175132271503113898. \tag{52}$$

The $z_{1\star}$ singularity is on the imaginary axis and is the closest to the real domain. The other two are further away (hidden) and symmetrically located with respect to the imaginary axis. The corresponding Z singularities are

$$Z_{1\star} = 0.6307173770893952917, \tag{53}$$

$$Z_{2\star}^\pm = 0.2140094820693456182 \pm \mathrm{i}\ 0.2473645913888956747. \tag{54}$$

are shown in Fig. 5.

To apply the BPH method we generate the Fourier harmonics with $k = 1, \ldots, N = 1000$ using the third Fourier–Lagrangian representation (19). The

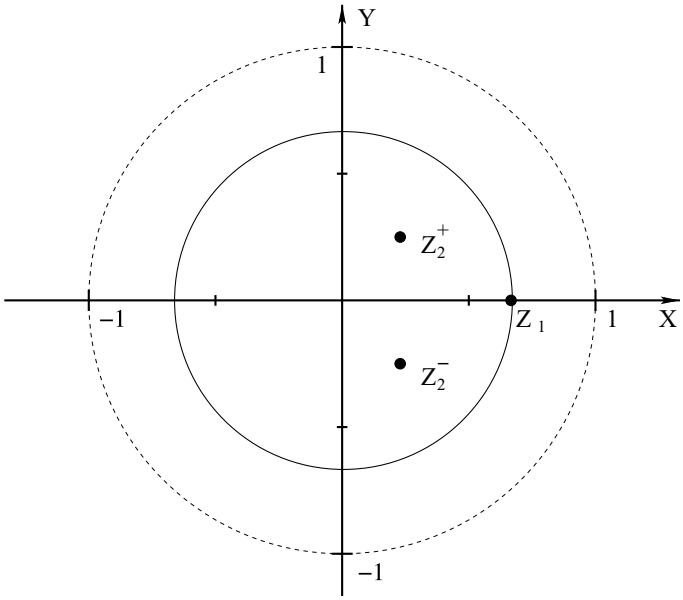

Fig. 5. Positions in Z-plane of the singularities for the 3-mode initial condition. Continuous line: circle of convergence; dashed line: image of the real domain by the map $z \mapsto \mathrm{e}^{-\mathrm{i}z}$.

Lagrangian integrals are again calculated with 80-digit precision and 120-digit working precision. The Borel transform is calculated for 20 values of ϕ between 0 and $\pi/2$ (a symmetry $\phi \to -\phi$ makes it unnecessary to take $\phi < 0$ and for $\phi > \pi/2$ the indicatrix is negative). For the mesh we take $r_0 = 1$. The total number of points on each ray is $M = 500$. Along each selected ray, application of six-stage asymptotic interpolation gives us C, α and h. We can check that the indicatrix is piecewise a cosine function as implied by (37). Least square fits allow us to identify the parameters of these cosine functions and thereby to find the locations of the singularities. We recover the known values with an accuracy of about 10^{-6}. We found that the accuracy on "hidden singularities" is comparable to that on directly visible ones. We also found that $N = 1000$ is not sufficiently asymptotic for a 13-stage analysis of the kind described in Sec. 3.1.

7. CONCLUDING REMARKS

One central theme of this paper is the use of a Borel transform, in conjunction with Pólya's theorem, to reveal singularities not directly accessible from the asymptotic behavior of the Taylor/Fourier coefficients. A very useful property of the Borel transform of a Taylor series (in inverse powers of Z) is that its large-distance behavior encodes information not only about those singularities of the Taylor series located on its convergence circle, but also about other singularities "hidden" inside this circle. Actually the Borel transform, followed by a

Borel–Laplace transformation is a way of performing analytic continuation. Recovering hidden singularities from a Taylor series has important applications in a number of fields; many of the known techniques have been reviewed by Guttmann.[9]

To the best of our knowledge Pólya's theorem has never been used as a numerical tool for identifying singularities. The theorem is of a very general nature and assumes nothing about the nature of the singularities; this has the great advantage that we do not have to distinguish between true and spurious singularities, as is the case, for example, when using Padé approximants and related methods. The principal drawbacks are that (i) not all hidden singularities are accessible, only those located on the convex hull of the singular set, (ii) pairs or clusters of singularities situated too close to each other may not be easily distinguishable, and (iii) enough terms in the series must be known to be able to actually obtain the asymptotic behavior of the Borel transform. When hundreds to thousands of Taylor coefficients are known, alternative mathematically well-founded techniques may become competitive, for example the old Weierstrass analytic continuation method; thanks to recent algorithmic discoveries it can be performed quite efficiently.[39,40]

The other theme of this paper is the asymptotic interpolation method of van der Hoeven which is here used both directly (when Darboux's theorem is applicable) and indirectly by means of Pólya's theorem. When a large number of Taylor/Fourier coefficients are known with sufficient accuracy, asymptotic interpolation can give truly remarkable results, providing us not only with very accurate leading terms but also with several subleading corrections. As we have seen in Sec. 3, there is usually a well-defined relation between the number of subleading correction terms and the number of stages of the procedure which can be achieved. The latter depends crucially on the number of known coefficients and on their precision. For example, if the data have only double precision, it is unlikely that more than six stages can be achieved. Asymptotic interpolation might than be viewed as an overkill compared to more standard techniques, but it is worth stressing that asymptotic interpolation is very easy to implement.

Which kinds of problems are most likely to fall within the prongs of full-strength Borel–Pólya–Hoeven-type analysis? This depends crucially on the computational complexity of the problem, that is the dependence of CPU requirement and storage on the number of coefficients N. As pointed out by Guttmann,[9] phase transition problems formulated on a lattice require usually enumerating diagrams and the number of these tends to grow exponentially with order, while fluid dynamics problems generally have only polynomial complexity. In connection with phase transitions our BPH method is likely to be less precise than alternative methods such as differential approximants, but it can usefully supplement them to ascertain that the singularities identified are not artefacts.

In fluid dynamics one outstanding problem is the issue of finite-time blow-up for the three-dimensional incompressible Euler flow with smooth initial data.[10,41] For initial data having simple trigonometric polynomial form, one can determine numerically a number of coefficients of the Taylor expansion in time of the enstrophy (integral of one-half the squared vorticity). This was done for the Taylor–Green flow by Brachet *et al.*[42] (yielding 40 non-vanishing coefficients calculated with quadruple working precision) and for the Kida–Pelz flow by Pelz and Gulak[43] (yielding 16 non-vanishing coefficients having at least 40-digit precision). Because the number of coefficients is rather small, there is no consensus on what the results imply for blow-up. Such calculations have a complexity $O(N^5)$ which can however be reduced to $O(N^4)$ (up to logs) using the method of relaxed multiplication.[39] It is likely that a state-of-the-art calculation for flows with simple trigonometric polynomial initial conditions can give up to several hundred non-vanishing Taylor coefficients of the enstrophy, with a working precision of several hundred digits. Another problem which can be tackled by series analysis is the analytic structure of the two-dimensional incompressible vortex sheet (Kelvin–Helmholtz instability). It is known that an initially analytic interface will develop a singularity in its shape after a finite time. Moore has made a prediction regarding this singularity[44] which has been studied by various numerical techniques.[16,45] Again there is no consensus on the type of this singularity.

It is of course of interest to extend to several dimensions the BPH method, here presented only in the one-dimensional case. We observe that there exist multi-dimensional generalizations of the Borel transform[46–48] and that the the asymptotic interpolation method can also in principle be extended to several dimensions.[11] In several dimensions, singularities are not point-like; they reside on extended objects such as analytic manifolds and can have a much more involved structure than in one dimension. It is possible to partially reconstruct such objects using a variant of BPH. Furthermore, we note that Pólya's theorem has been extended to several complex dimensions[48] (it is then referred to as the Ivanov–Stavskiĭ theorem). Information on singularities can then in principle be obtained numerically in a way analogous to what has been done in Sec. 5. Such issues will be discussed elsewhere.

ACKNOWLEDGMENTS

We are very much indebted to J. van der Hoeven for having introduced us to his asymptotic interpolation method and to E.J. Weniger for his detailed advice on extrapolation techniques. We have also benefited very much from discussions with J. Bec, M. Blank, H. Frisch, T. Matsumoto, D. Mitra, R. Pandit and A.K. Tsikh.

REFERENCES

1. S. Pincherle, Sulla risoluzione dell'equazione funzionale $\sum h_\nu \phi(x+\alpha_\nu) = f(x)$ a coefficienti costanti, *Memorie della R. Academia delle scienze dell'Istituto di Bologna Serie IV* **IX**:45–71 (1888). French translation: *Acta Mathematica*. **48**:279–304 (1926).
2. E. Borel, Mémoire sur les séries divergentes. *Ann. Sci. 'Ecole Normale Sup.* **16**:9–131 (1899). http://www.numdam.org/item?id=ASENS_1899_3_16__9_0
3. E. Borel, *Leçons sur les Séries Divergentes*, (Gauthier-Villars, reprinted by Éditions Jacques Gabay, Paris, 1928).
4. J. C. Le Guillou and J. Zinn-Justin (eds.), *Large-Order Behaviour of Perturbation Theory* (North-Holland, Amsterdam, 1990).
5. B. Shawyer and B. Watson, *Borel's Method of Summability*. (Oxford U.P., Oxford, 1994).
6. B. Yu. Sternin and V. E. Shatalov, *Borel–Laplace Transform and Asymptotic Theory* (CRC Press, Boca Raton, 1996).
7. G. Pólya, Untersuchungen über Lücken und Singularitäten von Potenzreihen. *Math. Z.* **29**:549–640 (1929).
8. M. D. Van Dyke, Computer-extended series. *Ann. Rev. Fluid Mech.* **16**:287–309 (1984).
9. A. J. Guttmann, Asymptotic Analysis of Power-Series Expansions. In *Phase Transitions*, C. Domb and J. Lebowitz, (eds.) Vol. 13, (pp. 1–234, 1989).
10. U. Frisch, T. Matsumoto and J. Bec, Singularities of the Euler equation? Not out of the blue! *J. Stat. Phys.* **113**:761–781 (2003).
11. J. van der Hoeven, Algorithms for asymptotic interpolation, preprint 2006–12 *Dep. Math. Univ. Paris-Sud, submitted to J. Symbolic Comput.* (2006); see also http://www.math.u-psud.fr/~vdhoeven/Publs/2006/interpolate.ps.gz
12. G. Darboux, Mémoire sur l'approximation des fonctions de très grands nombres. *J. de Mathématiques Pures et Appliquées* **4**:5–56 and 377–416 (1878).
13. P. Henrici, *Applied and Computational Complex Analysis*, Vol. 2. (John Wiley and Sons, 1977).
14. C. Hunter and B. Guerrieri, Deducing the properties of singularities of functions from their Taylor series coefficients. *SIAM J. Appl. Math.* **39**:248–263 (1980), erratum: **41**:203 (1981).
15. J. Zinn-Justin, Analysis of Ising model critical exponents from high temperature series expansions. *J. Physique* **40**:969–975 (1979).
16. M. J. Shelley, A study of singularity formation in vortex sheet motion by a spectrally accurate vortex method. *J. Fluid Mech.* **244**:493–526 (1992).
17. W. Pauls, T. Matsumoto, U. Frisch and J. Bec, Nature of complex singularities for the 2D Euler equation. *Physica D* **219**:40–59 (2006) (nlin.CD/0510059).
18. G. F. Carrier, M. Krook and C. E. Pearson, *Functions of a Complex Variable: Theory and Technique* (McGraw-Hill, New York, 1966).
19. P. Wynn, On a Procrustean technique for the numerical transformation of slowly convergent sequences and series. *Proc. Camb. Phil. Soc.* **52**:663–671 (1956).
20. P. Wynn, The rational approximation of functions which are formally defined by a power series expansion. *Mathemat. Comput.* **14**:147–186 (1960).
21. E. J. Weniger, Nonlinear sequence transformations for the acceleration of convergence and the summation of divergent series. *Comput. Phys. Rep.* **10**:189–371 (1989) (math.NA/0306302).
22. C. Brezinski and M. Redivo Zaglia, *Extrapolation Methods* (North-Holland, 1991).
23. I. Jensen and A. J. Guttmann, Self-avoiding polygons on the square lattice. *J. Phys. A: Math. Gen.* **32**:4867–4876 (1999).
24. I. Jensen, A parallel algorithm for enumeration of self-avoiding polygons on the square lattice. *J. Phys. A: Math. Gen.* **36**:5731–5745 (2003).
25. I. Jensen, Honeycomb lattice polygons and walks as a test of series analysis techniques. *J. Phys.: Conf. Ser.* **42**:163–178 (2006).

26. J. Ecalle, Introduction aux Fonctions Analysables et Preuve Constructive de la Conjecture de Dulac (Actualités mathématiques. Hermann, Paris, 1992).
27. J. van der Hoeven, Automatic Asymptotics, Thesis, Orsay (1997) http://www.math.u-psud.fr/~vdhoeven/Books/phd.ps.gz
28. J. van der Hoeven, Transseries and Real Differential Algebra, Lecture in Math., Springer, to appear.
29. J. D. Fournier et U. Frisch, L'équation de Burgers déterministe et statistique. *J. Méc. Th. Appl.* **2**:699–750 (1983).
30. U. Frisch and J. Bec, Burgulence. In *Les Houches 2000: New Trends in Turbulence*, M. Lesieur, A. Yaglom and F. David (eds.) (Springer EDP-Sciences, pp. 341–383, 2001). (nlin.CD/0012033).
31. G. W. Platzman, An exact integral of complete spectral equations for unsteady one-dimensional flow. *Tellus* **16**: 422–431 (1964).
32. M. Abramovitz and I. A. Stegun, *Handbook of Mathematical Functions* (Dover Publications, 1965).
33. P. Debye, Näherungsformeln für die Zylinderfunktionen für große Werte des Arguments und die unbeschränkt veränderliche Werte des Index. *Math. Ann.* **67**: 535–558 (1908).
34. G. N. Watson, *A Treatise on the Theory of Bessel Functions* (Cambridge University Press, 1922).
35. B. Ya. Levin, Lectures on Entire Functions (American Mathematical Society, Providence, 1996).
36. L. Bieberbach, Analytische Fortsetzung, Springer, Berlin, 1955. Russian translation: Analitich-eskoye Prodolzhenye, Nauka, Moscow, 1967.
37. F. W. J. Olver, *Asymptotics and Special Functions* (Academic Press, 1974).
38. J. Müller, Convergence acceleration of Taylor sections by convolution. *Constr. Appr.* **15**:523–536 (1999).
39. J. van der Hoeven, Relax, but don't be too lazy. *J. Symbolic Comput.* **34**:479–542 (2002).
40. J. van der Hoeven, On effective analytic continuation, preprint Dép. Math. Orsay, http://www.math.u-psud.fr/~vdhoeven/Publs/2006/riemann.ps.gz
41. A. J. Majda and A. L. Bertozzi, *Vorticity and Incompressible Flow*. (Cambridge University Press, Cambridge, 2000).
42. M. E. Brachet, D. I. Meiron, S. A. Orszag, B. G. Nickel, R. H. Morf and U. Frisch, Small-scale structure of the Taylor–Green vortex. *J. Fluid Mech.* **167**:411–452 (1983).
43. R. B. Pelz and Y. Gulak, Evidence for a real-time singularity in hydrodynamics from time series analysis. *Phys. Rev. Lett.* **79**:4998–5001 (1997).
44. D. W. Moore, The spontaneous appearance of a singularity in the shape of an evolving vortex sheet. *Proc. R. Soc. London A* **365**:105–119 (1979).
45. D. I. Meiron, G. R. Baker and S. A. Orszag, Analytic structrue of vortex sheet dynamics. Part 1. Kelvin–Helmholtz instability. *J. Fluid Mech.* **114**:283–298 (1982).
46. L. A. Aizenberg and V. M. Trutnev, A Borel summation method for n-tuple power series. *Sibirsk. Matem. Zh.* **12**(6):1895–1901 (1971).
47. V. M. Trutnev, The radial indicator in the theory of Borel summability with some applications. *Sibirsk. Matem. Zh.* **13**(3):659–664 (1972).
48. L. I. Ronkin, Introduction to the Theory of Entire Functions of Several Complex Variables. *Transl. Math. Monographs*, Vol. 44, AMS (1974).

4.2 Two-dimensional generalization of the BPH-method

A two-dimensional generalization of the BPH method, discussed in [PF07] is in principle straightforward. Let there be given a double series

$$F(\xi_1, \xi_2) = \sum_{n_1=0}^{\infty} \sum_{n_2=0}^{\infty} \hat{F}(n_1, n_2)\, \xi_1^{n_1} \xi_2^{n_2}. \tag{4.1}$$

As we have in Section 4, singularities of $F(\xi_1, \xi_2)$ can be analyzed by studying the singularities of its (p, q)-diagonal $d_{(p,q)}(\zeta)$ for various rational directions (p, q). The singularities of the (p, q)-diagonal can be studied by the one-dimensional BPH method. Thus, we can obtain numerically the functions $\delta_\nu(\theta)$ and $\phi_\nu(\theta, m)$ (we will refer to ϕ_ν as the *phase*) and reconstruct from them the contour and the cocontour. One essential difficulty is, however, the nonuniqueness of the phase $\phi_\nu(\theta, m)$.

Here we give a simple example. Suppose that $\phi(\theta, m)$ is given as

$$\phi(\theta, m) = \pi \pm \frac{2\pi m}{\sqrt{p^2 + q^2}}. \tag{4.2}$$

The resulting distribution of values is represented on Fig. 4.1. Chosing for example the

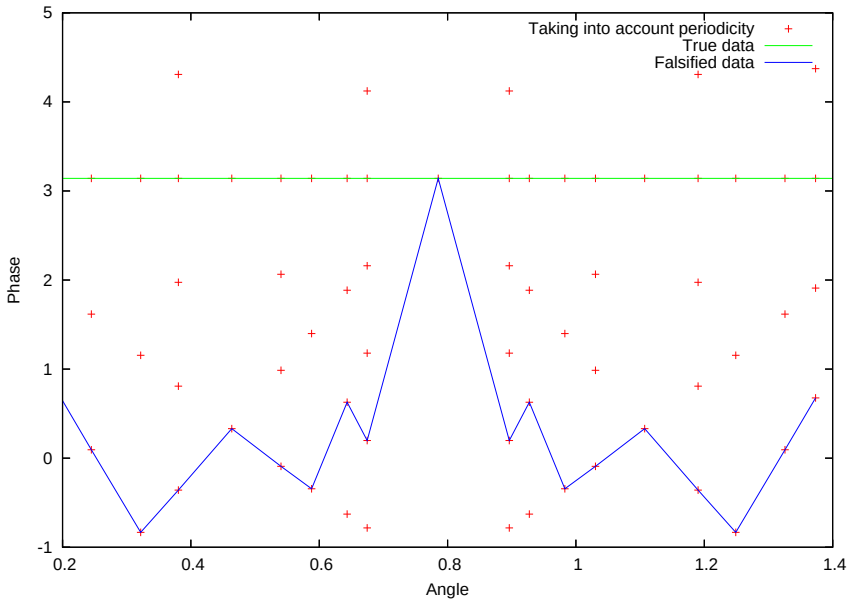

Figure 4.1: Equation (4.2), represented for various rational directions. The falsified data, represented by the blue line, are obtained by chosing the values of $\phi(\theta, m)$ which are closest to zero.

values of $\phi(\theta, m)$ which are closest to zero, we obtain a completely chaotic distribution of points which does not in any way resemble the original function $\phi(\theta) = \pi$. Actually, this "falsified" representation of $\phi(\theta)$ is what we observe in practice when using the two-dimensional BPH method numerically.

4.2.1 Testing the two-dimensional BPH method

To test the two-dimensional BPH method, we propose to analyze the singularities of the rational function $F(\xi_1, \xi_2) = 1/P(\xi_1, \xi_2)$. Here, $P(\xi_1, \xi_2)$ is the polynomial corresponding

to the first example ("dimer model") in Section 3.2.4

$$P(\xi_1, \xi_2) = 1 + \xi_1 + \xi_2 + \frac{e^t}{\xi_1 \xi_2}. \tag{4.3}$$

Numerically, the coefficients of the Taylor expansion are most conveniently calculated from a linear recursion relation (linear partial difference equation with constant coefficients) corresponding (see Section 4.2.2) to the polynomial (4.3)

$$\hat{F}(k_1+2, k_2+2) + \hat{F}(k_1+1, k_2+1)e^{-t} + \hat{F}(k_1+1, k_2)e^{-t} + \hat{F}(k_1, k_2+1)e^{-t} = 0, \tag{4.4}$$

initialized as $\hat{F}(k_1, k_2) = 0$ for $k_1 \leq 0$ or $k_2 \leq 0$, except for $\hat{F}(0, 0) = 1$.

To test the two-dimensional generalization of the BPH method I have calculated the solution of Equation (4.4) using high-precision arithmetics with resolution up to 1000×1000. Then, together with Takeshi Matsumoto, I have applied the 2D BPH method to determine the contour and the cocontour of the polynomial (4.3).

First, as shown on Figs. 4.2 and 4.3, we have extracted the phase $\phi(\theta)$ by demanding

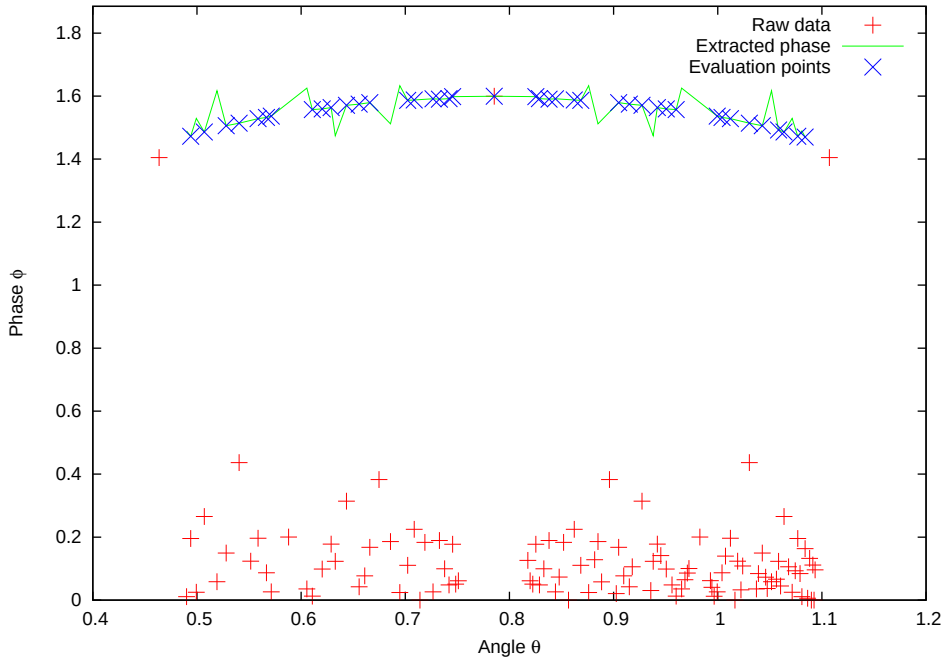

Figure 4.2: Data obtained from the numerical analysis of the Borel transform of the diagonal along various rational directions are represented by red crosses $+$. Data obtained by taking into account the periodicity are represented by the green line $-$. Data obtained by omitting the points with too large scattering are represented by blue crosses $\times$.

that it be continuous. It is seen that the scattering of the extracted data is quite large. This is due to the insufficient convergence of the Borel transform for the rarely populated directions (p, q). However, by omitting the points which are too far off, we are nevertheless able to reconstruct the cocontour, as is shown on Fig. 4.4.

4.2.2 Asymptotics of solutions of linear partial difference equations with constant coefficients

Given that the main numerical method of calculating solutions of various equation in this thesis are recursion relations (partial difference equations), we remark that asymptotics of

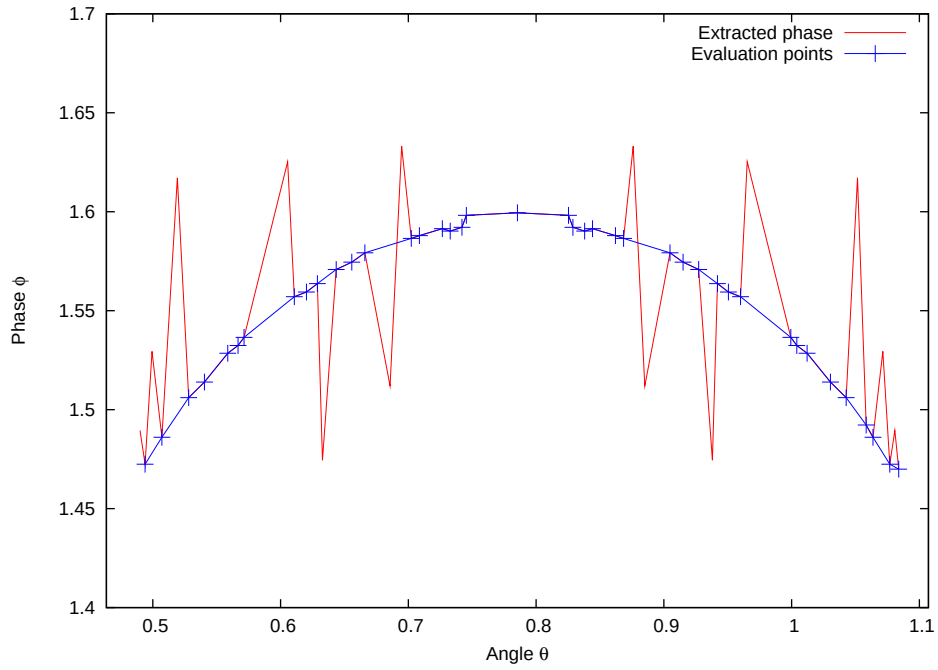

Figure 4.3: Data extracted by using the two-dimensional BPH method by taking into account the periodicity (enlarged). Data displaying too large deviations are omitted.

solutions of linear partial difference equations with constant coefficients can be determined analytically by using the methods presented in Chapter 4 (see also [LPTs05]). Consider the two-dimensional difference equation

$$\sum_{(k_1',k_2')\in A} c(k_1',k_2')\hat{F}(k_1+k_1',k_2+k_2') = 0, \qquad (k_1,k_2)\in\mathbb{Z}_+^2 \tag{4.5}$$

where A is a finite subset of $\mathbb{Z}_+^2$ and $c(k_1',k_2')$ are constants. The *characteristic polynomial* of (4.5) is defined as

$$Q(\xi_1,\xi_2) = \sum_{(k_1',k_2')\in A} c(k_1',k_2')\xi_1^{k_1}\xi_2^{k_2}. \tag{4.6}$$

With a two-dimensional generalization of the Z-transform (which is used to solve ordinary linear difference equations, see [Ela05]) it can be shown that for for suitable initial conditions, solutions of (4.5) are given by the coefficients of the Taylor expansions of functions $P(\xi_1,\xi_2)/Q(\xi_1,\xi_2)$, see [Lei04]. The exact form of $P(\xi_1,\xi_2)$ depends on the choice of the initial conditions for (4.5); in the simplest cases $P(\xi_1,\xi_2)$ is a polynomial.

We now observe, that for such initial data the asymptotic expansion of the solution of (4.5) is determined by (3.54). A similar result has been obtained in [LPTs05], however, under quite restrictive assumptions on the form of the characteristic polynomial $Q(\xi_1,\xi_2)$.

4.2.3 Other possible generalizations of the BPH method to two dimensions

Consider again the double series (4.1). One possible definition of the Borel transformed series[1] is

$$(\mathcal{B}F)(\zeta_1,\zeta_2) = \sum_{k_1=0}^{\infty}\sum_{k_2=0}^{\infty}\frac{\hat{F}(k_1,k_2)}{k_1!k_2!}\zeta_1^{k_1}\zeta_2^{k_2}, \tag{4.7}$$

[1]Note that there exist other extensions of the Borel transform to several dimensions, see [AT71, Tru72].

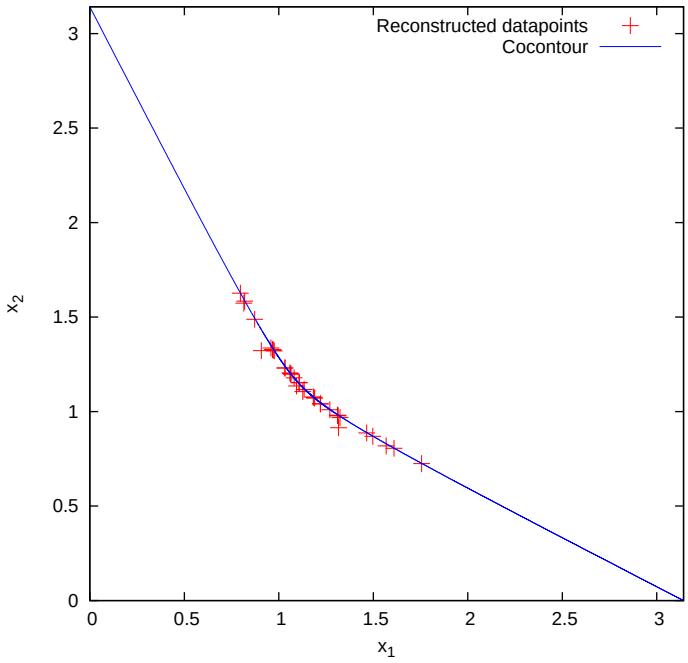

Figure 4.4: Numerical reconstruction of the cocontour in comparison with the exact solution.

see e.g. [Ron74]. Analogously to the one-dimensional case it can be shown that, if the domain of convergence of the series (4.1) contains the origin, then $(\mathcal{B}F)(\zeta_1, \zeta_2)$ is an entire function. As in [PF07], it is convenient to introduce the function

$$F^{\mathrm{BL}}(\xi_1, \xi_2) = \sum_{k_1=0}^{\infty} \sum_{k_2=0}^{\infty} \frac{\hat{F}(k_1, k_2)}{\xi_1^{k_1+1} \xi_2^{k_2+1}}. \tag{4.8}$$

Then the relation between $F^{\mathrm{BL}}(\xi_1, \xi_2)$ and $(\mathcal{B}F)(\zeta_1, \zeta_2)$ is given by a two-dimensional Laplace integral.

Actually, the rate of exponential growth of $F^{\mathrm{BL}}(\xi_1, \xi_2)$ can be related to the domain of analyticity of the function $F^{\mathrm{BL}}(\xi_1, \xi_2)$ by the Ivanov–Stavskii theorem, analogously to the one-dimensional case of the Pólya theorem. For an exact formulation we refer to [Ron74].

Using this theorem to obtain numerically information on the complex singularities would constitute a wellcome complement to the two-dimensional BPH method presented before.

Part II

Self-similar nonstationary solutions of ideal hydrodynamic equations

Chapter 5

Short-time expansion of the Burgers equation

The short-time asymptotic expansion for the one-dimensional inviscid Burgers equation has been introduced in [Fri83]. For the simple initial condition $-1/2 \sin z$ we perform the short-time asymptotic expansion to all orders and analyze its relation to the time Taylor expansions. After this we study the short-time asymptotics of the 2D Burgers equation. As we shall see in the following chapters, this approach can be easily generalized to various instances of inviscid hydrodynamical equations such as the 2D Euler equation, 2D MHD and 3D Euler equation.

5.1 One-dimensional Burgers equation

To illustrate the idea underlying the time-Taylor series analysis we begin by appying it to the complex singularities of the one-dimensional Burgers equation. Such singularities have been extensively studied over the years (see e.g. [BF84, SCE96, Sen97a, Sen97b]) and are now well understood. Furthermore, we can largely benefit from the possibility to obtain analytical solutions and are not obliged to limit ourselves to numerics.

We start with the solution of the complexified one-dimensional 2π-periodic Burgers equation with the initial condition $u^{(0)}(z) = (-1/2)\sin z$. For this simple initial condition we can solve (3.37) explicitly. For convenience we write the solution as a sum

$$u(z,t) = u_+(z,t) + u_-(z,t) \tag{5.1}$$

of two functions $u_+(z,t)$ and $u_-(z,t)$, analytic in the lower and in the upper half-planes respectively:

$$\begin{aligned} u_+(z,t) &= \sum_{k=1}^{\infty} \hat{u}_+(k,t) \mathrm{e}^{-\mathrm{i}kz}, \\ u_-(z,t) &= \sum_{k=1}^{\infty} \hat{u}_-(k,t) \mathrm{e}^{\mathrm{i}kz}. \end{aligned} \tag{5.2}$$

An explicit expression[1] for $\hat{u}_+(k,t)$ (as well as for $\hat{u}_-(k,t)$) is obtained using the Fourier-Lagrangian representation [FF83]

$$\hat{u}_+(k,t) = \frac{1}{\mathrm{i}\,kt} J_k(kt/2), \qquad k > 0. \tag{5.3}$$

[1] It has been found by G. Platzman in 1964, see [Pla64].

However, the methods presented above cannot be applied to more interesting cases, such as incompressible Euler equation or MHD equations. On the contrary, short-time asymptotic expansion and time-series analysis can be easily generalized to study (mostly numerically) complex space-time singularities of such equations.

We begin by showing how to obtain an explicit solution of (3.37) by the short-time asymptotic expansion introduced in [Fri83]. Inserting the time-Taylor series expansion for the velocity

$$u(z,t) = \sum_{n=0}^{\infty} t^n u^{(n)}(z), \tag{5.4}$$

into the Burgers equation (3.37), we obtain the recursion relations

$$u^{(n+1)} = -\frac{1}{n+1} \sum_{m=0}^{n} u^{(m)}\, \partial_z u^{(n-m)}. \tag{5.5}$$

Analogously to (5.1) we represent each function $u^{(n)}$ as a sum of two functions $u_+^{(n)}$ and $u_-^{(n)}$ analytic in the lower and the upper half-planes, respectively. Actually, the functions $u_+^{(m)}$ are polynomials in $\mathrm{e}^{-\mathrm{i}\,z}$

$$u_+^{(m)}(z) = \sum_{k \in J_+^{(m)} \subset \mathbb{Z}} \hat{u}_+^{(m)}(k)\, \mathrm{e}^{-\mathrm{i}\,kz}, \tag{5.6}$$

with the support $J_+^{(m)}$ given by

$$J_+^{(m)} = \begin{cases} \left\{ i \in \mathbb{Z}\backslash\{0\} \,|\, i = 2l,\ l = 1, ..., \frac{m+1}{2} \right\} & \text{for } m \text{ odd} \\ \left\{ i \in \mathbb{Z}\backslash\{0\} \,|\, i = 2l+1,\ l = 0, ..., \frac{m}{2} \right\} & \text{for } m \text{ even} \end{cases} \tag{5.7}$$

Using (5.6) and (5.2) the function $u_+(z,t)$ can be written as a double series in t and $\mathrm{e}^{-\mathrm{i}\,z}$

$$u_+(z,t) = \sum_{m=0}^{\infty} \sum_{k \in J_+^{(m)} \subset \mathbb{Z}} \hat{u}_+^{(m)}(k) t^m \mathrm{e}^{-\mathrm{i}\,kz}. \tag{5.8}$$

Similar reasoning applies to the function $u_-(z,t)$ which we write as a double series in t and $\mathrm{e}^{\mathrm{i}\,z}$

$$u_-(z,t) = \sum_{m=0}^{\infty} \sum_{k \in J_-^{(m)} \subset \mathbb{Z}} \hat{u}_-^{(m)}(k) t^m \mathrm{e}^{\mathrm{i}\,kz}. \tag{5.9}$$

For convenience we introduce the following notation:

$$z_+ = z + \mathrm{i}\,\ln t, \qquad z_- = z - \mathrm{i}\,\ln t. \tag{5.10}$$

Using this notation we rewrite series (5.8) and (5.9) as

$$\begin{aligned} u_+(z,t) &= \sum_{n=0}^{\infty} \sum_{k=1}^{\infty} \hat{u}_+^{(2n+k-1)}(k)\, t^{2n-1} \mathrm{e}^{-\mathrm{i}\,kz_+}, \\ u_-(z,t) &= \sum_{n=0}^{\infty} \sum_{k=1}^{\infty} \hat{u}_-^{(2n+k-1)}(-k)\, t^{2n-1} \mathrm{e}^{\mathrm{i}\,kz_-} \end{aligned} \tag{5.11}$$

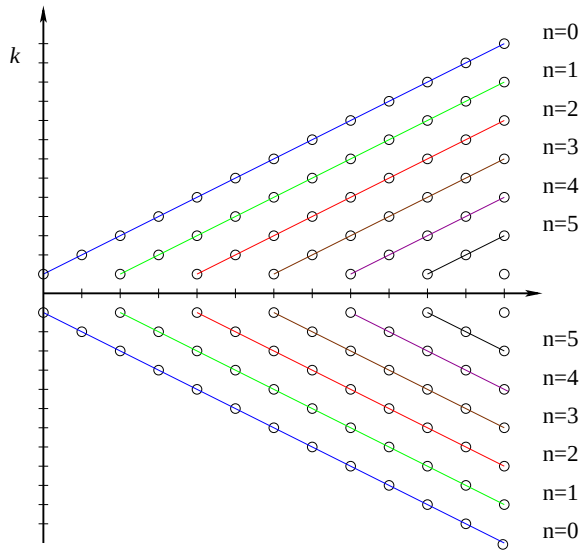

Figure 5.1: On this figure we represent the support of the series (5.8) in the (m, k) space.

see Fig. 5.1. Defining the functions

$$\begin{aligned} v_+^{(n)}(z_+) &= \sum_{k=1}^{\infty} \hat{u}_+^{(2n+k-1)}(k)\, \mathrm{e}^{-\mathrm{i}kz_+} = \sum_{k=1}^{\infty} \hat{v}_+^{(n)}(k)\, \mathrm{e}^{-\mathrm{i}kz_+}, \\ v_-^{(n)}(z_-) &= \sum_{k=1}^{\infty} \hat{u}_-^{(2n+k-1)}(-k)\, \mathrm{e}^{\mathrm{i}kz_-} = \sum_{k=1}^{\infty} \hat{v}_-^{(n)}(k)\, \mathrm{e}^{\mathrm{i}kz_-}. \end{aligned} \tag{5.12}$$

we represent $u_+(z,t)$ and $u_-(z,t)$ by their short-time asymptotic expansions

$$\begin{aligned} u_+(z,t) &= \sum_{n=0}^{\infty} v_+^{(n)}(z_+)\, t^{2n-1}, \\ u_-(z,t) &= \sum_{n=0}^{\infty} v_-^{(n)}(z_-)\, t^{2n-1}. \end{aligned} \tag{5.13}$$

Now we remark that $v_+^{(n)}(z_+)$ and $v_-^{(n)}(z_-)$ are solutions of an infinite system of ordinary differential equations which is obtained by substituting the expansion

$$u(z,t) = \sum_{n=0}^{\infty} t^{2n-1} \left[v_+^{(n)}(z_+) + v_-^{(n)}(z_-) \right] \tag{5.14}$$

into the Burgers equation (3.37). In particular, for $v_+^{(0)}(z_+)$ we get the *similarity equation*, see [Fri83]

$$(-1 + \mathrm{i}\,\partial_{z_+}) v_+^{(0)} + v_+^{(0)} (\partial_{z_+} v_+^{(0)}) = 0, \tag{5.15}$$

where the solution has to satisfy

$$v^{(0)} \simeq -\frac{\mathrm{i}}{4}\, \mathrm{e}^{-\mathrm{i}z_+}, \qquad \operatorname{Im} z \to -\infty. \tag{5.16}$$

The solution can be written explicitly in terms of Lambert's W function [CGHJK96]

$$v_+^{(0)}(z_+) = \mathrm{i}\, W\left(-\frac{1}{4} \mathrm{e}^{-\mathrm{i}z_+} \right). \tag{5.17}$$

Analogously, $v_-^{(0)}(z_-)$ is given by

$$v_-^{(0)}(z_-) = -\mathrm{i}\, W\left(-\frac{1}{4}\mathrm{e}^{\mathrm{i}\, z_-}\right). \tag{5.18}$$

Note that (5.17) and (5.18) correspond to the exact solutions

$$\begin{aligned} u_+^{\mathrm{as}}(z,t) &= \frac{\mathrm{i}}{t} W\left(-\frac{t}{4}\mathrm{e}^{-\mathrm{i}\, z}\right), \\ u_-^{\mathrm{as}}(z,t) &= \frac{1}{\mathrm{i}\, t} W\left(-\frac{t}{4}\mathrm{e}^{\mathrm{i}\, z}\right), \end{aligned} \tag{5.19}$$

of the Burgers equation (3.37) with initial conditions $-(\mathrm{i}/4)\mathrm{e}^{-\mathrm{i}\, z}$ and $(\mathrm{i}/4)\mathrm{e}^{\mathrm{i}\, z}$, see also [Wei03]. Thus, at short times the solution of (3.37) with the initial condition $(-1/2)\sin z$ is asymptotically close to a linear superposition of the two solutions with initial conditions given above. This can be readily seen by comparing the Fourier series of $u_+^{\mathrm{as}}(z,t)$

$$\frac{1}{\mathrm{i}\, t}\sum_{k=1}^{\infty} \frac{k^{k-1}}{k!}\left(\frac{t\mathrm{e}^{-\mathrm{i}\, z}}{4}\right)^k, \tag{5.20}$$

with the Fourier series (5.3) of the exact solution. Using Hadamard's factorization theorem [Ahl79] for the Bessel function J_k of order k

$$J_k(\xi) = \frac{\xi^k}{2^k k!}\prod_{n=1}^{\infty}\left(1 - \frac{\xi^2}{j_{k,\,n}}\right), \tag{5.21}$$

where $j_{k,\,n}$ denotes the nth zero of J_k, we obtain the following reperesentation

$$u_+(z,t) = \frac{1}{\mathrm{i}}\sum_{k=1}^{\infty}\frac{(kt)^{k-1}}{4^k k!}\prod_{n=1}^{\infty}\left(1 - \frac{(kt)^2}{j_{k,\,n}}\right)\mathrm{e}^{-\mathrm{i}\, kz}. \tag{5.22}$$

From this representation follows that $u_+^{\mathrm{as}}(z,t)$ is asymptotic to $u_+(z,t)$ for short times and large values of $\mathrm{Im}\, z$. Furthermore, the short-time asymptotic expansion (5.13) can be recovered from (5.22) by formally expanding the infinite product and ordering the resulting expression according to powers of t.

Equation (5.15) which governs the leading-order term is a nonlinear ordinary differential equation. On the contrary, equations governing the subdominant terms are linear inhomogeneous equations, for example the equation for $v_+^{(1)}$ has the form

$$\begin{aligned} &(1 + \mathrm{i}\,\partial_{z_+})v_+^{(1)} + v_+^{(0)}\,(\tilde{\partial}_+ v_+^{(1)}) + v_+^{(1)}\,(\partial_{z_+} v_+^{(0)}) - \\ &\frac{\mathrm{i}}{4}\mathrm{e}^{\mathrm{i}\, z_+}(\partial_{z_+} v_+^{(0)}) + \frac{1}{4}\mathrm{e}^{\mathrm{i}\, z_+} v_+^{(0)} = 0. \end{aligned} \tag{5.23}$$

The homogeneous part is determined by the interaction of $v_+^{(1)}$ with the leading-order term $v_+^{(0)}$ whereas the sorce term is governed by the interaction between the two complex conjugate singularities, located in the upper and the lower half-planes. This of course is valid for all $v(n)_+$ and $v(n)_-$.

The Fourier series representation can be determined explicitly for all orders $u_+^{(n)}$ and is given by

$$\begin{aligned} &v_+^{(n)}(z_+) = (-1)^n\,\frac{1}{2^{2n}}\,\frac{1}{n!}\times \\ &\sum_{k=1}^{\infty}\left(\prod_{l=1}^{n-1}(k+n+l)\right) a_{k+2n-1}^{(n)}\left(\frac{-\mathrm{e}^{-\mathrm{i}\, z_+}}{4}\right)^k, \end{aligned} \tag{5.24}$$

where

$$a_k^{(n)} = (-1)^{k+1}(2n-1)\sum_{l=0}^{k} \frac{(l-(2n-1))^{l-1}}{l!}\,\frac{(k-l)^{k-l}}{(k-l)!}. \tag{5.25}$$

An analogous expression can be obtained for $v_-^{(n)}$.

5.2 Burgers equation: additional remarks

Geometry of the singular set and the Fourier–Taylor expansion of the solution

Actually, as has been pointed out by K. Ohkitani[2], the solution (5.17) of the one-dimensional Burgers equation in the short-time asymptotic régime can also be obtained by Moore's asymptotic analysis [Moo79], originally developed for the Kelvin–Helmholtz problem: one assumes that the initial condition is of the form $u^{(0)}(z) = \varepsilon \sin z$ and expands the solution using ε as small parameter, see also [Mur97]. The leading order solution is then given by (5.17).

Having obtained analytically the complete Taylor expansion in time and the Fourier expansion in space, one may ask what information on the geometrical structure of the corresponding solution in time-space it gives us. The Fourier–Taylor coefficients of the series representation (5.8) of the solution with the initial condition $u^{(0)}(z) = (-1/2)\sin z$ are determined by Equation (5.24). As we have seen in Chapters 3 and 4, from these coefficients we can find the space-time singularities closest to the origin $(t, z) = (0, 0)$. In other words, we can determine the boundary of the complement of the amoeba corresponding to the Fourier–Taylor expansion (5.8).

Actually, this set constitutes a part of the contour of the (space-time) singular manifold of $u(z, t)$. Thus, on Fig. 5.2 we represent a part of the contour which includes it. Obviously, the explicit description of the singularities and thus of the contour is given as the set of points (3.39) at which the Jacobian of the Lagrangian map vanishes.

We observe that the singularities which are obtained from the Fourier–Taylor expansion (as explained above) are actually different from the real-time singularities of $u(z, t)$. Namely, the singularities which can be reconstructed from (5.8) correspond to the singularities of $u(z, t)$ in imaginary time. The singularities of the short-time asymptotic solutions (5.17) and (5.18) constitute the asymptotic directions of the amoeba.

Extension of the short-time asymptotic approach to more complicated initial conditions of the polynomial type

It would be interesting to extend the short-time asymptotic approach to initial conditions which are more complicated than the simple initial condition $u^{(0)}(z) = (-1/2)\sin z$ in order to study the effects of interactions of different harmonics. We note that for multimode initial conditions such as

$$u^{(0)}(z) = \lambda_1 \sin z + \lambda_2 \sin 2z, \tag{5.26}$$

it is quite easy to give an analytic description of the singular set.

Short-time asymptotics of the Burgers equation in several dimensions

We finally note that the short-time asymptotic approach can be easily extended to more than one dimension. However, we have preferred to introduce the multi-dimensional version of

[2]Private communication.

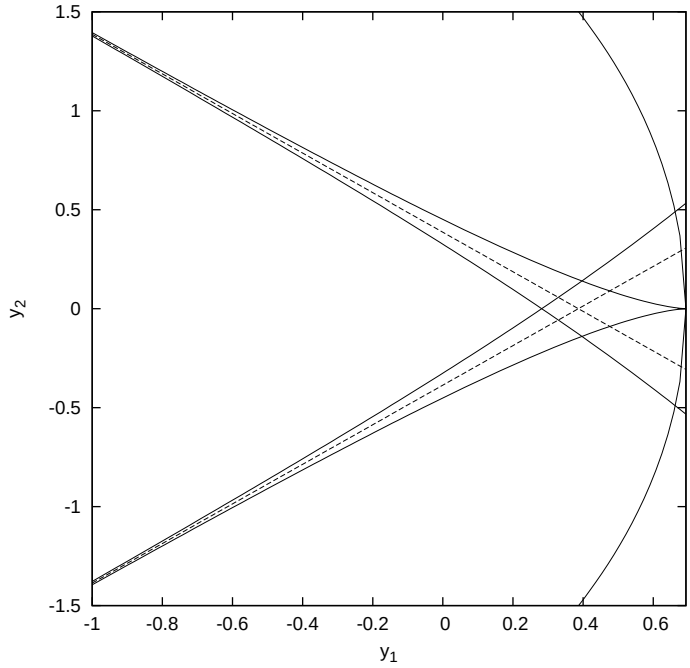

Figure 5.2: A part of the contour of the set of singularities of the solution of the one-dimensional Burgers equation with the initial condition $u^{(0)}(z) = (-1/2)\sin z$. The horizontal axis corresponds to the $\ln|t|$ (the time is also complex) and the vertical axis is y. The solid line represents the contour. The dashed lines correspond to the singularities of the asymptotic solutions (5.17) and (5.18).

the short-time asymptotic approach on less academic examples than the Burgers equation. They will be discussed in the three following chapters.

Chapter 6

Euler equations in two dimensions

In this chapter we study the short-time asymptotic expansion of the two-dimensional Euler equation on the domain $[0, 2\pi) \times [0, 2\pi) + \mathrm{i}\,\mathbb{R}^2$. Just as in the case of the Burgers equation in Chapter 5, short-time asymptotic solutions are here solutions of the Euler equations with complex valued initial conditions having two initial modes (two interacting plane waves) $\mathrm{e}^{-\mathrm{i}\,\mathfrak{p}\cdot z}$ and $\mathrm{e}^{-\mathrm{i}\,\mathfrak{q}\cdot z}$. For such initial conditions, the Euler equation has self-similar solutions whose determination can be reduced to solving a suitable time-independent problem. In Section 6.1 we give a formulation of this problem for arbitrary initial wave numbers $\mathfrak{p}$ and $\mathfrak{q}$, obtaining a generalized version of the *similarity equation* introduced in [FMB03]. It turns out that the only relevant parameters are the aspect ratio $\eta = |\mathfrak{q}|/|\mathfrak{p}|$ and the angle ϕ between the basic modes $\mathfrak{p}$ and $\mathfrak{q}$.

Noting that the isosceles case $\eta = 1$ does not develop any higher harmonics other than the two basic modes, I make a perturbative study of the generalized similarity equation using $\varepsilon = \eta - 1$ as small parameter, see Section 6.2. At the first order a linear partial differential equation is obtained which is a slight modification of the passive scalar equation introduced in [PMFB06]. Singularities of its solutions can be described explicitly, see also [PMFB06]. In particular, this model has a scaling exponent $\alpha = 5/2$ for the algebraic prefactor of the Fourier coefficients of the stream function which does not depend on ϕ. Numerically, I use van der Hoeven's asymptotic interpolation method [Hoe06] to obtain the transseries expansion of the solution in the Fourier space.

Solutions of the full nonlinear similarity equation have been studied for various values of the parameters η and ϕ using high-precision numerical calculations. We observed in [PMFB06] that the scaling of the solutions in the Fourier space seems to depend on the angle ϕ (but not on the ratio η), thus being non-universal.

To determine whether a clean scaling $\alpha = 5/2$ is found for solutions of the similarity equation, I used the fact that the *renormalized* representation introduced in Section 6.1 allows us to analyze directly the limiting case $\phi \to 0$ (which has a trivial solution in the standard representation and becomes non-trivial only after an appropriate rescaling of the coordinates), see Section 6.3. The scaling exponent α for $\phi = 0$ is found with high accuracy (absolute error of about 10^{-7} over different rational directions) to be $5/2$. Furthermore, using van der Hoeven's asymptotic interpolation procedure we determine the first four subleading terms in the transseries expansion of the solution in the Fourier space. We find that the structure of this transseries expansion is the same as the transseries expansion of the solution of the linear equation for the near isosceles case in Section 6.2, which may give us a hint for the missing theory, at least in the case $\phi = 0$.

In the last Section 6.4 we discuss the relation between the non-universality of the scaling exponent $\alpha(\phi)$ and depletion of nonlinearity. We also make some remarks on the problem of going beyond the short-time asymptotics.

6.1 General framework

The short-time asymptotic régime for the 2D Euler equation

$$\partial_t \nabla^2 \Psi(z_1, z_2) - J(\Psi, \nabla^2 \Psi) = 0. \tag{6.1}$$

was introduced in [FMB03] and further developed in [MBF05, PMFB06], in which I was involved (see Section 6.5). As I showed, for initial conditions which are trigonometric polynomials the solutions of the Euler equation in the short-time asymptotic régime can be reduced to solving a problem with a to two-mode intial condition of the type

$$\Psi_0(z_1, z_2) = \hat{F}(\mathfrak{p}) \mathrm{e}^{-\mathrm{i}\,\mathfrak{p}\cdot z} + \hat{F}(\mathfrak{q}) \mathrm{e}^{-\mathrm{i}\,\mathfrak{q}\cdot z}. \tag{6.2}$$

Analogously to the case of the 2D Burgers equation, it is easy to see [PMFB06] that the solution of the Euler equation (6.1) is of the form

$$\psi(z_1, z_2; t) = \frac{1}{t} F(\tilde{z}_1, \tilde{z}_2), \qquad (\tilde{z}_1, \tilde{z}_2) = (z_1 + \mathrm{i}\,\lambda_1 \ln t, z_2 + \mathrm{i}\,\lambda_2 \ln t), \tag{6.3}$$

where

$$\lambda_1 = \frac{\mathfrak{q}_2 - \mathfrak{p}_2}{\mathfrak{p}_1 \mathfrak{q}_2 - \mathfrak{q}_1 \mathfrak{p}_2}, \qquad \lambda_2 = -\frac{\mathfrak{q}_1 - \mathfrak{p}_1}{\mathfrak{p}_1 \mathfrak{q}_2 - \mathfrak{q}_1 \mathfrak{p}_2}.$$

In this chapter we are going to study solutions of (6.1) with initial conditions (6.2). In particular, they are solutions of a suitable time-independent problem.

6.1.1 Fourier representation

Here out goal is to study numerically the nature of complex singularities depending on the angle between the two initial modes, denoted here by $\mathfrak{p}$ and $\mathfrak{q}$. In the short-time régime the nth coefficient of the time series expansion corresponding to (5.5) is given by

$$\Psi^{(n)}(z_1, z_2) = \sum_{\sigma=0}^{n+1} \hat{F}((n+1-\sigma)\mathfrak{p} + \sigma \mathfrak{q}) \mathrm{e}^{-\mathrm{i}\,(n+1-\sigma)\mathfrak{p}\cdot z} \mathrm{e}^{-\mathrm{i}\,\sigma \mathfrak{q}\cdot z}. \tag{6.4}$$

For convenience we write the Fourier coefficients as

$$\hat{F}^{(n)}\left[(n+1-\sigma)\mathfrak{p} + \sigma \mathfrak{q}\right] = (\mathfrak{p} \wedge \mathfrak{q})^n \, \hat{G}^{(n)}(\sigma) \left(\hat{F}(\mathfrak{p})\right)^{n+1-\sigma} \left(\hat{F}(\mathfrak{q})\right)^{\sigma}, \tag{6.5}$$

where the renormalized coefficients $\hat{G}^{(n)}(\sigma)$ satisfy the recursion relations

$$\begin{aligned} \hat{G}^{(n+1)}(\sigma) = &-\frac{1}{n+1} \frac{1}{|(n-\sigma+2)\mathfrak{p} + \sigma \mathfrak{q}|^2} \\ &\sum_{m=0}^{n} \sum_{\tau=0}^{\sigma} |(n-m-(\sigma-\tau)+1)\mathfrak{p} + (\sigma-\tau)\mathfrak{q}|^2 \\ &\left[(m+1)(\sigma-\tau) - (n-m+1)\tau\right] \hat{G}^{(m)}(\tau) \hat{G}^{(n-m)}(\sigma-\tau), \end{aligned} \tag{6.6}$$

and have initial values $\hat{G}^{(0)}(0) = \hat{G}^{(0)}(1) = 1$. It follows from (6.6) that we have the identity

$$\hat{G}^{(n)}(\sigma |\, \mathfrak{p}, \mathfrak{q}) = (-1)^n \hat{G}^{(n)}(n+1-\sigma |\, \mathfrak{q}, \mathfrak{p}). \tag{6.7}$$

Furthermore, $\hat{G}^{(n)}(0) = \hat{G}^{(n)}(n+1) = 0$ for $n \geq 1$. The first few coefficients are as

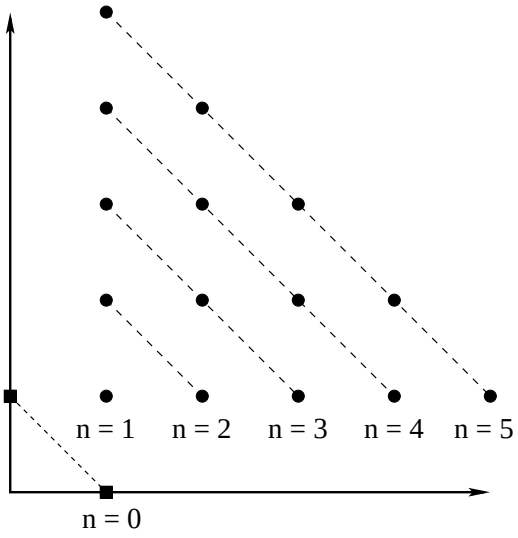

Figure 6.1: Excited modes of the recursion relation for the short-time asymptotics with initial modes $\mathfrak{p}$ and $\mathfrak{q}$.

follows

$$\begin{aligned}
\hat{G}^{(1)}(1) &= -\frac{|\mathfrak{q}|^2-|\mathfrak{p}|^2}{|\mathfrak{p}+\mathfrak{q}|^2};\\
\hat{G}^{(2)}(1) &= \frac{1}{2}\,\frac{|\mathfrak{q}|^2-|\mathfrak{p}|^2}{|\mathfrak{p}+\mathfrak{q}|^2}\,\frac{|\mathfrak{p}+\mathfrak{q}|^2-|\mathfrak{p}|^2}{|2\mathfrak{p}+\mathfrak{q}|^2};\\
\hat{G}^{(3)}(1) &= -\frac{1}{6}\,\frac{|\mathfrak{q}|^2-|\mathfrak{p}|^2}{|\mathfrak{p}+\mathfrak{q}|^2}\,\frac{|\mathfrak{p}+\mathfrak{q}|^2-|\mathfrak{p}|^2}{|2\mathfrak{p}+\mathfrak{q}|^2}\,\frac{|2\mathfrak{p}+\mathfrak{q}|^2-|\mathfrak{p}|^2}{|3\mathfrak{p}+\mathfrak{q}|^2};\\
\hat{G}^{(3)}(2) &= \frac{1}{3}\,\frac{|\mathfrak{q}|^2-|\mathfrak{p}|^2}{|\mathfrak{p}+\mathfrak{q}|^2}\,\frac{|\mathfrak{p}+\mathfrak{q}|^2-|\mathfrak{q}|^2}{|\mathfrak{p}+2\mathfrak{q}|^2}\,\frac{|\mathfrak{p}+2\mathfrak{q}|^2-|\mathfrak{p}|^2}{|2\mathfrak{p}+2\mathfrak{q}|^2}+\\
&\quad\frac{1}{3}\,\frac{|\mathfrak{q}|^2-|\mathfrak{p}|^2}{|\mathfrak{p}+\mathfrak{q}|^2}\,\frac{|\mathfrak{p}+\mathfrak{q}|^2-|\mathfrak{p}|^2}{|2\mathfrak{p}+\mathfrak{q}|^2}\,\frac{|2\mathfrak{p}+\mathfrak{q}|^2-|\mathfrak{q}|^2}{|2\mathfrak{p}+2\mathfrak{q}|^2}.
\end{aligned} \tag{6.8}$$

Note that the coefficients $\hat{G}^{(n)}(\sigma\,|\,\mathfrak{p},\mathfrak{q})$ are rational functions of $\mathfrak{p}$ and $\mathfrak{q}$. Furthermore, from the representation (6.8) follows that these coefficients are defined for arbitrary $\mathfrak{p}$, $\mathfrak{q}$, even for complex ones, not needed here. Furthermore, analogously to [PMFB06], recursion relation (6.6) can be easily solved along the edges

$$\begin{aligned}
\hat{G}^{(n)}(1) &= (-1)^n\frac{1}{n!}\prod_{\sigma=0}^{n-1}\frac{|\sigma\mathfrak{p}+\mathfrak{q}|^2-|\mathfrak{p}|^2}{(\sigma+1)\mathfrak{p}+\mathfrak{q}|^2},\\
\hat{G}^{(n)}(n) &= \frac{1}{n!}\prod_{\sigma=0}^{n-1}\frac{|\mathfrak{p}+\sigma\mathfrak{q}|^2-|\mathfrak{q}|^2}{|\mathfrak{p}+(\sigma+1)\mathfrak{q}|^2}.
\end{aligned} \tag{6.9}$$

For bookkeeping purposes, we give in Appendix A a few higher order coefficients $G^{(n)}(\sigma)$ (actually only those with $n=4$).

As we have observed numerically, all coefficients $\hat{G}^{(n)}(\sigma)$ except one can be made positive upon multiplying them by $(-1)^{n+1-\sigma}$, in complete analogy to [PMFB06].

6.1.2 Physical space: pseudohydrodynamics

We shall now introduce the generating function of $\hat{G}^{(n)}(\sigma)$ by

$$\check{G}(\check{z}_1,\check{z}_2)=G^{(0)}(0)e^{\check{z}_1}+G^{(0)}(1)e^{\check{z}_2}+\sum_{n=1}^{\infty}\sum_{\sigma=1}^{n}\hat{G}^{(n)}(\sigma)e^{\sigma\check{z}_1}e^{(n+1-\sigma)\check{z}_2}, \tag{6.10}$$

where $(\check{z}_1,\check{z}_2)\in\mathbb{C}^2$ are the coordinates corresponding to the imaginary plane. In the physical space $\check{G}(\check{z}_1,\check{z}_2)$ satisfies the generalized similarity equation

$$\begin{aligned}&|\mathfrak{p}|^2(\check{\partial}_1^2G)+2\mathfrak{p}\cdot\mathfrak{q}(\check{\partial}_1\check{\partial}_2G)+|\mathfrak{q}|^2(\check{\partial}_2^2G)-|\mathfrak{p}|^2(\check{\partial}_1^3G)-(|\mathfrak{p}|^2+2\mathfrak{p}\cdot\mathfrak{q})(\check{\partial}_1^2\partial_2G)-\\&(|\mathfrak{q}|^2+2\mathfrak{p}\cdot\mathfrak{q})(\check{\partial}_1\check{\partial}_2^2G)-|\mathfrak{q}|^2(\check{\partial}_2^3G)=|\mathfrak{p}|^2\left((\check{\partial}_1G)(\check{\partial}_1^2\check{\partial}_2G)-(\check{\partial}_2G)(\check{\partial}_1^3G)\right)+\\&2\mathfrak{p}\cdot\mathfrak{q}\left((\check{\partial}_1G)(\check{\partial}_1\check{\partial}_2^2G)-(\check{\partial}_2G)(\check{\partial}_1^2\check{\partial}_2G)\right)+|\mathfrak{q}|^2\left((\check{\partial}_1G)(\check{\partial}_2^3G)-(\check{\partial}_2G)(\check{\partial}_1\check{\partial}_2^2G)\right),\end{aligned} \tag{6.11}$$

with boundary conditions

$$\check{G}(\check{z}_1,\check{z}_2)\simeq e^{z_1}+e^{\check{z}_2},\quad \operatorname{Re}\check{z}_1,\ \operatorname{Re}\check{z}_2\to-\infty. \tag{6.12}$$

The short-time asymptotic solution of the Euler equation $F(\tilde{z}_1,\tilde{z}_2)$ can be obtained from $\check{G}(\check{z}_1,\check{z}_2)$ as follows

$$\begin{aligned}F(\tilde{z}_1,\tilde{z}_2)=\frac{1}{\mathfrak{p}\wedge\mathfrak{q}}\,G\Big[&-\mathrm{i}\ \mathfrak{p}\cdot\tilde{z}+\ln\mathfrak{p}\wedge\mathfrak{q}+\ln F^{(0)}(0),\\&-\mathrm{i}\ \mathfrak{q}\cdot\tilde{z}+\ln\mathfrak{p}\wedge\mathfrak{q}+\ln F^{(0)}(1)\Big].\end{aligned} \tag{6.13}$$

Introducing the notation

$$\check{\Delta}_{(\mathfrak{p},\mathfrak{q})}=|\mathfrak{p}|^2\,\check{\partial}_1^2+2\,\mathfrak{p}\cdot\mathfrak{q}\,\check{\partial}_1\check{\partial}_2+|\mathfrak{q}|^2\,\check{\partial}_2^2, \tag{6.14}$$

we can rewrite (6.11) as

$$\check{\Delta}_{(\mathfrak{p},\mathfrak{q})}\check{G}=\big(\check{\partial}_1G+1\big)\big(\check{\partial}_2\,\check{\Delta}_{(\mathfrak{p},\mathfrak{q})}\check{G}\big)-\big(\check{\partial}_2\check{G}-1\big)\big(\check{\partial}_1\,\check{\Delta}_{(\mathfrak{p},\mathfrak{q})}\check{G}\big). \tag{6.15}$$

Analogously to [PMFB06], defining a modified stream function

$$\check{H}(\check{z}_1,\check{z}_2)=\check{G}(\check{z}_1,\check{z}_2)+\check{z}_1-\check{z}_2, \tag{6.16}$$

we get a *stationary pseudo-hydrodynamic* equation

$$\check{\Delta}_{(\mathfrak{p},\mathfrak{q})}H=\check{J}(H,\ \check{\Delta}_{(\mathfrak{p},\mathfrak{q})}H). \tag{6.17}$$

The scale invariance of (6.11) implies that the function $G(z_1,z_2)$ remains unchanged when $\mathfrak{p}$ and $\mathfrak{q}$ are multiplied by the same factor. Therefore, without any loss of generality we can set $\mathfrak{p}=(1,0)$. To emphasize the fact that the solution depends only on two relevant parameters, the aspect ratio and the angle between $\mathfrak{p}$ and $\mathfrak{q}$, we introduce the following notation: $|\mathfrak{q}|=\eta$ and ϕ for the angle between $\mathfrak{p}$ and $\mathfrak{q}$. Then $\mathfrak{p}\cdot\mathfrak{q}=\eta\cos\phi$. Assuming that $\eta\neq0$ the generalized similarity equation can be written as

$$\check{\Delta}_{(\phi,\eta)}H=\check{J}(H,\check{\Delta}_{(\phi,\eta)}H), \tag{6.18}$$

where

$$\Delta_{(\phi,\eta)}=\frac{1}{\eta}\,\check{\partial}_1^2+2\,\cos\phi\,\check{\partial}_1\check{\partial}_2+\eta\,\check{\partial}_2^2. \tag{6.19}$$

6.2 Perturbative study of the similarity equation

Equation (6.18) does not seem to have any simple solutions except for the case $\eta = 1$. Obviously, when $\eta = 1$, there are no higher order harmonics and we have the following solution of the similarity equation

$$G_0 = \mathrm{e}^{\check{z}_1} + \mathrm{e}^{\check{z}_2}, \qquad H_0 = \check{z}_1 - \check{z}_2 + \mathrm{e}^{\check{z}_1} + \mathrm{e}^{\check{z}_2}. \tag{6.20}$$

Thus, it is natural to use $\varepsilon = \eta - 1$ as small parameter, writing $G = G_0 + \varepsilon G_1 + \varepsilon^2 G_2 + ...$ and $H = H_0 + \varepsilon H_1 + \varepsilon^2 H_2 + ...$ To the leading order we get

$$\check{J}(H_0, \check{\Delta}_{(\phi,1)} H_0) = \check{\Delta}_{(\phi,1)} H_0, \tag{6.21}$$

and to the order ε

$$\begin{aligned} \check{J}(H_0, \check{\Delta}_{(\phi,1)} H_1) + \check{J}(H_1, \check{\Delta}_{(\phi,1)} H_0) + \check{J}(H_0, (\partial_2^2 - \partial_1^2) H_0) = \\ \check{\Delta}_{(\phi,1)} H_1 + (\check{\partial}_2^2 - \check{\partial}_1^2) H_0. \end{aligned} \tag{6.22}$$

Clearly, (6.20) is the solution of the zeroth order equation. The first order equation can be rewritten as

$$(1-\mathrm{e}^{\check{z}_2})\check{\partial}_1 \check{\Delta}_{(\phi,1)} H_1 + (1+\mathrm{e}^{\check{z}_1})\check{\partial}_2 \check{\Delta}_{(\phi,1)} H_1 - \check{\Delta}_{(\phi,1)} H_1 + \mathrm{e}^{\check{z}_2}(\check{\partial}_1 H_1) - \mathrm{e}^{\check{z}_1}(\check{\partial}_2 H_1) = -2\,\mathrm{e}^{\check{z}_1}\mathrm{e}^{\check{z}_2}. \tag{6.23}$$

Equation (6.23) is probably easiest to analyze in terms of the representation (6.10) (in the Fourier space). Defining for simplicity $\hat{\Omega}(k_1, k_2) = (-1)^{k_1}(k_1^2 + 2\cos\phi k_1 k_2 + k_2^2)\hat{H}_1(k_1, k_2)$, we obtain the partial difference equation

$$\begin{aligned} & k_1\Big[\hat{\Omega}(k_1, k_2) - \hat{\Omega}(k_1, k_2 - 1)\Big] + k_2\Big[\hat{\Omega}(k_1, k_2) - \hat{\Omega}(k_1 - 1, k_2)\Big] = \hat{\Omega}(k_1, k_2) - \\ & k_1 \frac{\hat{\Omega}(k_1, k_2 - 1)}{k_1^2 + 2\cos\phi k_1(k_2 - 1) + (k_2 - 1)^2} - k_2 \frac{\hat{\Omega}(k_1 - 1, k_2)}{(k_1 - 1)^2 + 2\cos\phi(k_1 - 1)k_2 + k_2^2} - \\ & 2\delta_{k_1 1}\delta_{k_2 1}. \end{aligned} \tag{6.24}$$

Note that for $(k_1, k_2) \neq (1, 1)$ the source term $-2\delta_{k_1 1}\delta_{k_2 1}$ on the right-hand side drops out. Then, setting $k' = \sqrt{k_1^2 + (k_2 - 1)^2}$, $k'' = \sqrt{(k_1 - 1)^2 + k_2^2}$, $\theta' = \mathrm{Arc}\tan(k_2 - 1)/k_1$ and $\theta'' = \mathrm{Arc}\tan k_2/(k_1 - 1)$, Equation (6.24) can be written as

$$\begin{aligned} & \cos\theta\Big[\hat{\Omega}(k, \theta) - \hat{\Omega}(k', \theta')\Big] + \sin\theta\Big[\hat{\Omega}(k, \theta) - \hat{\Omega}(k'', \theta'')\Big] = \\ & \frac{1}{k}\hat{\Omega}(k, \theta) - \frac{\cos\theta}{(k')^2}\frac{\Omega(k', \theta')}{1 + \sin 2\theta' \cos\phi} - \frac{\sin\theta}{(k'')^2}\frac{\Omega(k'', \theta'')}{1 + \sin 2\theta'' \cos\phi}. \end{aligned} \tag{6.25}$$

Here, of course, we are mostly interested in the case $k \to \infty$. The high-k behavior of the Fourier coefficients is given by

$$\hat{\Omega}(k, \theta) \simeq k^{-\alpha+2}\mathrm{e}^{-\delta(\theta)k}, \tag{6.26}$$

where the e-folding rate $\delta(\theta)$ is determined by the left-hand side of (6.24), the next order term and its scaling exponent $\alpha = 5/2$ is determined by omitting all terms on the right-hand side except $\hat{\Omega}(k_1, k_2)$. The remaining terms are responsible only for higher order corrections.

Actually, the perturbative expansion introduced above can be made systematic by allowing for complex values of the parameter $\zeta = \eta - 1$. The function $H(\check{z}_1, \check{z}_2; \zeta)$ depends on three complex variables and is given by the solution of

$$\big(\check{\Delta}_\phi(\zeta) H\big) = \check{J}\Big(H, \big(\check{\Delta}_\phi(\zeta) H\big)\Big), \tag{6.27}$$

where the operator $\big(\Delta_\phi(\zeta)\big)$ is defined as

$$\big(\check{\Delta}_\phi(\zeta)\big) = \frac{1}{1+\zeta}\,\check{\partial}_1^2 + 2\cos\phi\,\check{\partial}_1\check{\partial}_2 + (1+\zeta)\,\check{\partial}_2^2. \tag{6.28}$$

The perturbative expansion for small ε corresponds to the (formal) Taylor expansion

$$H(\check{z}_1, \check{z}_2; \zeta) = z_1 - z_2 + \sum_{n=0}^{\infty} G_n(\check{z}_1, \check{z}_2)\,\zeta^n = \sum_{n=0}^{\infty} H_n(\check{z}_1, \check{z}_2)\,\zeta^n. \tag{6.29}$$

The functions $G_n(\check{z}_1, \check{z}_2)$ satisfy an infinite system of inhomogeneous linear partial differential equations which is given in Appendix B. Note also that $H(\check{z}_1, \check{z}_2; \zeta)$ can be represented as a triple Fourier–Taylor series

$$H(\check{z}_1, \check{z}_2; \zeta) = \check{z}_1 - \check{z}_2 + \sum_{k_1=0}^{\infty}\sum_{k_2=0}^{\infty}\sum_{n=0}^{\infty} \hat{G}(k_1, k_2; n)\,\mathrm{e}^{k_1\check{z}_1}\,\mathrm{e}^{k_2\check{z}_2}\zeta^n, \tag{6.30}$$

where the coefficients $\hat{G}(k_1, k_2; n)$ are determined through (6.20) and

$$H_n(\check{z}_1, \check{z}_2) = \sum_{k_1=0}^{\infty}\sum_{k_2=0}^{\infty} \hat{G}(k_1, k_2; n)\,\mathrm{e}^{k_1\check{z}_1}\,\mathrm{e}^{k_2\check{z}_2}, \quad n > 0. \tag{6.31}$$

The coefficients $\hat{G}(k_1, k_2; n)$ satisfy an infinite system of linear recursion relation which is also given in Appendix B.

We finally note that the ζ-dependence of $H(\check{z}_1, \check{z}_2; \zeta)$ can be studied by analyzing the coefficients $\hat{G}(k_1, k_2; n)$ along rational direction in the (k_1, k_2, n)-space.

6.3 Degenerate limit of the similarity equation

In this section we study the degenerate solution of the similarity equation in the limit $\phi \to 0$. Of course, in the case $\phi = 0$ the non-renormalized solution of the Euler equation (6.1) is stationary, comprising only the two initial modes. However, if we consider the renormalized functions $G(\check{z}_1, \check{z}_2)$ and $H(\check{z}_1, \check{z}_2)$ which have been rescaled with respect to $\sin\phi$ we see, for example from expressions (6.8), that they are nontrivial even for $\phi = 0$.

We first give the results of the analysis of the coefficients $G^{(n)}(\sigma)$, after which we briefly discuss the corresponding picture in the physical space.

6.3.1 Representation of the results in the Fourier space

The Fourier coefficients[1] of the solution $G^{(n)}(\sigma)$ have been calculated up to $N_{\max} = 2000$ and analyzed along rational directions (p, q) such that $p, q < 10$ (which gives 55 different rational directions) using the asymptotic interpolation procedure of van der Hoeven

[1] Note that we use the notations $G^{(n)}(\sigma) = G(k_1, k_2)$, with $k_1 = n + 1 - \sigma$ and $k_2 = \sigma$.

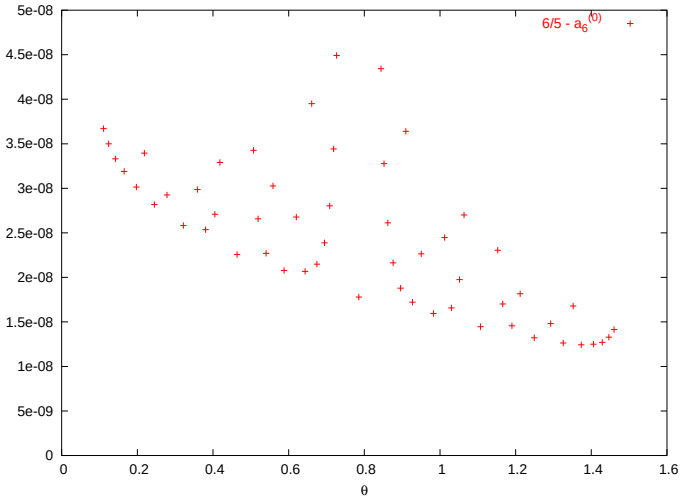

Figure 6.2: Difference between $3/\alpha$ for $\alpha = 5/2$ and the interpolation value $g^{(6)}(m_{\max})$.

[Hoe06]. The first six stages are the same as in [PF07] for the one-dimensional Burgers equation

$$\text{SR, -D, I, D, D, D,} \tag{6.32}$$

where we have used the same notation as in [PF07]. The leading order term and two subleading terms are the standard ones

$$G(k,\theta) \sim C(\theta) k^{-\alpha(\theta)} \mathrm{e}^{-\delta(\theta)k}, \tag{6.33}$$

where $(k_1, k_2) = m(p,q)$ for the rational direction (p,q). Fig. 6.2 shows the discrepancy of the scaling exponent, determined via the constant $a_6^{(0)}$ at the sixth stage, from the value $5/2$ as a function of the angle ϕ. It is seen that α differs from $5/2$ by less than 10^{-7}.

It is tempting to try to determine the nature of the following subdominant terms. The aim is twofold: firstly, it allows us to find the transseries expansion of the solutions, secondly, the parameters $\delta(\theta)$, α and $C(\theta)$ can be calculated more precisely. For this, we continue the procedure beyond the sixth stage. First we identify the nature of the remainder at the sixth stage,

$$g^{(6)}(m) = \frac{3}{\alpha} + \omega(m), \tag{6.34}$$

analyzing the data from the most populated direction $(p,q) = (1,1)$ and using seven more stages

$$\text{D, I, R, D, I, D, D.} \tag{6.35}$$

The value of the constant $a_1 3^{(0)}$ obtained at the thirteenth stage (which is an *interpolation stage* in the terminology of [PF07]) is remarkably close to $2/3$, thus suggesting a $1/m^2$ correction in (6.34). However, for the sparsely populated rational directions the convergence to the value $2/3$ is not very good, see Fig. 6.3. Still, the nature of the transseries expansion of $G(k,\theta)$ very likely does not depend on the particular rational direction (p,q), the observed discrepancy being due to the lack of asymptoticity for sparsely populated rational directions.

Thus, using the data from the direction $(1,1)$, I identified two additional subleading terms in the transseries expansion of $G(k,\theta)$

$$G(k,\theta) = C(\theta) k^{-\frac{5}{2}} \mathrm{e}^{-\delta(\theta)k} \left[1 + \frac{b_1(\theta)}{k} + \frac{a_2(\theta) \ln k}{k^2} + O\left(\frac{1}{k^2}\right) \right]. \tag{6.36}$$

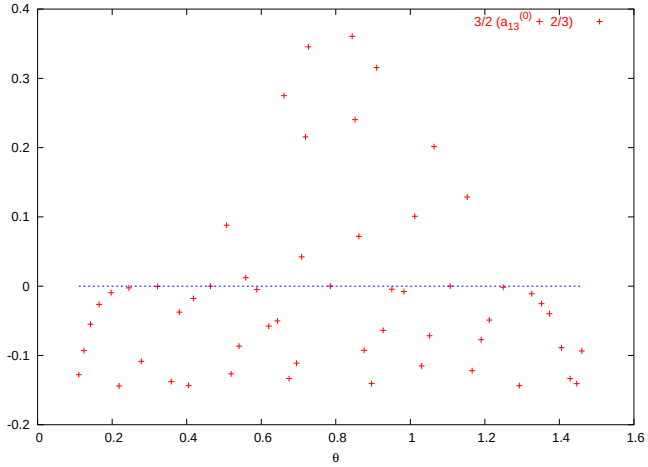

Figure 6.3: Determination of subdominant terms in (6.34).

Actually, the same transseries expansion is also obtained for the solutions of the linear equation at the first order perturbative expansion in $\varepsilon = \eta - 1$ in Section 6.2. The coefficient $a_2(\theta)$ of the logarithmic correction has been measured using modified interpolation stages (starting from the sixth stage)

$$\text{D, I, D, D, D,} \tag{6.37}$$

which are slighly different from those in (6.35), see Fig. 6.4. As can be seen, the lack

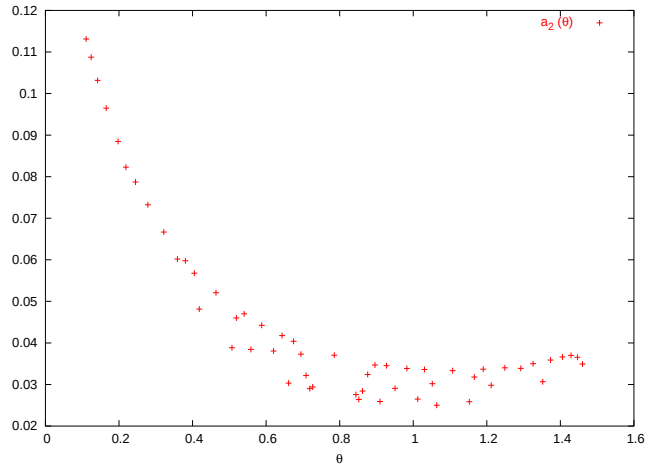

Figure 6.4: Logarithmic correction in the transseries expansion (6.36).

of asymptoticity for sparsely populated directions introduces quite significant errors in the determination of $a_2(\theta)$. Therefore, I did not use the input from $a_2(\theta)$ in determining the constants $b_1(\theta)$, $C(\theta)$ and $\delta(\theta)$. Note also that only after having determined the subdominant term $a_2(\theta)\ln k/k^2$ responsible for the correction $\omega(m)$ to the constant at the sixth stage in (6.34) was I able to estimate whether the inclusion of the subdominant term $b_1(\theta)/k$ is meaningful. For example, if the correction to (6.34) were of the type $1/m$ we would find a subdominant term of the type $a_1(\theta)\ln k/k$ which would clearly dominate over $b_1(\theta)/k$. In our case (6.36) the inclusion of the constant $b_1(\theta)$, represented on Fig. 6.5, turns out to be justified. The e-folding rate $\delta(\theta)$ is represented on Fig. 6.6. Note that for θ close to 0 and $\pi/2$ the function $\ln\delta(\theta)$ seems to be linear. On Fig. 6.7 we represent the second subleading

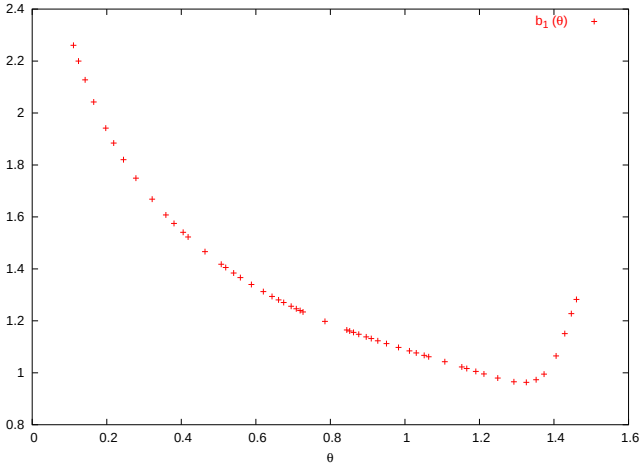

Figure 6.5: Third subleading correction of the type $b_1(\theta)/k$.

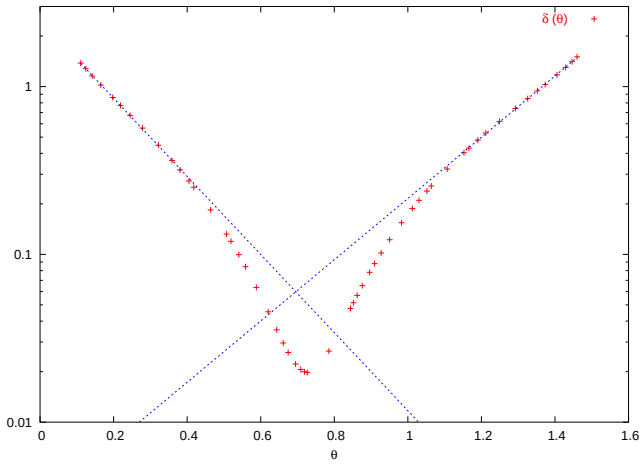

Figure 6.6: Leading-order asymptotics: $\delta(\theta)$ in lin-log coordinates.

term $C(\theta)$. Note that it stays almost constant for values of θ not too close neither to 0 nor to $\pi/2$.

6.3.2 Similarity equation in the physical space

For $\phi = 0$ the Laplacian (6.19) becomes $(\check{\partial}_1/\sqrt{\eta} + \sqrt{\eta}\,\check{\partial}_2)^2$. Introducing the coordinates

$$\begin{aligned} \bar{z}_1 &= \sqrt{\eta}\,\check{z}_1 + \frac{\check{z}_2}{\sqrt{\eta}}, \qquad & \bar{z}_2 &= \sqrt{\eta}\,\check{z}_1 - \frac{\check{z}_2,}{\sqrt{\eta}} \\ \check{z}_1 &= \frac{1}{2\sqrt{\eta}}(\bar{z}_1 + \bar{z}_2), \qquad & \check{z}_2 &= \frac{\sqrt{\eta}}{2}(\bar{z}_1 - \bar{z}_2), \end{aligned} \tag{6.38}$$

we can can reduce it to the second derivative with respect to $\bar{z}_1$, that is $4\bar{\partial}^2$. The similarity equation (6.17) then becomes

$$-\bar{\partial}_1^2 2H = \bar{J}(2H, \bar{\partial}_1^2 2H), \tag{6.39}$$

with initial condition

$$\frac{1}{2\sqrt{\eta}}(\bar{z}_1 + \bar{z}_2) - \frac{\sqrt{\eta}}{2}(\bar{z}_1 - \bar{z}_2) + \exp\left[\frac{1}{2\sqrt{\eta}}(\bar{z}_1 + \bar{z}_2)\right] + \exp\left[\frac{\sqrt{\eta}}{2}(\bar{z}_1 - \bar{z}_2)\right]. \tag{6.40}$$

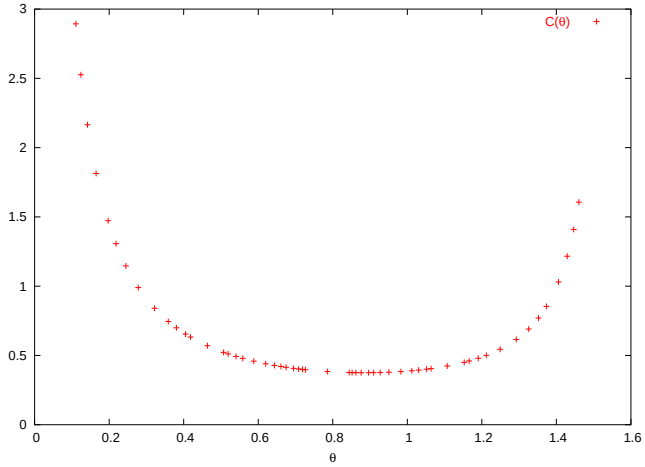

Figure 6.7: Second subleading term

Equation (6.15) can be represented analogously. Note that the "vorticity" term in (6.39) is a derivative with respect to only one coordinate, which agrees well with the intuitive definition of depletion as a reduction to one dimension. Still, even this reduced similarity equation is strongly nonlinear, due to the presence of the term $\bar{J}(2H, \bar{\partial}_1^2 2H)$.

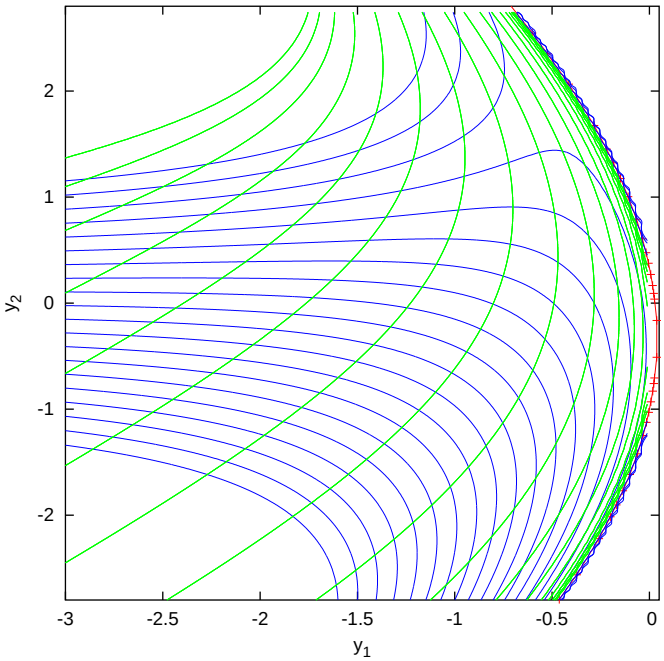

Figure 6.8: The stream lines of the global stream function H (blue lines) and the singular manifold reconstructed from the Fourier data (red points and red line). The superimposed vorticity is represented by green lines.

6.3.3 Geometry of the pseudohydrodynamical flow

The positivity relation, namely that $(-1)^{n+1-\sigma}\hat{G}^{(n)}(\sigma) \geq 0$ for all n, σ except for $n = 0$, $\sigma = 0$, implies that the part of the contour corresponding to the boundary of the amoeba of the singular manifold of $G(\check{z}_1, \check{z}_2)$ lies over the point $(\pi, 0)$. Thus we find it convenient

to give a two-dimensional representation of the functions $H(\bar{z}_1, \bar{z}_2)$ and $\bar{\partial}_1^2 H(\bar{z}_1, \bar{z}_2)$. As expected, it turns out that the general geometrical structure of the flow in the degenerate case $\phi = 0$ is the same as in the case $\phi = \pi/2$, studied in [PMFB06], see Fig. 6.8.

6.4 Some concluding remarks on the two-dimensional Euler equation

6.4.1 Nonuniversal nature of singularities

As we have observed numerically by varying the basic modes $\mathfrak{p}$ and $\mathfrak{q}$, the algebraic prefactor exponent α seems to be independent of the aspect ratio $\eta = |\mathfrak{q}|/|\mathfrak{p}|$, and to depend only on the angle ϕ between the two basic modes. In particular, the extremely clean scaling $\alpha = 5/2$ observed in the limiting case $\phi \to 0$ is the same as the scaling of the solution obtained for the near isosceles case by the $(\eta - 1)$ expansion in 6.2. But even more significantly: the structure of the transseries expansion is the same for both models.

For finite non-vanishing ϕ the scaling exponent is a function $\alpha(\phi)$ of the angle between the initial modes. Numerical results indicate that for $\phi \to \pi$ the scaling exponent approaches the value $\alpha = 3$. Actually, this value is the same as the scaling exponent for the solution of the two-dimensional Burgers equation.

These numerical observations suggest the following heuristic explanation of the angle dependence of α: the essentially flat geometry of the singular manifold for α close to zero (see Fig. 6.9) means that the nonlinearity of the flow is almost completely depleted. Thus, it

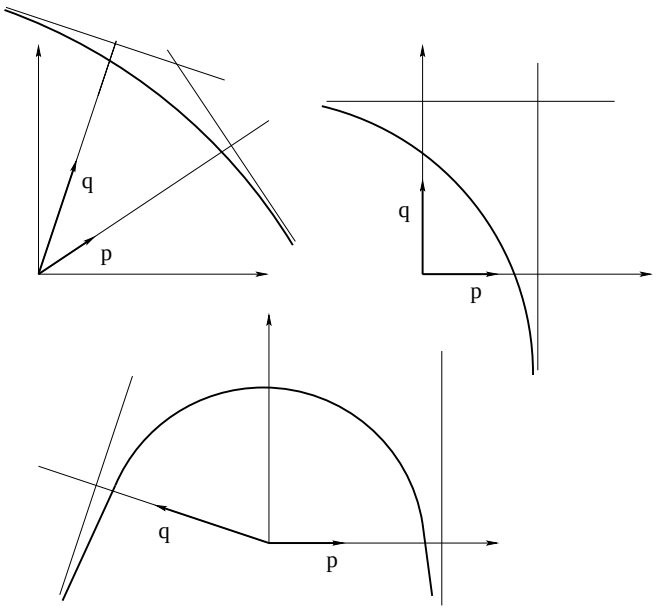

Figure 6.9: Geometry of the singular manifold in dependence on the initial modes $\mathfrak{p}$ and $\mathfrak{q}$.

is not surprising that the nature of the singularities is almost the same as in the linear case. On the contrary, when the singular manifold is strongly curved, almost folded back on itself (see Fig. 6.9), as it is the case for $\phi \to \pi$, the nonlinearity is almost the same as for the Burgers equation which has no depletion phenomenon.

Actually, as has been pointed out by Claude Bardos[2], there is at least one other instance of nonuniversality of solutions of the Euler equation. As is noted in [BT07], solutions

[2]Private communication.

of the Kelvin–Helmholtz problem starting from analytic initial conditions can have almost arbitrary singularities (Proposition 7.2 in [BT07]). The problem setting is of course quite different from the one I studied.

6.4.2 Short-time asymptotic expansion beyond leading order

Until now we were discussing almost exclusively the two-mode initial condition (6.2). However, from the mathematical point of view the most important case is the one in which the initial stream function is real valued. The simplest real-valued initial condition with non-trivial dynamics is the following

$$\Psi_0(z_1, z_2) = \hat{F}(\mathfrak{p})\mathrm{e}^{-\mathrm{i}\,\mathfrak{p}\cdot z} + \hat{F}(\mathfrak{q})\mathrm{e}^{-\mathrm{i}\,\mathfrak{q}\cdot z} + \hat{F}^*(\mathfrak{p})\mathrm{e}^{\mathrm{i}\,\mathfrak{p}\cdot z} + \hat{F}^*(\mathfrak{q})\mathrm{e}^{\mathrm{i}\,\mathfrak{q}\cdot z}. \tag{6.41}$$

As is well known, for $t \to 0$ and $z \to \infty$ the solution $\psi(z)$ behaves as a solution with initial condition of the type (6.2), the exact relationship depending on the ratio y_2/y_1. More precisely, the vectors $\mathfrak{p}$, $\mathfrak{q}$, $-\mathfrak{p}$ and $-\mathfrak{q}$ divide the k-space into four angular sectors. The two basic modes in the initial condition (6.2) are determined by the ratio y_2/y_1, that is y has to be in the sector defined by these two modes.

Thus, depending on the direction of y we get four different asymptotic solutions corresponding to the pairs of modes $(\mathfrak{p}, \mathfrak{q})$, $(-\mathfrak{p}, \mathfrak{q})$ and so on. For short times the sum of these four solutions asymptotically coincides with the solution of (6.1), (6.41). Geometrically these four solutions represent four singularities approaching the real domain following a logarithmical law. Replacing the actual solution by a sum of these four contributions amounts to neglecting the nonlinear interactions between them. One possibility to extend beyond the short-time asymptotic approximation is to make an asymptotic expansion of the solution in powers of $1/t$, analogously to the expansion (5.13) which was used for the Burgers equation. Since the resulting expressions turn out to be somewhat lengthy, we have preferred to give the actual formulae and their derivation in Appendix A.

The obtained system of recursion relations allows us to calculate numerically the space-time Fourier–Taylor coefficients for solutions of the two-dimensional Euler equation with initial conditions (6.41). For the two-dimensional Euler equation we proceed in a way quite analogous to the Burgers case. There is, however, one essential difference: in the case of the Euler equation we did non succeed in finding analytical solutions!

A preliminary numerical study of the higher-order terms in the asymptotic short-time expansion indicates that the positivity of the Fourier coefficients which we have observed for the leading-order term is lost. This loss of positivity is of course due to the interaction of the singularities.

6.5 Supplementary material

Available online at www.sciencedirect.com
SCIENCE DIRECT
Physica D 219 (2006) 40–59
PHYSICA D
www.elsevier.com/locate/physd

Nature of complex singularities for the 2D Euler equation

W. Pauls[a,b], T. Matsumoto[c,a], U. Frisch[a,*], J. Bec[a]

[a] CNRS UMR 6202, Observatoire de la Côte d'Azur, BP 4229, 06304 Nice Cedex 4, France
[b] Fakultät für Physik, Universität Bielefeld, Universitätsstraße 25, 33615 Bielefeld, Germany
[c] Department of Physics, Kyoto University, Katashirakawa Oiwakecho Sakyo-ku, Kyoto 606-8502, Japan

Received 24 October 2005; received in revised form 6 April 2006; accepted 12 May 2006

Communicated by E. Vanden-Eijnden

Abstract

A detailed study of complex-space singularities of the two-dimensional incompressible Euler equation is performed in the short-time asymptotic régime when such singularities are very far from the real domain; this allows an exact recursive determination of arbitrarily many spatial Fourier coefficients. Using high-precision arithmetic we find that the Fourier coefficients of the stream function are given over more than two decades of wavenumbers by $\hat{F}(\boldsymbol{k}) = C(\theta)k^{-\alpha}\mathrm{e}^{-k\delta(\theta)}$, where $\boldsymbol{k} = k(\cos\theta,\ \sin\theta)$. The prefactor exponent α, typically between 5/2 and 8/3, is determined with an accuracy better than 0.01. It depends on the initial condition but not on θ. The vorticity diverges as $s^{-\beta}$, where $\alpha+\beta = 7/2$ and s is the distance to the (complex) singular manifold. This new type of non-universal singularity is permitted by the strong reduction of nonlinearity (depletion) which is associated to incompressibility. Spectral calculations show that the scaling reported above persists well beyond the time of validity of the short-time asymptotics. A simple model in which the vorticity is treated as a passive scalar is shown analytically to have universal singularities with exponent $\alpha = 5/2$.
© 2006 Elsevier B.V. All rights reserved.

Keywords: Euler equation; Singularities

Und es wallet und siedet und brauset und zischt,
Wie wenn Wasser mit Feuer sich mengt,
Bis zum Himmel spritzet der dampfende Gischt,
Und Flut auf Flut sich ohn' Ende drängt...
Friedrich von Schiller, from *Der Taucher* [1]

1. Introduction

A quarter of a millennium has elapsed since Euler published for the first time what is now known as the Euler equations of hydrodynamics [2]. There has not been much celebration but this may just reflect our embarrassment at not having made enough progress. Actually, Leonhard Euler warned us. At the end of his 1755 paper he wrote: "However all that the Theory of fluids holds, is contained in the two equations above, so that in the pursuit of the research we are not lacking the principles of Mechanics, but solely the Analysis, which is not yet cultivated enough for this design: hence we see clearly, which discoveries are left for us to make in this Science, before we can attain a more perfect Theory of the motion of fluids".[1] (A paper in Latin *Principia motus fluidorum*, published a few years after the paper in French, contains the basic equations and was already presented under a different title to the Berlin Academy in 1752.)

Euler considered both the compressible and incompressible cases. Here we are concerned only with the latter which is particularly difficult in view of the global nature of the incompressibility constraint. One of the most important open questions concerning the "analysis" of the Euler equations is the well-posedness: does initially smooth 3D flow, which is known to remain smooth for short times, eventually "blow up",

[1] In French: Cependant tout ce que la Théorie des fluides renferme, est contenu dans les deux équations rapportées cy-dessus, de sorte que ce ne sont pas les principes de Méchanique qui nous manquent dans la poursuite de ces recherches, mais uniquement l'Analyse, qui n'est pas encore assés cultivée, pour ce dessein: et partant on voit clairement, quelles découvertes nous restent encore à faire dans cette Science, avant que nous puissions arriver à une Théorie plus parfaite du mouvement des fluides.

* Corresponding author. Tel.: +33 4 92003035; fax: +33 4 92003058.
E-mail address: uriel@obs-nice.fr (U. Frisch).

0167-2789/$ - see front matter © 2006 Elsevier B.V. All rights reserved.
doi:10.1016/j.physd.2006.05.011

that is become singular in a finite time (see, e.g. Refs. [3,4])? In two dimensions it has been known since the 1930's that flow in a bounded domain, initially sufficiently smooth, never blows up [5,6]. It was also shown that if such a 2D flow is initially analytic it will stay so forever [7–9]. However, in the course of time, such flow can develop very fine scales and there is a large discrepancy between the analytic estimation of how the smallest scale decreases in time (a double exponential) and what is found in numerical simulations (a simple exponential; see, e.g., Ref. [10]).

The likely cause of the discrepancy is *depletion*, the phenomenon by which high-Reynolds number or inviscid incompressible flow tends to organize itself into structures having vastly reduced nonlinearities (see, e.g., Ref. [11]). Depletion, which is still very poorly understood, may hold the key for understanding why 3D high-Reynolds number flow seems never to blow up, at least in simulations.[2] In this paper we shall focus on the two-dimensional case.

There are well-known 2D examples of depletion, such as flows which depend only on one Cartesian coordinate or on the radial polar coordinate. Such flows are however steady and thus globally depleted, with no dynamics. In this paper we shall be interested in 2D flow with an initial stream function which is a real trigonometric polynomial in the space variables, of the sort already considered in Refs. [4,12]. These are the 2D counterparts of well-known 3D flows such as Taylor–Green and Kida–Pelz [13–17] which have been used for (so far inconclusive) investigation of finite-time blow-up. Our 2D flows have generally non-trivial dynamics and display locally very strong depletion.

Trigonometric polynomials are instances of entire functions, that is, functions which are analytic in the whole complex domain. The only singularities of such functions are at complex infinity. The solution of the Euler equations at times $t > 0$ sufficiently small can then be extended analytically into the complex domain [7–9]. There is strong numerical evidence in 2D and also in 3D that such flow does not stay entire and develops singularities at certain complex locations for any $t > 0$ [10,14,4,12]. Complex singularities are usually detected through the Fourier transforms of the solution: roughly, there is an exponential tail related to the distance of the nearest singularity from the real domain, accompanied by an algebraic prefactor related to the nature (also called type or structure) of the singularities.

Little is known about the nature of complex singularities of the Euler equations. In Refs. [4] and [12] it is shown numerically for the 2D case with the initial stream function $\cos x_1 + \cos 2x_2$ that the complex singularities lie on a smooth manifold and that the vorticity becomes infinite when approaching the singular manifold; there is however considerable uncertainty as to the scaling law of this divergence. In Ref. [18] the motion of preexisting complex-space singularities is studied analytically but their nature is kept quite arbitrary. In Ref. [19] traveling-wave solutions with a pure imaginary velocity are studied for 3D axisymmetrical flow with swirl; using an ultra-high precision[3] numerical method, the singularities in the complexified axial variable are mapped out as a function of the (real) radial variable and found to lie on a smooth curve; the nature of the singularities is obtained using a "sliding fit" method. In Ref. [20], for the vortex sheet problem with an initially analytic interface, the nature of complex singularities of the interface is obtained using an ultra-high precision method and a "pointwise fit". The sliding fit and the pointwise fit are very closely related to the method we use in Section 3.1 and we shall come back to this matter. Since the work of Krasny [21], it appears that ultra-high precision is a prerequisite for obtaining numerical information on the nature of singularities, particularly when they are in the complex domain.

From a *theoretical* point of view, for many nonlinear equations of mathematical physics a very successful tool in studying the nature of singularities has been dominant balance and its refined versions such as Painlevé analysis [22]. Dominant balance analysis typically gives *universal* singularities, that is singularities whose positions may depend on the initial conditions but their nature does not. The simplest instance is the 1D viscous Burgers equation whose complex-space singularities are simple poles, obtainable by balancing the nonlinear term against the viscous one. For the d-dimensional incompressible Euler equations, attempts to use dominant balance fail because of the particular structure of the nonlinearity: if we assume that the solution becomes singular on a complex manifold of dimension $d - 1$, the nonlinearity vanishes to leading order. This is just a consequence of the simplest form of depletion, the vanishing of nonlinearity for solutions which depend on a single spatial coordinate. The nature of singularities cannot be obtained by a dominant balance argument; actually, as we shall see, complex singularities of the 2D Euler equation display a very unusual *non-universality*.

In this paper we will mainly discuss the *short-time asymptotic régime* presented in Ref. [4] and extensively used in Ref. [12] which gives us the most accurate information on the nature of complex singularities.[4] After briefly introducing it in Section 2 we will show that this régime can be reformulated as a "pseudo-hydrodynamic" Euler problem, in which all the action including the singularities takes place in a plane extending in the pure imaginary directions, but our usual hydrodynamic intuition is still applicable. The short-time asymptotics allows us to obtain recurrence relations for spatial Fourier components involving only wavectors $\boldsymbol{k} = (k_1, k_2)$ with $k_1 \geq 0$ and $k_2 \geq 0$, a feature which is also present in the Moore approximation for vortex sheets [23] and its generalization to smooth flow [19]; as a consequence Fourier components can be calculated in ultra-high precision without any truncation error. In Section 3 we present the numerical evidence for simple scaling laws

[2] For the case of 3D inviscid Euler flow there is no truly conclusive evidence in favor of blow-up [4,17]. Furthermore, if the flow is initially analytic, any real singularity will have to be preceded by complex-space singularities [8,9].

[3] That is, higher than double precision.

[4] Henceforth, Ref. [12] will be cited as MBF.

associated to complex singularities and determine the nature of the singularities with high precision. Analyzing short-time asymptotics for different initial conditions, we find that the singularities are non-universal. In Section 4 we describe the global and local geometry of the pseudo-hydrodynamic flow, including depletion of nonlinearity which is especially strong near the singularities.

Sections 3 and 4 both involve a mixture of numerical results and of theoretical arguments, some heuristic, some more rigorous. We must stress that at the moment we do understand various features of the solution, in particular why the scaling exponent for singularities does not depend on the direction, but we failed so far to reproduce by theory the non-universal scaling exponents observed for the singularities. Nevertheless by moving to yet another level of toy-modeling (the equivalent for our problem of considering the vorticity as a passive scalar in a prescribed velocity field), we can determine the nature of the corresponding complex singularities using dynamical systems tools (Section 5). The nature of these "advection" singularities is however universal and therefore does not reproduce an essential feature of the nonlinear Euler flow. Finally, conclusions, open problems and a tentative road map for future research on blow-up are presented in Section 6. To make the present paper reasonably self-contained we shall occasionally re-derive results already found in Ref. [4] and MBF.

2. Short-time asymptotics and pseudo-hydrodynamics

We are interested in the short-time asymptotics for the 2D Euler equation, written in terms of the stream function

$$\partial_t \nabla^2 \Psi(\boldsymbol{x}, t) - J(\Psi, \nabla^2 \Psi) = 0, \tag{1}$$

where $\boldsymbol{x} = (x_1, x_2)$ and $J(f, g) \equiv \partial_1 f \partial_2 g - \partial_1 g \partial_2 f$. The initial condition $\Psi_0(\boldsymbol{x}) \equiv \Psi(\boldsymbol{x}, 0)$ is a real 2π-periodic trigonometric polynomial of the form $\Psi_0(\boldsymbol{x}) = \sum_{\boldsymbol{k}} \hat{F}^{(0)}(\boldsymbol{k})\, \mathrm{e}^{\mathrm{i}\boldsymbol{k}\cdot\boldsymbol{x}}$, where the sum has only a finite number of terms. Here $\boldsymbol{k} = (k_1, k_2)$, where k_1 and k_2 are signed integers. The short-time asymptotics is simplest when the initial condition has only two orthogonal Fourier modes, as in Refs. [4,12] where the assumed initial condition is

$$\Psi_0(\boldsymbol{x}) = \cos x_1 + \cos 2x_2. \tag{2}$$

In what follows we shall call this initial condition the Standard Orthogonal Case (SOC). One of our present goals is to investigate to what extent complex singularities are or are not universal; we are thus naturally led to considering more general cases, having, for example, more than two modes in the initial conditions. In the Appendix it will be shown that the short-time asymptotic régime for the multimode case can be reduced to a set of two-mode initial conditions. We may thus without loss of generality limit ourselves to two-mode initial conditions of the form

$$\Psi_0(\boldsymbol{x}) = h_1\, \mathrm{e}^{\mathrm{i}\,\mathfrak{p}\boldsymbol{x}} + h_2\, \mathrm{e}^{\mathrm{i}\,\mathfrak{q}\boldsymbol{x}} + \text{c.c.} \tag{3}$$

Here c.c. stands for "complex conjugate", $\mathfrak{p} = (\mathfrak{p}_1, \mathfrak{p}_2)$ and $\mathfrak{q} = (\mathfrak{q}_1, \mathfrak{q}_2)$ are two vectors with signed integer components. Furthermore, we assume that $\mathfrak{p}$ and $\mathfrak{q}$ are not parallel and do not have the same modulus since otherwise the two-mode initial condition is a time-independent solution of the Euler equation. By performing if needed a suitable translation, we can then assume that h_1 and h_2 are positive. Finally, since our goal here is primarily to demonstrate non-universality of the nature of the singularities with respect to the initial conditions, we shall not strive for the greatest generality and limit ourselves to *basic modes* with non-negative components such that $\mathfrak{p}_1\mathfrak{q}_2 - \mathfrak{q}_1\mathfrak{p}_2 > 0$.

Eq. (1) has a solution in the form of a Taylor series in the time variable

$$\Psi(\boldsymbol{x}, t) = \sum_{n\geq 0} \Psi_n(\boldsymbol{x})\, t^n, \tag{4}$$

where Ψ_0 is the initial condition and the $\Psi_n(\boldsymbol{x})$'s for $n \geq 1$ are easily shown to satisfy the recursion relations:

$$\nabla^2 \Psi_{n+1} = \frac{1}{n+1} \sum_{m+p=n} J(\Psi_m, \nabla^2 \Psi_p). \tag{5}$$

For the two-mode initial condition (2) all the $\Psi_n(\boldsymbol{x})$ are trigonometric polynomials that can be continued analytically to complex locations $\boldsymbol{z} = \boldsymbol{x} + \mathrm{i}\,\boldsymbol{y}$. Since the initial condition has its singularities at infinity, we expect, by continuity, that at short times the singularities will have large imaginary parts $|y_1|$ and $|y_2|$. Let us now suppose that $y_1 \to +\infty$ and $y_2 \to +\infty$ in such a way that their ratio y_2/y_1 stays finite but arbitrary. Obviously, the four vectors $(\mathfrak{p}_1, \mathfrak{p}_2)$, $(-\mathfrak{p}_1, -\mathfrak{p}_2)$, $(\mathfrak{q}_1, \mathfrak{q}_2)$ and $(-\mathfrak{q}_1, -\mathfrak{q}_2)$ divide the $\boldsymbol{k}$-space into four angular sectors so that, for example, in the first angular sector $\mathfrak{p}_2/\mathfrak{p}_1 \leq y_2/y_1 \leq \mathfrak{q}_2/\mathfrak{q}_1$. Then, for $\boldsymbol{z}$ such that $\boldsymbol{y}$ lies in the first angular sector, to leading order any additional factor t in the expansion (4) is accompanied by either a factor $\mathrm{e}^{-i\,\mathfrak{p}\boldsymbol{z}}$ or a factor $\mathrm{e}^{-i\,\mathfrak{q}\boldsymbol{z}}$, thus giving amplitude factors $t\mathrm{e}^{\mathfrak{p}\boldsymbol{y}}$ and $t\mathrm{e}^{\mathfrak{q}\boldsymbol{y}}$, respectively. When $t \to 0$ and $|\boldsymbol{y}| \to \infty$ these factors remain finite, provided $\mathfrak{p}\cdot\boldsymbol{y}$ and $\mathfrak{q}\cdot\boldsymbol{y}$ are shifted by $\ln t$. This suggests that the short-time asymptotics is obtained by the *similarity ansatz*

$$\Psi(\boldsymbol{z}, t) = (1/t) F(\tilde{\boldsymbol{z}}), \tag{6}$$

$$\tilde{\boldsymbol{z}} = (\tilde{z}_1, \tilde{z}_2) \equiv (z_1 + \mathrm{i}\,\lambda_1 \ln t,\ z_2 + \mathrm{i}\,\lambda_2 \ln t), \tag{7}$$

where λ_1 and λ_2 are determined by

$$\lambda_1 = \frac{\mathfrak{p}_2 - \mathfrak{q}_2}{\mathfrak{q}_1\mathfrak{p}_2 - \mathfrak{q}_2\mathfrak{p}_1} \quad \text{and} \quad \lambda_2 = \frac{\mathfrak{q}_1 - \mathfrak{p}_1}{\mathfrak{q}_1\mathfrak{p}_2 - \mathfrak{q}_2\mathfrak{p}_1}. \tag{8}$$

Substitution in (1) gives the *similarity equation*

$$\tilde{\nabla}^2(-1 + \mathrm{i}\,\lambda_1\tilde{\partial}_{z_1} + \mathrm{i}\,\lambda_2\tilde{\partial}_{z_2})F = \tilde{J}(F, \tilde{\nabla}^2 F), \tag{9}$$

where the tilde means that the partial derivatives are taken with respect to the new variables. The initial condition (2) becomes an asymptotic boundary condition

$$F(\tilde{\boldsymbol{z}}) \simeq h_1 \mathrm{e}^{-\mathrm{i}\,\mathfrak{p}\tilde{\boldsymbol{z}}} + h_2 \mathrm{e}^{-\mathrm{i}\,\mathfrak{q}\tilde{\boldsymbol{z}}}, \quad \tilde{y}_1 \to -\infty, \tilde{y}_2 \to -\infty. \tag{10}$$

In (9) the second and third terms on the l.h.s. can be viewed as stemming from the advection by a pure imaginary constant "drift velocity". This is because we are following

the singularities coming "down" from complex infinity. It is important to observe that (9) is an exact consequence of the Euler equation. The only place where an approximation is made is in the boundary condition (10) where harmonics containing for example $e^{+i\,\mathbf{p}\tilde{z}}$ and $e^{+i\,\mathbf{q}\tilde{z}}$ are discarded because such terms are exponentially subdominant at short times.

In what follows we shall generally limit ourselves to the SOC, giving occasionally an indication of what is valid for more general two-mode cases. The general case can easily be handled but we wish to avoid burdening the reader with unnecessarily complicated statements and equations.

The function $F(\tilde{z})$, which is 2π-periodic in $\tilde{x}_1$ and π-periodic in $\tilde{x}_2$, is analytic in the product of the half-spaces $\tilde{y}_1 \le 0$ and $\tilde{y}_2 \le 0$ and thus its spatial Fourier series has only harmonics of the form $e^{-i\,(k_1\tilde{z}_1+k_2\tilde{z}_2)}$ with $k_1 \ge 0$ and $k_2 \ge 0$. Its Fourier series is here written as[5]

$$F(\tilde{z}_1,\tilde{z}_2) = \sum_{k_1=0}^{\infty}\sum_{k_2=0}^{\infty}(-1)^{k_1}\hat{F}(k_1,k_2)e^{-i\,k_1\tilde{z}_1}e^{-i\,k_2\tilde{z}_2}. \tag{11}$$

The reason for the presence of the factor $(-1)^{k_1}$ will become clear shortly. The Fourier coefficients $\hat{F}(\boldsymbol{k}) \equiv \hat{F}(k_1,k_2)$ can be calculated recursively from the relation given in MBF which follows from (9)

$$\hat{F}(k_1,k_2) = -\frac{1}{k_1+k_2/2-1}\,\frac{1}{|\mathbf{k}|^2} \times \sum_{p_1=0}^{k_1}\sum_{p_2=0}^{k_2}(\mathbf{p}\wedge\mathbf{k})|\mathbf{k}-\mathbf{p}|^2\hat{F}(p_1,p_2)\hat{F}(k_1-p_1,k_2-p_2). \tag{12}$$

Here, $\mathbf{p}\wedge\mathbf{k} \equiv p_1k_2 - p_2k_1$. Because there are no Fourier harmonics with negative k_1 or k_2, the convolutions in (12) only involve positive arguments. This feature, which allows truncation-free determination of Fourier coefficients, is also present in the Moore approximation for the vortex sheet problem and in its generalization to axisymmetrical flow [19, 23]. The initialization of the recursion relations requires the knowledge of the coefficients along the "edges", that is the half-lines $k_1 = 0$ and $k_2 = 0$. In the present case $\hat{F}(0,2) = 1/2$ and $\hat{F}(1,0) = -1/2$ while all the other edge harmonics are zero.[6] It has been shown in MBF that, with the choice made above in (11), the coefficient $\hat{F}(1,0)$ is the only one that is negative. All the other ones are non-negative. This result has so far only been established by (very solid) numerical computations and holds for all the two-mode initial conditions studied. As we shall see, this has important consequences for the geometry of singularities.

We shall now show that (9) can be reformulated as the steady solution of a *pseudo-hydrodynamic* problem in a suitable imaginary plane. Since we are working with analytic functions, we can replace the complex partial derivatives $\tilde{\partial}_{z_1}$ and $\tilde{\partial}_{z_2}$ by $-i\,\tilde{\partial}_{y_1}$ and $-i\,\tilde{\partial}_{y_2}$, holding the x-coordinates fixed. In terms of such y-derivatives (9) becomes an equation with real coefficients. If we furthermore choose x_1 and x_2 such that the boundary condition (10) becomes real then the solution "above such points" F is also real. This happens for $x_1 = 0, \pi$ and for $x_2 = 0, \pi/2, \pi, 3\pi/2$. The positivity of all but one of the Fourier coefficients defined in (11) with the factor $(-1)^{k_1}$ amounts to stating that, after moving the origin to $(\pi, 0)$, all but one of the usual Fourier coefficients of F are positive. As we shall see in Section 4, this gives us the possibility of analyzing the (short-time) complex singularities by focusing solely on the y-plane above $(\pi, 0)$. This point turns out also to be a center of symmetry for the Euler flow with the initial condition (2), but it is not clear whether this matters.[7] Henceforth we shall consider the y-plane above $(\pi, 0)$.

We define a pseudo-stream function in terms of the y-coordinates (from now on we drop the tilde on the y variables for notational simplicity)

$$\psi(\boldsymbol{y}) = \psi(y_1,y_2) \equiv \frac{1}{2}y_1 - y_2 + F(\pi + i\,y_1, i\,y_2), \tag{13}$$

$$= \frac{1}{2}y_1 - y_2 + \sum_{\boldsymbol{k}}\hat{F}(\boldsymbol{k})\,e^{\boldsymbol{k}\cdot\boldsymbol{y}}, \tag{14}$$

where the two linear terms on the r.h.s. have been introduced to avoid having an additional advection term. Note that because of these terms, ψ is not the continuation to complex coordinates of a function periodic in x_1 and x_2.

It is now elementary to check that (9) and (10) are equivalent to taking the steady-state (τ-independent) solution of the pseudo-hydrodynamic equation

$$\partial_\tau\nabla^2\psi - J(\psi,\nabla^2\psi) = -\nabla^2\psi, \tag{15}$$

with the asymptotic boundary condition (for $y_1,\ y_2 \to -\infty$)

$$\psi(y_1,y_2) - \frac{1}{2}y_1 + y_2 \simeq -\frac{1}{2}e^{y_1} + \frac{1}{2}e^{2y_2}. \tag{16}$$

Here, in order to bring out familiar hydrodynamic notation, we have introduced a pseudo-time variable τ.[8] We are using $\nabla = (\partial_1,\ \partial_2)$ for ∇_y and the Jacobian J has its usual definition in terms of y-derivatives. We now introduce a pseudo-velocity and a pseudo-vorticity by the usual definitions[9]:

$$\boldsymbol{v} = (v_1,v_2) \equiv (\partial_2\psi, -\partial_1\psi) \tag{17}$$

$$= -(1,1/2) + \sum_{\boldsymbol{k}}(k_2,-k_1)\,\hat{F}(\boldsymbol{k})\,e^{\boldsymbol{k}\cdot\boldsymbol{y}}, \tag{18}$$

$$\omega \equiv -\nabla^2\psi, \tag{19}$$

$$= \sum_{\boldsymbol{k}} -k^2\,\hat{F}(\boldsymbol{k})\,e^{\boldsymbol{k}\cdot\boldsymbol{y}}, \tag{20}$$

[5] In MBF k_1 and k_2 were defined with the opposite sign.

[6] In the general case of two basic modes $\mathbf{p}$ and $\mathbf{q}$, the main change with respect to the SOC is the replacement in (12) of the denominator $k_1 + k_2/2 - 1$ by $\lambda_1k_1 + \lambda_2k_2 - 1$, where λ_1 and λ_2 are defined in (8).

[7] Note that streamlines have a hyperbolic structure near $(\pi, 0)$, but an elliptic structure near $(0, 0)$ which is also a center of symmetry.

[8] If we allow the function F and thus ψ to also depend on t and set $\tau = \ln(1/t)$, we obtain precisely (15).

[9] The true velocity is actually pure imaginary in the y-plane and the true vorticity is $-\omega$.

in terms of which (15) reads

$$[\partial_\tau \omega] + \boldsymbol{v} \cdot \nabla \omega + \omega = 0, \tag{21}$$

with the boundary conditions (for $y_1,\ y_2 \to -\infty$)

$$\boldsymbol{v} \simeq \left(-1,\ -\frac{1}{2}\right), \quad \omega \simeq \frac{1}{2}\mathrm{e}^{y_1} - 2\mathrm{e}^{2y_2}. \tag{22}$$

For other initial conditions, only the boundary condition (22) must be modified. The τ-derivative term has been put within square brackets since we are only interested in the steady-state solution. Note that the pseudo-hydrodynamic formulation in the y-plane is that of a quasi-two-dimensional flow in a 3D container with bottom friction producing a Rayleigh drag. In this formulation $\tau \to +\infty$ as we approach the initial instant. An alternative interpretation is to define τ as $\ln t$, to avoid reversing the course of time, and then to change the signs of $\boldsymbol{v}$ and of ω and replace the Rayleigh drag by an instability.

In the pseudo-hydrodynamic formulation it is now obvious that the problem is invariant under an arbitrary translation $\boldsymbol{h} = (h_1,\ h_2)$ in y-space. By (14), such a translation amounts to a factor $\mathrm{e}^{\boldsymbol{k}\cdot\boldsymbol{h}}$ on the Fourier coefficients $\hat{F}(\boldsymbol{k})$. It follows, as noted in MBF, that the set of initial conditions $\Psi_0(\boldsymbol{x}) = \mathrm{e}^{h_1}\cos x_1 + \mathrm{e}^{2h_2}\cos 2x_2$ is equivalent to the SOC as long as $\boldsymbol{h}$ is within the analyticity domain. Similarly, a translation in k-space with integer components $(n_1,\ n_2)$ is equivalent to multiplying $F(\pi + \mathrm{i}\, y_1,\ \mathrm{i}\, y_2)$ by the exponential factor $\mathrm{e}^{n_1 y_1 + n_2 y_2}$ in y-space. The exponential being an entire function, this changes neither the positions nor the nature of the singularities at finite distance.

3. Numerical investigation of scaling laws in Fourier space

We shall show in this section that the solution of the Euler equation in the short-time asymptotic régime defined in the previous section has remarkably clean scaling properties in Fourier space. By this we mean that the wavenumber dependence of the Fourier coefficients is represented as a decreasing exponential multiplied by an algebraic prefactor whose exponent can be measured very accurately. Such a functional form is not surprising. In fact the exponential is the signature of the location of a singularity while the prefactor encodes the nature of the singularity. For one-dimensional analytical functions with isolated singularities in the complex space this is well known: a singularity at $z_\star$ of the form $(z - z_\star)^\rho$ has a signature in the modulus of the Fourier transorm at high wavenumbers k of the form $C|k|^{-\rho-1}\mathrm{e}^{-\delta|k|}$, where δ is the distance of $z_\star$ to the real axis (see, e.g., Ref. [24]). Such asymptotic results have been extended in the 1990's to the Fourier transforms of periodic analytical functions of several complex variables when the wavevector $\boldsymbol{k}$ tends to infinity with a fixed rational slope $\tan\theta = k_2/k_1 = p/q$, where p and q are relative prime integers [25–27].

When the Fourier coefficients are obtained numerically, there is a maximum wavenumber $k_{\max}$. Unless it is taken very large, there will be very few points on the line of slope p/q as soon as q is not a very small integer. But a large value of $k_{\max}$ entails extremely small Fourier coefficients because of the exponential decrease with the wavenumber. Thus, as stressed in MBF, very high precision may be needed to avoid swamping by the rounding errors. Truncation errors are not an issue in the short-time asymptotic régime since the Fourier coefficients can be calculated from (12) with arbitrary accuracy.

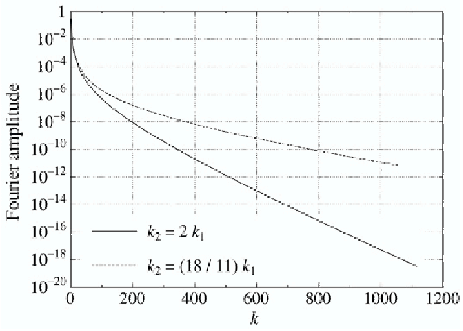

Fig. 1. Fourier coefficients of the stream function F along two lines of different slopes as a function of $k \equiv |\boldsymbol{k}|$ in lin–log coordinates.

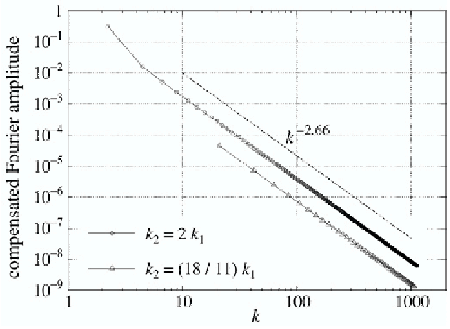

Fig. 2. Same as in Fig. 1 after division by $\exp(-\delta k)$ (compensated Fourier coefficients) in log–log coordinates. Most of the points are in the asymptotic power-law régime, at least visually.

The data obtained for the SOC initial condition in MBF had wavenumbers $k \equiv |\boldsymbol{k}|$ up to 1000 or 2000, depending on the direction and were calculated with 35-digit accuracy.[10] Most of the results presented here are based on the 35-digit calculation. Additional calculations are also presented here with various initial conditions, with up to 100-digit precision and wavenumbers which can reach 4000 in particular directions. We note that the MPFUN90 package for high-precision calculation used in MBF, here and in Ref. [19] makes use of fast Fourier transform techniques. Thus the CPU time per multiplication, as a function of the number of digits N, is proportional to $N \log N$ [28].

We now show that it is quite easy in principle to observe scaling by analyzing the behavior of the Fourier coefficients in directions of rational slope. Figs. 1 and 2 give two examples of the analysis of Fourier coefficients along straight lines through

[10] In MBF it was stated that, when using only double-precision (15-digit) accuracy, unacceptably large errors are obtained beyond wavenumber 800. Actually, as pointed out by Zimmermann (private communication), the double-precision calculation can be modified in such a way that, up to wavenumber 1000, the relative error on Fourier modes does not exceed 10^{-5}.

the origin[11] in a direction of rational slope, using the data from MBF for the Fourier coefficients of the stream function with SOC initial conditions. The first case has $k_2/k_1 = 2$, the direction with the largest number of grid points having non-vanishing Fourier coefficients. The second case has $k_2/k_1 = 18/11$, the direction with the slowest decrease of the Fourier coefficients. Fig. 1, which shows the Fourier coefficients in lin–log coordinates, reveals an exponential tail $\propto \mathrm{e}^{-\delta k}$; a least square fit gives $\delta = 0.021$ for the first case and $\delta = 0.0065$ for the second case.[12] In Fig. 2 we show the "compensated" Fourier coefficients obtained by dividing by the exponential term; the result is then represented in log–log coordinates in order to look for an algebraic prefactor $\propto k^{-\alpha}$. The quality of the scaling obtained is impressive: over most of the range we cannot on a log–log plot visually distinguish the prefactor from a power law with exponent $\alpha = 8/3$. As we shall see, the exponent does not depend on the direction chosen.

3.1. Technique for capturing algebraic prefactors

Determining the scaling properties as done above by use of least square fits, compensating exponentials and log–log plots is not optimally adapted for delicate issues such as studying the dependence of the prefactor exponent on the direction of the wavector or on the initial conditions. As pointed out by Shelley [20], it is better to remove some of the subjective biases present in a least square fit (such as choosing the range in k). We shall make use of his method of point-wise fit (also used in Ref. [19], where it is called a sliding fit), followed by an extrapolation step as now explained.

In $\boldsymbol{k}$-space, a direction of rational positive slope is characterized by $k_2/k_1 = \tan\theta = q/p$ (where the positive integers p and q are taken to be relative primes). All the $\boldsymbol{k}$ vectors on the line of slope p/q through the origin are thus of the form $\boldsymbol{k} = n\boldsymbol{k}_0$, where $\boldsymbol{k}_0 \equiv (p, q)$ and n is a positive integer. What we have seen at the beginning of Section 3 suggests that for a given direction of rational slope $\tan\theta$, the Fourier coefficients of the stream function can be represented, for sufficiently large k, as

$$\hat{F} \simeq C(\theta) k^{-\alpha(\theta)} \mathrm{e}^{-\delta(\theta)k}. \tag{23}$$

Henceforth α, C and δ will be referred to as the prefactor exponent, the constant and the decrement, respectively. When there is no ambiguity, the θ-dependence will be omitted. Following Ref. [20], let us assume for a moment that (23) holds exactly and let us set $\hat{F}_n(\boldsymbol{k}_0) \equiv \hat{F}(n\boldsymbol{k}_0)$. It then follows that if we know $\hat{F}_n(\boldsymbol{k}_0)$ for any three consecutive values, say $n-1$, n and $n+1$, we can determine C, α and δ by

$$\alpha = \frac{\ln\left(\frac{\hat{F}_{n-1}(\boldsymbol{k}_0)\hat{F}_{n+1}(\boldsymbol{k}_0)}{\hat{F}_n^2(\boldsymbol{k}_0)}\right)}{\ln\left(\frac{n^2}{(n-1)(n+1)}\right)}, \tag{24}$$

[11] All the lattice lines of a given rational slope have the same high-k asymptotics, due to the observation made at the end of Section 2.

[12] Why the minimum value is so small is a matter we shall come back to in Section 5.

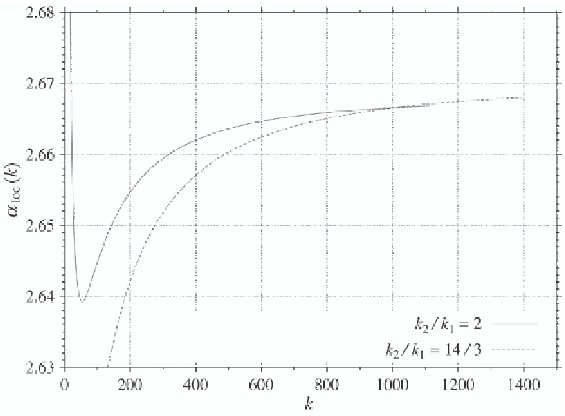

Fig. 3. Local prefactor exponent $\alpha_{\mathrm{loc}}(k)$ versus wavenumber for two values of the slope.

$$\delta = \frac{1}{|\boldsymbol{k}_0|}\left[\ln\left(\frac{\hat{F}_n(\boldsymbol{k}_0)}{\hat{F}_{n+1}(\boldsymbol{k}_0)}\right) + \alpha \ln\left(\frac{n}{n+1}\right)\right], \tag{25}$$

$$\ln C = \ln \hat{F}_n(\boldsymbol{k}_0) + \alpha \ln[(n)|\boldsymbol{k}_0|] + n|\boldsymbol{k}_0|\delta. \tag{26}$$

The expression (24) for α follows immediately by noticing that in the combination $\hat{F}_{n-1}\hat{F}_{n+1}/\hat{F}_n^2$ the constant C and the exponential factor both drop out. The other two expressions are readily established by taking the logarithm of (23).

Of course, we have no reason to expect that (23) holds *exactly* for arbitrary wavenumbers. At best it will hold asymptotically at large wavenumbers. Nevertheless we can use (25) *and* (26) to calculate a *local prefactor exponent* $\alpha_{\mathrm{loc}}(k)$, which depends on the wavenumber. Here we have chosen to use as arguments of the local quantities the wavenumber $k = n|\boldsymbol{k}_0|$.

The typical behavior of $\alpha_{\mathrm{loc}}(k)$ is shown in Fig. 3 for two directions. For large values of k the curves grow to an asymptotic value close to 8/3. Globally, $\alpha_{\mathrm{loc}}(k)$ is found to be non-monotonic when $\theta < \theta_\star$ with $\tan\theta_\star$ close to 3 (but not very sharply defined) and monotonic above $\theta_\star$.

To estimate the asymptotic value α_∞ we must *extrapolate* the data beyond the largest available wavenumber at which they are known with acceptable accuracy. Since the only causes of error in $\alpha_{\mathrm{loc}}(k)$ are rounding errors, we can measure such errors by comparing runs having different levels of precision. Fig. 4 shows the discrepancy (absolute error) of $\alpha_{\mathrm{loc}}(k)$ obtained with 15- and 35-digit precision. The error is seen to grow with the wavenumber in an approximately exponential fashion, the highest value being about 10^{-8} around wavenumber 1000. We shall see that the error involved in the extrapolation may be much larger than 10^{-8}.

One well-known difficulty with extrapolation is that the problem may not be well-posed unless one has additional information on the functional form of the convergence to zero of the remainder $\alpha_\infty - \alpha_{\mathrm{loc}}(k)$. In Ref. [20], which deals with the shape of a vortex sheet continued analytically to complex parameters, it is assumed that branch singularities of unknown exponent are present and that the high-k behavior of the one-dimensional Fourier transform can be obtained from Laplace's

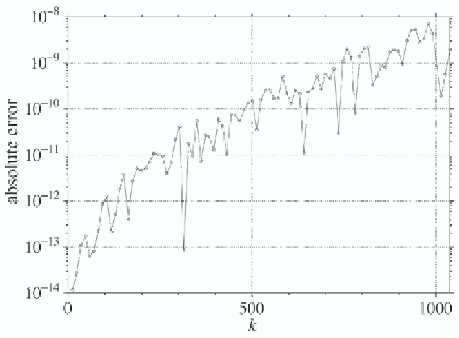

Fig. 4. Discrepancy between 15- and 35-digit calculation of the local prefactor exponent $\alpha_{\rm loc}(k)$ along $k_2/k_1 = 5/3$, as an estimate of the absolute error on $\alpha_{\rm loc}$.

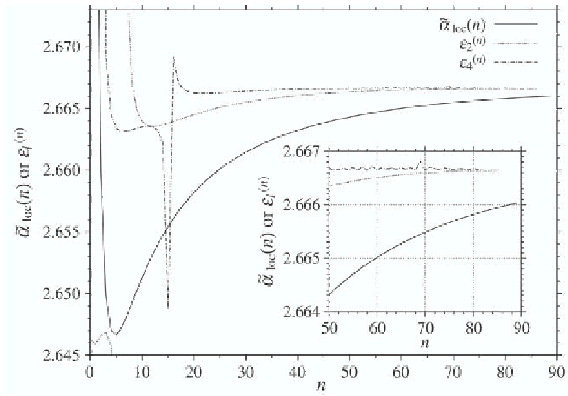

Fig. 5. Local prefactor exponent $\tilde{\alpha}_{\rm loc}(n)$ for the nth point along the line $k_2/k_1 = 5/3$ which has $(k_1, k_2) = (5n, 3n)$; it is shown together with its second- and fourth-order epsilon-algorithm extrapolated values. Inset: enlargement for $n > 50$.

method to leading and first subleading orders; the inclusion of the first subleading correction allows a much improved determination of the exponent. This extrapolation procedure is equivalent to assuming that the remainder $\alpha_\infty - \alpha_{\rm loc}(k)$ goes to zero as $1/k$. For our problem, unfortunately no simple functional form of the remainder, such as algebraic, exponential or inverse logarithmic decrease, gives a satisfactory fit. An efficient extrapolation method for a wide range of functional behaviors of the remainder is the *epsilon algorithm* of Wynn [29], related to the Shanks transform method [30]. It is an algorithm for acceleration of convergence of a sequence $S = (s^{(0)}, s^{(1)}, s^{(2)}, \ldots, s^{(i)}) \in \mathbb{C}$, and it comprises the following initialization and iterative phases.

Initialization: For $n = 0, 1, 2, \ldots$

$$\varepsilon_{-1}^{(n)} = 0 \quad \text{(artificially)}, \quad \varepsilon_0^{(n)} = s^{(n)}. \tag{27}$$

Iteration: For $n = 0, 1, 2, \ldots$

$$\varepsilon_{l+1}^{(n)} = \varepsilon_{l-1}^{(n+1)} + [\varepsilon_l^{(n+1)} - \varepsilon_l^{(n)}]^{-1}. \tag{28}$$

After a few iterations of the algorithm, applied to 35-digit SOC data, the $\varepsilon_l^{(n)}$'s with even l become almost constant and give an estimate of the *extrapolated exponents* (see Fig. 5). The epsilon-algorithm extrapolated exponents will be used when discussing results (unless otherwise stated). We have also used the recently introduced asymptotic interpolation method of van der Hoeven [31] which strips off successively leading and subleading terms by suitable transformations before doing the interpolation. This method works impressively for the passive scalar model discussed in Section 5 for which both leading and subleading terms in the high-k expansion can be determined from numerical data. In the nonlinear case, the asymptotic interpolation method gives exponents consistent with those determined by the epsilon algorithm with a relative error of about 10^{-3}; we have so far not been able to determine numerically the functional form of subleading corrections. As we shall see in Section 4.3, theory tells us that α should not depend on the angle θ. We suspect that θ-dependent subleading corrections account for the slight apparent variation of α with θ, reported in Section 3.2.

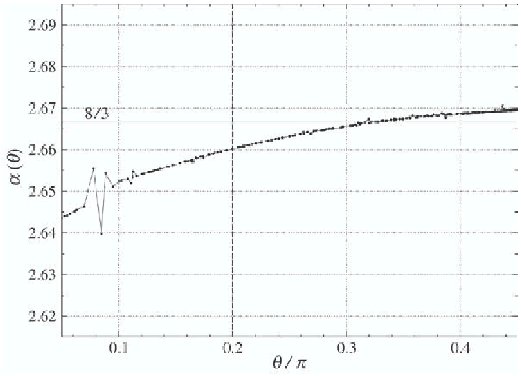

Fig. 6. Angular dependence of the prefactor exponent $\alpha(\theta)$ for the SOC (extrapolated by the epsilon algorithm). Below $\theta = 0.2\pi$ (long dashed line) the extrapolation cannot be trusted.

3.2. Results for the SOC

For the SOC, whose initial stream function is $\cos x_1 + \cos 2x_2$, we now use the method described in Section 3.1 to calculate the prefactor exponent $\alpha(\theta)$, the decrement $\delta(\theta)$ and the constant $C(\theta)$.

Figs. 6–8 show the angular variation of α, δ and C, respectively, excluding near-edge ranges where θ is close to 0 or $\pi/2$ which deserve separate discussion (see Section 3.4).

The most striking result is the very weak angular dependence of the prefactor exponent, which over the range $0.2\pi < \theta < 0.45\pi$ is given by $\alpha = 2.66 \pm 0.01$, consistent with the theory which predicts independence on θ (Section 4.3). This immediately leads to asking if $\alpha_{\rm SOC} = 8/3$. The short answer is: we do not know. We shall come back to this at length.

The angular dependence of δ has already been reported in MBF where it was measured by decomposing the set of directions into small angular sectors.[13] We find that $\delta(\theta)$

[13] In MBF θ was varying in the third quadrant; here, because of the aforementioned change of notation θ varies in the first quadrant. Furthermore,

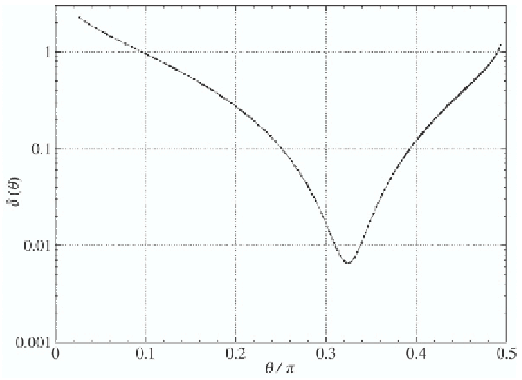

Fig. 7. Angular dependence of the decrement $\delta(\theta)$ for SOC.

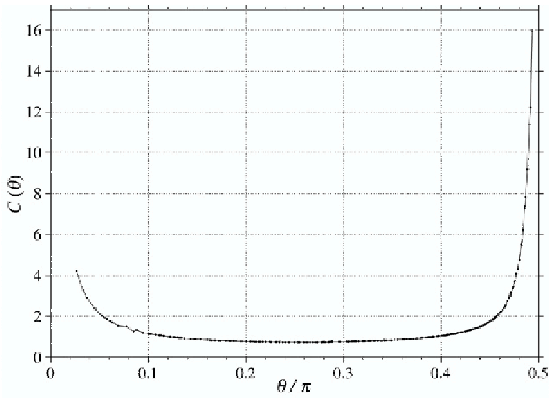

Fig. 8. Angular dependence of the constant $C(\theta)$ for SOC.

achieves a minimum value $\delta_\star \approx 0.0065$ at $\theta_\star \approx 0.324\pi$ and it becomes large near the edges. In MBF it was reported that the shell-summed amplitude of $\hat{F}(\boldsymbol{k})$

$$A(k) \equiv \sum_{k\le|\boldsymbol{k}|\le k+1} |\hat{F}(\boldsymbol{k})|, \tag{29}$$

a kind of discrete angle average, behaves as $C'k^{-2.16}\mathrm{e}^{-\delta_\star k}$ for large k. This is consistent with the present result. Indeed for large k, we can evaluate the shell sums (29) by integrating over $k\mathrm{d}\theta$ using (23) and steepest descent near $\theta_\star$. This changes the prefactor from $k^{-\alpha}$ to $k^{-\alpha+1-1/2} \approx k^{-2.16}$.

Finally, $C(\theta)$ is quite flat in the interval $0.1 < \theta < 0.4$.

3.3. Non-universality of the scaling exponent

Having established the angle-independence of the prefactor exponent, we now investigate its dependence on the initial condition. What happens when we change from the SOC (given by (2)) to another initial condition? Since 35-digit computations take up to one month of CPU, we generally used 15-digit

the method used in MBF was less accurate than the present one and there are thus small discrepancies in the values reported.

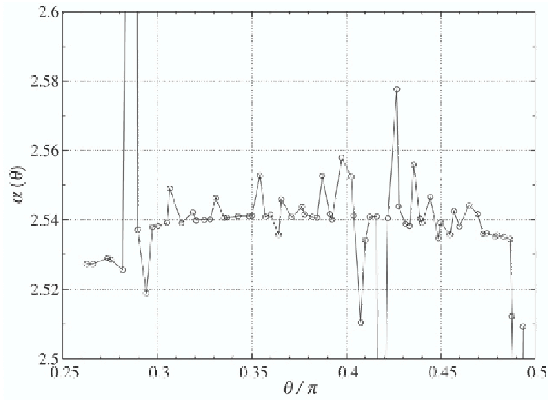

Fig. 9. Angular dependence of the prefactor exponent $\alpha(\theta)$ for the "45-degree" initial condition $\Psi_0(\boldsymbol{x}) = \cos 2x_1 + \cos(x_1 + x_2)$.

accuracy but there is one important exception (see below). At first we changed the SOC to

$$\Psi_0(\boldsymbol{x}) = \cos x_1 + \cos 3x_2, \tag{30}$$

for which the basic modes in the short-time asymptotics are (1, 0) and (0, 3) between which there is the same 90-degree angle as for the SOC. The prefactor exponent was again indistinguishably close to $8/3$. For a while this led us to conjecturing the universality of the $8/3$ exponent. Well ... until we tried

$$\Psi_0(\boldsymbol{x}) = \cos(x_1 + x_2) + \cos 2x_2, \tag{31}$$

whose basic modes are (1, 1) and (0, 2), forming an angle of 45 degrees. This gave us an exponent $\alpha \approx 2.54$. The same exponent was obtained with

$$\Psi_0(\boldsymbol{x}) = \cos(x_1 + x_2) + \cos px_2, \tag{32}$$

with $p = 1, 3, 4$, whose basic modes are different but also form an angle of 45 degrees. We also did some exploration of the direction dependence of α and, just as for the SOC, did not find any. As we shall see in Section 4.3, independence on the direction can be shown to hold.

All this was pointing towards non-universality of the prefactor exponent, that is dependence on the initial condition or at least on the angle between the basic modes. To ascertain the non-universality we performed a 100-digit computation for (31) with $k_{\max} = 1000$. Fig. 9 gives the epsilon-algorithm extrapolated values of the local prefactor exponent for this calculation as a function of θ.

Except near the edges the exponent stays very close to 2.54.[14] The discrepancy between 2.54 and 2.66 vastly exceeds the estimated error on the prefactor exponent, as discussed in Section 3.1. Finally, we report that for all cases discussed in this section on non-universality, the positivity of all the Fourier coefficients except one holds, just as for the SOC.

[14] The anomalously low value around $\theta/\pi = 0.42$ is caused by a large denominator in the corresponding slope (79/21) which does not permit a reliable determination of α.

3.4. Intermediate asymptotics near the edges

In this section we discuss only the SOC, but the theoretical results presented are easily generalized. We have seen that on any line of strictly positive and finite rational slope the Fourier coefficients decrease exponentially at high k (up to algebraic prefactors). This is not true for lines of vanishing and infinite slope. We can explicitly calculate from the recursion relation (12) all the coefficients having either $k_2 = 2$ or $k_1 = 1$. Indeed along such "edge lines" the recursion relations take the form of first-order linear homogeneous finite difference equations

$$\hat{F}(k_1, 2) = \frac{1}{k_1} \frac{k_1^2 - 2k_1 + 4}{k_1^2 + 2^2} \hat{F}(k_1 - 1, 2), \tag{33}$$

$$\hat{F}(1, k_2) = \frac{2}{k_2} \frac{k_2^2 - 4k_2 + 1}{1 + k_2^2} \hat{F}(1, k_2 - 2). \tag{34}$$

At large orders, essentially each coefficient on a horizontal or vertical edge line is obtained by dividing by k_1 or $k_2/2$ the adjacent lower-order coefficient. Thus they are decreasing roughly as $1/k_1!$ or $1/(k_2/2)!$. More precisely, using standard asymptotic methods for difference equations [32], it is easily shown that for integer $m \to \infty$

$$\hat{F}(m, 2) \sim \hat{F}(1, 2m) \sim m^{-5/2} \mathrm{e}^m m^{-m}, \tag{35}$$

which decreases faster than exponentially.

If we now consider a "near edge" direction with θ close to 0 or to $\pi/2$ we expect that the edge behavior will manifest itself as intermediate asymptotics making it hard to obtain clean scaling for the prefactor. We can however easily predict the θ-dependence of the decrement δ by the following argument. When θ is small, the line through the origin of slope $\tan\theta \approx \theta$ will intersect the edge $k_2 = 2$ at $k_1 \approx 2/\theta$. At this point, by (35), the logarithm of the Fourier amplitude is given to leading order by $-(2/\theta)\ln(2/\theta)$. Assuming that, on the line of slope θ, this point is within the region of exponential fall-off with decrement $\delta(\theta)$, we obtain

$$-(2/\theta)\ln(2/\theta) \approx -(2/\theta)\delta(\theta), \tag{36}$$

which gives (for $\theta \to 0$)

$$\delta(\theta) \approx \ln\left(\frac{2}{\theta}\right). \tag{37}$$

Near the other edge, we obtain by a similar argument (for $\theta \to \pi/2$)

$$\delta(\theta) \approx \frac{1}{2} \ln\left(\frac{1}{\pi - 2\theta}\right). \tag{38}$$

We turn now to numerical study of the near edge behavior of Fourier coefficients. So far we have determined such coefficients in regions having comparable extensions in the k_1 and k_2 directions. The structure of the recursion relation allows us however to determine the coefficients in rectangular domains having a very small or very large aspect ratio. We have seen that the local prefactor exponent behaves non-monotonically with the wavenumber when θ is below a critical value.[15] Consistently, we have found that for small θ's a more complex behavior is observed than for θ's close to $\pi/2$. We have thus studied the former in more detail. Because of the slow convergence to asymptotics we need wavenumbers much larger than in MBF, so we used rectangular domains of size 4000×480 near $\theta = 0$ and of size 200×4000 near $\theta = \pi/2$. Fig. 10 shows the variation with the wavenumber of the local prefactor exponent $\alpha_{\mathrm{loc}}(k)$ for various small θ's. It is seen that when θ decreases, the wavenumber at which $\alpha_{\mathrm{loc}}(k)$ achieves its minimum increases and thus the extrapolation of α becomes more difficult. The situation is much more favorable for the determination of the decrement, because it is (logarithmically) large.

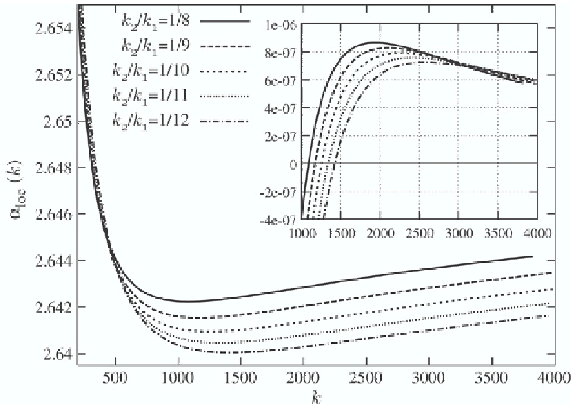

Fig. 10. Wavenumber dependence of local prefactor exponent α_{loc} for various small θ. Inset: $\mathrm{d}\alpha_{\mathrm{loc}}(k)/\mathrm{d}k$.

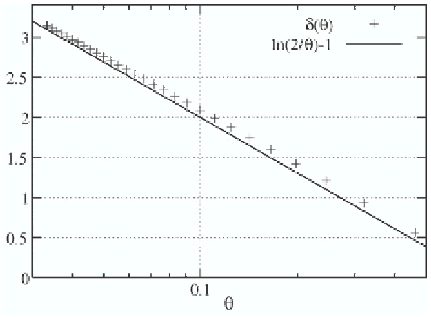

Fig. 11. Angle dependence of the decrement δ for small θ in lin–log coordinates (crosses). The continuous line is the theoretical prediction.

Fig. 11 shows the measured decrement together with a theoretical prediction $\delta(\theta) = \ln(2/\theta) - 1$ which includes a subleading correction to the leading-order prediction (37), obtained by a partially heuristic procedure. Near $\theta = \pi/2$ the decrement has also logarithmic scaling (not shown), consistent with the leading-order prediction (38) but not very clean. As to the constant $C(\theta)$, we found that it becomes large near the edges. For $\theta \to 0$ the behavior is roughly $C(\theta) \propto 1/\theta$ but

[15] This may be related to the fact that the global structure seen in Fig. 14 is far from being symmetrical in y_1 and y_2.

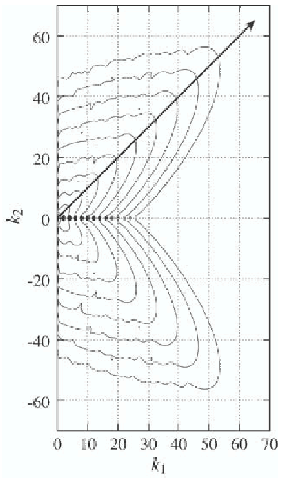

Fig. 12. Contours of the absolute value of the Fourier coefficients (logarithmic scale) of the stream function at $t = 0.8$ by full spectral simulation for the SOC.

there are substantial uncertainties because the constant C is quite sensitive to small errors made on δ and α.

3.5. Beyond short times

In MBF it was shown, for the SOC initial condition, that deviations from short-time asymptotics become important around $t = 0.1$. More precisely, deviations from the law $\delta(t) \propto \ln(1/t)$ become visible (see Fig. 2 of MBF). We now investigate numerically the issue of persistence of the $k^{-2.66}$ law for the SOC beyond the time of validity of short-time asymptotics. For this we must use a full spectral simulation with time-marching as in Refs. [4,12]. A priori there is no need to use a resolution in excess of 1024^2 since we shall see that the $k^{-2.66}$ law deteriorates significantly after $t = 1$. At that time, the decrement $\delta \approx 0.4$, which implies that the flow is extremely well resolved with 1024^2 modes. Fig. 12 shows the behavior of the absolute value[16] of the Fourier coefficients of the stream function at $t = 0.8$ in the (k_1, k_2)-plane (because of the Hermitian symmetry we are not showing negative k_1). It is seen that there is a direction of slowest decrease which has $k_2/k_1 \approx 1$. At short times the slowest decrease had $k_2/k_1 \approx 18/11$ but this direction changes in the course of time. Fig. 13 shows the usual exponential decrease with an algebraic prefactor for the Fourier amplitude in the direction of slope unity at $t = 0.8$. Beyond wavenumber 85, rounding errors take over (the calculation has 15-digit precision). The same procedure, applied at much later times, for example at $t = 1.9$, still shows some kind of exponential tail but the data are far too wiggly to permit the extraction of a reliable power-law prefactor. We have also repeated the analysis beyond short times for the flow with initial condition $\cos(x_1 + x_2) + \cos 2x_2$, where the basic modes make an angle of 45 degrees. At time $t = 1.4$ the prefactor exponent is around 2.58, quite close to the value 2.54 reported at short times.

[16] Because of the symmetry of the SOC, the Fourier coefficients are real.

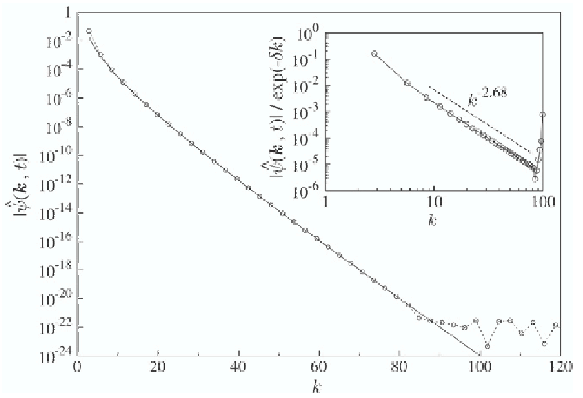

Fig. 13. Absolute value of the Fourier coefficients of the stream function at $t = 0.8$ along the rational direction $k_2/k_1 = 1$ in lin–log coordinates. A least square fit (continuous line) gives $ck^{-2.68}e^{-0.429k}$. The inset shows the same data after division by $e^{-0.429k}$ in log–log coordinates.

Let us now discuss some of the limitations involved in the search for prefactor scaling beyond the short-time asymptotics. We begin with practical limitations. With 1024^2 modes the direction of rational slope $k_2/k_1 = 1$ has about 30 points before encountering 15-digit rounding level. Other directions have typically only ten points and this makes precise determination of the decrement δ and the prefactor exponent α impossible. We thus cannot comment on any possible angular dependence of α. Calculations with higher resolution require higher precision in order to lower the rounding noise level and this in turn requires enormous computer resources by a time-marching full spectral method if we demand that temporal truncation error be at rounding level.

There is a more fundamental issue regarding the validity of the short-time asymptotic régime. For the SOC, this régime breaks down around $t = 0.1$, as far as the temporal behavior of $\delta(t)$ is concerned. Actually the short-time approximation is strongly non-uniform with respect to the wavenumber: high wavenumbers show discrepancies at much earlier times than 0.1. For example we know that, in the short-time régime, all the Fourier coefficients except one are non-negative, but as early as $t = 10^{-3}$, a 90-digit calculation by time-marching shows that Fourier coefficients start oscillating in sign beyond wavenumber forty.[17] By $t = 0.8$ such oscillations are found in the 15-digit calculation whenever $k_2/k_1 > 2$, irrespective of wavenumber. In the presence of such oscillations, the functional form we have used in the short-time asymptotics $\propto k^{-\alpha}e^{-\delta k}$ is clearly invalid. What is happening has a geometric interpretation which is more readily understood after reading the first page of Section 4. In the short-time régime the positivity of the Fourier coefficients implies that the singular manifold is in the y-plane. Note, however, that in this régime we are ignoring interactions with Fourier harmonics

[17] It matters how precisely we let $t \to 0$ and $k \to \infty$. For a fixed value of t, however small, the high-k régime discussed in most of this paper may be just an intermediate asymptotic régime. It is conceivable that the non-universality found here is confined to this particular asymptotic régime.

from quadrants other than the first one since they only contribute subdominant terms in the short-time expansion of the hydrodynamic fields. When such terms are taken into account it is likely that singularities obtained at leading order will be mostly advected by a modified velocity field which carries the singularities slightly out of the y-plane without changing their nature, as happens in the work of Tanveer and Speziale [18]. Of course, positivity of the Fourier coefficients will be lost but not necessarily their scaling properties. Observe also that the y-plane being a plane of symmetry, this picture implies that there are several pieces of the singular manifold very close to the y-plane. In Fourier space they produce a kind of interference pattern which at first has very long wavelength (in k). This wavelength becomes shorter and shorter as time advances and the singular manifold moves further away from the y-plane.[18]

4. The geometry of the pseudo-hydrodynamic flow

In two-dimensional simulations of hydrodynamics, considerable insight is usually obtained by looking at flow features in the physical space. This is much simpler in two dimensions than in three, provided that the relevant features are in the *real* $\mathbb{R}^2$ space. Here the most important features are in the *complex* $\mathbb{C}^2$ space, which is equivalent to having four real dimensions. Fortunately, as explained in Section 2, we can make use of only two real dimensions by working in the y-plane above $(z_1, z_2) = (\pi, 0)$ which extends in the (pure) imaginary directions. As already briefly mentioned in Section 4 of MBF, the positivity of all the Fourier coefficients $\hat{F}(k_1, k_2)$ (except $\hat{F}(1, 0)$) and the exponential decrease with the wavenumber imply that the solution to the (short-time asymptotic) Euler equation has a line of singularities $\mathcal{S}$ in the (y_1, y_2)-plane. Indeed, since only harmonics with non-negative k_1 and k_2 are present, we may rewrite (13) and (14) as a Taylor series in two variables

$$\psi(\mathbf{y}) - \frac{1}{2}y_1 + y_2 = \sum_{k_1=0}^{\infty}\sum_{k_2=0}^{\infty} \hat{F}(k_1, k_2)\, \zeta_1^{k_1}\, \zeta_2^{k_2}, \tag{39}$$

$$\zeta_1 \equiv \mathrm{e}^{y_1}, \quad \zeta_2 \equiv \mathrm{e}^{y_2}. \tag{40}$$

If we now hold y_2 (and thus ζ_2) fixed and sum over k_2, we obtain a Taylor series in ζ_1 such that all its coefficients (except possibly the first one) are positive. By Vivanti's theorem [33], if such a series has a finite radius of convergence (as is the case here because of the aforementioned exponential decrease), the singularity in the complex ζ_1-plane nearest to the origin is on the positive real axis at a location $y_1 = y_1^\star(y_2)$, which depends on y_2. The function $y_1^\star(y_2)$ defines an object which we here call the *singular manifold* and is the edge of the analyticity domain $y_1 < y_1^\star(y_2)$.[19] A standard theorem about multi-dimensional Taylor series states that their domain of convergence is logarithmically convex (see, e.g., Ref. [34]).

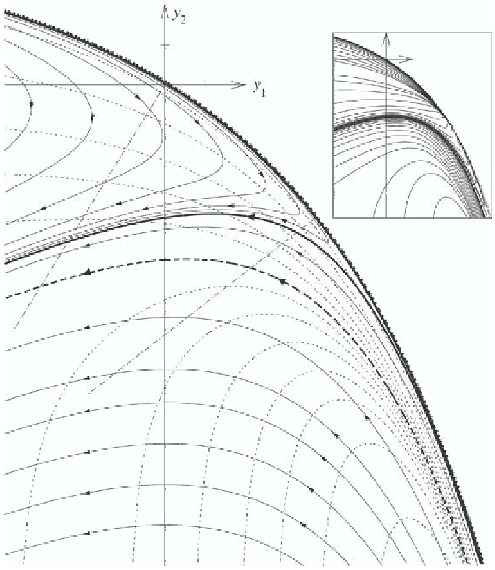

Fig. 14. Global geometry of the flow in the y-plane. Streamlines (solid lines) and iso-vorticity lines (thin-dotted lines) are shown. Thick-solid-crenated line: singular manifold; thick-solid line: U-turn separatrix ($\psi \approx 0.5$); thick-dashed line: vorticity separatrix ($\omega = 0$ and $\psi = \ln 2$). The ticks on the two axes correspond to coordinate 0.25. Inset: Contours of absolute value of the cotangent of the angle between the streamlines and the iso-vorticity lines as a measure of depletion of nonlinearity.

In our case this just means that the analyticity domain in the y-plane is convex. As shown in MBF using slightly different notation, the singular manifold can be constructed either as the envelope of the family of straight lines $y_1 \cos\theta + y_2 \sin\theta = \delta(\theta)$ (where the decrement δ has been defined in Section 3) or as the envelope of analyticity disks.

To numerically construct the pseudo-hydrodynamic solution in the y-plane from the Fourier data we use (14) for the stream function, (18) for the velocity and (20) for the vorticity. Although our Fourier data typically have 35 decimal digits, it suffices to truncate them to 16 digits to obtain the various relevant fields in y-space with a good accuracy.

4.1. Presentation of the y-plane results

We begin with global topological features and then turn to a more local and more quantitative description. Fig. 14 gives a global view of the flow in the y-plane.[20] The outer edge of the flow region, which passes very close to the origin is the singular manifold. At large distances on the upper left and the lower right, respectively, the singular manifold has logarithmic branches. Close to the singular manifold, the streamlines follow it until they make a U-turn and eventually plunge into the third quadrant ($y_1 < 0, y_2 < 0$) where they become straight with slope $1/2$ at large distances. An important feature is the U-*turn separatrix*, above which stream lines make U-turns which

[18] Somewhat similar interference patterns are obtained when the short-time asymptotics is extended to the Navier–Stokes equation (with viscosity scaling as $1/t$).

[19] More correctly, the singular manifold is a (perhaps analytic) manifold in $\mathbb{C}^2$ whose intersection with the y-plane is designated here by the same name.

[20] When magnifying this figure, ADOBE READER® 7 or higher is recommended.

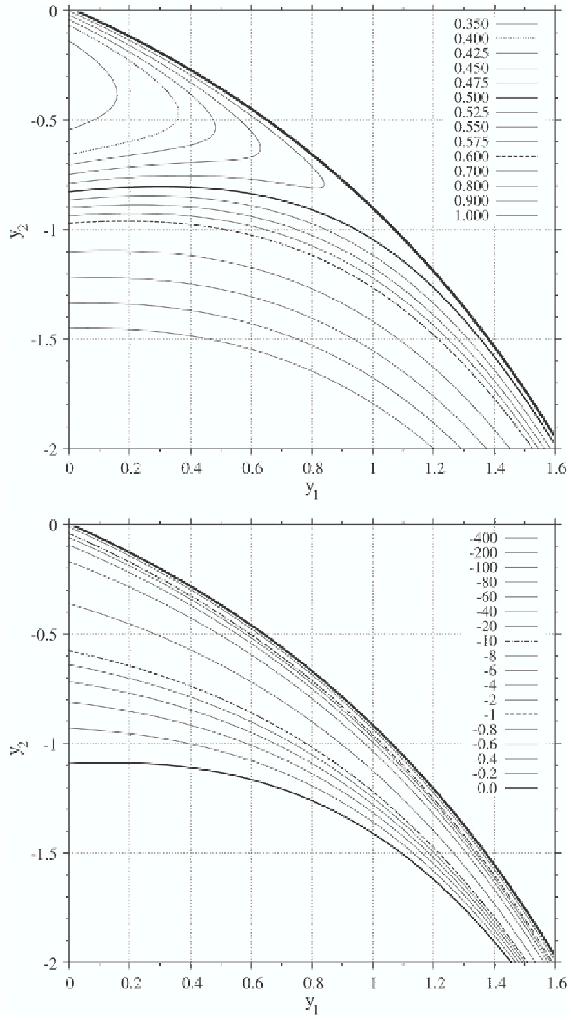

Fig. 15. Enlargements of Fig. 14 around the point $(y_1, y_2) = (0.8, -1.0)$ showing the streamlines (upper figure) and the vorticity contours (lower figure). Only negative vorticity contours are shown.

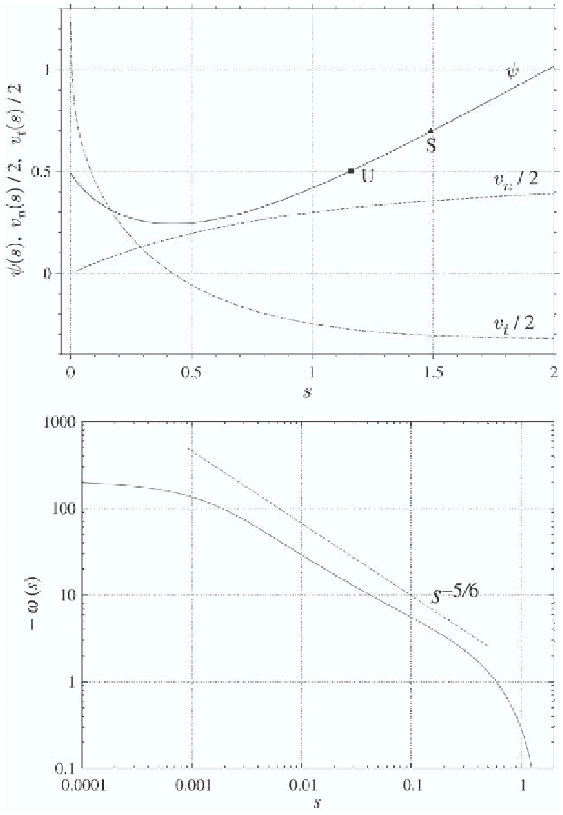

Fig. 16. Upper figure: stream function ψ, velocity components (suitably rescaled) v_n and v_t normal and parallel to the singular manifold along the line of cut normal to the singular manifold passing through the origin, shown as a dashed-dotted line on Fig. 14. U and S identify the places where the cut intersects the U-turn separatrix and the vorticity separatrix. Lower figure: negative vorticity along the same cut in log–log coordinates.

become increasingly sharp when moving to the lower right, and below which there are no U-turns. Vorticity contours starting close to the singular manifold far on the upper left get pressed increasingly close into the singular manifold when moving to the lower right. The *vorticity separatrix* divides negative vorticity (above) and positive vorticity (below). It approaches the singular manifold in the lower right but not as fast as the U-turn separatrix. In view of the Jacobian formulation of the Euler equation, the vorticity separatrix is clearly also a streamline. Hence, the strong depletion of nonlinearity evidenced by accumulation of contour lines near this separatrix on the inset of Fig. 14. The depletion is here measured by plotting the absolute value of the cotangent of the angle between $\nabla\psi$ and $\nabla\omega$.

Fig. 15 shows the stream function and the vorticity with more details in a region of particular interest. Increasingly sharp U-turns of the stream lines are seen when moving to the lower right into the narrowing channel separating the singular manifold from the U-turn separatrix. It is seen that the vorticity becomes very large and negative near the singular manifold, while the stream function remains finite with a value around $\psi = 0.5$, the same as on the U-turn separatrix. Thus, the singular manifold, which is simultaneously a limiting case of a streamline and of a vorticity contour, displays strong depletion of nonlinearity as seen on the inset of Fig. 14. We also looked at the velocity field (not shown); close to the singular manifold the velocity is parallel to this manifold and decreases in modulus when moving down and to the right. Note that, contrary to the vorticity, the velocity does not grow explosively when approaching the singular manifold; there is no numerical evidence against the plausible assumption that the velocity has a finite limit on the singular manifold which is tangent to this manifold. Similarly, the pressure (not shown) also appears to have a finite limit on the singular manifold.

For a better quantitative grasp we show in Fig. 16 a one-dimensional cut of the two-dimensional fields along the normal to the singular manifold passing through the origin, shown as a dashed-dotted line on Fig. 14. It is seen that the stream

function takes the finite value $\psi_{\text{sing}} \approx 0.5$ on the singular manifold and the same value at the U-turn separatrix and that the vorticity follows approximately a power law $-\omega \propto s^{-\beta}$ with $0.7 < \beta < 0.9$, where s is the distance to the singular manifold. The scaling is however rather poor; it gets even worse when repeating the same analysis along the other dashed line normal to the singular manifold, shown on Fig. 14. It is also seen that at the singular manifold the normal velocity vanishes linearly. We now turn to comments and theoretical explanation of most of these features.

4.2. Bridging k-space and y-space results

As we shall now see, it is quite obvious to relate the *leading-order* asymptotics (23) of the Fourier coefficients at large k and the *leading-order* behavior near the singular manifold in y-space. To explain the poor scaling observed for the vorticity in y-space, we need to take into account subleading corrections as we shall also discuss. The "Fourier–Laplace" representations (14), (18) and (20) for the (pseudo-hydrodynamic) stream function, the velocity and the vorticity, connect k- and y-space functions. Consider, for example, the vorticity; using (23) and polar coordinates $\boldsymbol{k} = k(\cos\theta,\ \sin\theta)$ we can rewrite it as

$$\omega(\boldsymbol{y}) = -\sum_{\boldsymbol{k}} C(\theta) k^{-\alpha+2} \mathrm{e}^{-kh(\theta;\boldsymbol{y})}, \tag{41}$$

$$h(\theta;\boldsymbol{y}) \equiv \delta(\theta) - y_1\cos\theta - y_2\sin\theta. \tag{42}$$

The convergence properties at high wavenumbers of this sum will depend crucially on the sign of the decrement $h(\theta;\boldsymbol{y})$. If

$$\min_{\theta} h(\theta;\boldsymbol{y}) > 0, \tag{43}$$

all the exponentials are decaying and the sum will be finite. If the minimum is negative, the sum is divergent. In the borderline case of a vanishing minimum, the algebraic prefactors will determine convergence. If $\delta(\theta)$ is a smooth function of θ, as our numerical results suggest, the minimum corresponds to a vanishing derivative with respect to θ. Hence, the borderline case is characterized by the following two equations:

$$\delta(\theta) - y_1\cos\theta - y_2\sin\theta = 0, \tag{44}$$

$$\delta'(\theta) + y_1\sin\theta - y_2\cos\theta = 0, \tag{45}$$

where $\delta'(\theta)$ is the derivative of $\delta(\theta)$. Those points $\boldsymbol{y}_\star(\theta) = (y_{\star 1},\ y_{\star 2})$ which satisfy (44) and (45) are on the singular manifold. Conversely, $\delta(\theta)$ is the distance from the origin to the tangent at the singular manifold which has the slope $\theta - \pi/2$ (see Fig. 17). It follows that the singular manifold is the envelope of such lines. In MBF this result was derived by Poincaré's pinching argument.

From (44) and (45) it is easily shown that the near-edge behavior of $\delta(\theta)$ given by (37) and (38) implies logarithmic branches for the singular manifold: $y_2 \simeq (1/2)\ln(-y_1)$ for large negative y_1 and $y_1 \simeq \ln(-y_2)$ for large negative y_2.

We observe that $s \equiv \min_\theta h(\theta;\boldsymbol{y})$ is the shortest Euclidean distance of $\boldsymbol{y}$ to the singular manifold, with a plus sign when $\boldsymbol{y}$ is below the singular manifold and a minus sign when it is above. Let us assume that $\boldsymbol{y}$ is below or on the singular manifold

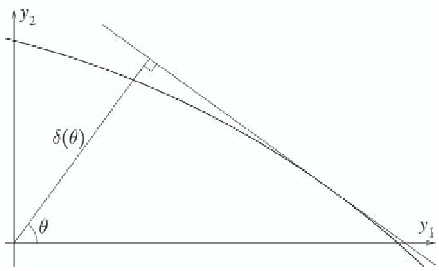

Fig. 17. Construction of the singular manifold from the logarithmic decrement $\delta(\theta)$.

and let us denote by $\theta_\star(\boldsymbol{y})$ the value of θ where the minimum is achieved. Near this minimum we can Taylor-expand the decrement

$$h(\theta;\boldsymbol{y}) = s + \frac{1}{2}h''_\star(\theta-\theta_\star)^2 + O((\theta-\theta_\star)^3), \tag{46}$$

where $h''_\star \equiv \partial^2 h(\theta_\star,\boldsymbol{y})/\partial\theta^2$. The convergence of the sum (41) depends only on the high-k behavior, where we can, to leading order, replace the sum by an integral over $k\mathrm{d}k\mathrm{d}\theta$, to obtain a "continuous approximation"

$$\omega_{\text{cont}}(\boldsymbol{y}) = -\int_0^{2\pi}\mathrm{d}\theta\int_0^\infty \mathrm{d}k\, C(\theta)k^{-\alpha+3}\,\mathrm{e}^{-kh(\theta;\boldsymbol{y})}. \tag{47}$$

When s vanishes or is small and positive, we can evaluate the angular integral in (47) by steepest descent

$$\omega_{\text{cont}}(\boldsymbol{y}_\star) \simeq -C(\theta_\star)\sqrt{\frac{2\pi}{h''_\star}}\int_0^\infty \mathrm{d}k k^{-\alpha+5/2}\,\mathrm{e}^{-ks}. \tag{48}$$

On the singular manifold, $s = 0$ and it is clear that the integral over k is ultraviolet-divergent as soon as $\alpha \geq 3/2$. All the values of the prefactor exponent α considered in this paper are at least $5/2$ and thus give an *infinite vorticity at the singular manifold*. The same analysis applied to the stream function and to the velocity gives ultraviolet-convergent integrals. For small positive s, we obtain from (48)

$$\omega_{\text{cont}}(\boldsymbol{y}_\star) \simeq -C(\theta_\star)\sqrt{\frac{2\pi}{h''_\star}}\,\Gamma(7/2-\alpha)\,s^{-\beta}, \tag{49}$$

$$\beta = \frac{7}{2} - \alpha, \tag{50}$$

where $\Gamma(\cdot)$ denotes the Gamma function.

For SOC initial conditions, $\alpha \approx 8/3$, and thus the vorticity diverges to leading order with a $s^{-5/6}$ law, when approaching the singular manifold. The subleading corrections causing the poor scaling seen in Section 4.1 are of various sorts. First, there are subleading corrections to (23) whose simplest manifestation is the discrepancy between the local scaling exponent $\alpha_{\text{loc}}(k)$ and its extrapolated value α_∞, as discussed in Section 3.1. As already stated, we do not know the functional form of such corrections. Second, there are subleading corrections coming from having approximated the Fourier–Laplace sums by integrals. It is easily shown that they contribute $O(s^0)$ to the

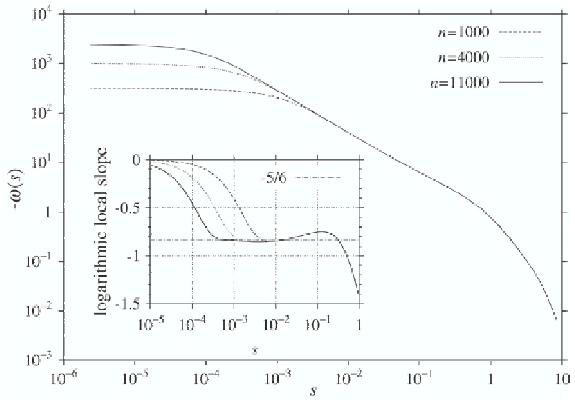

Fig. 18. Same as lower part of Fig. 16 but for the synthetic data with various values of the maximum wavenumber n. Inset: corresponding logarithmic local slopes. The predicted scaling exponent is $-5/6$.

vorticity in y-space. Third, there are the subleading corrections to the continuous approximation (47), which may be shown to be $O(s^{-1/3})$. A simple way to determine how much the scaling is degraded by the second and third type of corrections is to use *synthetic data* for which the Fourier coefficients are given exactly by (23). It is then easy to change the resolution $n \times n$ and to find out how large n should be for clean leading-order scaling to emerge. We performed such a calculation with C and α constant and the values of $\delta(\theta)$ taken from the actual Euler SOC data. From the synthetic data, using (20) we then calculate a synthetic vorticity $\omega_{\text{synth}}(\boldsymbol{y})$ just as in Section 4.1. Fig. 18 shows $-\omega_{\text{synth}}(\boldsymbol{y})$ in log–log coordinates for three values of n. The lowest one, $n = 1000$, is comparable to what is used in the actual Euler calculation: the scaling is very poor. Only when we increase the resolution more than tenfold to $n = 11{,}000$ do we begin to see a clean $s^{-5/6}$ scaling.

4.3. Theory of y-plane pseudo-hydrodynamics

The starting point for theory in the y-plane is of course the pseudo-hydrodynamic vorticity equation and its boundary conditions far into the third quadrant, derived in Section 2 and repeated here for convenience:

$$\boldsymbol{v} \cdot \nabla\omega + \omega = 0, \tag{51}$$

$$\boldsymbol{v} \simeq \left(-1,\ -\frac{1}{2}\right), \quad \omega \simeq \frac{1}{2}\mathrm{e}^{y_1} - 2\mathrm{e}^{2y_2}, \quad y_1,\ y_2 \to -\infty. \tag{52}$$

Alternatively we can rewrite (51) as $J(\psi, \omega) = \omega$ or as $J(\psi, \ln|\omega|) = 1$. Thus the map from $(y_1,\ y_2)$ to $(\psi,\ \ln|\omega|)$ is area preserving. The vorticity separatrix was defined by $\omega = 0$; so that the Jacobian of the stream function and of the vorticity is zero along this line. Hence it is also a streamline.[21] It is easily shown that the value of the streamfunction on this line is $\ln 2$. Indeed, as we follow the vorticity separatrix far into the third quadrant, we obtain from (52) that $y_1 \simeq 2y_2 + 2\ln 2$. Since $\psi = (1/2)y_1 - y_2$ (up to exponentially small terms), we obtain the result claimed. We have also checked numerically that the value of the stream function on the vorticity separatrix is $\ln 2$ to at least three decimal places.

Depletion of nonlinearity near the singular manifold prevents us from using the dynamical equation (51) to derive the scaling exponent of the singularities by, for example, balancing to leading order the two terms in (51). Nevertheless, such balancing gives some useful information, such as the vanishing of the normal component $v_n(s)$ of the velocity near the singular manifold (for $s \to 0$) and the independence on position of the exponent β characterizing the divergence of the vorticity. Since β and the prefactor exponent α are related by $\alpha + \beta = 7/2$, this will establish the independence of α on θ, which was rather strongly supported by the numerical results reported in Section 3. We now derive these results. In what follows, points $\boldsymbol{y}_\star$ on the singular manifold are parameterized by the angle θ between the y_1-axis and the outgoing normal.

To show the vanishing of $v_n(s)$ for $s \to 0$, it is convenient to use as *local coordinates* near the singular manifold the angle θ and the distance s. We denote by $v_n(s, \theta)$ and $v_t(s, \theta)$ the components of the velocity along the inward normal and along the tangent in the direction of increasing θ. For small s, to leading order, (51) becomes

$$\left[v_n(s,\theta)\partial_s + v_t(s,\theta)\frac{1}{R(\theta)}\partial_\theta\right]\omega(s,\theta) \simeq -\omega(s,\theta), \tag{53}$$

where $R(\theta)$ is the radius of curvature of the singular manifold (the arclength is given by $R(\theta)\mathrm{d}\theta$). We now assume that $\omega \propto s^{-\beta}$ (with $\beta > 0$). If $v_n(0, \theta)$ did not vanish, the first term on the l.h.s. of (53) would be proportional to $s^{-\beta-1}$, which for small s could not be balanced by any of the other terms of the equation. The argument actually implies the stronger result that the normal velocity v_n cannot vanish more slowly than s^1. The technique of Section 4.2 on bridging k-space and y-space results can be used to show that $\partial v_n/\partial s$ remains finite at the singular manifold, although it has the same dimension as the vorticity which becomes infinite.[22] Thus v_n actually vanishes linearly with s.

For the independence of β on θ, we integrate (51) along a typical streamline passing near the singular manifold between two points M_0 (far from the singular manifold) and M_1 (within a small distance s_1), so that there is a U-turn in between which is assumed not to be close to either M_0 or M_1 (see Fig. 19). We obtain

$$\frac{\omega(M_1)}{\omega(M_0)} = \exp\left\{\int_{M_0}^{M_1} \frac{\mathrm{d}\ell}{|\boldsymbol{v}(\ell)|}\right\}. \tag{54}$$

The streamline is here parameterized by the arclength ℓ measured from an arbitrary reference point and growing when moving into the upper far left, opposite to the direction of

[21] By changing ω into $1/\omega$ in (51), we can show similarly that the singular manifold, at which $1/\omega = 0$, is also a streamline.

[22] In the proof one uses the vanishing of the normal component of the velocity at the singular manifold, a consequence of the singular manifold being a streamline.

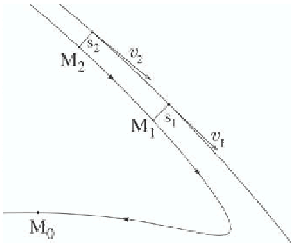

Fig. 19. A typical streamline passing near the singular manifold and performing a U-turn. Although this figure uses the actual data rather then being a sketch, the distance between the streamline and the singular manifold has been somewhat increased for legibility.

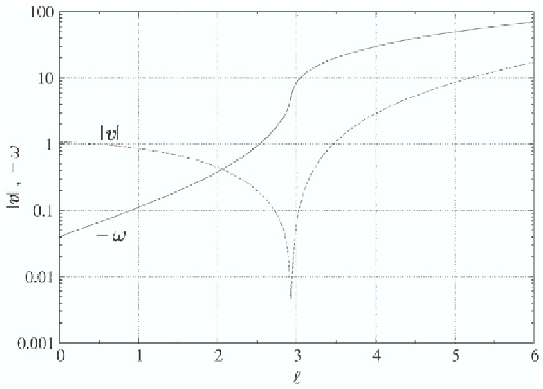

Fig. 20. Modulus of the velocity and vorticity (changed sign) versus arclength ℓ along the streamline shown in Fig. 19 which has $\psi \approx 0.47$. The point M_0 is taken near $\ell = 2.5$; the U-turn, M_1 and M_2 are near $\ell = 3$, $\ell = 3.2$, $\ell = 3.5$, respectively.

the velocity. When moving from M_0 to M_1 the smallest velocities and thus the leading-order contribution to the integral $\int_{M_0}^{M_1} \mathrm{d}\ell/|\boldsymbol{v}(\ell)|$ are expected to come from the immediate neighborhood of the U-turn. We have checked this conjecture numerically by calculating the vorticity and the modulus of the velocity along a streamline chosen to have a rather sharp but well-resolved U turn (see Fig. 20).

We assume now that the vorticity near the singular manifold is given to leading order by $\omega = c(\theta)s^{-\beta(\theta)}$, where we temporarily leave the possibility that the exponent β depends on the parameter θ associated to the nearest point on the singular manifold. We take a second point M_2 on the same streamline but further away from the U-turn. We then have (to leading order)

$$\omega(M_1) \simeq c(\theta_1)s_1^{-\beta(\theta_1)}, \tag{55}$$

$$\omega(M_2) \simeq c(\theta_2)s_2^{-\beta(\theta_2)}, \tag{56}$$

where $(s_1,\ \theta_1)$ and $(s_2,\ \theta_2)$ are the local coordinates for M_1 and M_2. From (54), applied successively to M_1 and M_2, we find that

$$\frac{\omega(M_2)}{\omega(M_1)} \simeq \exp\left\{\int_{M_1}^{M_2} \frac{\mathrm{d}\ell}{|\boldsymbol{v}(\ell)|}\right\}. \tag{57}$$

Between M_1 and M_2 the streamline is close to the singular manifold and the velocity is dominated by its tangential component; hence we can replace the r.h.s. of (57) by an integral along the singular manifold and obtain to leading order

$$\frac{\omega(M_2)}{\omega(M_1)} \simeq K_{12} \equiv \exp\left\{\int_{\theta_1}^{\theta_2} \mathrm{d}\theta\, \frac{R(\theta)}{v_t(\theta)}\right\}, \tag{58}$$

which depends neither on s_1 nor on s_2. We now observe that the solenoidal character of the velocity implies (again to leading order)

$$s_1 v_t(\theta_1) \simeq s_2 v_t(\theta_2). \tag{59}$$

It follows from (58) and (59) that

$$\omega(M_2) \simeq c_2\left[\frac{s_1 v_1}{v_2}\right]^{-\beta(\theta_2)} \simeq K_{12}\, c_1 s_1^{-\beta(\theta_1)}. \tag{60}$$

Comparison of the middle and the rightmost members gives

$$\beta(\theta_1) = \beta(\theta_2), \quad c_2 = K_{12}\, c_1 \left[\frac{v_1}{v_2}\right]^{\beta}. \tag{61}$$

This establishes the independence of the vorticity scaling exponent on θ.

5. A passive scalar model

As shown in Ref. [35], simple advection of a passive scalar by a prescribed velocity field with just a few Fourier harmonics can easily lead to singularities because fluid particles may come from or go to (complex) infinity in a finite time. In the present context of short-time asymptotics, the equivalent of a passive scalar model is to treat the (pseudo-hydrodynamic) vorticity ω in (21) as a passive scalar advected by a prescribed velocity. The simplest prescribed velocity we can take is

$$\boldsymbol{v}_{\mathrm{P}}(\boldsymbol{y}) = \left(-1,\ -\frac{1}{2}\right) + \left(\mathrm{e}^{2y_2},\ \frac{1}{2}\mathrm{e}^{y_1}\right), \tag{62}$$

obtained from the stream function

$$\psi_{\mathrm{P}} \equiv \frac{1}{2}y_1 - y_2 - \frac{1}{2}\mathrm{e}^{y_1} + \frac{1}{2}\mathrm{e}^{2y_2}. \tag{63}$$

This velocity field includes the drift $(-1,\ -1/2)$ resulting from the shifts of the original coordinates by terms proportional to $\ln t$ and the contributions from the basic modes. For our passive scalar model we use the vorticity equation (21) with the inclusion of an inhomogeneous term whose precise form does not matter (as long as it does not have itself any singularity): the singularities of the passive vorticity stem solely from advection. Specifically, the passive scalar model is defined by

$$\boldsymbol{v}_{\mathrm{P}} \cdot \nabla\omega + \omega = \frac{3}{2}\mathrm{e}^{y_1+2y_2}, \tag{64}$$

where the r.h.s. is taken to be the interaction term of the two basic modes. It is easy to write down Fourier-space recursion relations for this model and to show that all the Fourier coefficients are positive. Numerical solution of the recursion relations gives the usual type of scaling with a very clean

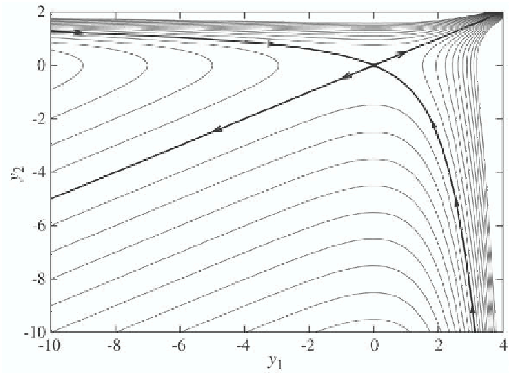

Fig. 21. Streamlines in the y plane for the passive scalar model given by (63), which has a hyperbolic stagnation point at the origin. Thick line with arrows pointing to the origin: stable manifold of the associated dynamical system (65) which is also the singular manifold for the vorticity. Thick line with arrows pointing away from the origin: unstable manifold.

prefactor exponent $\alpha = 5/2$.[23] In the y-space this implies a blow-up of the vorticity $\omega \propto s^{-1}$ as function of the distance s to the singular manifold.

Actually all these results can be derived in a rather straightforward manner by working in the y-space, as we now explain. Eq. (64) can be integrated along the characteristics. For this we consider the conservative dynamical system of fluid particle trajectories in the velocity field $\boldsymbol{v}_{\mathrm{P}}$:

$$\frac{\mathrm{d}}{\mathrm{d}\tau}\boldsymbol{y} = \boldsymbol{v}_{\mathrm{P}}(\boldsymbol{y}). \tag{65}$$

The integral lines are the lines $\psi_{\mathrm{P}} = \text{const.}$, which are shown in Fig. 21. At the origin there is a hyperbolic stagnation point near which we have $\psi_{\mathrm{P}} = -(1/4)y_1^2 + y_2^2 + O(|\boldsymbol{y}|^3)$. The associated unstable manifold is simply $y_1 = 2y_2$, while the stable manifold is the other solution to $\psi_{\mathrm{P}} = 0$.

This hyperbolic stagnation point at the origin completely determines the scaling of the vorticity. Indeed, in Section 4.3 we derived from the vorticity equation (21) an expression (54) which shows that large vorticities stem from low-velocity regions. This derivation, which did not make use of the fact that the vorticity is the curl of the velocity, remains valid for the passive scalar model (except for minor changes due to the presence of an inhomogeneous term). In the fully nonlinear case, the low velocities were due to the increasingly sharp U-turns described in Section 4.1. In the present much simpler case, they are just due to the passage near the hyperbolic stagnation point. As we follow a streamline upstream (i.e. to increasing arclengths ℓ in the notation of Section 4.3) we come closer and closer to the stable manifold. The latter thus plays the role of the singular manifold. By the same argument as used in Section 4.3 the scaling of the vorticity near the stable/singular manifold is the same everywhere. It suffices to determine it locally near the stagnation point. One way is to parameterize the streamline by the distance s to the stable manifold (more precisely to its tangent at the origin, since we are doing a local analysis). By (54), the growth of the vorticity is controlled by

$$\exp\left\{\int^{\ell} \frac{\mathrm{d}\ell'}{|\boldsymbol{v}(\ell')|}\right\} = \exp\left\{\int^{s} \frac{\mathrm{d}s'}{v_n(s')}\right\}, \tag{66}$$

where $v_n(s)$ is the velocity component along the (inward) normal $\boldsymbol{n} = (-1/\sqrt{5}, -2/\sqrt{5})$ to the stable manifold at the origin. Near a hyperbolic stagnation point we have $v_n(s) = \lambda s + O(s^2)$, where λ is the positive eigenvalue of the velocity gradient $\partial_i v_j$ at the stagnation point. Here, it is elementary to show that $\lambda = 1$. Using this in (66) we find that the vorticity $\omega \propto s^{-1}$, as claimed. This argument is easily adapted to the passive scalar models for other two-mode initial conditions, such as those discussed in Section 3.3. The same s^{-1} behavior is always obtained, which is thus universal, contrary to what happens in the full nonlinear case.

Although the passive scalar model does not predict the exact and non-universal character of the vorticity blow-up for the full nonlinear problem, the singular manifold is given quite accurately by the passive scalar model. In particular it is immediately checked that both have the same logarithmic branches (at least to leading order). Furthermore, in the passive scalar model the stable/singular manifold goes exactly through the origin while in the full nonlinear problem it passes within a distance $\delta \approx 0.0065$, as shown in MBF. It may be that such agreements are due to the presence of very strong depletion of nonlinearity in the full problem, thereby making a simple linear advection model quite relevant.

Actually, the passive scalar model can be systematically improved by enriching the prescribed velocity field through addition of higher-order modes. A simple way to do this is to take all the Fourier modes such that $k_1 + k_2/2 \leq n + 1$. For SOC, we have studied these "enriched" passive scalar models for various values of n. They all possess a hyperbolic stagnation point. The associated positive eigenvalue λ_n becomes larger than unity when $n \geq 1$. The first few values for the corresponding prefactor exponent $\alpha_n = 7/2 - 1/\lambda_n$ are: $\alpha_0 = 2.5$, $\alpha_1 \approx 2.594$, $\alpha_2 \approx 2.613$. For larger values of n, the growth is very slow; for example $\alpha_{20} \approx 2.618$. We also observed that, as n grows, the stagnation point moves to the right and down and the angle between its stable and unstable manifolds decreases. It is likely that, for $n \to \infty$, the stagnation point is pushed to infinity in such a way that its stable and unstable manifold tend to the singular manifold and to the U-turn separatrix for the nonlinear problem, while $\alpha_n \to \alpha$, but the convergence may be slow.

6. Conclusion

The present paper, like Refs. [4] and MBF, is mainly concerned with the short-time asymptotics of the 2D Euler equation in situations where complex-space singularities are born at infinity at time $t = 0+$. Let us first summarize the main findings of this work, which uses a mixture of ultra-high precision computations (with up to 100-digit accuracy) and of theory. Our work is specifically concerned with initial

[23] With the already cited asymptotic interpolation method [31] the exponent α is found to differ from 5/2 by less than 10^{-11}.

conditions in the form of a trigonometric polynomial; it is shown in the Appendix that this problem can generically be reduced to one with only two modes. A very detailed description of the complex singularities is given. For all cases studied, the Fourier coefficients except one are found to be non-negative (this was already reported for SOC in MBF). In any direction of rational slope $\tan\theta$ not too close to the edges of the Fourier domain, the coefficients of the stream function converge very quickly with increasing wavenumbers k to the form $C(\theta)k^{-\alpha}\mathrm{e}^{-k\delta(\theta)}$. The prefactor exponent α, determined with better than one per cent accuracy, is independent of θ but is not universal: when the initial modes are orthogonal, it is indistinguishable from $8/3 \approx 2.66$, whereas with a 45 degree angle between the initial modes it takes the value 2.54. We cannot rule out that α depends also on the moduli of the initial modes but we have no evidence that it does.

It is shown that the singularity problem can be reformulated as an ordinary steady-state (pseudo)hydrodynamic problem in a suitable y-plane corresponding to pure imaginary coordinates. The complex singularities are in this y-plane on a smooth (possibly analytic) curve extending to infinity with logarithmic branches. The vorticity diverges as $s^{-\beta}$, where s is the distance to the singular manifold and $\alpha + \beta = 7/2$. We give a full description of the geometry of streamlines and vorticity contours in the y-plane (Fig. 14). Increasingly sharp U-turns of the streamlines near the lower logarithmic branch of the singular manifold give rise to the vorticity scaling. Very strong depletion of nonlinearity near the singular manifold prevents application of dominant balance to determine the scaling exponent of singularities and is likely to be the reason for the very unusual non-universality of the singularities. Finally it is shown that the scaling behavior of the prefactor persists in time significantly beyond the validity of the short-time asymptotics, at least as intermediate asymptotics. However, we do not know if the non-universality of the singularities found in the short-time régime carries over to the full Euler equation.

The main theoretical shortcomings of this work are our inability so far to prove the positivity of Fourier coefficients and to derive the prefactor exponent α (or the vorticity divergence exponent β) from the initial conditions (we also failed to identify the nature of subleading corrections to (23)). We have nevertheless gained some qualitative understanding with the passive scalar model of Section 5 that ignores the back reaction of the vorticity on the velocity but which sheds interesting light on the mechanism for producing singularities. In this toy model, scaling is controlled by a stagnation point of the velocity field, whereas in the full nonlinear problem the stagnation point is rejected to infinity.

We have described our findings in some detail, hoping that colleagues will be able to help us with the missing theory.

In principle the methods used for the 2D short-time Euler problem can be extended to various other short-time problems. One instance is the short-time régime for the 2D ideal incompressible MHD equations. A preliminary study for this case indicates that the positivity result does not survive: Fourier amplitudes display oscillations revealing a richer geometry of the singular manifold which can no more be captured in terms of just the imaginary coordinates $\boldsymbol{y}$. In mathematical terms, one has to study the amoeba and coamoeba of the singular manifold.[24] Oscillations can be handled by techniques similar to those discussed here, as has already been done in Ref. [19].

Another natural extension of our study is to the 3D Euler equations which also have a short-time régime. This is rather straightforward. A direct extension of the algorithm used in two dimensions requires CPU resources (time complexity) proportional to $k_{\max}^6$ instead of $k_{\max}^4$. This becomes prohibitively large when $k_{\max}$ exceeds a few hundred. In principle, the time complexity can be reduced to $k_{\max}^3$ (with logarithmic corrections) by using FFT's and the recent technique of "relaxed multiplications" [37]. However, in the calculations reported in MBF and the present paper the magnitude of Fourier coefficients can vary by several hundred orders of magnitude; this requires special precautions when applying FFT's unless one is prepared to use several hundred digits.

We remind the reader that our long term goal is to find out about blow-up in three dimensions (3D). We hope this will not take another 250 years. Progress may however be painfully slow if, as we expect, numerical experimentation is to play an important part. Indeed, the amazingly fast growth of computer power observed over the last 50 years becomes much less spectacular when translated in terms of resolution achievable in 3D simulations.[25] As more powerful computers become available for investigation of 3D blow-up, it would not be advisable to use the new resources exclusively for increasing the spatial resolution. Experience on the advantage of ultra-high precision for singularity studies from the work of Krasny [21], Shelley [20], Caflisch [19] and also from our own work suggest that it is not safe to use less than 30–35 digits. Using flows with symmetries such as the Taylor–Green [13,14] or the Kida–Pelz [15–17] flow to boost the resolution introduces a possible element of non-genericity, but we can always use such flows to sharpen our tools and then, as computers become more powerful, turn to flows without symmetry.

Have the results reported in MBF and the present paper brought us closer to this Holy Grail of 3D blow-up? In a direct way, we cannot infer anything regarding 3D real blow-up from a 2D study of complex singularities at short times. We have however learned that in this rather restricted framework, singularities are located on very smooth objects (possibly analytic manifolds); because the fastest spatial variation is then in the direction perpendicular to the singular manifold, the singularities have strongly depleted nonlinearity in a suitable frame. We have already good evidence that in 2D this smoothness property is not limited to the short-time régime [4]. In 3D such a

[24] In d-dimensional algebraic geometry one deals with an algebraic manifold in complex coordinates $\zeta_1, \dots \zeta_d$ and the amoeba is defined as the image of the manifold under the map $\zeta_1 \mapsto y_1 \equiv \ln|\zeta_1|, \dots, \zeta_d \mapsto y_d \equiv \ln|\zeta_d|$. The coamoeba is similarly defined in terms of the argument functions of the ζ's. The complex exponentials $\mathrm{e}^{-\mathrm{i}z_1}, \dots, \mathrm{e}^{-\mathrm{i}z_d}$, play here the role of the ζ_i's. The name amoeba has been proposed by Gelfand et al. [36] because amoebae sometimes have pseudopods resembling those of microscopic protozoa. Coamoebae have been introduced by Tsikh and Passare (private communication).

[25] At the moment the highest resolution accessible in 15-digit precision for three-dimensional flow without any special symmetries is 2048^3 [38,39].

property would be both a curse, since dominant balance cannot be used, and perhaps a blessing, since it might well slow down (indefinitely?) the approach of singularities to the real domain.

Acknowledgments

We are grateful to M. Blank, H. Frisch, J. van der Hoeven, D. Mitra, A. Pumir, A. Sobolevskiĭ, A.K. Tsikh, P. Zimmermann and an anonymous referee for useful discussions and comments. Part of this work was done while the authors participated in "Frontiers of Non Linear Physics" (Nizhny Novgorod, Russia, July 5–12, 2004) and in "Singularities, coherent structures and their role in intermittent turbulence" (Warwick, UK, September 9–17, 2005). TM and JB were supported by the Grant-in-Aid for the 21st Century COE "Center for Diversity and Universality in Physics" from the Japanese Ministry of Education. TM was supported by the Japanese Ministry of Education Grant-in-Aid for Young Scientists [(B), 15740237, 2003] and by the French Ministry of Education. UF was supported by the Grant-in-Aid for the 21st Century COE "Center of Excellence for Research and Education on Complex Functional Mechanical Systems" from the Japanese Ministry of Education. WP had partial support from the European network EU RTN no. HPRN-CT-2002-00282 'Hyké. JB, UF and WP had partial support from the Fédération de Recherche Wolfgang Doeblin (FR 2800 CNRS). Part of the computational resources were provided by the Yukawa Institute for Theoretical Physics (Kyoto) and by the Mésocentre SIGAMM (Nice).

Appendix. Reduction of multimode initial conditions

Here we shall show that the short-time asymptotics of two-dimensional Euler flows with generic initial conditions of trigonometric polynomial type can be reduced to the study of two-mode initial conditions. In Section 2 we have seen that with two initial modes $\mathfrak{p}$ and $\mathfrak{q}$ the behavior of the stream function $\Psi(z,t)$ for large imaginary arguments $|y_1|$, $|y_2|$ can be described by the *similarity ansatz* (6) and (7). It relies on the fact that when $\boldsymbol{y}$ is such that $\mathfrak{p}_2/\mathfrak{p}_1 \le y_2/y_1 \le \mathfrak{q}_2/\mathfrak{q}_1$ the leading-order factors accompanying each factor t in the time–Taylor expansion (4) are either $\mathrm{e}^{-\mathrm{i}\mathfrak{p}z}$ or $\mathrm{e}^{-\mathrm{i}\mathfrak{q}z}$. In the limit $|\boldsymbol{y}| \to \infty$, $t \to 0$ we can make such terms finite by shifting simultaneously $\mathfrak{p}\cdot\boldsymbol{y}$ and $\mathfrak{q}\cdot\boldsymbol{y}$ by $\ln t$.

The similarity ansatz as explained above is however not applicable to the case of more than two initial modes. Instead, we have to reduce the multimode initial condition to various two-mode problems which can be handled in the usual way. Let us illustrate this by looking at a simple three-mode initial condition

$$\Psi_0(\boldsymbol{x}) = h_1\mathrm{e}^{\mathrm{i}\mathfrak{p}\boldsymbol{x}} + h_2\mathrm{e}^{\mathrm{i}\mathfrak{q}\boldsymbol{x}} + +h_3\mathrm{e}^{\mathrm{i}\mathfrak{r}\boldsymbol{x}} + \text{c.c.}, \tag{A.1}$$

in which the vectors $\mathfrak{p}$, $\mathfrak{q}$ and $\mathfrak{r}$ are listed in angular counterclockwise order. As in Section 2, to avoid pathologies, we assume that the vectors $\mathfrak{p}$, $\mathfrak{q}$, $\mathfrak{r}$ are not parallel and not of the same length. In the Taylor expansion (4) each factor t will now be accompanied by a factor $\mathrm{e}^{-\mathrm{i}\mathfrak{p}z}$, $\mathrm{e}^{-\mathrm{i}\mathfrak{q}z}$ or $\mathrm{e}^{-\mathrm{i}\mathfrak{r}z}$. Note that, in the limit $|\boldsymbol{y}| \to \infty$, $t \to 0$, we cannot simultaneously make the terms $t\mathrm{e}^{\mathfrak{p}\boldsymbol{y}}$, $t\mathrm{e}^{\mathfrak{q}\boldsymbol{y}}$ and $t\mathrm{e}^{\mathfrak{r}\boldsymbol{y}}$ remain finite. Indeed, we cannot translate $\boldsymbol{y}$ in such a way that all three scalar products $\mathfrak{p}\cdot\boldsymbol{y}$, $\mathfrak{q}\cdot\boldsymbol{y}$ and $\mathfrak{r}\cdot\boldsymbol{y}$ are shifted by $\ln t$. If $\mathfrak{p}_2/\mathfrak{p}_1 \le y_2/y_1 \le \mathfrak{q}_2/\mathfrak{q}_1$ the factors $t\mathrm{e}^{\mathfrak{p}\boldsymbol{y}}$ and $t\mathrm{e}^{\mathfrak{q}\boldsymbol{y}}$ will dominate, while if $\mathfrak{q}_2/\mathfrak{q}_1 \le y_2/y_1 \le \mathfrak{r}_2/\mathfrak{r}_1$ the factors $t\mathrm{e}^{\mathfrak{q}\boldsymbol{y}}$ and $t\mathrm{e}^{\mathfrak{r}\boldsymbol{y}}$ will dominate. In each case the three-mode initial condition (A.1) is reduced to a two-mode problem involving either $\mathfrak{p}$ and $\mathfrak{q}$ or $\mathfrak{q}$ and $\mathfrak{r}$.

Let us now turn to the general multimode case with an initial stream function of the form

$$\Psi_0(z_1,z_2) = \sum_{(k_1,k_2)\in\operatorname{supp}\hat{F}^{(0)}} \hat{F}^{(0)}(k_1,k_2)\mathrm{e}^{-\mathrm{i}k_1z_1}\mathrm{e}^{-\mathrm{i}k_2z_2}. \tag{A.2}$$

Here, we assume Hermitian symmetry[26] $\hat{F}^{(0)*}(k_1,k_2) = \hat{F}^{(0)}(-k_1,-k_2)$ and we take the sum over all wavevectors for which the Fourier coefficients $\hat{F}^{(0)}(k_1,k_2)$ do not vanish, called the *support* of $\hat{F}^{(0)}$ and denoted $\operatorname{supp}\hat{F}^{(0)}$. The fact that $\operatorname{supp}\hat{F}^{(0)}$ is a finite set plays a crucial part in our analysis. Let us suppose for simplicity that all initial modes have different lengths, that is $|(k_1',k_2')| \ne |(k_1'',k_2'')|$ for all pairs (k_1',k_2') and $(k_1'',k_2'') \in \operatorname{supp}\hat{F}^{(0)}$.

As we have seen before, it is necessary to distinguish between different directions in the $\boldsymbol{y}$-space when taking the limits $|\boldsymbol{y}| \to \infty$, $t \to 0$. Therefore we let $|y_1|, |y_2| \to \infty$ while keeping the ratio y_2/y_1 fixed. By Hermitian symmetry, it is enough to consider only the case $y_1 \to +\infty$. Assuming as in Section 2 that

$$\Psi(z,t) = \sum_{n=0}^{\infty} \Psi_n(z)\, t^n, \tag{A.3}$$

and denoting by $\hat{F}^{(n)}(\boldsymbol{k})$ the Fourier coefficients of Ψ_n we obtain easily from the Euler equation the following recursion relations for the Fourier coefficients of the $(n+1)$th "generation":

$$\hat{F}^{(n+1)}(k_1,k_2) = -\frac{1}{n+1}\frac{1}{|k|^2} \times \sum_{m+p=n}\ \sum_{\boldsymbol{k}'+\boldsymbol{k}''=\boldsymbol{k}} (\boldsymbol{k}'\wedge\boldsymbol{k}'')|\boldsymbol{k}''|^2\hat{F}^{(m)}(k_1',k_2')\hat{F}^{(p)}(k_1'',k_2''), \tag{A.4}$$

which allows us to compute $\hat{F}^{(n+1)}(\boldsymbol{k})$ in terms of the previous generations $\hat{F}^{(m)}(\boldsymbol{k})$ and $\hat{F}^{(p)}(\boldsymbol{k})$ with $m, p \ge 0$ and $m+p=n$. From (A.4) it follows immediately that $\hat{F}^{(n)}$ has finitely many non-vanishing modes.

We now identify the modes in the nth generation which give the leading-order contributions to $\Psi_n(z)$ for a fixed ratio y_2/y_1. For this we use the notion of *Newton polytope* of $\operatorname{supp}\hat{F}^{(0)}$. It is defined as the convex hull (in the usual sense) of the set $\operatorname{supp}\hat{F}^{(0)}$, as for example represented (taking into account the Hermitian symmetry) on Fig. 22 for a typical initial condition. We shall call *relevant* those initial modes lying on the boundary of the Newton polytope of $\operatorname{supp}\hat{F}^{(0)}$ (black circles indicated by arrows on Fig. 22). The relevant modes divide the $\boldsymbol{k}$-space into

[26] In fact, this condition is not essential. We could as well consider more general sets $\operatorname{supp}\hat{F}^{(0)}$.

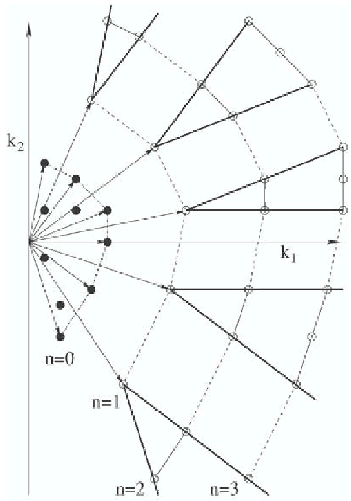

Fig. 22. Construction of relevant Fourier modes in various angular sectors. Black circles: initial modes; dash-dotted lines: boundary of the Newton polytope of the initial modes; white circles: higher-order modes associated to nth generation. Thick lines show the edges of the various angular sectors.

angular sectors, analogously to the three-mode case presented above.

Let now $\boldsymbol{k}'$ and $\boldsymbol{k}''$ be two relevant modes defining an angular sector such that $\boldsymbol{k}' \wedge \boldsymbol{k}'' > 0$. The vectors $\boldsymbol{k}'$ and $\boldsymbol{k}''$ define an angular sector in the $\boldsymbol{y}$-space such that $k_2'/k_1' \leq y_2/y_1 \leq k_2''/k_1''$. For these directions the leading-order terms in $\Psi_n(\boldsymbol{z})$ are proportional to $\mathrm{e}^{(n'\boldsymbol{k}'+n''\boldsymbol{k}'')\cdot\boldsymbol{y}}$ with $n', n'' \geq 1$ and $n' + n'' = n + 1$; the terms corresponding to other Fourier modes are subdominant. Clearly, we would have obtained the same dominant terms if we had started from just the two initial modes $\boldsymbol{k}'$ and $\boldsymbol{k}''$. We can now apply the similarity ansatz, shifting $\boldsymbol{k}' \cdot \boldsymbol{y}$ and $\boldsymbol{k}'' \cdot \boldsymbol{y}$ by $\ln t$. Let us remark that while it is possible to eliminate the time variable by a global similarity ansatz for two-mode asymptotics, it is in general impossible to do so for more than two modes.

In the exceptional cases where two or more relevant modes have the same length one must take into account the fact that the Fourier coefficient of their sum vanishes. The description of the leading-order contributions in the nth generation becomes slightly more involved than in the generic case, but the leading-order behavior in a fixed direction y_2/y_1 is still dominated by two-mode asymptotics.

Summarizing, we have shown that the study of the short-time asymptotics of Euler flows with multimode initial conditions can be reduced to the analysis of various two-mode asymptotics in angular sectors defined by a suitable set of relevant initial modes, namely those on the boundary of the Newton polytope of the initial modes.

References

[1] And it bubbles and seethes, and it hisses and roars, As when fire is with water commix'd and contending, And the spray of its wrath to the welkin up-soars, And flood upon flood hurries on, never-ending (translation by Edward, Lord Lytton).
[2] L. Euler, Principes généraux du mouvement des fluides, Histoire de l'Académie des Sciences et des Belles-Lettres de Berlin 11 (1755) 1757, 274–315.
[3] A.J. Majda, A.L. Bertozzi, Vorticity and Incompressible Flow, Cambridge University Press, Cambridge, 2000.
[4] U. Frisch, T. Matsumoto, J. Bec, Singularities of the Euler equation? Not out of the blue! J. Stat. Phys. 113 (2003) 761–781.
[5] E. Hölder, Über die unbeschränkte Fortsetzbarkeit einer stetigen ebenen Bewegung in einer unbegrenzten inkompresiblen Flüssigkeit, Math. Z. 37 (1933) 727–738.
[6] W. Wolibner, Un théorème sur l'existence du mouvement plan d'un fluide parfait, homogène, incompressible, pendant un temps infiniment long, Math. Z. 37 (1933) 698–726.
[7] C. Bardos, S. Benachour, M. Zerner, Analyticité des solutions périodiques de l'équation d'Euler en deux dimensions, C. R. Acad. Sci. Paris 282 A (1976) 995–998.
[8] S. Benachour, Analyticité des solutions de l'équation d'Euler en trois dimensions, C. R. Acad. Sci. Paris 283 A (1976) 107–110.
[9] S. Benachour, Analyticité des solutions des équations d'Euler, Arch. Ration. Mech. Anal. 71 (1976) 271–299.
[10] C. Sulem, P.L. Sulem, H. Frisch, Tracing complex singularities with spectral methods, J. Comput. Phys. 50 (1983) 138–161.
[11] U. Frisch, Turbulence, the Legacy of A.N. Kolmogorov, Cambridge University Press, Cambridge, 1995.
[12] T. Matsumoto, J. Bec, U. Frisch, The analytic structure of 2D Euler flow at short times, Fluid Dyn. Res. 36 (2005) 221–237.
[13] G.I. Taylor, A.E. Green, Mechanism of the production of small eddies from large ones, Proc. R. Soc. A 158 (1937) 499–521.
[14] M.E. Brachet, D.I. Meiron, S.A. Orszag, B.G. Nickel, R.H. Morf, U. Frisch, Small-scale structure of the Taylor–Green vortex, J. Fluid Mech. 167 (1983) 411–452.
[15] S. Kida, Three-dimensional periodic flows with high-symmetry, J. Phys. Soc. Japan 54 (1985) 2132–2136.
[16] R.B. Pelz, Y. Gulak, Evidence for a real-time singularity in hydrodynamics from time series analysis, Phys. Rev. Lett. 79 (1997) 4998–5001.
[17] C. Cichowlas, M.E. Brachet, Evolution of complex singularities in Kida–Pelz and Taylor–Green inviscid flows, Fluid Dyn. Res. 36 (2005) 239–248.
[18] S. Tanveer, C.G. Speziale, Singularities of the Euler equation and hydrodynamic stability, Phys. Fluids A 5 (1993) 1456–1465.
[19] R.E. Caflisch, Singularity formation for complex solutions of the 3D incompressible Euler equation, Physica D 67 (1993) 1–18.
[20] M.J. Shelley, A study of singularity formation in vortex sheet motion by a spectrally accurate vortex method, J. Fluid Mech. 244 (1992) 493–526.
[21] R. Krasny, A study of singularity formation in a vortex sheet by the point-vortex approximation, J. Fluid Mech. 167 (1986) 65–93.
[22] J. Weiss, M. Tabor, G. Carnevale, The Painlevé property for partial differential equations, J. Math. Phys. 24 (1983) 552–559.
[23] D.W. Moore, The spontaneous appearance of a singularity in the shape of an evolving vortex sheet, Proc. R. Soc. Lond. A 365 (1979) 105–119.
[24] G.F. Carrier, M. Krook, C.E. Pearson, Functions of a Complex Variable: Theory and Technique, McGraw-Hill, New York, 1966.
[25] A.K. Tsikh, Conditions for absolute convergence of series of Taylor coefficients of meromorphic functions of two variables, Math. USSR Sbornik 74 (1993) 336–360.
[26] A.G. Orlov, On asymptotics of Taylor coefficients of rational functions of two variables, Russian Math. (Iz. Vuz) 37 (6) (1993) 23–30 (translated from: Izv. Vuzov Mat. 37 (6) (1993) 26–33).
[27] A.G. Orlov, About asymptotics of Taylor coefficients of algebraic functions, Siberian Math. J. 35 (1994) 1125–1137 (in Russian).
[28] D.H. Bailey, A fortran-90 based multiprecision system, RNR Technical Report, RNR-94-013, 1995. See also http://crd.lbl.gov/~dhbailey/.
[29] P. Wynn, The rational approximation of functions which are formally defined by a power series expansion, Math. Comput. 14 (1960) 147–186.

[30] D. Shanks, Non-linear transformations of divergent and slowly convergent, sequences, J. Math. Phys. 34 (1955) 1–42.
[31] J. van der Hoeven, Algorithms for asymptotic interpolation, J. Symbolic Comput. (2006) (submitted for publication). Preprint 2006-12 Dep. Math. Univ. Paris-Sud. See also http://www.math.u-psud.fr/~vdhoeven/Publs/2006/interpolate.ps.gz.
[32] C.M. Bender, S.A. Orszag, Advanced Mathematical Methods for Scientists and Engineers, McGraw-Hill, 1978.
[33] P. Dienes, The Taylor Series, an Introduction to the Theory of Functions of a Complex Variable, Oxford University Press, 1931.
[34] B.V. Shabat, Introduction to Complex Analysis Part II: Functions of Several Variables, American Mathematical Society, 1992.
[35] W. Pauls, T. Matsumoto, Lagrangian singularities of steady two-dimensional flows, Geophys. Astrophys. Fluid Dyn. 99 (2005) 61–75.
[36] I. Gelfand, M. Kapranov, A. Zelevinsky, Discriminants, Resultants and Multidimensional Determinants, Birkhäuser, Boston, 1994.
[37] J. van der Hoeven, Relax, but don't be too lazy, J. Symbolic Comput. 34 (2002) 479–542.
[38] K. Itakura, A. Uno, M. Yokokawa, M. Saito, T. Ishihara, Y. Kaneda, Performance tuning of a CFD code on the Earth Simulator, NEC Res. Dev. 44 (2003) 115–120.
[39] Y. Kaneda, T. Ishihara, M. Yokokawa, K. Itakura, A. Uno, Energy dissipation rate and energy spectrum in high resolution direct numerical simulations of turbulence in a periodic box, Phys. Fluids 15 (2003) L21–L42.

Chapter 7

2D MHD equations

7.1 Short-time asymptotic régime for the 2D MHD equations

In this section we shall study the short-time asymptotics for two-dimensional ideal conducting flow governed by the two-dimensional MHD equations

$$\begin{aligned} &\partial_t \nabla^2 \Psi = J(\Psi, \nabla^2 \Psi) - J(A, \nabla^2 A) \\ &\partial_t A = J(\Psi, A). \end{aligned} \tag{7.1}$$

Here, Ψ is the stream function and A is the magnetic potential. Just as in the case of the Euler equation, in the short-time régime the solutions of (7.1) with trigonometric polynomial initial conditions are reducible to solving a problem with only two-modes in the initial condition.

A general two-mode initial condition is the MHD analogue of (6.2), namely

$$\begin{aligned} \Psi_0(z_1, z_2) &= \hat{F}(\mathfrak{p}) \mathrm{e}^{-\mathrm{i}\,\mathfrak{p}\cdot z} + \hat{F}(\mathfrak{q}) \mathrm{e}^{-\mathrm{i}\,\mathfrak{q}\cdot z}, \\ A_0(z_1, z_2) &= \hat{F}_{\mathrm{m}}(\mathfrak{p}) \mathrm{e}^{-\mathrm{i}\,\mathfrak{p}\cdot z} + \hat{F}_{\mathrm{m}}(\mathfrak{q}) \mathrm{e}^{-\mathrm{i}\,\mathfrak{q}\cdot z}. \end{aligned} \tag{7.2}$$

The nth coefficients in the time series expansion for the solution of (7.1) have a form similar to that of the two-dimensional Euler equation (6.4)

$$\begin{aligned} \Psi^{(n)} &= \sum_{\sigma=0}^{n+1} \hat{F}((n+1-\sigma)\mathfrak{p} + \sigma\mathfrak{q}) \mathrm{e}^{-\mathrm{i}\,(n+1-\sigma)\mathfrak{p}\cdot z} \mathrm{e}^{-\mathrm{i}\,\sigma\mathfrak{q}\cdot z}, \\ A^{(n)} &= \sum_{\sigma=0}^{n+1} \hat{F}_{\mathrm{m}}((n+1-\sigma)\mathfrak{p} + \sigma\mathfrak{q}) \mathrm{e}^{-\mathrm{i}\,(n+1-\sigma)\mathfrak{p}\cdot z} \mathrm{e}^{-\mathrm{i}\,\sigma\mathfrak{q}\cdot z}. \end{aligned} \tag{7.3}$$

For the two-dimensional MHD equations we can also renormalize the Fourier coefficients just as in (6.5)

$$\begin{aligned} \hat{F}^{(n)}\left[(n+1-\sigma)\mathfrak{p} + \sigma\mathfrak{q}\right] &= (\mathfrak{p} \wedge \mathfrak{q})^n \, \hat{G}^{(n)}(\sigma), \\ \hat{F}_{\mathrm{m}}^{(n)}\left[(n+1-\sigma)\mathfrak{p} + \sigma\mathfrak{q}\right] &= (\mathfrak{p} \wedge \mathfrak{q})^n \, \hat{G}_{\mathrm{m}}^{(n)}(\sigma). \end{aligned} \tag{7.4}$$

The coefficients $\hat{G}^{(n)}(\sigma)$ and $\hat{G}^{(n)}(\sigma)$ are then easily found to satisfy the recursion relations

$$\begin{aligned}
&\hat{G}^{(n+1)}(\sigma) = -\frac{1}{n+1}\,\frac{1}{|(n-\sigma+2)\mathfrak{p}+\sigma\mathfrak{q}|^2}\sum_{m=0}^{n}\sum_{\tau=0}^{\sigma}\\
&|(n-m-(\sigma-\tau)+1)\mathfrak{p}+(\sigma-\tau)\mathfrak{q}|^2\times[(m+1)(\sigma-\tau)-(n-m+1)\tau]\\
&\left[\hat{G}^{(m)}(\tau)\hat{G}^{(n-m)}(\sigma-\tau)-\hat{G}_{\mathrm{m}}^{(m)}(\tau)\hat{G}_{\mathrm{m}}^{(n-m)}(\sigma-\tau)\right],\\
&\hat{G}_{\mathrm{m}}^{(n+1)}(\sigma) =\\
&-\frac{1}{n+1}\sum_{m=0}^{n}\sum_{\tau=0}^{\sigma}[(m+1)(\sigma-\tau)-(n-m+1)\tau]\,\hat{G}^{(m)}(\tau)\hat{G}_{\mathrm{m}}^{(n-m)}(\sigma-\tau),
\end{aligned}\tag{7.5}$$

initialized by

$$\begin{aligned}
\hat{G}^{(0)}(0) &= \hat{F}(\mathfrak{p}), \qquad \hat{G}^{(0)}(1) = \hat{F}(\mathfrak{q}),\\
\hat{G}_{\mathrm{m}}^{(0)}(0) &= \hat{F}_{\mathrm{m}}(\mathfrak{p}), \qquad \hat{G}_{\mathrm{m}}^{(0)}(1) = \hat{F}_{\mathrm{m}}(\mathfrak{q}).
\end{aligned}\tag{7.6}$$

As in the case of the short-time Euler equation, all the coefficients $\hat{G}^{(n)}(\sigma)$ and $\hat{G}^{(n)}(\sigma)$ can in principle be determined exactly. The first few coefficients are given by

$$\begin{aligned}
\hat{G}^{(1)}(1) =& -\frac{|\mathfrak{q}|^2-|\mathfrak{p}|^2}{|\mathfrak{p}+\mathfrak{q}|^2}\left[\hat{F}(\mathfrak{p})\hat{F}(\mathfrak{q})-\hat{F}_{\mathrm{m}}(\mathfrak{p})\hat{F}_{\mathrm{m}}(\mathfrak{q})\right],\\
\hat{G}_{\mathrm{m}}^{(1)}(1) =& -\hat{F}(\mathfrak{p})\hat{F}_{\mathrm{m}}(\mathfrak{q})+\hat{F}(\mathfrak{q})\hat{F}_{\mathrm{m}}(\mathfrak{p}),\\
G^{(2)}(1) =& \frac{1}{2}\frac{|\mathfrak{q}|^2-|\mathfrak{p}|^2}{|\mathfrak{p}+\mathfrak{q}|^2}\frac{|\mathfrak{p}+\mathfrak{q}|^2-|\mathfrak{p}|^2}{|2\mathfrak{p}+\mathfrak{q}|^2}\left(\hat{F}(\mathfrak{p})\right)^2\hat{F}(\mathfrak{q})+\\
&\frac{1}{2}\frac{|\mathfrak{p}+\mathfrak{q}|^2-|\mathfrak{p}|^2}{|2\mathfrak{p}+\mathfrak{q}|^2}\left(\hat{F}_{\mathrm{m}}(\mathfrak{p})\right)^2\hat{F}(\mathfrak{q})-\\
&\frac{1}{2}\frac{|\mathfrak{p}+\mathfrak{q}|^2-|\mathfrak{p}|^2}{|2\mathfrak{p}+\mathfrak{q}|^2}\left(1+\frac{|\mathfrak{q}|^2-|\mathfrak{p}|^2}{|\mathfrak{p}+\mathfrak{q}|^2}\right)\hat{F}(\mathfrak{p})\hat{F}_{\mathrm{m}}(\mathfrak{p})\hat{F}_{\mathrm{m}}(\mathfrak{q}),\\
\hat{G}_{\mathrm{m}}^{(2)}(1) =& \frac{1}{2}\left(\hat{F}(\mathfrak{p})\right)^2\hat{F}_{\mathrm{m}}(\mathfrak{q})-\frac{1}{2}\hat{F}(\mathfrak{p})\hat{F}(\mathfrak{q})\hat{F}_{\mathrm{m}}(\mathfrak{p})-\\
&\frac{1}{2}\frac{|\mathfrak{q}|^2-|\mathfrak{p}|^2}{|\mathfrak{p}+\mathfrak{q}|^2}\hat{F}(\mathfrak{p})\hat{F}_{\mathrm{m}}(\mathfrak{p})\hat{F}_{\mathrm{m}}(\mathfrak{q})+\\
&\frac{1}{2}\frac{|\mathfrak{q}|^2-|\mathfrak{p}|^2}{|\mathfrak{p}+\mathfrak{q}|^2}\left(\hat{F}_{\mathrm{m}}(\mathfrak{p})\right)^2\hat{F}_{\mathrm{m}}(\mathfrak{q}).
\end{aligned}\tag{7.7}$$

For the initial conditions of the type (7.2) the dependence on the amplitudes of the initial conditions is not as explicit as in the case of the two-dimensional Euler equation. Contrary to the two-dimensional Euler cases we cannot render the problem independent of the initial ampitudes by performing a suitable imaginary translation. The solutions of (7.5) with initial conditions (7.6) depend on two real and two complex parameters. The two real parameters are the aspect ratio $\eta = |\mathfrak{q}|/|\mathfrak{p}|$ of the two basic vectors and the angle ϕ between $\mathfrak{p}$ and $\mathfrak{q}$. The two amplitude-dependent complex parameters are obtained by reducing the four complex initial amplitudes using translation invariance.

Furthermore, it may be shown from the explicit formulae (7.7) for the first few coefficients that the positivity which we observed for the two-dimensional Euler equation is not conserved generically.

The counterpart of (7.5) in the physical space is given by

$$\begin{aligned}\check{\Delta}_{(\mathfrak{p},\mathfrak{q})}G &= (\check{\partial}_1 G+1)(\check{\partial}_2\check{\Delta}_{(\mathfrak{p},\mathfrak{q})}G)-(\check{\partial}_2 G-1)(\check{\partial}_1\check{\Delta}_{(\mathfrak{p},\mathfrak{q})}G)-\\ &(\check{\partial}_1 G_{\mathrm{m}})(\check{\partial}_2\check{\Delta}_{(\mathfrak{p},\mathfrak{q})}G_{\mathrm{m}})+(\check{\partial}_2 G_{\mathrm{m}})(\check{\partial}_1\check{\Delta}_{(\mathfrak{p},\mathfrak{q})}G_{\mathrm{m}}),\\ G_{\mathrm{m}} &= (\check{\partial}_1 G+1)(\check{\partial}_2 G_{\mathrm{m}})-(\check{\partial}_2 G-1)(\check{\partial}_1 G_{\mathrm{m}}),\end{aligned} \tag{7.8}$$

or, in terms of the modified stream function $H(\check{z}_1,\check{z}_2)$ introduced in Chapter 6

$$\begin{aligned}\check{\Delta}_{(\mathfrak{p},\mathfrak{q})}H &= \check{J}(H,\check{\Delta}_{(\mathfrak{p},\mathfrak{q})}G)-\check{J}(G_{\mathrm{m}},\check{\Delta}_{(\mathfrak{p},\mathfrak{q})}G_{\mathrm{m}}),\\ G_{\mathrm{m}} &= \check{J}(H,G_{\mathrm{m}}).\end{aligned} \tag{7.9}$$

Here $G_{\mathrm{m}}(\check{z}_1,\check{z}_2)$ is defined analogously to $G(\check{z}_1,\check{z}_2)$ in (6.10) by

$$\check{G}_{\mathrm{m}}(\check{z}_1,\check{z}_2)=G_{\mathrm{m}}^{(0)}(0)\mathrm{e}^{\check{z}_1}+G_{\mathrm{m}}^{(0)}(1)\mathrm{e}^{\check{z}_2}+\sum_{n=1}^{\infty}\sum_{\sigma=1}^{n}\hat{G}_{\mathrm{m}}^{(n)}(\sigma)\mathrm{e}^{\sigma\check{z}_1}\mathrm{e}^{(n+1-\sigma)\check{z}_2}. \tag{7.10}$$

7.2 Numerical study of the short-time asymptotics of the two-dimensional MHD equations

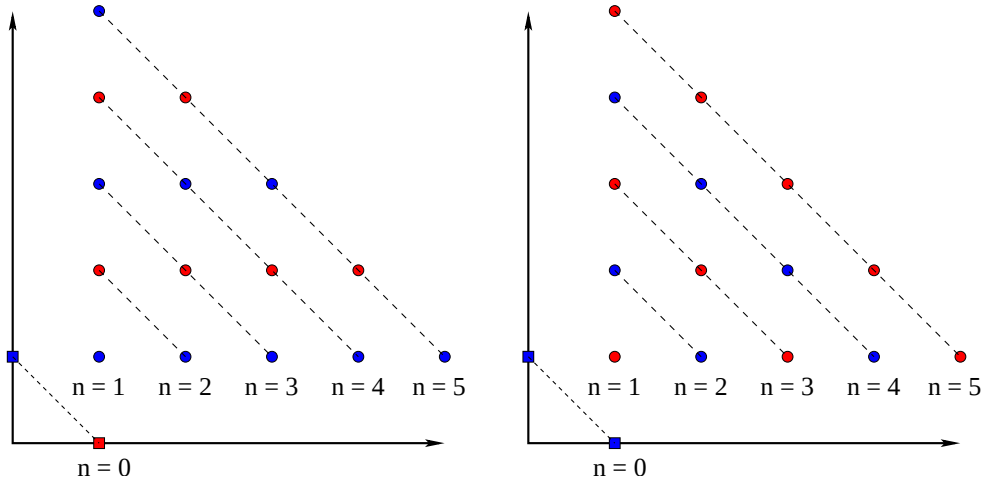

Figure 7.1: Excited modes for (i) purely magnetic and (ii) mixed initial conditions.

Exploring numerically the whole parameter space of solution to (7.5) is quite a formidable task. For the moment I have restricted my attention to two special initial conditions: (i) *purely magnetic* initial condition $\hat{F}(\mathfrak{p})=\hat{F}(\mathfrak{q})=0$, (ii) *mixed* initial condition with one non-vanishing amplitude in the velocity field and one in the magnetic field. In both cases the translation invariance allows us to eliminate the amplitides of the initial modes just as in the case of the two-dimensional Euler equation (6.5). A pathological feature of these initial conditions is that the velocity and magnetic modes $\hat{G}^{(n)}(\sigma)$ and $\hat{G}_{\mathrm{m}}^{(n)}(\sigma)$ are never excited simultaneously.

7.2.1 Purely magnetic initial conditions

In the case (i) of purely magnetic initial conditions we have found that, just as in the two-dimensional Euler case, all the Fourier coefficients of the renormalized stream function $\hat{G}^{(n)}(\sigma)$ except one can be made positive upon multiplying them by $(-1)^{n-\sigma}$. The same

applies to the renormalized magnetic potential $\hat{G}_{\mathrm{m}}^{(n)}(\sigma)$ which becomes positive after multiplication by $(-1)^{n+1-\sigma}$.

I have calculated the Fourier coefficients of the stream function and of the vector potential numerically – using high-precision arithmetics – for various values of the basic vectors $\mathfrak{p}$ and $\mathfrak{q}$, with resolution up to $N_{\max} = 2000$. The numerical data have then been analyzed along various rational direction. It is found that for high wavenumbers the asymptotic behavior is of the same type as in the case of the two-dimensional Euler equation[1]

$$\hat{G}(k,\theta) \sim C(\theta)k^{-\alpha(\theta)}\mathrm{e}^{-\delta(\theta)}, \qquad \hat{G}_{\mathrm{m}}(k,\theta) \sim C_{\mathrm{m}}(\theta)k^{-\alpha_{\mathrm{m}}(\theta)}\mathrm{e}^{-\delta_{\mathrm{m}}(\theta)}. \tag{7.11}$$

Numerically the evidence is that α is equal to α_{m}.

There are now at least three questions which can be addressed regarding the scaling exponents α and α_{m}: firstly, do $\alpha(\theta)$ and $\alpha_{\mathrm{m}}(\theta)$ really depend on θ, secondly, are their values different, and, thirdly, if $\alpha(\theta)$ and $\alpha_{\mathrm{m}}(\theta)$ are independent of θ, how do their values vary when we change the basic modes $\mathfrak{p}$ and $\mathfrak{q}$?

For various choices of the basic vectors $\mathfrak{p}$ and $\mathfrak{q}$ I have found that the angular variation of $\alpha(\theta)$ and $\alpha_{\mathrm{m}}(\theta)$ (measured numerically by using the asymptotic interpolation method, cf Chapter 5) is significantly stronger than in the case of the two-dimensional Euler equation. For example, in the case $\mathfrak{p} = (1,0)$, $\mathfrak{q} = (0,2)$, $N_{\max} = 2000$ I measure $\alpha \approx 3/2$, $\alpha_{\mathrm{m}} \approx 3/2$, with variations of order 10^{-2}. It is conjectured that the scaling exponents α and α_{m} do not depend on θ and that the apparently observed angular variations are due to strong subleading-order corrections. I note that with the currently available resolution it is not possible to identify such corrections numerically.

By measuring α and α_{m} for various basic modes I found that $\alpha \approx 3/2$ and $\alpha_{\mathrm{m}} \approx 3/2$. I thus conjecture, that the scaling exponent $\alpha = 3/2 = \alpha_{\mathrm{m}}$ is universal for the two-

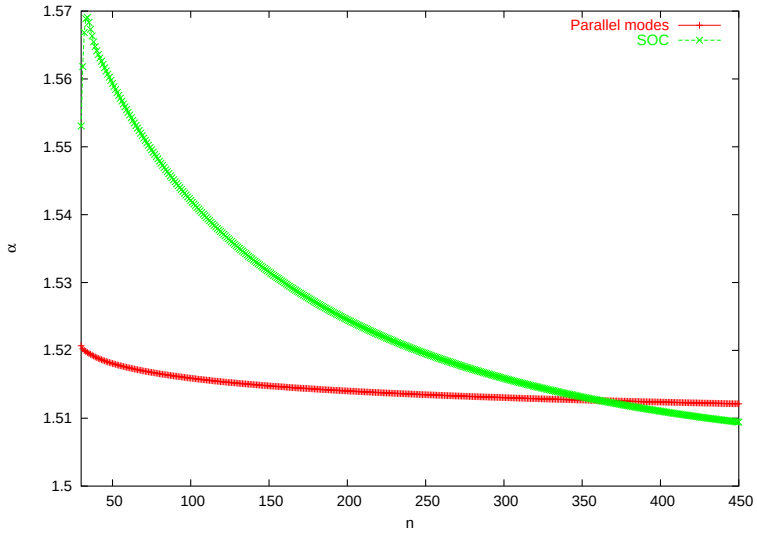

Figure 7.2: Scaling exponents α measured along the rational direction $(1,1)$ for initial conditions of the purely magnetic type with basic vectors $\mathfrak{p} = (1,0)$, $\mathfrak{q} = (0,2)$ (SOC) and $\mathfrak{p} = (1,0)$, $\mathfrak{q} = (2,0)$ (parallel modes).

dimensional MHD equations.

[1] We use the notation $\hat{G}^{(n)}(\sigma) = \hat{G}(k_1,k_2)$ and $\hat{G}_{\mathrm{m}}^{(n)}(\sigma) = \hat{G}_{\mathrm{m}}(k_1,k_2)$, with $k_1 = n+1-\sigma$ and $k_2 = \sigma$.

7.2.2 Mixed initial conditions

Due to the positivity of the Fourier coefficients the purely magnetic case does not have geometric properties differing substantially from those of the pure Euler case. The singularities which are closest to the real domain are located "above" the symmetry point $(\pi, 0)$, just as in the case of the two-dimensional Euler equation. As I have found numerically, the mixed case (in which we have only one non-vanishing initial amplitude in the stream function and one in the magnetic potential) has new life.

For example, for the initial conditions $\mathfrak{p} = (1, 0)$, $\mathfrak{q} = (0, 2)$, $\hat{G}(1, 0) = 0$, $\hat{G}(0, 1) = 1$, $\hat{G}_{\mathrm{m}}(1, 0) = 1$, $\mathrm{G}(0, 1) = 0$ the Fourier coefficients $\hat{G}(k_1, k_2)$ and $\hat{G}_{\mathrm{m}}(k_1, k_2)$ are not positive anymore. This indicates that the singularities "split", a phenomenon which is also observed beyond the short-time régime for solutions of the Euler equation.

The geometry of singularities can studied, for example, by the two-dimensional generalization of the Borel–Pólya–Hoeven method presented in Chapter 5. We also note, that the two-dimensional BPH method allows us to determine the value of the scaling exponents α and α_{m} and thus, to test the conjectured universality.

Chapter 8

3D Euler equation

8.1 Short-time asymptotic régime for the three-dimensional Euler equation

In this chapter we represent briefly the short-time asymptotic expansion for the three-dimensional Euler equation. Just as in the cases of the two-dimensional Euler and MHD equations at short time the problem is reducible to one with a small number of initial modes, here three, whose general form is

$$\begin{aligned} v_1(z_1,z_2,z_3) &= v_1^{(0)}(\mathfrak{p})\mathrm{e}^{-\mathrm{i}\,\mathfrak{p}\cdot z} + v_1^{(0)}(\mathfrak{q})\mathrm{e}^{-\mathrm{i}\,\mathfrak{q}\cdot z} + v_1^{(0)}(\mathfrak{r})\mathrm{e}^{-\mathrm{i}\,\mathfrak{r}\cdot z} \\ v_2(z_1,z_2,z_3) &= v_2^{(0)}(\mathfrak{p})\mathrm{e}^{-\mathrm{i}\,\mathfrak{p}\cdot z} + v_2^{(0)}(\mathfrak{q})\mathrm{e}^{-\mathrm{i}\,\mathfrak{q}\cdot z} + v_2^{(0)}(\mathfrak{r})\mathrm{e}^{-\mathrm{i}\,\mathfrak{r}\cdot z} \\ v_3(z_1,z_2,z_3) &= v_3^{(0)}(\mathfrak{p})\mathrm{e}^{-\mathrm{i}\,\mathfrak{p}\cdot z} + v_3^{(0)}(\mathfrak{q})\mathrm{e}^{-\mathrm{i}\,\mathfrak{q}\cdot z} + v_3^{(0)}(\mathfrak{r})\mathrm{e}^{-\mathrm{i}\,\mathfrak{r}\cdot z}. \end{aligned} \tag{8.1}$$

Because of the incompressibility[1] condition the initial amplitudes have to satisfy

$$\mathfrak{p}\cdot v^{(0)}(\mathfrak{p}) = 0, \quad \mathfrak{q}\cdot v^{(0)}(\mathfrak{q}) = 0, \quad \mathfrak{r}\cdot v^{(0)}(\mathfrak{r}) = 0. \tag{8.2}$$

The similarity ansatz is given by

$$v(z;t) = \frac{1}{t}\tilde{v}(\tilde{z}), \qquad (z + \mathrm{i}\,\boldsymbol{\lambda}\ln t), \tag{8.3}$$

where the vector $\boldsymbol{\lambda}$ is given by

$$\begin{aligned} \lambda_1 &= \frac{1}{\det(\mathfrak{p},\mathfrak{q},\mathfrak{r})}\left(\mathfrak{q}_2\mathfrak{r}_3 - \mathfrak{q}_3\mathfrak{r}_2 + \mathfrak{p}_3\mathfrak{r}_2 - \mathfrak{p}_2\mathfrak{r}_3 + \mathfrak{p}_2\mathfrak{q}_3 - \mathfrak{p}_3\mathfrak{q}_2\right) \\ \lambda_2 &= \frac{1}{\det(\mathfrak{p},\mathfrak{q},\mathfrak{r})}\left(\mathfrak{q}_3\mathfrak{r}_1 - \mathfrak{q}_1\mathfrak{r}_3 + \mathfrak{p}_1\mathfrak{r}_3 - \mathfrak{p}_3\mathfrak{r}_1 + \mathfrak{p}_3\mathfrak{q}_1 - \mathfrak{p}_1\mathfrak{q}_3\right) \\ \lambda_3 &= \frac{1}{\det(\mathfrak{p},\mathfrak{q},\mathfrak{r})}\left(\mathfrak{q}_1\mathfrak{r}_2 - \mathfrak{q}_2\mathfrak{r}_1 + \mathfrak{p}_2\mathfrak{r}_1 - \mathfrak{p}_1\mathfrak{r}_2 + \mathfrak{p}_1\mathfrak{q}_2 - \mathfrak{p}_2\mathfrak{q}_1\right). \end{aligned} \tag{8.4}$$

Here $\det(\mathfrak{p},\mathfrak{q},\mathfrak{r})$ is the determinant of the matrix

$$(\mathfrak{p},\mathfrak{q},\mathfrak{r})^T = \begin{pmatrix} \mathfrak{p}_1 & \mathfrak{p}_2 & \mathfrak{p}_3 \\ \mathfrak{q}_1 & \mathfrak{q}_2 & \mathfrak{q}_3 \\ \mathfrak{r}_1 & \mathfrak{r}_2 & \mathfrak{r}_3 \end{pmatrix}. \tag{8.5}$$

[1] Since the incompressiblity condition has been for the first time derived by d'Alembert, it has been proposed to refer to it as d'Alembert's condition [DF07].

8.1.1 Fourier space representation

For the initial condition (8.1) the nth coefficient in the temporal Taylor expansion is a trigonometric polynomial supported on a polytope (2-simplex)

$$\boldsymbol{v}^{(n)}(z_1, z_2, z_3) = \sum_{\sigma_1+\sigma_2+\sigma_3=n+1} \hat{\boldsymbol{v}}^{(n)}(\sigma_1\mathfrak{p} + \sigma_2\mathfrak{q} + \sigma_3\mathfrak{r}) \exp\left[-\mathrm{i}\,(\sigma_1\mathfrak{p} + \sigma_2\mathfrak{q} + \sigma_3\mathfrak{r}) \cdot \boldsymbol{z}\right], \tag{8.6}$$

where $\sigma_1, \sigma_2, \sigma_3 \geq 0$. From the Euler equations and the trace formula for the Laplacian of the pressure the recursion relations for the Fourier coefficients can be found. For brevity we denote

$$\hat{\boldsymbol{v}}^{(n)}(\sigma_1\mathfrak{p} + \sigma_2\mathfrak{q} + \sigma_3\mathfrak{r}) = \hat{\boldsymbol{v}}^{(n)}(\sigma_1, \sigma_2, \sigma_3). \tag{8.7}$$

In order to avoid proliferation of complex notations we use the "imaginary" velocity $\hat{\boldsymbol{u}}^{(n)}$ defined through the relation $\hat{\boldsymbol{v}}^{(n)} = \mathrm{i}\,\hat{\boldsymbol{u}}^{(n)}$. An alternative to using the imaginary velocity is the use of the vector potential Ψ defined by $\boldsymbol{v} = \nabla \wedge \Psi$.

The recursion relations for $\hat{\boldsymbol{u}}^{(n)}$ are

$$\begin{aligned}
&\hat{\boldsymbol{u}}^{(n)}(\sigma_1, \sigma_2, \sigma_3) = -\frac{1}{n} \sum_{1\leq\sigma_1'+\sigma_2'+\sigma_3'\leq n} \\
&\Bigg(\Big\langle(\sigma_1 - \sigma_1')\mathfrak{p} + (\sigma_2 - \sigma_2')\mathfrak{q} + (\sigma_3 - \sigma_3')\mathfrak{r}\,,\ \hat{\boldsymbol{u}}^{(\sigma_1'+\sigma_2'+\sigma_3'-1)}(\sigma_1', \sigma_2', \sigma_3')\Big\rangle \times \\
&\hat{\boldsymbol{u}}^{(n-\sigma_1'-\sigma_2'-\sigma_3')}(\sigma_1 - \sigma_1', \sigma_2 - \sigma_2', \sigma_3 - \sigma_3') - \frac{\sigma_1\mathfrak{p} + \sigma_2\mathfrak{q} + \sigma_3\mathfrak{r}}{|\sigma_1\mathfrak{p} + \sigma_2\mathfrak{q} + \sigma_3\mathfrak{r}|^2} \times \\
&\Big\langle\sigma_1'\mathfrak{p} + \sigma_2'\mathfrak{q} + \sigma_3'\mathfrak{r}\,,\ \hat{\boldsymbol{u}}^{(n-\sigma_1'-\sigma_2'-\sigma_3')}(\sigma_1 - \sigma_1', \sigma_2 - \sigma_2', \sigma_3 - \sigma_3')\Big\rangle \times \\
&\Big\langle(\sigma_1 - \sigma_1')\mathfrak{p} + (\sigma_2 - \sigma_2')\mathfrak{q} + (\sigma_3 - \sigma_3')\mathfrak{r}\,,\ \hat{\boldsymbol{u}}^{(\sigma_1'+\sigma_2'+\sigma_3'-1)}(\sigma_1', \sigma_2', \sigma_3')\Big\rangle\Bigg).
\end{aligned} \tag{8.8}$$

Here $\langle\,\cdot\,,\,\cdot\,\rangle$ denotes the standard scalar product. The coefficients for the first generation $n = 1$ are

$$\begin{aligned}
&\hat{\boldsymbol{u}}^{(1)}(0,0,2) = \hat{\boldsymbol{u}}^{(1)}(0,0,2) = \hat{\boldsymbol{u}}^{(1)}(0,0,2) = 0, \\
&\hat{\boldsymbol{u}}^{(1)}(0,1,1) = 2\,\frac{\mathfrak{q}+\mathfrak{r}}{|\mathfrak{q}+\mathfrak{r}|^2}\,\langle\mathfrak{r}, \hat{\boldsymbol{u}}^{(0)}(0,1,0)\rangle\,\langle\mathfrak{q}, \hat{\boldsymbol{u}}^{(0)}(0,0,1)\rangle - \langle\mathfrak{q}, \hat{\boldsymbol{u}}^{(0)}(0,0,1)\rangle\,\hat{\boldsymbol{u}}^{(0)}(0,1,0) - \\
&\langle\mathfrak{r}, \hat{\boldsymbol{u}}^{(0)}(0,1,0)\rangle\,\hat{\boldsymbol{u}}^{(0)}(0,0,1) \\
&\hat{\boldsymbol{u}}^{(1)}(1,0,1) = 2\,\frac{\mathfrak{p}+\mathfrak{r}}{|\mathfrak{p}+\mathfrak{r}|^2}\,\langle\mathfrak{r}, \hat{\boldsymbol{u}}^{(0)}(1,0,0)\rangle\,\langle\mathfrak{p}, \hat{\boldsymbol{u}}^{(0)}(0,0,1)\rangle - \langle\mathfrak{p}, \hat{\boldsymbol{u}}^{(0)}(0,0,1)\rangle\,\hat{\boldsymbol{u}}^{(0)}(1,0,0) - \\
&\langle\mathfrak{r}, \hat{\boldsymbol{u}}^{(0)}(1,0,0)\rangle\,\hat{\boldsymbol{u}}^{(0)}(0,0,1) \\
&\hat{\boldsymbol{u}}^{(1)}(1,1,0) = 2\,\frac{\mathfrak{p}+\mathfrak{q}}{|\mathfrak{p}+\mathfrak{q}|^2}\,\langle\mathfrak{q}, \hat{\boldsymbol{u}}^{(0)}(1,0,0)\rangle\,\langle\mathfrak{p}, \hat{\boldsymbol{u}}^{(0)}(0,1,0)\rangle - \langle\mathfrak{p}, \hat{\boldsymbol{u}}^{(0)}(0,1,0)\rangle\,\hat{\boldsymbol{u}}^{(0)}(1,0,0) - \\
&\langle\mathfrak{q}, \hat{\boldsymbol{u}}^{(0)}(1,0,0)\rangle\,\hat{\boldsymbol{u}}^{(0)}(0,1,0)
\end{aligned} \tag{8.9}$$

In terms of the vector potential, the recursion relations become

$$\hat{\Psi}^{(n)}(\sigma_1,\sigma_2,\sigma_3) = \frac{1}{n}\frac{1}{|\sigma_1\mathfrak{p}+\sigma_2\mathfrak{q}+\sigma_3\mathfrak{r}|^2}\sum_{1\le\sigma_1'+\sigma_2'+\sigma_3'\le n}$$
$$\Big\langle\big((\sigma_1-\sigma_1')\mathfrak{p}+(\sigma_2-\sigma_2')\mathfrak{q}+(\sigma_3-\sigma_3')\mathfrak{r}\big)\wedge\big(\sigma_1'\mathfrak{p}+\sigma_2'\mathfrak{q}+\sigma_3'\mathfrak{r}\big)\,,\,\hat{\Psi}^{(\sigma_1'+\sigma_2'+\sigma_3'-1)}(\sigma_1',\sigma_2',\sigma_3')\Big\rangle\times$$
$$|(\sigma_1-\sigma_1')\mathfrak{p}+(\sigma_2-\sigma_2')\mathfrak{q}+(\sigma_3-\sigma_3')\mathfrak{r}|^2\,\hat{\Psi}^{(n-\sigma_1'-\sigma_2'-\sigma_3')}(\sigma_1-\sigma_1',\sigma_2-\sigma_2',\sigma_3-\sigma_3') -$$
$$|\sigma_1'\mathfrak{p}+\sigma_2'\mathfrak{q}+\sigma_3'\mathfrak{r}|^2\Big\langle(\sigma_1-\sigma_1')\mathfrak{p}+(\sigma_2-\sigma_2')\mathfrak{q}+(\sigma_3-\sigma_3')\mathfrak{r}\,,\,\hat{\Psi}^{(\sigma_1'+\sigma_2'+\sigma_3'-1)}(\sigma_1',\sigma_2',\sigma_3')\Big\rangle\times$$
$$\Big((\sigma_1-\sigma_1')\mathfrak{p}+(\sigma_2-\sigma_2')\mathfrak{q}+(\sigma_3-\sigma_3')\mathfrak{r}\Big)\wedge\hat{\Psi}^{(n-\sigma_1'-\sigma_2'-\sigma_3')}(\sigma_1-\sigma_1',\sigma_2-\sigma_2',\sigma_3-\sigma_3') \tag{8.10}$$

Contrary to the recursion relations for the two-dimensional Euler equation, the dependence on the initial amplitudes is rather non-trivial: it cannot be removed by applying translation invariance. This can be easily seen by a simple counting of the number of degrees of freedom.

The eighteen real degrees of freedom (or nine complex) in the amplitudes of the basic modes can be reduced to twelve due to translation invariance. The incompressibility conditions (8.2) imposes three further constraints. However, note that these do not affect the phases of the initial modes: the incompressibility condition reduces the number of degrees of freedom by three. Thus we are left with nine (real) degrees of freedom.

Already the exploration of the whole parameter space for some fixed basic modes is a quite demanding task. If we allow for varying the initial modes, the problem becomes even more complicated: the number of parameters is then equal to thirteen.

8.1.2 Similarity equation

Introducing a generating function for the vector potential

$$\Psi(z_1,z_2,z_3) = \hat{\Psi}^{(0)}(1,0,0)\mathrm{e}^{z_1} + \hat{\Psi}^{(0)}(0,1,0)\mathrm{e}^{z_2} + \Psi^{(0)}(0,0,1)\mathrm{e}^{z_3} + \sum_{n=1}^{\infty}\sum_{\sigma_1+\sigma_2+\sigma_3=n+1}\hat{\Psi}^{(n)}(\sigma_1,\sigma_2,\sigma_3)\mathrm{e}^{\sigma_1 z_1+\sigma_2 z_2+\sigma_3 z_3}, \tag{8.11}$$

we obtain the *similarity* equation for the vector stream function in the three-dimensional case

$$-\Delta_{(\mathfrak{p},\mathfrak{q},\mathfrak{r})}\Psi = \Big\{\Big[\partial_2\langle\mathfrak{p}\wedge\mathfrak{q}\,,\,\Psi\rangle-\partial_3\langle\mathfrak{r}\wedge\mathfrak{p}\,,\,\Psi\rangle-1\Big]\partial_1+\Big[\partial_3\langle\mathfrak{q}\wedge\mathfrak{r}\,,\,\Psi\rangle-\partial_1\langle\mathfrak{p}\wedge\mathfrak{q}\,,\,\Psi\rangle-1\Big]\partial_2+$$
$$\Big[\partial_1\langle\mathfrak{r}\wedge\mathfrak{p}\,,\,\Psi\rangle-\partial_2\langle\mathfrak{q}\wedge\mathfrak{r}\,,\,\Psi\rangle-1\Big]\partial_3\Big\}\Delta_{(\mathfrak{p},\mathfrak{q},\mathfrak{r})}\Psi - \langle\mathfrak{p}\,,\,\Delta_{(\mathfrak{p},\mathfrak{q},\mathfrak{r})}\Psi\rangle\,\partial_1\Big[\partial_1\,\mathfrak{p}\wedge\Psi+\partial_2\,\mathfrak{q}\wedge\Psi+\partial_3\,\mathfrak{r}\wedge\Psi\Big] -$$
$$\langle\mathfrak{q}\,,\,\Delta_{(\mathfrak{p},\mathfrak{q},\mathfrak{r})}\Psi\rangle\,\partial_2\Big[\partial_1\,\mathfrak{p}\wedge\Psi+\partial_2\,\mathfrak{q}\wedge\Psi+\partial_3\,\mathfrak{r}\wedge\Psi\Big] - \langle\mathfrak{r}\,,\,\Delta_{(\mathfrak{p},\mathfrak{q},\mathfrak{r})}\Psi\rangle\,\partial_3\Big[\partial_1\,\mathfrak{p}\wedge\Psi+\partial_2\,\mathfrak{q}\wedge\Psi+\partial_3\,\mathfrak{r}\wedge\Psi\Big] \tag{8.12}$$

Similar equations can be obtained for the imaginary velocity $\boldsymbol{u}$ and the vorticity.

8.2 Numerical study of the short-time asymptotics for the three-dimensional Euler equations

The short-time three-dimensional Euler equation in its most general formulation, such as (8.10) cannot be easily studied by numerical methods, due to the large number of degrees

of freedom. I have then decided to limit myself to simple instances of initial conditions , namely the Kida–Pelz flow

$$\begin{aligned} u_1 &= \sin x_1 \left(\cos 3x_2 \cos x_3 - \cos x_2 \cos 3x_3\right), \\ u_2 &= \sin x_2 \left(\cos 3x_3 \cos x_1 - \cos x_3 \cos 3x_1\right), \\ u_3 &= \sin x_3 \left(\cos 3x_1 \cos x_2 - \cos x_1 \cos 3x_2\right), \end{aligned} \tag{8.13}$$

and the flow

$$\begin{aligned} u_1 &= h_{1,2} \sin x_2 + h_{1,3} \sin x_3, \\ u_2 &= h_{2,1} \sin x_1 + h_{2,3} \sin x_3, \\ u_3 &= h_{3,1} \sin x_1 + h_{3,2} \sin x_2. \end{aligned} \tag{8.14}$$

Note that the latter becomes especially simple when all coefficients $h_{i,j}$ are equal. I propose to call this particular flow a *permutation flow*. The initial condition is then given by

$$u_1 = h \sin x_2 + h \sin x_3, \quad u_2 = h \sin x_1 + h \sin x_3, \quad u_3 = h \sin x_1 + h \sin x_2. \tag{8.15}$$

Actually, this initial condtion is strongly reminiscent of the initial condition which was recently introduced by K. Ohkitani using the Clebsch variables $\lambda = \sin x_1 + \sin x_2 + \sin x_3$ and $\mu = \cos x_1 + \cos x_2 + \cos x_3$.

So far, I have studied numerically solutions of (8.8) for three different initial conditions corresponding to the short-time asymptotics of: (i) the Kida–Pelz flow (8.13) (resolutions $N_{\max} = 100$), (ii) the permutation flow (8.15) with $h = 1/4$ (resolution $N_{\max} = 100$) and (iii) a special case of the flow (8.14) with $h_{1,2} = h_{2,3} = h_{3,1} = 0.52$, $h_{1,3} = h_{2,1} = h_{3,2} = 0$ (resolution $N_{\max} = 200$). Contrary to the case of the two-dimensional Euler equation and the MHD equations, all calculations have been done with double precision. Indeed, with the algorithms I am using presently to evaluate the recursion relations (8.9), high-precision calculations with resolutions of order 100 are not feasible.[2]

The asymptotic form of the Fourier coefficients in all the three cases has been found to be of the usual form of an exponential with an algebraic prefactor

$$u_i(k, \theta, \phi) \sim C_i(\theta, \phi) k^{-\alpha} \mathrm{e}^{-\delta(\theta,\phi)k}, \tag{8.16}$$

where $(k_1, k_2, k_3) = k(\cos\theta \sin\phi, \sin\theta \sin\phi, \cos\phi)$. Contrary to the two-dimensional case, the Fourier coefficient are not positive anymore and cannot be made positive by a translation. Still, along rational directions $(k_1, k_2, k_3) = n(p, q, r)$ the Fourier coefficients do not oscillate. Thus, we can analyze these coefficients by the same methods as in [PMFB06] and Chapter 6; in particular we can use the asymptotic interpolation method to obtain the algebraic prefactor exponent α. Although our data have been calculated with double precision, it turns out that this is just enough to be able to reach the sixth stage of the asymptotic interpolation procedure (as defined in [PF07]).

First we report the results obtained in case (iii) corresponding to the initial condition (8.14). Here we find $\alpha \approx 2.58 \pm 0.03$. The error bars are in particular due to the numerical noise introduced by using only double precision, see Fig. 8.1. One important exception are the Fourier coefficients along the rational directions corresponding to the *edges* (edges are cones constituting the boundary of the support set of the Fourier coefficients). For such directions we measure $\alpha \approx 1/2$.

[2] In principle, such questions can be handled by relaxed algorithms of the type described by van der Hoeven [Hoe02] and by high-precision fast Fourier transforms. I have started exploring this with colleagues but there are no results to report yet.

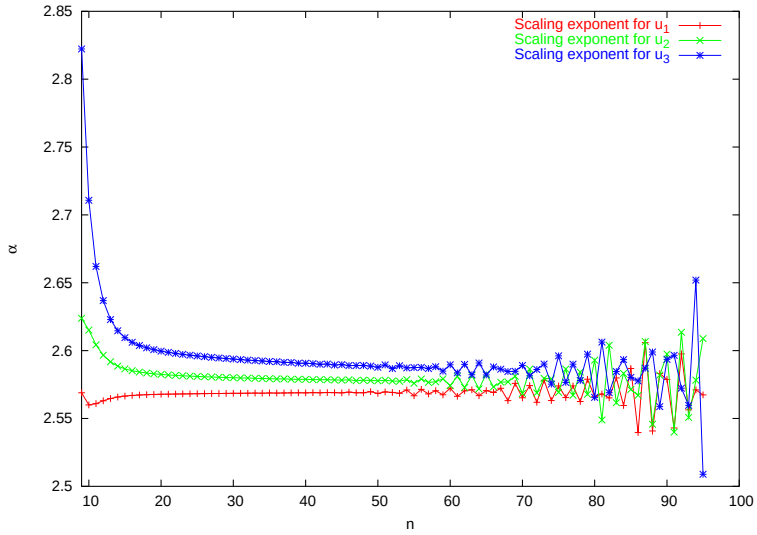

Figure 8.1: Case (iii): scaling exponent α obtained by the asymptotic interpolation method from the Fourier coefficients of the three components of the imaginary velocity $\boldsymbol{u}$ along the rational direction $(1, 2, 2)$. The numerical noise becomes significant beyond $n = 60$.

Except for the edges, we find that the scaling exponent α does not depend on the angles θ and ϕ. The angular variations which we observe are comparable to those in the two-dimensional case.

Consider now case (ii) which has the same basic modes but quite different initial amplitudes. For this case we measure within the numerical errors the same value of the algebraic prefactor exponent $\alpha \approx 2.58 \pm 0.03$, see Fig. 8.2 Therefore, we conjecture that

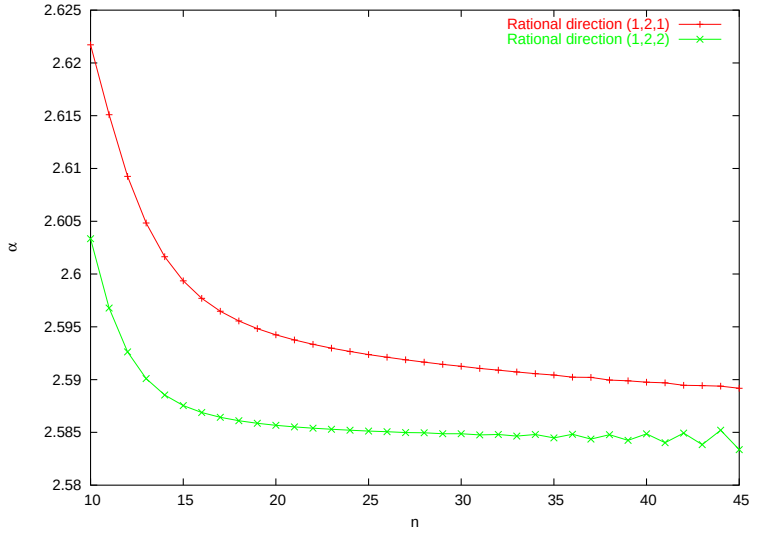

Figure 8.2: Case (ii): scaling exponent α obtained by the asymptotic interpolation method from the Fourier coefficients of one of the components of the imaginary velocity $\boldsymbol{u}$ along the rational directions $(1, 2, 2)$ and $(1, 2, 1)$. Note that because of the symmetry of the flow it suffices to analyze only one component.

the scaling exponent in the case of the three-dimensional Euler equation does not depend on the value of the initial amplitude, just as in the two-dimensional case.

It is instructive to consider the Kida–Pelz initial condition which has basic vectors different from those of the cases (ii) and (iii). For this initial condition we find that the scaling exponent $\alpha \approx 3$ (although the results are still quite preliminary), see Fig. 8.3. and

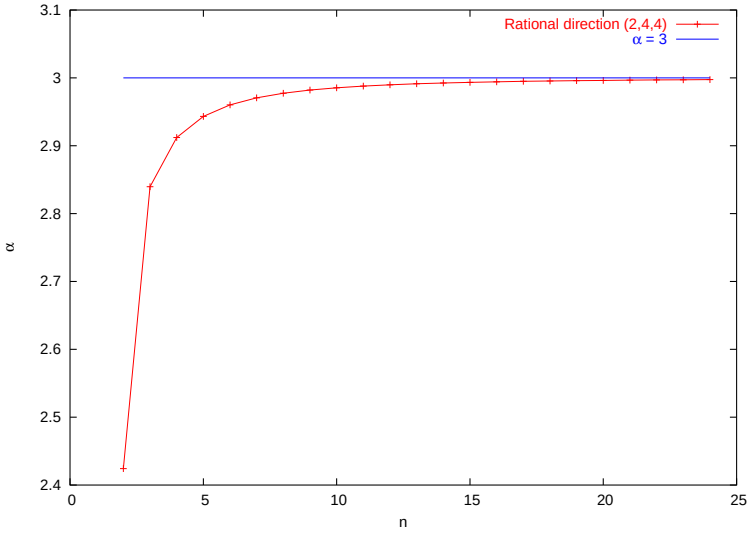

Figure 8.3: Kida–Pelz initial condition: scaling exponent α obtained by the asymptotic interpolation method from the Fourier coefficients of one of the components of the imaginary velocity $\boldsymbol{u}$ along the rational directions $(2, 4, 4)$.

is definitely different from the value observed in cases (ii) and (iii).

We conclude that both in two and three dimensions the nature of complex singularities of solutions of the Euler equation depends on the initial conditions and is therefore *nonuniversal*.

Part III

Complex Lagrangian singularities

Chapter 9

Lagrangian description of singularities

Consider again solutions of the two-dimensional Euler equation

$$\partial_t \nabla^2 \Psi(z_1, z_2) - J(\Psi, \nabla^2 \Psi) = 0. \tag{9.1}$$

on the complex torus (real-periodic domain) with the initial condition $\Psi(z, 0) = \Psi_0$. The Lagrangian description is given in terms of the Lagrangian mapping $z = Z(,t)$

$$\partial_t Z = v(Z, t), \qquad Z(c, 0) = c, \tag{9.2}$$

where $c = a + \mathrm{i}\, b \in \mathbb{T}^2_{\mathbb{C}}$. We denote the inverse Lagrangian map (or the "back-to-labels" map) by $C(z, t)$. As is well known, in two dimensions the vorticity is advected by the flow, so that the vorticity can be written as $\omega(z, t) = \omega_0(C(z, t))$.

From this relation follows that there are two possibilities by which complex singularities of the solutions of the two-dimensional Euler equation can arise: (i) by advecting of fluid particles from the complex infinity, (ii) by $C(z, t)$ becoming singular.

In the former case the map $C(z, t)$ becomes infinite because fluid particles which at time t are located at the point z were initially located at infinty. Note that in this case the vorticity has to be infinite. Concerning the latter case, it is at the moment not quite clear whether and by which mechanism the inverse Lagrangian mapping $C(z, t)$ can develop singularities when $|C(z, t)|$ stays bounded. We remark that on the real domain both types of singularities are excluded: the first type is excluded just because fluid particles stay confined in the real periodic domain, and the second one is not permitted because of the global regularity of the two-dimensional Euler flow. Actually, recently some numerical evidence has been given [MBF07] that "escaping to the infinity" is the only mechanism by which complex singularities are created in two dimensions.

Another reason for studying the complex singularities in the Lagrangian coordinates is to understand the role of depletion. Indeed, it is found that the strongest depletion of nonlinearity occurs in the neighborhood of singularities. Thus, complex Lagrangian signularities seem to be most appropriate to study its Lagrangian counterpart.

Note that no simple definition of depletion can be given in the Lagrangian coordinates as compared to the Eulerian case, where depletion means roughly vanishing of the nonlinear term in the Euler equation. Actually, there exist stationary solutions of the Euler equation which are completely depleted in the Eulerian frame and which exhibit very complicated Lagrangian behavior, e.g. Lagrangian chaos.

9.1 Lagrangian singularities of two-dimensional Eulerian flows in the short-time asymptotic régime

In this section we make some remarks on possible studies of the Lagrangian singularities of the two-dimensional Euler equation

$$\partial_t \nabla^2 \Psi - J(\Psi, \nabla^2 \Psi) = 0, \tag{9.3}$$

with the initial conditions

$$\Psi_0(z_1, z_2) = \hat{F}(\boldsymbol{p}) e^{-i\boldsymbol{p}\cdot\boldsymbol{z}} + \hat{F}(\boldsymbol{q}) e^{-i\boldsymbol{q}\cdot\boldsymbol{z}}. \tag{9.4}$$

As we know, its solution is given by

$$\Psi(z_1, z_2 p; t) = \frac{1}{t} F(\tilde{z}_1, \tilde{z}_2), \tag{9.5}$$

with

$$\tilde{z}_1 = z_1 + i\lambda_1 \ln t, \quad \tilde{z}_2 = z_2 + i\lambda_2 \ln t, \tag{9.6}$$

where $F(\tilde{z}_1, \tilde{z}_2)$ satisfies the corresponding similarity equation.

Let us now consider the inverse Lagrangian displacement

$$\boldsymbol{d}(\boldsymbol{z}, t) = \boldsymbol{C}(\boldsymbol{z}, t) - \boldsymbol{c}, \tag{9.7}$$

which satisfies the equation

$$\partial_t \boldsymbol{d} + \boldsymbol{u} \cdot \nabla \boldsymbol{d} = -\boldsymbol{u}. \tag{9.8}$$

Since the velocity field has the self-similar form

$$\boldsymbol{u}(\boldsymbol{z}, t) = \frac{1}{t} \boldsymbol{v}(\tilde{\boldsymbol{z}}, t), \tag{9.9}$$

it is easy to see that

$$\boldsymbol{d}(\boldsymbol{z}, t) = \boldsymbol{d}(\tilde{\boldsymbol{z}}), \tag{9.10}$$

and satisfies the following equation

$$(i\,\lambda_1 \partial_1 + i\,\lambda_2 \partial_2 + \boldsymbol{v} \cdot \nabla)\boldsymbol{d} = -\boldsymbol{v}. \tag{9.11}$$

This equation is easily converted into a recursion relation. Using the fact that the velocity field is known, a solution to this equation is can be readily calculated with very high precision. Thus, at least in the short-time asymptotic régime, we can analyze the singularities of the inverse Lagrangian map quite accurately. The calculation of the direct Lagrangian map is more laborious but is probably still feasible.

Once the Fourier coefficients of the inverse and the direct Lagrangian maps are known, it becomes possible to make a precise analysis of their singularities by using the tools presented in Chapter 4.

9.2 Lagrangian singularities of steady solutions of the Euler equation

Geophysical and Astrophysical Fluid Dynamics,
Vol. 99, No. 1, February 2005, 61–75

Taylor & Francis
Taylor & Francis Group

Lagrangian singularities of steady two-dimensional flow

WALTER PAULS†‡* and TAKESHI MATSUMOTO†§

†Observatoire de la Côte d'Azur, CNRS UMR 6202, BP 4229, 06304 Nice Cedex 4, France
‡Fakultät für Physik, Universität Bielefeld, Universitätsstraße 25, 33615 Bielefeld, Germany
§Dep. Physics, Kyoto University, Katashirakawa Oiwakecho Sakyo-ku,
Kyoto 606-8502, Japan

(*Received 11 March 2004; in final form 7 June 2004*)

The Lagrangian complex-space singularities of the steady Eulerian flow with stream function $\sin x_1 \cos x_2$ are studied by numerical and analytical methods. The Lagrangian singular manifold is analytic. Its minimum distance from the real domain decreases logarithmically at short times and exponentially at large times.

Keywords: Lagrangian coordinates; Singular manifold

1. Introduction

Singularities of the solutions of hydrodynamical problems in the complex space domain are important, for example, because they allow us to give an objective definition of an otherwise fuzzy concept of "smallest scale present in a flow". Specifically, if a flow is analytic in the space variable x for all x, it can be continued to complex $\mathbf{z} = \mathbf{x} + \mathrm{i}\mathbf{y}$ locations where it will generally have singularities on some complex set Σ. The minimum distance δ of Σ to the real domain, called the width of the analyticity strip, defines the smallest scale. Indeed, the modulus of the Fourier transforms of the velocity v decreases roughly as $\exp(-\delta k)$ at high wavenumbers k; thus the mesh needed in numerically simulating such a flow, e.g. by spectral methods, has to be significantly less than δ (Sulem *et al.*, 1983; Brachet, 1983). Furthermore, should the flow ever develop a real singularity at a finite real time t_*, it must be preceded by complex singularities at a distance $\delta(t)$ which continuously vanishes at t_* (Bardos *et al.*, 1976; Benachour, 1976 a,b). For incompressible flow actual measurements of $\delta(t)$, using high-resolution spectral simulations, indicate that $\delta(t)$ decreases in time, but in a way much tamer than suggested by the known rigorous estimates. In both two and three dimensions

*Corresponding author. E-mail: walter.pauls@physik.uni-bielefeld.de

Geophysical and Astrophysical Fluid Dynamics
ISSN 0309-1929 print: ISSN 1029-0419 online © 2005 Taylor & Francis Group Ltd
http://www.tandf.co.uk/journals
DOI: 10.1080/03091920412331312411

the behavior of $\delta(t)$ generally may well be exponential, but the best estimates are a decreasing double exponential in two dimensions and finite-time blow-up in three dimensions (see Frisch *et al.*, 2003, for review).

The standard explanation for this discrepancy is the phenomenon of nonlinear depletion, whereby the flow is found to organize itself into structures which have nearly vanishing nonlinearities (Frisch, 1995; Majda and Bertozzi, 2002). Note that one of the features characterising depletion can be the degree of velocity–vorticity alignment or "Beltramization" of the flow.

Till date, singularities in the complex domain had been studied in Eulerian coordinates. In the present paper, we analyse some aspects related to singular behaviour of flows extended into the complex domain in Lagrangian coordinates. One practical motivation of studying Lagrangian singularities in the complex domain concerns the structure of Eulerian singularities of a passive scalar. Indeed, consider a passive scalar[1] advected by an incompressible flow $\mathbf{v}$, whose density satisfies the continuity equation

$$\frac{\partial_t \theta}{\partial t} + \nabla \cdot (\theta \mathbf{v}) = 0, \tag{1}$$

as long as we can neglect molecular diffusion. Obviously, this can be solved by using Lagrangian coordinates:

$$\theta(\mathbf{x}, t) = \theta_0(\mathbf{a}(\mathbf{x}, t)), \tag{2}$$

where θ_0 is the initial density field and $\mathbf{a}(\mathbf{x}, t)$ is the inverse of the Lagrangian map $\mathbf{x}(\mathbf{a}, t)$, the latter satisfying the characteristic equation

$$\dot{\mathbf{x}} = \mathbf{v}(\mathbf{x}, t), \quad \mathbf{x}(\mathbf{a}, 0) = \mathbf{a}. \tag{3}$$

If θ_0 is devoid of singularities (entire function), it is clear that the singularities of the Eulerian field, continued to complex locations, $\theta(\mathbf{z}, t)$, will correspond to those (complex) fluid particles trajectories which have started at $t = 0$ at (complex) infinity. Furthermore, it implies that the width of the analyticity strip $\delta(t)$ for $\theta(\mathbf{x}, t)$ in Eulerian coordinates equals the width of the analyticity strip $\delta_{\mathrm{L}}(t)$ of the Lagrangian map $\mathbf{x}(\mathbf{a}, t)$ for the time reversed flow. In section 4 we will use this correspondence to define the smallest scale of the passive scalar field $\theta(\mathbf{x}, t)$ at time t.

Note that the above argument can be applied to the two-dimensional vorticity. Assuming infiniteness of Eulerian vorticity at complex Eulerian singularities (Frisch *et al.*, 2003; Matsumoto *et al.*, 2004) it implies that the Eulerian singularities of solutions of the two-dimension Euler equation starting from entire initial data come from the complex infinity. Therefore, especially for the two-dimensional flows, some understanding of complex singularities in Lagrangian coordinates, even for a very simple flow, can shed light on the nature of Eulerian complex singularities.

[1]Similar remarks can be made about a passive magnetic field.

Orszag (2003) pointed out that the phenomenon of depletion is intrinsically Eulerian and has no Lagrangian counterpart.[2] Thus, it is expected that Lagrangian singularities are stronger — or at least closer to the real domain – than Eulerian ones. An extreme form of depletion[3] is to work with a Beltrami flow given by a steady solution of the incompressible Euler equation such as the ABC flow in three dimensions or the two-dimensional cellular flow with stream function

$$\psi(x_1, x_2) = \sin x_1 \cos x_2 \tag{4}$$

and velocity

$$v_1 = -\sin x_1 \sin x_2, \quad v_2 = -\cos x_1 \cos x_2. \tag{5}$$

The latter is much simpler, because the Lagrangian map can be obtained explicitly in terms of elliptic functions (Dombre *et al.*, 1986, Appendix A). Moreover, it represents a special case ($A=1$, $B=1$, and $C=0$) of the ABC flow, obtained by applying a transformation of coordinates of the type used in Dombre *et al.*, (1986, Appendix A) and reducing the non-trivial dynamics to two dimensions. Our goal in this paper will be to obtain for this flow the complex singularities in Lagrangian coordinates.

The Lagrangian velocity[4] is defined just by the change of variables, that is, as $\mathbf{v}_{\text{L}}(\mathbf{a}, t) \equiv \mathbf{v}(\mathbf{x}(\mathbf{a}, t))$ where $\mathbf{x}(\mathbf{a}, t)$ is the solution of (3) with the velocity given by (5). Of course, such flow being steady, completely lacks Eulerian singularities (except at complex infinity). However, as we shall see, it develops *real* Lagrangian singularities in infinite time.

The outline of the paper is as follows. In section 2, we explicitly construct the singular set, the explicit construction of the Lagrangian map being relegated to Appendix A. In section 3 the Lagrangian velocity, its Fourier transform and $\delta(t)$ are determined numerically. Section 4 is devoted to the short-time and long-time asymptotics.

2. Analytic structure of the singular manifold

We consider the cellular flow on $\mathbb{T}^2 \equiv [0, 2\pi] \times [0, 2\pi]$ defined by (4) and (5). Because of the symmetries of this flow the full periodicity domain can be decomposed into four cells, figure 1a. For convenience, in figure 1 b, we represent the cell $[0, \pi] \times [-\pi/2, \pi/2]$. The Lagrangian map $\mathbf{x}(\mathbf{a}, t)$ is the solution of

$$\dot{x}_1 = -\sin x_1 \sin x_2, \quad \dot{x}_2 = -\cos x_1 \cos x_2 \tag{6}$$

with the initial conditions

$$x_1(\mathbf{a}, 0) = a_1, \quad x_2(\mathbf{a}, 0) = a_2. \tag{7}$$

[2]There are indications that depletion in the three-dimensional Lagrangian coordinates exists (Ohkitani, 2002), nevertheless it seems to be weaker than in the Eulerian coordinates. Furthermore, our definition of depletion (Frisch, 1995) is somewhat different from Ohkitani's definition of depletion, measuring the preference of the vorticity for being aligned with a certain eigendirection of the rate-of-strain tensor (the Eulerian case) and the Cauchy-Green tensor (the Lagrangian case).

[3]Observe that the nonlinear terms of the two-dimensional and three-dimensional Euler equations completely vanish for the flows (4) and the ABC flow, respectively.

[4]We cannot work with the Lagrangian vorticity since it remains constant along trajectories and thus constant in Lagrangian coordinates; the same applies to the stream function for any steady two-dimensional flow.

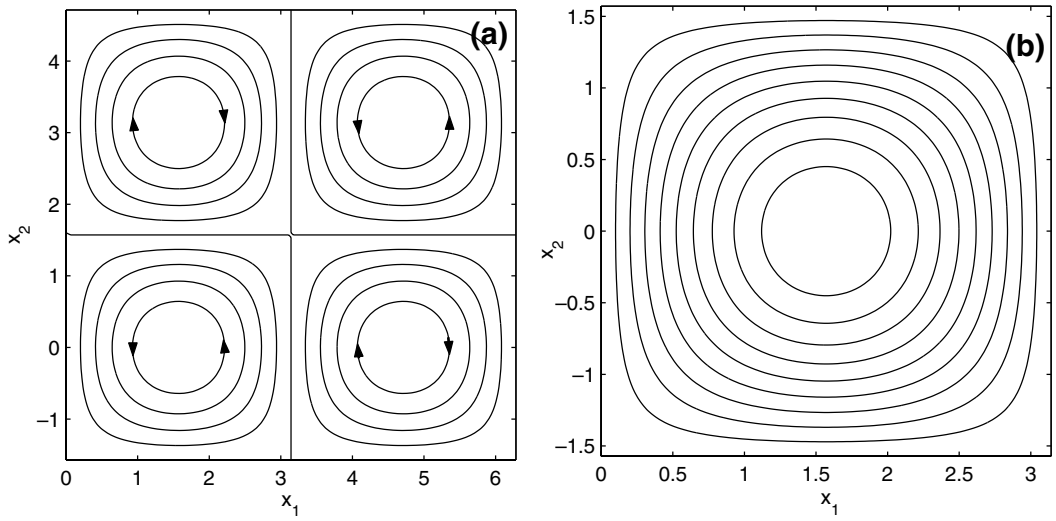

Figure 1. Streamlines for the flow defined by (4) in the (a) flow box, (b) in the basic cell.

When fluid particles start at complex locations they will stay in the complex domain. We then denote the complexified Lagrangian position by $c = a + \mathrm{i}b$ and the complexified Eulerian position by $z = x + \mathrm{i}y$. The complex Lagrangian stream function is $\xi(c, t) \equiv \psi(z(c, t))$ and the complex Lagrangian velocity is $v_{\mathrm{L}}(c, t) \equiv v(z(c, t))$.

Since the Eulerian velocity v is an entire function of z,[5] the Lagrangian velocity can become singular only where the Lagrangian map becomes singular; furthermore it is easily shown that the only way $z(c, t)$ can become singular, for a finite real t and a complex c, is by going to (complex) infinity.

The explicit solution to (6) is given in the Appendix in terms of elliptic functions. Its form implies the existence of singularities, associated to certain poles of suitable elliptic functions. This is however not the simplest way to actually construct the singular set $\Sigma(t)$, a time-dependent complex manifold of complex dimension one, that is which can be parametrized in terms of one complex parameter. For the construction it is simpler to observe (i) that the value of the complex stream function ξ does not change along fluid particle trajectories and (ii) that the stream function, being the product of $w_1 \equiv \sin z_1$ and $w_2 \equiv \cos z_2$, the only way z can run to infinity while conserving the stream function is to have either $w_1 \to \infty$ and $w_2 \to 0$ or conversely.

In terms of the w_1 and w_2 variables, the equations for fluid particle trajectories can be rewritten as

$$\dot{w}_1 = -w_1\sqrt{1 - w_1^2}\sqrt{1 - w_2^2}, \quad \dot{w}_2 = w_2\sqrt{1 - w_2^2}\sqrt{1 - w_1^2} \tag{8}$$

with now complex initial conditions

$$w_1(0) = \sin c_1, \qquad w_2(0) = \cos c_2, \tag{9}$$

corresponding to the initial conditions (7).

[5]An entire function is analytic for all z but can still be singular at infinity.

Obviously, the product $\xi = w_1 w_2$ is an integral of motion: this expresses just that for steady flow particles move along streamlines. One can take advantage of this integral of motion to rewrite (8) as a single equation in terms for example of the variable $u \equiv w_1/\xi$, as

$$\dot{u} = -\mathrm{i}\sqrt{1-u^2}\sqrt{1-\xi^2 u^2}, \qquad u(0) = u_0 = (1/\xi)\sin c_1. \tag{10}$$

This equation allows to express the time variable t in terms of the initial and current values of u by an elliptical integral:

$$\mathrm{i}t = -\int_{u_0}^{u(t)} \frac{\mathrm{d}s}{\sqrt{(1-s^2)(1-\xi^2 s^2)}}. \tag{11}$$

We turn now to the determination of the singularities, that is those initial complex locations $\mathbf{c}^\star = (c_1^\star, c_2^\star)$ which go to infinity at time t. Because of the symmetries of the flow we can, without loss of generality, assume that when $\mathbf{z} \to \infty$ at time t, we have $w_2 \to \infty$ and $w_1 \to 0$ and hence $u(t) = 0$. It follows then from (10) that the singular values of u_0 are such that

$$\mathrm{i}t = -\int_{u_0}^{0} \frac{\mathrm{d}s}{\sqrt{(1-s^2)(1-\xi^2 s^2)}}. \tag{12}$$

The inverse of the elliptical integral is the elliptic sn function (Abramovitz and Stegun, 1965). Thus u_0 can be expressed as an elliptic function. Since, by (10), $w_1(0) = \xi u_0$, we obtain

$$w_1(0) = \xi\,\mathrm{sn}(\mathrm{i}t, \xi), \qquad w_2(0) = \mathrm{ns}(\mathrm{i}t, \xi), \tag{13}$$

where $\mathrm{ns} \equiv 1/\mathrm{sn}$. Alternatively, since the sn and ns functions of imaginary arguments can be expressed in terms of the sc function, defined as $\mathrm{sc} \equiv \mathrm{sn}/\mathrm{cn}$, and its reciprocal cs, we have

$$w_1(0) = \mathrm{i}\xi\,\mathrm{sc}(t, \sqrt{1-\xi^2}), \qquad w_2(0) = -\mathrm{i}\,\mathrm{cs}(t, \sqrt{1-\xi^2}). \tag{14}$$

By (9), we can express the singular Lagrangian locations at time t as

$$c_1^\star = \arcsin\left[\mathrm{i}\,\xi\mathrm{sc}(t, \sqrt{1-\xi^2})\right], \qquad c_2^\star = \arccos\left[\mathrm{i}\,\mathrm{cs}(t, \sqrt{1-\xi^2})\right]. \tag{15}$$

This constitutes the parametric representation of the singular manifold $\Sigma(t)$, the parameter being the complex stream function ξ. Obviously, the functions appearing in this representation are multivalued. More precisely, the singular manifold has infinitely many sheets.

It is well known that elliptic functions are real for real values of the parameters. Therefore, $\Sigma(t)$ will have a non-trivial part "above" the hyperbolic stagnation points,

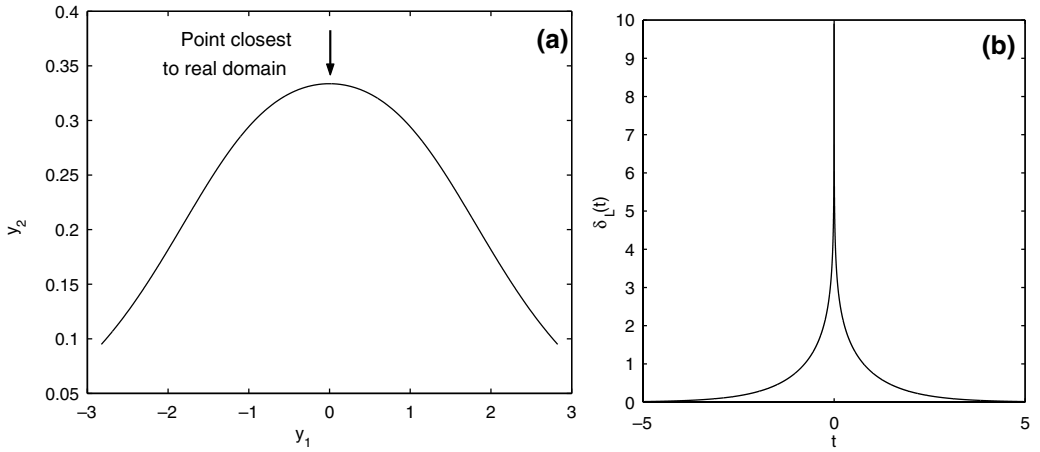

Figure 2. (a) The cut of the singular manifold on the imaginary (y_1, y_2)-plane is represented. The point closest to the origin lies on the y_2-axis. (b) Here the value of the closest distance from singular manifold to the real domain, $\delta(t)$, is represented for both positive and negative times.

namely the four corners in figure 1 b.[6] By symmetry, it is enough to consider one of them. We take $(a_1, a_2) = (0, \pi/2)$ and easily obtain the following parametric representation of the singular locations having this stagnation point as real part:

$$b_1^* = \operatorname{arc\,sinh}\Big[\xi\,\mathrm{sc}(t, \sqrt{1-\xi^2})\Big], \qquad b_2^* = \operatorname{arc\,sinh}\Big[-\mathrm{cs}(t, \sqrt{1-\xi^2})\Big]. \tag{16}$$

Using the parametrization (16) in figure 2 a, we have represented the curve obtained as intersection of the singular manifold with the set of points with real coordinates fixed at $(x_1, x_2) = (0, \pi/2)$, that is the trace of the singular manifold on the pure imaginary plane lying above the corresponding stagnation point. Here "trace on" is used with its mathematical meaning of "intersection with".

The width of the Lagrangian analyticity strip $\delta_{\mathrm{L}}(t)$ is obtained by finding the point(s) on the singular manifold closest to the real domain. It seems likely that these points will be located over the points where the flow exhibits a special structure. Indeed, expanding (15) locally in its Taylor series confirms that the points closest to the real domain lie above the hyperbolic stagnation points. The upper left and the lower right stagnation points have $b_1^* = 0$, while the upper right and the lower left stagnation points have $b_2^* = 0$. The distance from the real domain is easily shown to be given by

$$\delta_{\mathrm{L}}(t) = \left|\operatorname{arcsinh}\left(\frac{1}{\sinh t}\right)\right|. \tag{17}$$

Figure 2 b is a plot of $\delta_{\mathrm{L}}(t)$ showing both positive and negative times.

As we have mentioned in the introduction, $\delta_{\mathrm{L}}(t)$ of the time reversed flow gives the width of the analyticity strip in Eulerian coordinates for a passive scalar satisfying (1) with the same velocity field (5). Indeed, singularities for the passive scalar correspond to (complex) fluid particles which are mapped back to infinity in time t.

[6] By "above" we mean at complex locations whose real parts are the stagnation points.

Note that the symmetry of the cellular flow used here implies that $\delta_L(t)$ is an even function of time so that $\delta_L(t)$ of the original flow coincides with the Eulerian $\delta(t)$ for the passive scalar field.

3. Numerical integration in Lagrangian coordinates

In this section, we obtain the width $\delta_L(t)$ of the Lagrangian analyticity strip by numerically calculating the Fourier transform of the velocity in Lagrangian coordinates and then applying the method of tracing complex singularities (Sulem *et al.*, 1983) to relate the Fourier transform to $\delta_L(t)$. Our method is implemented for the steady cellular flow given by (4), but can in principle, be applied to any steady solution of the Euler equation in both two and three dimensions.

We need to calculate the Lagrangian Fourier coefficients, which are here obtained as follows. First, we calculate the Lagrangian map $\mathbf{x}(\mathbf{a}, t)$ by solving the characteristic equations (6) with a fourth-order Runge-Kutta method for N^2 initial conditions $\mathbf{a} = ((2\pi/N)l, (2\pi/N)m)$ $(l, m = 0, 1, \ldots, N-1)$, which form a regular square grid in the Lagrangian marker space. We obtain then the Lagrangian velocity field by just changing variables:

$$\mathbf{v}_L(\mathbf{a}, t) \equiv \mathbf{v}(\mathbf{x}(\mathbf{a}, t),\ t), \tag{18}$$

where $\mathbf{v}(\mathbf{x})$ is given by (5). The Lagrangian velocity Fourier coefficients are given by

$$\hat{\mathbf{v}}_L(\mathbf{k},\ t) = \frac{1}{N^2} \sum_{\mathbf{a}} \mathbf{v}_L(\mathbf{a}, t)\, e^{-i\mathbf{k}\cdot\mathbf{a}}. \tag{19}$$

For measuring the width δ_L, it is convenient to define the shell-summed amplitude $A_k^{(\mathbf{v}_L)}$ of $\hat{\mathbf{v}}_L(\mathbf{k})$ as

$$A_k^{(\mathbf{v}_L)} = \sum_{k \le |\mathbf{k}| < k+1} |\hat{\mathbf{v}}_L(\mathbf{k})|. \tag{20}$$

The Lagrangian width δ_L is then obtained by fitting the shell-summed amplitude to an exponential with an algebraic prefactor:

$$A_k^{(\mathbf{v}_L)} \propto k^{-\alpha} \exp(-\delta_L k). \tag{21}$$

We first discuss how to obtain the width $\delta_L(t)$ at short times when it is very large (since it is infinite at $t = 0$). Obtaining $\delta_L(t)$ with a double-precision calculation is not feasible because the Fourier amplitudes $A_k^{(\mathbf{v}_L)}$ fall off too quickly as a function of the wavenumber and thus get lost in the roundoff noise. So we need to solve the equation (6) with higher precision.[7] In practice we divide the time interval $10^{-12} \le t \le t$ into four parts: (i) $10^{-12} \le t < 10^{-9}$, (ii) $10^{-9} \le t < 10^{-6}$, (iii) $10^{-6} \le t < 10^{-3}$,

[7]We use here the package MPFUN90 (Bailey, 1995).

(iv) $10^{-3} \leq t < 1$. For each part, we use different time step Δt and precision: (i) $\Delta t = 10^{-12}$ and 48-digit precision, (ii) $\Delta t = 10^{-9}$ and 36-digit precision, (iii) $\Delta t = 10^{-6}$ and 24-digit precision, (iv) $\Delta t = 10^{-3}$ and 15-digit (double) precision. These precisions, for each Δt, are the best we can handle with the fourth-order Runge-Kutta scheme. Note that in Frisch *et al.* (2003) a 90-digit spectral calculation was used for obtaining the short-time behavior of $\delta(t)$ in Eulerian coordinates for two-dimensional Euler flow with non-trivial Eulerian dynamics; in the present case, the accuracy of the shell-summed amplitudes $A_k^{(\mathbf{v}_\mathrm{L})}$ is constrained by the accuracy of the time integration scheme of (6).[8] Also we encounter the difficulty that a long-time integration causes serious accumulation of error in vorticity, which eventually breaks the conservation of vorticity (in two-dimensional vorticity should be conserved along each fluid particle trajectory). That is the reason why we split the time interval $10^{-12} < t < 1$ into four parts and use different Δt for each part to avoid this accumulation. Figure 3 shows the shell-summed amplitude $A_k^{(\mathbf{v}_\mathrm{L})}$ and the width of the Lagrangian analyticity strip $\delta_\mathrm{L}(t)$ at short times $10^{-12} \leq t \leq 1$. As seen in figure 3 a, the number of points in $A_k^{(\mathbf{v}_\mathrm{L})}$ to be fitted is small. We checked that, for several measured $\delta_\mathrm{L}(t)$'s shown in figure 3 b, a calculation with smaller Δt and higher precision for the same instance gives the same value of $\delta_\mathrm{L}(t)$. In this sense, we believe the measured $\delta_\mathrm{L}(t)$ is reliable in spite of the very limited data points. From figure 3 b, a clean logarithmic decay of $\delta_\mathrm{L}(t)$ is observed for more than 10 decades.

Now we turn to the numerical determination of the long-time behavior of the width of the Lagrangian analyticity strip. The calculation is straightforward: the characteristic equation (6) is solved with standard double precision using a time step $\Delta t = 10^{-3}$. The number of grid points is 4096^2. Figure 4 shows $A_k^{(\mathbf{v}_\mathrm{L})}$ and $\delta_\mathrm{L}(t)$ at long times, $0 < t \leq 5$. The temporal decrease of $\delta_\mathrm{L}(t)$ is exponential in this regime.

This indicates that exponentially small-scale structure is generated in the Lagrangian coordinates by this steady flow. To illustrate this, we first show in figure 5 the deformation of the initially regular grid caused by the flow. As seen in figure 5, the Eulerian field is squeezed around the hyperbolic stagnation points along the contracting direction. We then plot contours of the modulus of the corresponding displacement $|\mathbf{x}(\mathbf{a}, t) - \mathbf{a}|$ in the Lagrangian coordinates for various instances in figure 6. Here we can clearly see that the small-scale structures centered at hyperbolic stagnation points are generated in the Lagrangian coordinates. The exponential decrease of $\delta_L(t)$ corresponds to the exponential decrease of the width of the structure in the Lagrangian coordinates centered at the hyperbolic stagnation points.

4. Short-time and long-time behavior

The parametric representation (15) for the singular manifold at arbitrary times is somewhat cumbersome. At short times we can use suitable expansions of the

[8]We cannot take higher precision than the order of $(\Delta)^4$, which is the error level of the fourth-order Runge-Kutta method employed here. If we take higher precision than that, we find that a bump appears in the shell-summed applitude $A_k^{(\mathbf{v}_\mathrm{L})}$ around the level of $(\Delta)^4$. This is perhaps due to the fact that the equation (6) is integrated in the physical space. In Frisch, Matsumoto and Bec (2003), the Euler equation was integrated with the same fourth order Runge-Kutta scheme but in the Fourier space, and this may considerably decrease the error (more precisely, the factor in front of $(\Delta)^4$ is exponentially small for large k).

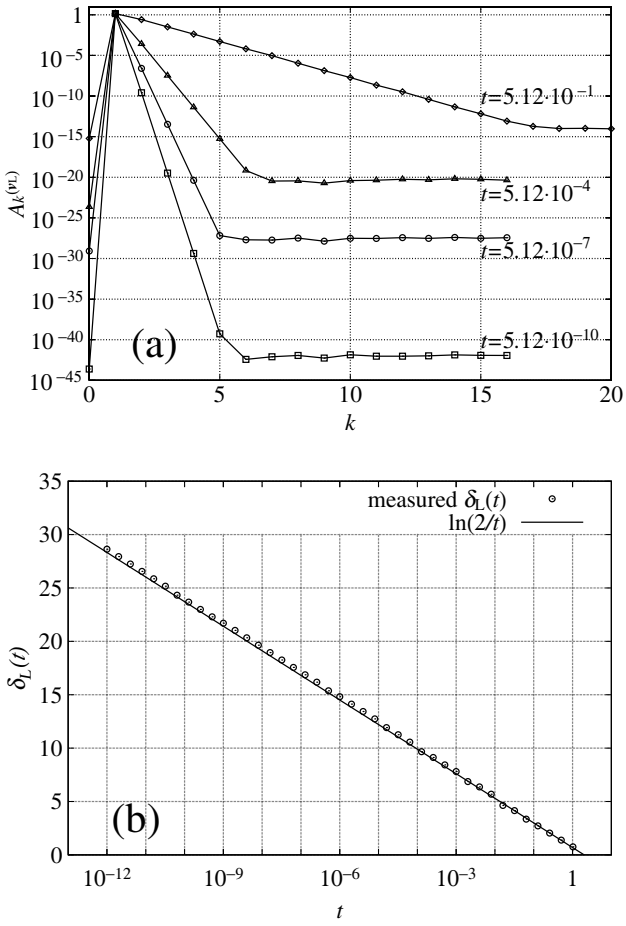

Figure 3. (a) Shell-summed amplitudes of the Lagrangian velocity $A_k^{(v_L)}$ for four different short times calculated with the number of grid points 32^2 and 64^2. (b) Log-linear plot of the width of the Lagrangian analyticity strip $\delta_L(t)$ measured as the logarithmic decrement of $A_k^{(v_L)}$ at short times $10^{-12} \leq t \leq 1$.

trigonometric and elliptic functions (Abramovitz and Stegun, 1965) and obtain to leading order

$$c_1^\star \simeq \arcsin(i\,\xi t), \qquad c_2^\star \simeq \frac{\pi}{2} + i\,\ln\left(\frac{2}{t}\right), \tag{22}$$

from which it follows readily that the width of the analyticity strip is

$$\delta_L(t) \simeq \ln\frac{2}{t}, \qquad t \to 0. \tag{23}$$

Hence the Lagrangian $\delta_L(t)$ follows a logarithmic law at short time.

We now observe that a short-time logarithmic law for the Eulerian $\delta(t)$ has been obtained by Frisch *et al.* (2003) (see also Matsumoto *et al.*, 2004) for two-dimensional flow with a finite number of initial Fourier harmonics. In the present case the Eulerian dynamics are trivial since the flow is time-independent. We believe that a logarithmic law for the short-time behavior of the Lagrangian $\delta_L(t)$ is quite general for *steady* solutions of the Euler equation with a finite number of harmonics

70 W. Pauls and T. Matsumoto

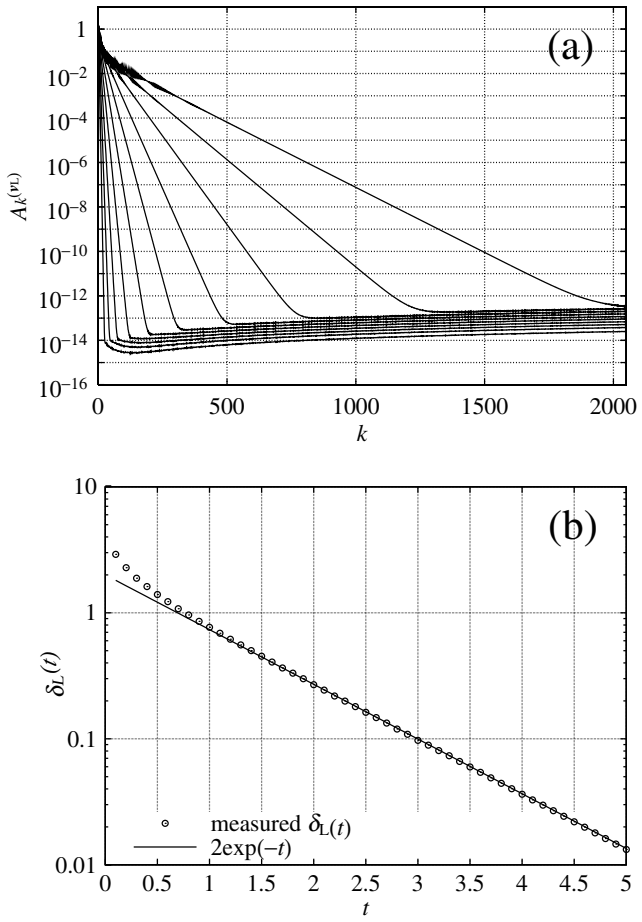

Figure 4. (a) Shell-summed amplitudes of the Lagrangian velocity $A_k^{(v_L)}$ for 10 different instances ($t = 0.5, 1.0, \ldots, 5.0$) calculated with the number of grid points 4096^2. (b) Linear-log plot of the width of the Lagrangian analyticity strip $\delta_L(t)$ measured as the logarithmic decrement of $A_k^{(v_L)}$ at long times $t \leq 5$.

in any dimension $d \geq 2$. Roughly, the argument is as follows. Let n be the degree of the highest-order Fourier harmonic; the velocity at complex locations a large distance y from the real domain grows as $\exp(ny)$. Singularities in Lagrangian coordinates at time t correspond to fluid particles which emanated initially from infinity or, equivalently, which are mapped to infinity in a time t under the reversed flow. The latter also grows as $\exp(ny)$ at large y. A fluid particle located initially within a distance $\delta_L \gg 1$ of the real domain and having an imaginary component of the velocity $O\exp(ny)$ will escape to infinity in a time approximately given by

$$t = \int_{\delta_L}^{\infty} e^{-ny} dy = \frac{1}{n} e^{-n\delta_L}. \tag{24}$$

It follows that

$$\delta_L(t) \simeq \frac{1}{n} \ln \frac{1}{nt}. \tag{25}$$

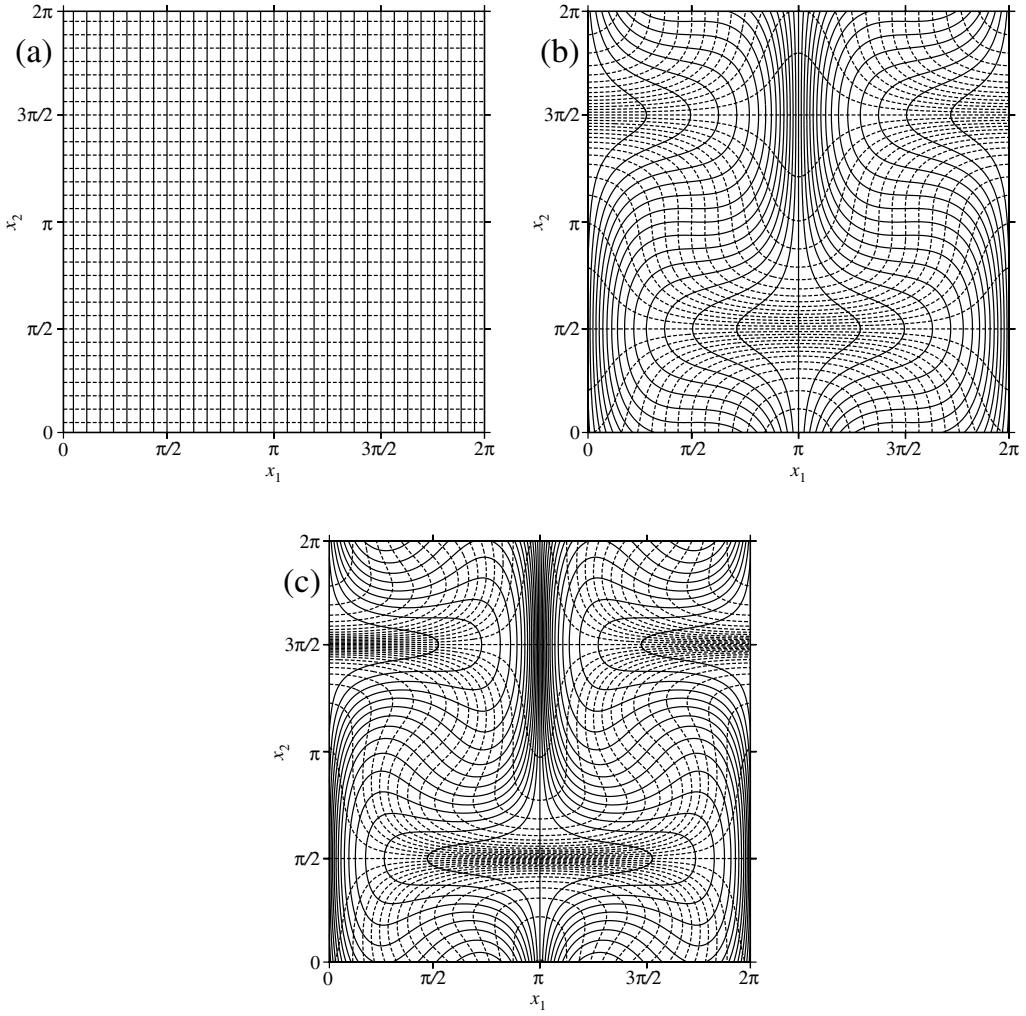

Figure 5. (a) Regular grids in the Eulerian coordinates (x_1, x_2) at time $t = 0$. (b) Advected regular grids by the steady flow at time $t = 1.6$, which indicate the Lagrangian map $\mathbf{x}(\mathbf{a}, t)$ in the Eulerian coordinates. (c) Advected regular grids at time $t = 2.4$.

It is not clear whether this law for the Lagrangian δ_L will carry over to flow having non-trivial Eulerian dynamics.

We now turn to the long-time behavior. In Eulerian coordinates for non-trivial dynamics, the best proven lower bound for $\delta(t)$ is a decreasing double exponential (see Frisch *et al.*, 2003, and references therein). But numerical simulations usually give a simple exponential decrease (Sulem *et al.*, 1983; Frisch *et al.*, 2003). The Lagrangian δ_L for the steady cellular flow considered here is given by (17), which has an obvious expansion at large t

$$\delta_L(t) \simeq 2e^{-t}, \qquad t \to \infty, \tag{26}$$

which agrees with the numerical simulations of section 3. Note that the nearest singularities are located "above" the hyperbolic stagnation points of the flow (5).

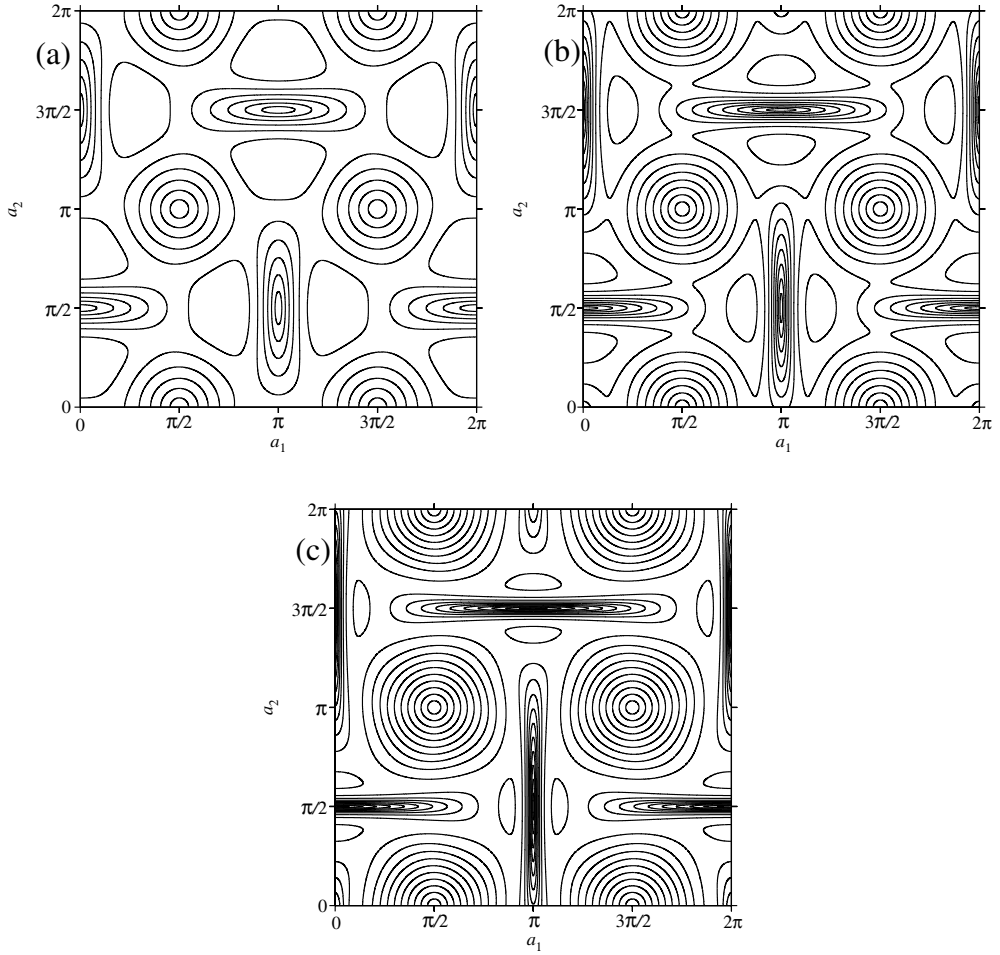

Figure 6. (a) Contours of the modulus of the displacement $|\mathbf{x}(\mathbf{a}, t) - \mathbf{a}|$ at time $t = 1.6$ in the Lagrangian coordinates (a_1, a_2). Contour levels are $\pi/15, 2\pi/15, \ldots$ (b) Same as (a) but for $t = 2.4$. (c) Same as (a) but for $t = 3.2$.

As we have remarked in section 1, $\delta_L(t)$ allows us to give an objective definition of the smallest scale for the passive scalar advected by the flow (5). According to formula (26), this scale decreases exponentially in time which, as we have noted in section 3, reflects the squeezing of the flow around the hyperbolic stagnation points. The exponential temporal rate of deformation of passive scalar structures transversal to the streamlines can be explained by dimensional reasoning.

We note that the period of motion of a particle along a trajectory with the stream function $\Psi(\mathbf{a})$ is given by $4K(\sqrt{1 - \Psi^2(\mathbf{a})})$ (see Appendix A, formula (A.4) and Lawden, 1989) changing from 2π in the centre of the cell to infinity at the boundaries. Obviously, for a passive scalar field which is not constant[9] along the streamlines, such as for example $\theta(x_1, x_2) = \cos x_1 \sin x_2$, the most intensive mixing will be observed near the hyperbolic stagnation points. Let us consider the flow near the stagnation point $(0, \pi/2)$ at the point $\mathbf{a} = (a_1, \pi/2 - a_2)$. The displacement of a fluid particle starting

[9]If a passive scalar field is constant along the streamlines there will be no mixing.

at $\mathbf{a}$ becomes significant at the time $t \sim K(\sqrt{1-\Psi^2(\mathbf{a})})$. Since $\Psi(\mathbf{a})$ is small, we use the approximative expression (see Whittaker and Watson, 1927)

$$K(\sqrt{1-\Psi^2(\mathbf{a})}) \approx \ln \frac{4}{\Psi(\mathbf{a})} \tag{27}$$

and obtain

$$a_1 a_2 \sim \mathrm{e}^{-t}. \tag{28}$$

Hence the smallest spatial scale for the passive scalar will decrease exponentially in time.

In this paper, it is found that hyperbolic stagnation points can be a key in the analysis of the Lagrangian analyticity strip of the steady solution (4) to the two-dimensional Euler equation. Currently we are investigating the Lagrangian $\delta_{\mathrm{L}}(t)$ of the three-dimensional steady solutions (the ABC flows and more general Beltrami flows Majda and Bertozzi, 2002) of the three-dimensional Euler equations. Since such flows can be chaotic, an interesting question is which stretching — caused by the chaos or the hyperbolic stagnation points — dominates. A preliminary result indicates that the nearest singularities are again above the hyperbolic stagnation points at large times. The details of the study of the three-dimensional steady flows will be reported elsewhere. It is also of interest to point out that for kinematic dynamos in three-dimensional[10] steady flows, the fastest growth of the magnetic field is frequently observed near hyperbolic stagnation points (Soward, 1994) despite the presence of the chaotic stretching.

A question for further study remains whether the behaviour of the Lagrangian $\delta_{\mathrm{L}}(t)$ does exhibit some structural stability with respect to hyperbolic stagnation points.

Acknowledgments

We are grateful to J. Bec and U. Frisch for useful discussions. Computational resources were provided by the Yukawa Institute (Kyoto). This research was supported by the European Union under contract HPRN-CT-2000-00162 and by the Indo-French Centre for the Promotion of Advanced Research (IFCPAR 2404-2). WP would like to thank U. Frisch, A. Degenhard and Yu. G. Kondratiev for their support and help. TM was supported by the Japanese Ministry of Education Grant-in-Aid for Young Scientists [(B), 15740237, 2003] and also received partial support from the French Ministry of Education. WP acknowledges partial support from the European network EU RTN no. HPRN-CT-2002-00282 'Hyke'.

References

Abramovitz, M. and Stegun, I.A., *Handbook of Mathematical Functions*, 1965 (Dover Publications).

Bailey, D.H., A fortran-90 based multiprecision system. *RNR Technical Report*, 1995, **RNR-94-013**. See also http://crd.lbl.gov/~dhbailey/

[10]Because of the two-dimensional theorem three dimensions are required.

Bardos, C., Benachour, S. and Zerner, M., Analyticité des solutions périodiques de l'équation d'Euler en deux dimensions. *C. R. Acad. Sc. Paris* 1976, **282** A, 995–998.
Benachour, S., Analyticité des solutions de l'équation d'Euler en trois dimensions. *C. R. Acad. Sc. Paris*, 1976a, **283** A, 107–110.
Benachour, S., Analyticité des solutions des équations d'Euler. *Arch. Rat. Mech. Anal.*, 1976b, **71**, 271–299.
Brachet, M.E., Meiron, D.I., Orszag, S.A., Nickel, B.G., Morf, R.H. and Frisch, U., Small-scale structure of the Taylor-Green vortex. *J. Fluid Mech.*, 1983, **130**, 411–452.
Dombre, T., Frisch, U., Greene, J.M., Hénon, M., Mehr, A. and Soward, A.M., Chaotic streamlines in the ABC flows. *J. Fluid Mech.*, 1986, **167**, 353–391.
Frisch, U., *Turbulence. The legacy of A.N. Kolmogorov*, 1995 (Cambridge University Press: Cambridge).
Frisch, U., Matsumoto, T. and Bec, J., Singularities of Euler flow? Not out of the blue!. *J. Stat. Phys.*, 2003, **113**, 761–781.
Lawden, D.F., *Elliptic Functions and Applications*, 1989 (Springer-Verlag).
Majda, A.J. and Bertozzi, A.L., *Vorticity and Incompressible Flow*, 2002 (Cambridge University Press: Cambridge).
Matsumoto, T., Bec, J. and Frisch, U., The analytic structure of 2D Euler flow at short times, 2004, *Fluid Dyn. Res.* (in press).
Ohkitani, K., Numerical study of comparison of vorticity and passive vectors in turbulence and inviscid flows. *Phys. Rev.* E, 2002, **65**, 046304.
Orszag, S.A., Private communication to U. Frisch, 2003.
Soward, A.M., Fast dynamos, In *Lectures on Solar and Planetary Dynamos*, edited by M.R.E. Proctor and A.D. Gilbert, p. 181–217, 1994 (Cambridge University Press: Cambridge).
Sulem, C., Sulem, P.L. and Frisch, H., Tracing complex singularties with spectral methods. *J. Comput. Phys.*, 1983, **50**, 138–161.
Whittaker, E.T. and Watson, G.N., *A Course of Modern Analysis*, 1927 (Cambridge University Press: Cambridge).

Appendix

A. *Explicit construction of the Lagrangian map*

The system of ordinary differential equations (6) can be solved by a simple adaptation of what is done for an integrable case of the ABC flow in (Dombre *et al.*, 1986, Appendix A). For completeness we give the full derivation, which is quite elementary.

Taking the derivative of (6) with respect to time we obtain a system of two decoupled differential equations

$$2\ddot{x}_1 = \sin 2x_1, \qquad 2\ddot{x}_2 = -\sin 2x_2 \tag{A.1}$$

satisfying the initial conditions (7) and

$$\dot{x}_1(\mathbf{a}, 0) = -\sin a_1 \sin a_2, \qquad \dot{x}_2(\mathbf{a}, 0) = -\cos a_1 \cos a_2. \tag{A.2}$$

Equation (5.1) is obviously the same as a set of pendulum equations describing nonlinear oscillations around the origin for the x_2-variable and around $\pi/2$ for the x_1-variable. Let us just consider the x_2-variable. The equation has the first integral

$$\frac{1}{2}\dot{x}_2^2 - \frac{1}{4}\cos 2x_2 = \frac{1}{4} - \frac{1}{2}\sin^2 a_1 \cos^2 a_2 = \frac{1}{4}\big(1 - 2\Psi^2(\mathbf{a})\big), \tag{A.3}$$

which expresses the conservation of energy. From this equation we obtain by standard integration (Lawden, 1989)

$$\sin x_2(\mathbf{a}, t) = \sqrt{1 - \Psi^2(\mathbf{a})}\,\mathrm{sn}\left(t + \int_0^{a_2} \frac{d\tilde{x}}{\sqrt{(1 - \Psi^2(\mathbf{a})) - \sin^2 \tilde{x}}}, \sqrt{1 - \Psi^2(\mathbf{a})} \right). \qquad \text{(A.4)}$$

Obviously, since the poles of the sn function do not lie on the real axis (Lawden, 1989; Abramovitz and Stegun, 1965), solutions of (6) are periodic and non-singular for real initial conditions. The only possibility for an orbit to come across a pole and thereby to go to infinity is to start at a suitable complex location.

Lagrangian singularities of steady two-dimensional flow

Walter Pauls and Takeshi Matsumoto*

Fakultät für Physik, Universität Bielefeld, Bielefeld, Germany [1].

*Department of Physics, Kyoto University, Kyoto, Japan.

Abstract

The complex-space singularities in the Lagrangian frame of a class of stationary solutions to the three-dimensional incompressible Euler equation (integrable case of the Arnold-Beltrami-Childress flows) are studied by analytical and numerical methods. We obtain full analytic description of the singular manifold in terms of elliptic and inverse trigonometric functions. The distance from the real space to the closest complex Lagrangian singularity (width of the Lagrangian analyticity strip) decreases logarithmically at short times and exponentially at large times. Numerical simulations confirm these observations.

Introduction

There are several reasons for studying singularities of solutions to hydrodynamical equations (such as the Navier-Stokes or Euler equations) in the complex spatial domain. The most important one among them is related to the issue of a finite-time blowup. Namely, it is still not clear whether a solution to the three dimensional incompressible Navier-Stokes or Euler equation with real analytic initial conditions satisfying periodic boundary conditions can become singular in a finite time.

In the case of the Euler equation, a key observation is that, if a singularity appears in the real domain, it is necessarily preceded by the one in the complex domain (see [1] for details). Note that even if the real-space flow has no singularities, the velocity field continued into the complex domain can become singular at some complex locations which we denote by Σ. Therefore, measuring the distance from the real domain to the nearest complex singularity (called width of the analyticity strip) serves as a criterion of a finite-time blowup [2, 3] : vanishing the width means appearance of a singularity in the real space. The width also defines the smallest scale in the flow.

Usually, such complex singularities are considered in the Eulerian frame of reference (Eulerian coordinates). In this study we consider complex singularities in the Lagrangian frame of reference (Lagrangian coordinates). Knowledge of such complex Lagrangian singularities can help us, for example, to understand the behavior of small scale structures of a passive scalar. And, mathematically, it may reveal important aspects of time continuous complex dynamics, since the complexified Lagrangian map of analytical flows is a physical representative of complex analytical transformations depending on a continuous parameter. Here we further restrict[2] ourselves to Lagrangian singularities of a class of steady solutions to the incompressible 3D Euler equation, more specifically the integrable case of the well-known Arnold-Beltrami-Childress (ABC) flow ($A = 1, C = 0, 0 < B \leq 1$). For such flows, complex singularities in the Eulerian coordinates stay at the complex infinity forever. However, when working in the Lagrangian coordinates, we find a nontrivial set of complex singularities which is within a finite distance from the Lagrangian real domain at every finite time and reaches it in the infinite time limit. The merit of working with integrable steady solutions is that we can obtain a global analytic description of the Lagrangian complex singular manifold Σ. For the non-integrable case, due to the non-integrability (chaotic mixing) [4], the non-perturbative analytic expression of Σ is not available.

Analytic description of the set of complex Lagrangian singularities

We consider the integrable case ($C = 0$) of the well-known ABC flow [4]. The velocity field of the ABC flow is given by

$$\mathbf{v}(\tilde{x}_1, \tilde{x}_2, \tilde{x}_3) = (A \sin \tilde{x}_3 + C \cos \tilde{x}_2, B \sin \tilde{x}_1 + A \cos \tilde{x}_3, C \sin \tilde{x}_2 + B \cos \tilde{x}_1) \qquad (1)$$

[1] walter.pauls@physik.uni-bielefeld.de

[2] A study about complex Lagrangian singularities of the general time-dependent solutions to the Euler equation will be reported elsewhere.

which is a steady solution to the 3D Euler equation. By using a suitable transformation of coordinates and the conservation of the vorticity, the integrable case ($C = 0$) can be reduced to a two dimensional system. The equations of motion of the fluid particles are as follows

$$\dot{x}_1 = -\tfrac{1+B}{2}\sin x_1 \sin x_2 + \tfrac{1-B}{2}\cos x_1 \cos x_2; \tag{2}$$
$$\dot{x}_2 = -\tfrac{1+B}{2}\cos x_1 \cos x_2 + \tfrac{1-B}{2}\sin x_1 \sin x_2. \tag{3}$$

They have to satisfy the initial conditions $\mathbf{x}(\mathbf{a}, 0) = \mathbf{a}$ defining the Lagrangian map $\mathbf{x}(\mathbf{a}, t)$. Next we introduce the complex Eulerian variables $\mathbf{z} = \mathbf{x} + i\mathbf{y}$ as well as the complex Lagrangian variables $\mathbf{c} = \mathbf{a} + i\mathbf{b}$. The complexified stream function has the form

$$\xi = \frac{1+B}{2}\sin z_1 \cos z_2 + \frac{1-B}{2}\cos z_1 \sin z_2. \tag{4}$$

From now on we introduce a new coordinate system $w_1 = \sin z_1$, $w_2 = \cos z_2$. Using (4) in the new coordinates we can express w_2 as function of w_1

$$w_2^{\pm} = \frac{2\xi(1+B)w_1 \pm 2(1-B)\sqrt{B(-w_1^4 + [\tilde{\xi}^2+1]w_1^2 - \tilde{\xi}^2)}}{(1-B)^2 + 4Bw_1^2}, \qquad \text{where} \quad \tilde{\xi}^2 = \frac{4\xi^2 - (1-B)^2}{4B}. \tag{5}$$

Introducing a new variable $u \equiv w_1/\tilde{\xi}$ we obtain the following equation

$$\dot{u} = \pm i\sqrt{B}\sqrt{(1-u^2)(1-\tilde{\xi}^2u^2)}. \tag{6}$$

This equation allows to express t in terms of the initial and the current values of u that is u_0 and $u(t)$, respectively

$$i\sqrt{B}t = \mp \int_{u_0}^{u(t)} \frac{ds}{\sqrt{(1-s^2)(1-\tilde{\xi}^2s^2)}}. \tag{7}$$

Obviously, the complexified Lagrangian velocity field $\mathbf{v}(\mathbf{z}(\mathbf{c}, t))$ becomes infinite only if the complexified Lagrangian mapping becomes infinite, that is the fluid particles escape to the complex infinity. Therefore, at least one of the coordinates, say w_2 must become infinite. From (5) it follows that, if w_2 tends to infinity then, because of the finiteness of complexified stream function, w_1 must tend to $\pm i(1-B)/2\sqrt{B}$. Therefore, the time it takes a particle with initial position u_0 to escape to infinity is given by

$$i\sqrt{B}t = \pm \int_{\mp i(1-B)/2\tilde{\xi}\sqrt{B}}^{u_0} \frac{ds}{\sqrt{(1-s^2)(1-\tilde{\xi}^2s^2)}}. \tag{8}$$

Inverting this relation we obtain

$$w_1(0) = \mp\tilde{\xi}\,\mathrm{sn}\left(i\left[\sqrt{B}t - F\left(\arcsin i\,\frac{1-B}{2\tilde{\xi}\sqrt{B}},\ \tilde{\xi}\right)\right],\ \tilde{\xi}\right), \tag{9}$$

where $F(\cdot, \tilde{\xi})$ denotes the incomplete elliptic integral of the first kind with modulus $\tilde{\xi}$ and w_2 can be calculated using (5). Note, that as expected, for $B = 0$ the singularities are time independent and therefore located at the complex infinity.

Let us for simplicity restrict ourselves to the case $B = 1$. Then the singular set can be parametrized in terms of the complex stream function ξ as

$$w_1(0) = i\xi\,\mathrm{sc}(t, \sqrt{1-\xi^2}), \qquad w_2(0) = -i\,\mathrm{cs}(t, \sqrt{1-\xi^2}), \tag{10}$$

where the sc function is defined as $\mathrm{sc} \equiv \mathrm{sn}/\mathrm{cn}$ and cs is its reciprocal. By definition of coordinates w_1 and w_2 we can express the Lagrangian locations at which w_2 becomes singular at time t as

$$c_1^\star = \arcsin\left[i\xi\mathrm{sc}(t, \sqrt{1-\xi^2})\right], \qquad c_2^\star = \arccos\left[i\mathrm{cs}(t, \sqrt{1-\xi^2})\right]. \tag{11}$$

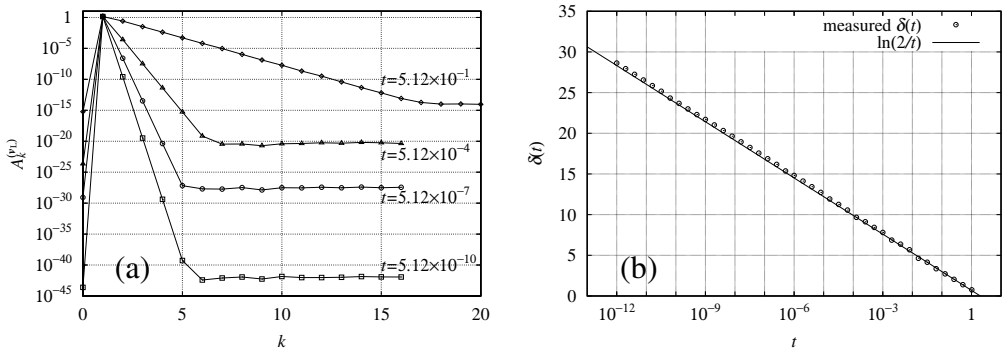

Figure 1: (a) Shell-summed amplitudes of the Lagrangian velocity $A_k^{(\mathbf{v}_\mathrm{L})}$ for four different short times calculated with the number of grid points 32^2 and 64^2. (b) Log-linear plot of the width of the Lagrangian analyticity strip $\delta(t)$ measured as the logarithmic decrement of $A_k^{(\mathbf{v}_\mathrm{L})}$ at short times $10^{-12} \leq t \leq 1$.

Since the functions appearing in these expressions are multivalued the singular manifold has infinitely many sheets. Furthermore, it has nontrivial intersection with the imaginary plane "above" the hyperbolic stagnation points, such as $(0, -\pi/2)$, see [5]. This fact is explained by an additional symmetry of the case $B = 1$ in comparison with the case $B \neq 1$. The minimal distance to from Σ to the real domain is given by

$$\delta(t) = |\mathrm{arcsinh}\left(\frac{1}{\sinh t}\right)|. \tag{12}$$

In the general case $0 < B \leq 1$ the short-time behaviour of the shortest distance $\delta(t)$ from the singular manifold Σ to the real domain at time t can be estimated using addition formula for the elliptic sn function [6]. We obtain

$$\delta(t) \sim \ln \frac{1}{t}, \tag{13}$$

analogously to the logarithmic short-time behaviour, found in [1] for nonstationary inviscid flows in Eulerian coordinates. On dimensional reasons we expect the same type of behaviour for all steady flows given by trigonometric polynomials [5].

The long-time behaviour of $\delta(t)$ crucially depends on the structure of the hyperbolic stagnation points of the flow. In long-time limit the nearest points of the singular manifold are located "above" the hyperbolic stagnation points and the width of the Lagrangian analyticity strip decays exponentially

$$\delta(t) \sim e^{-\sqrt{B}t}. \tag{14}$$

Numerical check

The above results on the long and short-time behaviours of $\delta(t)$ are checked using numerical simulations. We first calculate the Fourier coefficients of the reduced two-dimensional velocity field and then apply the method of tracing complex singularities [2] which relies on the fact that the energy spectrum at high wavenumbers is decaying exponentially as $\exp(-2\delta(t)|\mathbf{k}|)$.

The Lagrangian Fourier coefficients are obtained as follows. First, we calculate the Lagrangian map $\mathbf{x}(\mathbf{a}, t)$ by solving the equations of motion with a fourth order Runge-Kutta method for N^2 initial conditions $\mathbf{a} = ((2\pi/N)l,\, (2\pi/N)m)$ $(l,\, m = 0, 1, \ldots, N-1)$, which form a regular square grid in the Lagrangian marker space. We obtain then the Lagrangian velocity field by just changing variables:

$$\mathbf{v}_\mathrm{L}(\mathbf{a}, t) \equiv \mathbf{v}(\mathbf{x}(\mathbf{a},\, t)). \tag{15}$$

The Lagrangian velocity Fourier coefficients are given by

$$\hat{\mathbf{v}}_\mathrm{L}(\mathbf{k},\, t) = \frac{1}{N^2} \sum_{\mathbf{a}} \mathbf{v}_\mathrm{L}(\mathbf{a}, t)\, e^{-i\mathbf{k}\cdot\mathbf{a}}. \tag{16}$$

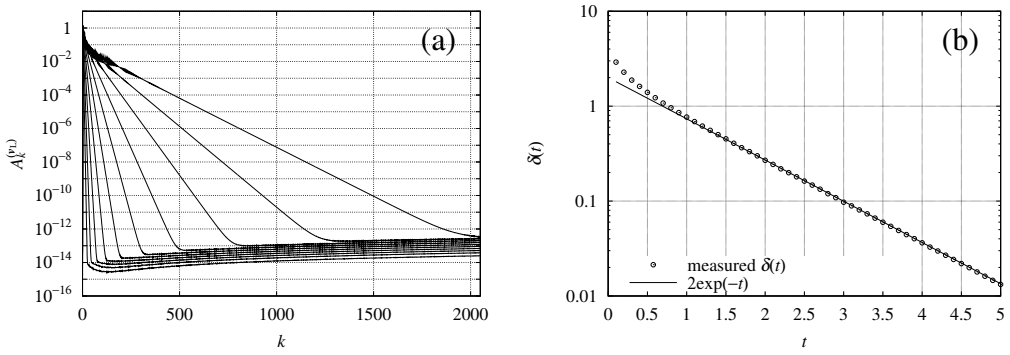

Figure 2: (a) Shell-summed amplitudes of the Lagrangian velocity $A_k^{(\mathbf{v}_\mathrm{L})}$ for 10 different instances ($t = 0.5, 1.0, \ldots, 5.0$) calculated with the number of grid points 4096^2. (b) Linear-log plot of the width of the Lagrangian analyticity strip $\delta(t)$ measured as the logarithmic decrement of $A_k^{(\mathbf{v}_\mathrm{L})}$ at long times $t \leq 5$.

For measuring the width δ, it is convenient to define the shell-summed amplitude $A_k^{(\mathbf{v}_\mathrm{L})}$ of $\hat{\mathbf{v}}_\mathrm{L}(\mathbf{k})$ as

$$A_k^{(\mathbf{v}_\mathrm{L})} = \sum_{k \leq |\mathbf{k}| < k+1} |\hat{\mathbf{v}}_\mathrm{L}(\mathbf{k})|. \tag{17}$$

The Lagrangian width δ is then obtained by fitting the shell-summed amplitude to an exponential with an algebraic prefactor:

$$A_k^{(\mathbf{v}_\mathrm{L})} \propto k^{-\alpha} \exp(-\delta k). \tag{18}$$

For the short and long-time behaviour, our numerical results confirm the analytical predictions, see Figures 1 and 2 for the case $B = 1$.

Discussion

The observed exponential decay (14) of the width of the analyticity strip $\delta(t)$ is connected with generation of small scale structures in the vicinity of the hyperbolic stagnation points [5]. The fluid particles are squeezed along the stable direction and are stretched along the unstable direction. Thus, for certain configurations of passive tracer an intensive mixing will take place at these stagnation points. It should be noted that this process is not related to the chaotic mixing since the velocity field which we have considered has integrable stream lines.

The analytically continued Lagrangian map $\mathbf{x}(\mathbf{a}, t)$ is an example of complex dynamical systems with continuous time. Here we have found that the set of its complex Lagrangian singularities is analytic. However, such boundaries generated by dynamical systems in the complex domain are often not smooth, even fractal. (An intensively studied example are dynamical systems given by iteration of analytic functions in one complex dimension, see for example [7].) An interesting question in this connection is in how far the structure of the Lagrangian singular manifold (algebraic variety, analytic manifold,...) reflects the integrability of the velocity field.

Acknowledgments

We are grateful to J. Bec and U. Frisch for useful discussions. Computational resources were provided by the Yukawa Institute (Kyoto). This research was supported by the European Union under contract HPRN-CT-2000-00162 and by the Indo-French Centre for the Promotion of Advanced Research (IFCPAR 2404-2). TM was supported by the Japanese Ministry of Education Grant-in-Aid for Young Scientists [(B), 15740237, 2003] and received also partial support from the French Ministry of Education. WP acknowledges partial support from the European network EU RTN no HPRN-CT-2002-00282 “Hyke”.

References

[1] U. Frisch, T. Matsumoto and J. Bec, *J. Stat. Phys.*, 2003, **113**, 761.

[2] C. Sulem, P. L. Sulem, H. Frisch, Tracing complex singularities with spectral methods, *J.Comput. Phys.* **50**, pp 138-161, 1983.

[3] U. Frisch, *Turbulence. The Legacy of Kolmogorov*, Cambridge University Press, 1995.

[4] T. Dombre, U. Frisch, J. M. Greene, M. Hénon, A. Mehr, A. M. Soward, Chaotic streamlines in the ABC flows, *J. Fluid Mech.* **167**, pp. 3553-391, 1986.

[5] W. Pauls and T. Matsumoto, Lagrangian singularities of steady two-dimensional flow, *Geophys. Astrophys. Fluid Dynamics*, in press.

[6] E. T. Whittaker and G. N. Watson, *A Course of Modern Analysis*, Cambridge at the University Press, 1927.

[7] N. Steinmetz, *Rational Iteration*, Walter de Gruyter, 1993.

Part IV

Stochastic diffusion in cellular flows at high Péclet numbers

Chapter 10

Probabilistic approach to passive scalar advection in cellular flows at high Péclet numbers

Transport in cellular flows from the viewpoint of stochastic differential equations

W. Pauls

July 18, 2006

1 Introduction

The behaviour of passive scalar tracers moving in a prescribed velocity field can be described using two equivalent formulations: (i) the passive scalar equation which in two dimensions can be written as

$$\partial_t \theta + \nabla^\perp H \cdot \nabla \theta = \varepsilon \Delta \theta, \tag{1}$$

(ii) probabilistic description in terms of stochastic differential equations

$$dX_t = -\partial_y H(X_t, Y_t) + \sqrt{2\varepsilon}\, dW_t^{(x)}; \tag{2a}$$

$$dY_t = \partial_x H(X_t, Y_t) + \sqrt{2\varepsilon}\, dW_t^{(y)}. \tag{2b}$$

Here $H(x, y)$ is a periodic stream function defined in such a way that the velocity field is given by $\mathbf{u} = (-\partial_y H, \partial_x H)$. In what follows the velocity field will always be deterministic and time-independent.

The subject of study in this report is the asymptotic behaviour of the process (2) in the limit $\varepsilon \to 0$. In fact, this question can be analyzed using the passive scalar equation (1). Here the homogenization technique from the theory of partial differential equations is applied which gives a description of the behaviour of solutions of (1) on large scales, see [1]. Separating slow and fast variables and performing a multiscale analysis one obtains the effective diffusion equation for the evolution of θ on large scales

$$\partial_t \theta = \nabla \cdot D_\varepsilon^* \nabla \theta. \tag{3}$$

The effective diffusivity D_ε^* is a constant matrix given by the following expression

$$D_\varepsilon^*(\mathbf{e}) = \langle (\varepsilon \mathbb{I} + \mathbf{\Psi})(\nabla \chi + \mathbf{e}) \cdot \mathbf{e} \rangle, \tag{4}$$

where χ is the solution of the so called cell problem

$$\nabla \cdot [(\varepsilon \mathbb{I} + \mathbf{\Psi})(\nabla \chi + \mathbf{e})] = 0. \tag{5}$$

Note that equation (5) has to be solved in the domain of periodicty of the streamfunction $H(x, y)$. One class of flows for which the cell problem (5) is amenable to analysis is a special

case of the well known ABC flow, namely the case $A = 1$, $C = 0$. The streamfunction is of the form

$$H(x, y) = \frac{1 + B}{2} \cos x \cos y + \frac{1 - B}{2} \sin x \sin y. \tag{6}$$

The case $B = 1$ has been treated in [2] using boundary layer techniques where it was shown that $D^*_\varepsilon = O(\sqrt{\varepsilon})$. More precisely, the boundary layer analysis is performed in a boundary layer of width $O(\sqrt{\varepsilon})$ which forms at the boundaries of the impermeable cells of the underlying velocity field $\nabla^\perp H(x, y)$. Heuristically, since the amount of the tracer transported along the boundary layer is proportional to its area, the effective diffusivity has to be proportional to $\sqrt{\varepsilon}$. An analytical solution of the cell problem in the boundary layer approximation was given in [3] using Wiener–Hopf technique. In the case $B < 1$ the effective diffusivity is anisotropic and as has been shown in [4] the effective diffusivity across the streamlines is of order $O(\varepsilon)$ while along the stream lines of the flow it is of order $O(1/\varepsilon)$.

The large-scale picture obtained by the homogenization approach as presented above does not give any information on the microscale structure of the diffusion processes happening in the flow. However, small scales do play a major role in the form of boundary layers which is typical for diffusion processes at high Péclet numbers.

In principle, stochastic differential equations (2) allow us to describe the diffusion of particles in much more detail. But how much information can we obtain on the limit $\varepsilon \to 0$? A standard approximating technique in this framework is the so called Wentzell–Freidlin method. It describes the behaviour of randomly perturbed Hamiltonian systems on large time scales at high Péclet numbers by means of continuous diffusion processes on graphs, as is explained in Section 2. A priori, this technique works only only for Hamiltonians $H(x, y)$ such that $H(x, y) \to +\infty$ when $|(x, y)| \to \infty$ and does not allow for existence of heteroclinic orbits.

If we try to apply this technique to the case of unbounded cellular flow with $H(x, y)$ given by (6) we arrive at a paradox. Namely, the transition from one cell to another will happen instantaneously no matter how large the spatial separation between the cells. Furthermore, the characteristic time scale of diffusion will be of order $O(1/\varepsilon)$ which contradicts the results obtained in the homogenization framework where the characteristic time scale is of order $O(1/\sqrt{\varepsilon})$.

However, for bounded domains this technique works for sufficiently small ε such that $1/\sqrt{\varepsilon}$ is much larger that the domain size (therefore it is not in contradiction to the homogenization method). This gives us an indication that the Wentzell-Freidlin method remains locally valid. In fact, it fails on unbounded domains because of its global structure which is determined by the method of "gluing" together single cells.

Actually, by changing the "gluing" prescription between the processes obtained in single cells we can make the Wentzell–Freidlin approach to be consistent with the results given by the homogenization. The main ingredient here is the conservation of probability: the probability current going out of a cell has to be matched with the probability current across the cell boundary (dominated by the boundary layer effects) into the neighbouring cells.

The structure of the present report is as follows: Section 2 is entirely devoted to the Wentzell–Freidlin technique. In Section 2.1 we explain the averaging principle for a single cell and its deterministic background. Asymptotics $\varepsilon \to 0$ of solutions to (2) on bounded domains is described in Section 2.2. In Section 2.3 we discuss some simple models for

diffusion in unbounded cellular flows. Furthermore, using results of numerical simulations we argue that the approximating process on unbounded domain will be discontinuous. In Section 3 we outline the procedure for obtaining this process and state the result. Possible applications are discussed in Section 4.

2 Random perturbation of Hamiltonian systems

For small values of ε (i.e. for high Péclet numbers) equations (2) describe small random perturbation of the determinstic system

$$\dot{x} = -\partial_y H(x(t), y(t)), \tag{7a}$$
$$\dot{y} = \partial_x H(x(t), y(t)) \tag{7b}$$

which represents the limiting case $\varepsilon = 0$. Heuristically one would expect that the behaviour of solutions to (2) in the limit $\varepsilon \to 0$ is to a large extent determined by the deterministic solutions, i.e. solutions of (7). The simplest ansatz of this type consists in making a perturbative expansion of solutions to (2) in powers of $\sqrt{\varepsilon}$ around the deterministic solutions[1], see [11, 12]. However, this approximation is of little use when we want to study long-time behaviour. Indeed, it works well only for a finite period of time (which also remains true when we include higher-order terms) and does not take into account the separation into fast and slow variables. The latter point is of special interest to us because the underlying structure of the deterministic case (to be described in Section 2.1.1) is at the basis of the approximating method discussed in Section 2.1.

2.1 Slow-scale motion inside a cell

2.1.1 Case of vanishing viscosity

In terms of (1) the deterministic case corresponds to the passive scalar equation with vanishing viscosity $\varepsilon = 0$

$$\partial_t \theta + \nabla^\perp H \cdot \nabla \theta = 0 \tag{8}$$

and an initial condition θ_0. The charateristics of this equation are given by (7) so that the solutions of the Cauchy problem for equation (8) can be constructed in terms of the one-parametric flow (by taking the inverse Lagrangian mapping) generated by the velocity field $\nabla^\perp H(x, y)$, see e.g. [5].

If we choose the streamfunction (6), then equations (7) can be solved explicitly, see [6]. For the particular case $B = 1$ the solution is given in terms of Jacobi elliptic functions (see [7])

$$x(t, h) = \arcsin\left(\sqrt{1-h^2}\,\mathrm{sn}(t, \sqrt{1-h^2})\right), \tag{9a}$$
$$y(t, h) = \arcsin\left(\sqrt{1-h^2}\,\mathrm{cd}(t, \sqrt{1-h^2})\right), \tag{9b}$$

[1] In the case of the Hamiltonian (6) with $B = 1$ the explicit solution of (7) given by (9) allows us to compute analytically the first order term in the expansion. It turns out to be a stochastic integral the integrand being a complicated expression involving Jacobi elliptic, hyperbolic and logarithmic functions.

where $x(0) = 0$ and $H(x, y) = h$ is kept fixed along a trajectory. Obviously, a particle initially located in one particlular cell will stay inside this cell. The period of motion along a level line with $H(x, y) = h$ is given by a complete elliptic integral $4K(\sqrt{1-h^2})$. For the special case $h = 0$ the equation of motion along the separatrix can be solved in terms of elementary functions

$$x(t, 0) = 2 \arctan e^t - \frac{\pi}{2}, \tag{10}$$

where the initial conditions are specified as $x(0, 0) = 0$ and $y(0, 0) = \pi/2$. Note that in the deterministic case it takes an infinite time to reach the equilibrium point $(\pi/2, \pi/2)$.

It is crucial for the following analysis that we can interpret (7) as a Hamiltonian system with one degree of freedom by identifying $(x, y) \to (p, q)$. The streamfunction $H(x, y) \to H(p, q)$ is then identified with the Hamiltonian of the system. As usually, an action variable $I(h)$ can be introduced as

$$I(h) = \frac{2}{\pi} \int_h^1 K\left(\sqrt{1-h'^2}\right) dh', \tag{11}$$

which is equal to the area inclosed inside the orbit $H(p, q) = h$ divided by 2π, see [8].

2.1.2 Effective Fokker-Planck equation

We will first study the behaviour of solutions to (2) with H given by (6) with $B = 1$ such that the particle is staying inside one cell. The typical technique for analyzing the evolution of slow variables of such a system subject to small random perturbations is the technique of averaging out the fast variables. Then an effective evolution equation for slow variables inside a cell is obtained in a way similar to the analysis of small perturbations in classical mechanics [8]. In the framework of stochastic differential equations this ansatz was introduced by Wentzell and Freidlin, see [12] and references therein. For analogous consideration in the framework of passive scalar equation see [17].

In our case the averaging principle can be briefly summarized as follows: Inside the cell the deterministic system (7) can be described in terms of motion on invariant tori. We parametrize these tori by the values of $H(x, y) = h$. In the perturbed system (at least for small perturbations) particles will still rotate rapidly along the tori, however they will slowly drift across the tori. To describe this slow drift we calculate $dH(X_t, Y_t)$. Using Itô's formula we obtain

$$dH(X_t, Y_t) = \sqrt{2\varepsilon}\, \nabla H(X_t, Y_t) \cdot d\mathbf{W}_t + \varepsilon\, \Delta H(X_t, Y_t) dt, \tag{12}$$

where $d\mathbf{W}_t = (dW_t^{(x)}, dW_t^{(y)})$ is the two-dimensional Brownian motion. Of course, we cannot evaluate the terms $\nabla H(X_t, Y_t) \cdot d\mathbf{W}_t$ and $\Delta H(X_t, Y_t)$ explicitly without solving equations (2). However, using the integral form of (12)

$$H(X_t, Y_t) = H(X_0, Y_0) + \sqrt{2\varepsilon} \int_0^t \nabla H(X_s, Y_s) \cdot d\mathbf{W}_s + \varepsilon \int_0^t \Delta H(X_s, Y_s) ds, \tag{13}$$

we see that because of the smallness of the perturbation (i) the second integral is approximately equal[2] to the integral $\int_0^t \langle \Delta H \rangle_{H=h}(X_s, Y_s) ds$, where

$$\langle \Delta H \rangle_{H=h} = \left(\oint \frac{dl}{|\nabla H|} \right)^{-1} \oint \frac{\Delta H}{|\nabla H|} \, dl \tag{14}$$

and the integrals are taken over the level set $\{(x, y) : \ H(x, y) = h\}$. Moreover, (ii) the first (stochastic) integral in (13) can be represented as

$$\int_0^t \nabla H(X_s, Y_s) \cdot d\mathbf{W}_s = W \left(\int_0^t |\nabla H(X_s, Y_s)|^2 ds \right), \tag{15}$$

where $W(\cdot)$ is a one-dimensional Wiener process. With the same argument as before $\int_0^t |\nabla H(X_s, Y_s)|^2 ds$ can be approximated by the ergodic average of $|\nabla H|^2$

$$\langle |\nabla H|^2 \rangle_{H=h} = \left(\oint \frac{dl}{|\nabla H|} \right)^{-1} \oint |\nabla H| \, dl \tag{16}$$

The obtained effective diffusion process is most conveniently formulated in terms of an effective Fokker-Planck equation with time rescaled as $t \to \varepsilon t$

$$\partial_t p = \partial_h^2 \left(A(h) p \right) - \partial_h \left(B(h) p \right) \tag{17}$$

The coefficients $A(h)$ and $B(h)$ given by

$$A(h) = \langle |\nabla H|^2 \rangle_{H=h}, \quad B(h) = \langle \Delta H \rangle_{H=h}. \tag{18}$$

In the case of H given by (6) with $B = 1$ these coefficients can be calculated explicitly using formulas (9)

$$A(h) = 2 \frac{E(\sqrt{1-h^2})}{K(\sqrt{1-h^2})} - 2h^2, \qquad B(h) = -2h. \tag{19}$$

Here $K(\cdot)$ and $E(\cdot)$ are complete elliptic integrals of the first and second kind, see [7, 15]. Note that instead of the Hamiltonian we could have used the action variable (11). Indeed, the formulation in terms of the action turns out to be very convenient for generalization of the averaging principle to higher dimensions.

2.2 Construction of an approximating Feller process (Wentzell-Freidlin technique)

In this subsection we study asymptotic behaviour of solutions of (2) constrained to a bounded domain (with periodic boundary conditions) approximating them by a process with essentially one-dimensional state space. We have seen that (17) specifies completely the behaviour of the system up to the first exit time out of a cell. Once having left the cell after some transitional time (during which it will stay in some neighbourhood of the boundary of the original cell) the particle will again slowly diffuse, either in the original cell or in another neighbouring cell.

[2] This is due to the averaging principle.

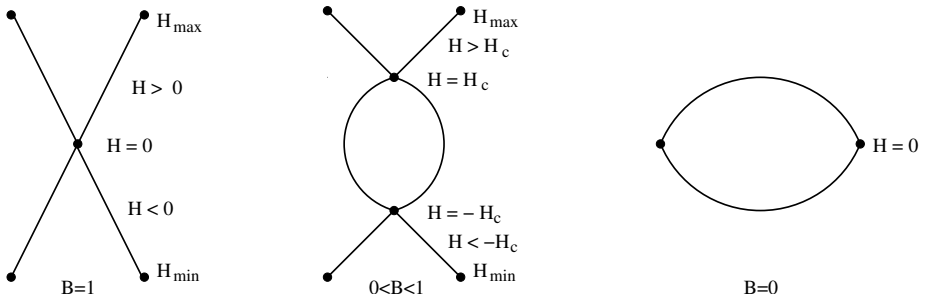

Figure 1: Reeb graphs of the flow (6) for the cases $B = 1$, $0 < B < 1$ and $B = 0$ on the domain of width $2\pi \times 2\pi$.

To describe the transition phase of the particle from one cell to another we need to (i) give a geometrical description of the way in which the cells are connected to each other, (ii) analyze in detail the behaviour of the diffusion process during this transition.

The geometrical description is given using the topological notion of a Reeb graph of $H(x, y)$ [9]. For a general Hamiltonian $H(x, y)$ it is defined in the following way: Let (x_c, y_c) be a critical point, i.e. a point such that $\nabla H(x_c, y_c) = 0$. Then each connected component of the level set $H^{-1}(H(x_c))$ is identified with a vertex. The points on the edges which connect the vertices are identified with connected components of the noncritical level sets $H^{-1}(H(x, y))$. Figure 1 shows the Reeb graphs of $H(x, y)$ given by (6) on the domain $[0, 2\pi] \times [0, 2\pi]$ for the cases $B = 0$, $0 < B < 1$, $B = 1$. Note that in the case $B = 1$ the edges of the Reeb graph correspond to the interior of the cells.

The geometrical description above suggests that the appropriate state space of the process approximating the solutions of (2) is the Reeb graph Γ of the Hamiltonian $H(x, y)$ with edges denoted by e_i and vertices denoted by O_k. In side each edge e_i the approximating process is governed by the evolution equation of the type (17)

$$\partial_t p_i = \partial_h^2 \left(A_i(h) p_i\right) - \partial_h \left(B_i(h) p_i\right) \tag{20}$$

To determine the process completely we have to specify the boundary conditions at the ends of each edge, "gluing" the edges together in a consistent way. This "gluing" procedure determines the behaviour of the process during the passage through the vertices of the graph. Physically it describes transitions of a particle from one cell to another.

Specifying boundary conditions for a stochastic process is in general a quite delicate point. One possibility to specify the boundary conditions is to require the approximating process to have "nice" mathematical properties.[3] In [13] all possible continuous Markov processes with Feller property[4] on graphs were described such that the diffusion inside an edge is governed by a second order elliptic operator (which can possibly depend on the edge). In our case the ellpitic operator is given by the right hand side of (20). Furthermore, at each edge the sum of the incoming probability currents has to vanish. This leads to the

[3] As we shall see later, this requirement is not always consistent with the behaviour of solutions of (2).
[4] This means that in course of time continuous distributions of probability remain continuous.

following boundary conditions at a vertex O_k

$$\sum_{i:\ e_i\sim O_k} J_i(O_k) = 0, \quad p_i(O_k) = p_j(O_k), \quad i,j : e_i \sim O_k,\ e_j \sim O_k \tag{21}$$

where $e_i, e_i \sim O_k$ denote the edges incident to the vertex O_k.

Thus, the approximating technique (in the following referred to as Wentzell–Freidlin technique) consists in (i) approximating the solutions of (2) inside of the cell by (17), (ii) gluing together the cells by matching continuously the probability distributions at the boundaries of the cells.

In the case of the Hamiltonian specified by (6) on bounded domain we expect that the process on the graph approximates well solutions of (2). Furthermore, similarly to [12] a particle spends a zero time (on the time scale εt) at the vertex. From this follows that once the particle reaches the cell (edge) boundary, it can hop instantaneously to any other cell. Furthermore, the behaviour of the process after it reaches the vertex does not depend on its prehistory, i.e. on the edge it came from. Thus, the transition probability from one edge to another is not dependent on their spatial separation. Note that for $\varepsilon \to 0$ this does not result in any contradiction, because of the very long relevant time $O(1/\varepsilon) \to \infty$.

Altogether the Wentzell–Freidlin technique yields the following picture for advection of passive scalar in a bounded domain: Let us chose an initial coondition which corresponds to the passive scalar being concentrated in the center of a cell at $t = 0$. Then, as time goes on, the passive scalar will slowly (i.e. on time scale $O(1/\varepsilon)$) diffuse untill it reaches the cell boundary. As soon as it reaches the boundary it will very quickly (instantaneously on time scale $O(1/\varepsilon)$) spread across the domain along the network of separatrices. After this the passive scalar will penetrate the cells on slow time scale $O(1/\varepsilon)$ untill the stationary distribution is established.

However, the above implies immediately that the Wentzell-freidlin technique cannot be applied in the unbounded case. Indeed, it would state that a transition from one edge to another happens instantaneously, no matter how large the spatial distance. It can also be readily seen from the structure of the Reeb graph corresponding to the unbounded case. Indeed, in this case the Reeb graph consists of one vertex with infinitely many incoming vertices.

2.3 Diffusion in cellular flows: unbounded case

As we have seen previously, the knowledge of the behaviour of solutions to (2) in the vicinity of the cell boundaries is of crucial importance. To describe this behaviour one has to take into account events such as a particle crossing of a separatrice and going to another cell. Qualitatively, we can discribe them as follows: We artificially separate the cells by channels (which play the role of the boundary layers along the separatrices) to take into account the transport along the boundaries. Let $\delta(\varepsilon)$ be the width of the channel. The motion of a particle consists of two types of events: (i) slow motion across streamlines inside the cells with typical time spent inside a cell $t_{\text{cell}} = O(1/\varepsilon)$ and mean square displacement $O(\varepsilon^0)$; (ii) fast transport in the channels with velocity of order $O(\varepsilon^0)$ and time spent inside the

channel $O(\delta^2/\varepsilon)$. The effective diffusion is given by

$$\kappa_{\text{eff}} = O\left(\frac{\langle X^2\rangle_{\text{channel}}}{t_{\text{cell}}}\right) = O\left(\delta^2\right) \tag{22}$$

Setting $\delta(\varepsilon) = \varepsilon^{\frac{1}{4}}$ we obtain $\kappa_{\text{eff}} = O(\sqrt{\varepsilon})$. However, the width of the channel is something that we have to insert by hand into this model. Furthermore, for solution of the cell problem the width of the boundary layer is usually assumed to be $\sqrt{\varepsilon}$. Nevertheless, this simple model is usefull because it gives an additional intuition about the nature of diffusion in the cellular flow. Indeed, numerical simulations of (2) show long flights along the cell boundaries interupted by trapping of the particle inside the cells, see Fig. 2.

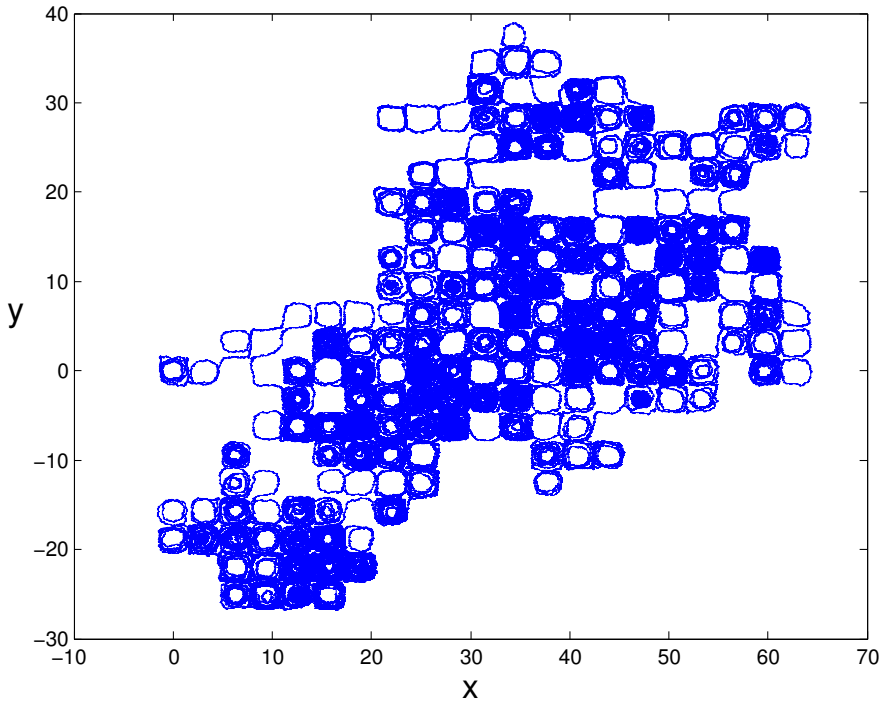

Figure 2: Random motion of a Brownian particle the cellular flow $B = 1$.

During the excursions the stochastique motion can be described by a very simple one-dimensional model

$$d\Theta_t = |\cos\Theta_t| + \sqrt{2\varepsilon}dW_t, \tag{23}$$

where $\theta \in [0, 4\pi]$. The backward Kolmogorov equation is given by

$$\partial_t p + |\cos\theta|\partial_\theta p = \varepsilon\partial_\theta^2 p. \tag{24}$$

Solutions[5] are most easily found by writing the drift $|\cos\Theta|$ as the derivative of the following continuous potential

$$V(\theta) = \begin{cases} -4k - \sin\theta & \text{for } x \in [-\frac{\pi}{2} + 2k\pi, \frac{\pi}{2} + 2k\pi]; \\ -2(2k+1) + \sin\theta & \text{for } x \in [-\frac{\pi}{2} + (2k+1)\pi, \frac{\pi}{2} + (2k+1)\pi], \end{cases} \tag{25}$$

such that $|\cos\theta| = -\partial_\theta V(\theta)$. Note that this potential contains two parts: a periodic part $V_0(\theta)$ with period π and a tilting force $F = \frac{2}{\pi}$. Obviously, the function $V_0(\theta) = V(\theta) + \theta F$ satisfies $V_0(\theta + \pi) = V_0(\theta)$. Stationary distributions are easily found which allows to determine the mean velocity and the effective diffusion

$$< v >= \lim_{t\to\infty} \frac{\mathbb{E}[\Theta_t]}{t} \qquad D = \lim_{t\to\infty} \frac{\mathbb{E}[\Theta_t^2] - (\mathbb{E}[\Theta_t])^2}{2t} \tag{26}$$

It turns out that the mean velocity does not vanish and the effective diffusion is proportional to $1/\epsilon$, see [22]. The behaviour of the diffusion process in the neighbourhood of the cell boundaries has been studied in [14] using boundary layer asymptotics. It turns out that the time a particle spends in a cell is of order $O(\varepsilon)$.

Note that events (i) and (ii) have two different time scales: (i) is on time scale $O(1/\sqrt{\varepsilon})$ while (ii) is on time scale $O(1/\varepsilon)$. A similar situation has been discussed in [18] for effective diffusion along a pipe with semiinfinite pipes branching off the main pipe. The fast motion happens inside the main pipe while trapping occurs inside the side branches.

Since the stochastic motion of a particle inside of the unbounded cellular flow is a mixture of random walk on the lattice of cells (jump process) and slow diffusion inside the cells (continuous process) we cannot expect the Wentzell–Freidlin technique to hold on unbounded domains. Indeed, as Fig. 3 shows, in numerical simulations of diffusion of passive tracer on the cellular flow (6) we find high gradients of the passive scalar accross the cell boundaries.

3 Approximating process with jumps

In this section we propose a generalization of Wentzell-Freidlin method to the case of unbounded domains. The main idea is to give up the mathematical condition of continuity of the process at the vertices of the Reeb graph which in the previous paragraph has been shown to inconsistent and allow for processes which can have jumps at vertices. The continuity condition has to be replaced by another condition which takes into account processes happening at the separatrices analyzing them more carefully than it has been done in Section 2.2.

We begin by outlining the procedure which can be used for obtaining the approximating process on the domain $\mathbb{R}^2$. We label each cell by a two-dimensional integer vector $(n_1, n_2) \in \mathbb{Z}^2$. The effective evolution equation inside each cell is given by

$$\partial_{\varepsilon t} p_{(n_1,n_2)} = \partial_h^2 \left(A(h) p_{(n_1,n_2)}\right) - \partial_h \left(B(h) p_{(n_1,n_2)}\right) \tag{27}$$

Consider now, analogously to [20] a water-pipe network $\Omega_N^\varepsilon = \{(x,y) \in \Omega : \ |H(x,y)| \leq N\sqrt{\varepsilon}\}$ around the separatrices. The corresponding water-pipe approximation is

$$\epsilon \Delta \theta_N^\varepsilon - \nabla^\perp H \cdot \nabla \theta_N^\varepsilon = 0, \qquad (x,y) \in \Omega_N^\varepsilon, \tag{28}$$

[5] Stochastic equations with periodic drift are intensively studied in [21].

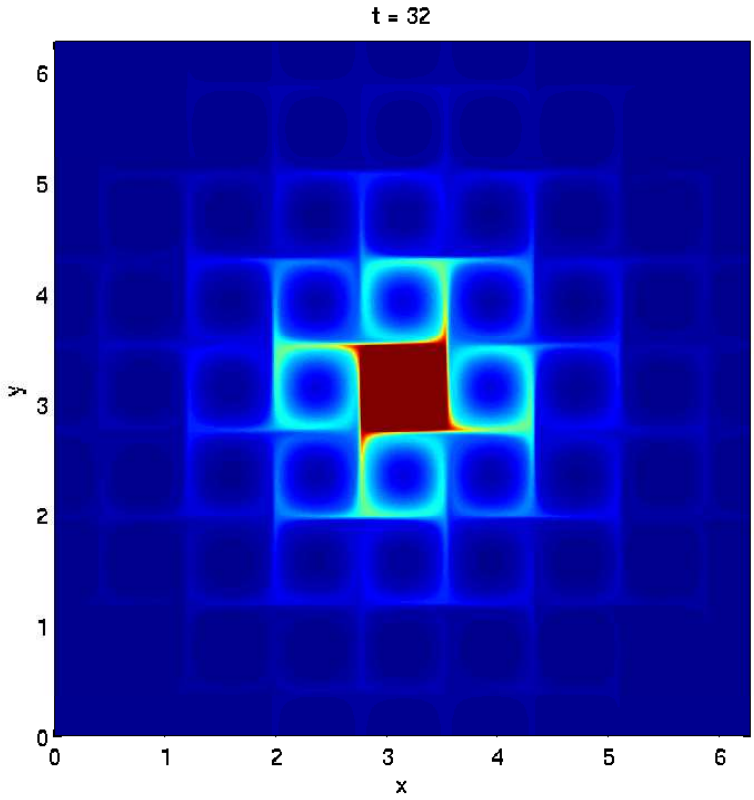

Figure 3: Diffusion in the cellular flow given by (6) with $B = 1$ for $\varepsilon = 0.0009765625$ at $t = 32$.

however, instead of zero gradient von Neumann boundary conditions at the level set

$$\mathcal{L}_{(n_1,n_2)}(N\sqrt{\varepsilon}) = \{(x,y) \in \Omega : \ |H(x,y)| = N\sqrt{\varepsilon}, \ (x,y) \text{ lies in the cell } (n_1,n_2)\} \tag{29}$$

used in [20], we introduce the following conditions

$$\frac{\partial \theta_N^\varepsilon}{\partial \mathbf{n}} = (D\theta)_{(n_1,n_2)}, \quad (x,y) \in \mathcal{L}_{(n_1,n_2)}(N\sqrt{\varepsilon}). \tag{30}$$

The two descriptions, in the interior of the cells and at the cell boundary, have to be glued together. It is here that the conservation of probability enters. We have to match probablity current leaving the edge with the probablity current entering the water-pipe network. This gives the equation

$$\oint_{\mathcal{L}_k(N\sqrt{\varepsilon})} (D\theta)_k dl = \varepsilon \left[B(h) p_{(n_1,n_2)}(h) - \partial_h \left(A(h) p_{(n_1,n_2)} \right) \right]_{h=N\sqrt{\varepsilon}}. \tag{31}$$

The expression on the right hand side is just the probability current entering the boundary of the cell.

Now we turn to description of the approximating process. First of all, in order to describe the transport from one cell to another in the asymptotics $\varepsilon \to 0$ we find it convenient to consider the network of lines connecting the neighbouring cells which is in fact a network dual to the water-pipe network. In our case of $H(x, y)$ given by (6) with $B = 1$ it is just the two-dimensional lattice $\mathbb{Z}^2$. At each vertex of this network we specify a function $f_{(n_1,n_2)}(t)$. This function serves as a boundary condition for the effective Fokker–Planck equation (27) (with the original time) in the cell (n_1, n_2). For a particle the probability of leaving this cell through the boundary adjacent to one of the neighbouring cell, e.g. the cell $(n_1, n_2 + 1)$ is proportional to $f_{(n_1,n_2+1)} - f_{(n_1,n_2)}$. Therefore the discontinuous part of the process is governed by the Laplace lattice operator on the lattice $\mathbb{Z}^2$

$$\Delta_{\mathbb{Z}^2} f_{(n_1,n_2)}(t) = f_{(n_1+1,n_2)}(t) + f_{(n_1-1,n_2)}(t) + f_{(n_1,n_2+1)}(t) + f_{(n_1,n_2-1)}(t) - 4f_{(n_1,n_2)}(t) \quad (32)$$

The evolution equation for $f_{(n_1,n_2)}(t)$ is then given by

$$\frac{d}{dt} f_{(n_1,n_2)} + \frac{d}{dt} \int p_{(n_1,n_2)}(h)dh = \Delta_{\mathbb{Z}^2} f_{(n_1,n_2)} \quad (33)$$

In this way we obtain a coupled system of equations which yield the complete description of the approximating process.[6]

4 Discusion

The generalization of the Wentzell–Freidlin technique proposed in the previous paragraph is easily generalized to the cases of nonperiodic cellular flows. In fact, it suffices to replace the Laplace operator on $\mathbb{Z}^2$ by the Laplace operator on the network (graph) dual to the network of separatrices of the original flow. Of course, the spectral properties of the graph Laplacian then depend strongly on the topological structure of the dual network. Therefore the cellular structure of the flow can nontrivially influence the solutions of (33).

One application of the Wentzell–Freidlin technique is connected to the study of reaction-diffusion equations. However, as has been stated in [10], in its usual formulation it is not applicable without any restrictions. The generalized form of this technique proposed in the report seems to be suitable to a wider range of applications, including nonperiodic cellular flows.

5 Acknowledgements

I would like to thank E. Vanden Eijnden, G. Papanicolaou, W. Young and J.-L. Thiffeault for helping me in my work on this project. Many thanks to G. Veronis and C. Doering for softball coaching. And of course, I would like to thank all fellows for the wonderful summer we spent together.

[6] In fact, analogous constructions were discussed in [19, 18].

References

[1] G. Papanicolaou, GFD lecture series, 2005.

[2] S. Childress, Alpha-effect in flux ropes and sheets, *Physics of the Earth and Planetary Interior* **20**, pp. 172–180, 1979.

[3] A. Soward, Fast dynamo action in a steady flow, *Journal of Fluid Mechanics* **180**, pp. 267–295, 1987.

[4] S. Childress and A. Soward, *Journal of Fluid Mechanics* **180**, pp. 267–295, 1987.

[5] V. I. Arnold, *Geometric Methods in the Theory of Ordinary Differential Equations*, Springer-Verlag, 1983.

[6] T. Dombre, U. Frisch, J. Green, M. Hénon, A. Mehr and A. Soward, Chaotic streamlines in the ABC flows, *Journal of Fluid Mechanics* **167**, pp. 353–391, 1986.

[7] M. Abramowitz and I.Stegun, Handbook of Mathematical Functions, Dover Publications, 1965.

[8] V. I. Arnold, *Mathematical Methods of Classical Mechanics*, Springer-Verlag, 1997.

[9] G. Reeb, Sur les points singuliers d'une forme de Pfaff completement integrable ou d'une fonction numérique, *Compte Rendus de l'Académie des Sciences* **222**, pp. 847–849, 1946.

[10] A. Fannjiang, A. Kiselev and L. Ryzhik, Quenching of reaction by cellular flows, Arxiv preprint math.AP/0505654, 2005.

[11] C. W. Gardiner, *Handbook of Stochastic Methods*, Springer-Verlag, 1983.

[12] M. I. Freidlin and A. D. Wentzell, *Random perturbations of dynamical systems*, second edition, Springer-Verlag, 1998.

[13] M. I. Freidlin and A. D. Wentzell, Diffusion process on graphs and the averaging principle, *Annals of Probability* **21**, pp. 2215–2245, 1993.

[14] L. Koralov, Random perturbations of 2-dimensional Hamiltonian flows, *Probability Theory and Related Fields* **129**, pp. 37-62, 2004.

[15] I. S. Gradstein and I. M. Ryzhik, *Tables of Integrals, Series and Products*, Academic, New York, 1980.

[16] A. Fannjiang and G. Papanicolaou, Convection enhanced diffusion for periodic flows, *SIAM Journal on Applied Mathematics* **54**, pp. 333–408, 1994.

[17] P. B. Rhines and W. R. Young, How rapidly is a passive scalar mixed within closed streamlines, *Journal of Fluid Mechanics* **133**, pp. 133–145, 1983.

[18] W. R. Young, Arrested shear dispersion and other models of anomalous diffusion, *Journal of Fluid Mechanics* **193**, pp. 129–149, 1988.

[19] W. Young, A. Pumir and Y. Pomeau, Anomalous diffusion of tracer in convection rolls, *Physics of Fluids* **1**, pp. 462–469, 1989.

[20] A. Novikov, G. Papanicolaou and L. Ryzhik, Boundary layers for cellular flows at high Péclet numbers,

[21] H. Risken, *The Fokker-Planck Equation*, Springer-Verlag, 1989.

[22] P. Reimann, C. Van den Broeck, H. Linke, P. Hänggi, J. M. Rubi, and A. Pérez-Madrid, Diffusion in tilted periodic potentials: enhancement, universality, and scaling, *Phys. Rev. E* **65**, 031104, 2002.

draft

Probabilistic analysis of the boundary layer diffusion in cellular flows at high Péclet number

G. Papanicolaou[1] and W. Pauls[2,3]

[1]*Department of Mathematics, Stanford University, Stanford, CA 94305, USA*
[2]*Labor. Cassiopée, UNSA, CNRS, OCA, BP 4229, 06304 Nice Cedex 4, France*
[3]*Fakultät für Physik, Universität Bielefeld, Universitätsstraße 25, 33615 Bielefeld, Germany*

(Dated: September 3, 2007)

We consider diffusion in a cellular (not necessarily periodic) flow in the high Péclet number limit. The limiting process is a continuous time Markov process with jumps on a state space constructed on the graph connnecting the separatrices of the flow.

I. INTRODUCTION

A standard way of studying the advection of a passive scalar field in a fluid is to use the passive scalar equation

$$\partial_t\theta + \nabla^\perp H\cdot\nabla\theta = \varepsilon\Delta\theta. \tag{1}$$

A more detailed picture which allows us to follow the trajectories of particles is given by the probabilistic description in terms of ordinary stochastic differential equations

$$dX_1^\varepsilon(t) = -\partial_2 H(X_1^\varepsilon(t), X_2^\varepsilon(t)) + \sqrt{2\varepsilon}\, dW_1(t), \tag{2a}$$
$$dX_2^\varepsilon(t) = \partial_1 H(X_1^\varepsilon(t), X_2^\varepsilon(t)) + \sqrt{2\varepsilon}\, dW_2(t). \tag{2b}$$

First we consider the case in which the velocity field is determined by a simple periodic stream function

$$H(x_1,x_2) = \sin x_1 \sin x_2. \tag{3}$$

In the PDE setting (1) the standard way to treat the large scale and long time behavior of θ is the homogenization approach [1], which is performed by separating fast and slow variables: $t\to t/\delta^2$, $(x_1,x_2)\to(x_1/\delta, x_2/\delta)$.

Here we just briefly recapitulate the essential points of the homogenization approach to Equation (1) for the velocity fields such as the one given by (3) (for more details see [2]). For initial conditions $\theta_0(x_1,x_2)$, which do not depend on fast variables, solutions of (1) converge to solutions of

$$\frac{\partial\bar\theta}{\partial t} = \sum_{i=1}^d\sum_{j=1}^d \sigma_{ij}\frac{\partial^2\bar\theta}{\partial x_i\partial x_j}, \tag{4}$$

with the same initial condition θ_0. The diffusion matrix σ (for convenience we apply it to a unit vector $\boldsymbol{e}$) is found by solving the stationary cell problem

$$\nabla\cdot\Big[(\varepsilon\boldsymbol{I}+\boldsymbol{H})(\nabla\chi_{\boldsymbol{e}}+\boldsymbol{e})\Big] = 0 \tag{5}$$

in the periodicity domain and calculating the quantity

$$\sigma(\varepsilon)\,\boldsymbol{e} = \langle(\nabla\chi_{\boldsymbol{e}}+\boldsymbol{e})\cdot(\nabla\chi_{\boldsymbol{e}}+\boldsymbol{e})\rangle, \tag{6}$$

where $\boldsymbol{I}$ is the unity matrix and $\boldsymbol{H}$ is the antisymmetric matrix given componentwise as $\epsilon_{ij}\,H(x_1,x_2)$ (ϵ_{ij} is antisymmetric and such that $\epsilon_{12}=1$, $\epsilon_{21}=-1$).

In probabilistic terms (4) means that for a fixed ε and for $t\to+\infty$ the process $(X_1^\varepsilon(t), X_2^\varepsilon(t))$ behaves like a Brownian motion with effective diffusivity

$$\sigma_{ij}(\varepsilon) = \lim_{t\to+\infty}\mathbb{E}_{T_0}\frac{X_i^\varepsilon(t)X_j^\varepsilon(t)}{t}, \tag{7}$$

where T_0 is the initial distribution of the process [3].

It was proven in [2] by variational methods that for $\varepsilon\to 0$ the effective diffusivity of the flow given by (3) scales like

$$\sigma_{ij}(\varepsilon) = \sqrt{\varepsilon}\,(\delta_{ij}c^* + o(1)). \tag{8}$$

Actually, this relation has been established by Childress in [4] by using boundary layer analysis. The constant c^* is determined by the solution of a suitable boundary problem and has been calculated analytically by Soward in [5].

Recently, relation (8) has been extended by Koralov in [6] who has shown that the $\sqrt{\varepsilon}$-scaling holds for general periodic cellular flows. Intuitively, this result can be explained as follows: a particle is being efficiently transported by the flow as long as it stays sufficiently close to the unbounded network of separatrices $\mathcal{L} := \{x\in\mathbb{R}^2 : H(x)=0\}$, $(x=(x_1,x_2))$ in a channel $V^\varepsilon := \{x : |H(x)|<\varepsilon^\alpha\}$ of width ε^α (note that this width is muich larger than the mean fluctuation of $X^\varepsilon(t)$). The mean square displacement is of order $\varepsilon^{\alpha-1/2}$. The transport is randomly interrupted when the particle is caught inside a cell, with an average trapping time of order $\varepsilon^{\alpha-1}$. Therefore, the effective diffusivity given by the ratio of these two quantities scales as square root of ε.

Here we recall in short the main steps by which (8) has been obtained in Ref. [6]. First, a discrete Markov chain $\tilde X^\varepsilon(\tau_n^\varepsilon)$ associated with $X^\varepsilon(t)$ on the restriction $\tilde{\mathcal{L}}$ of $\mathcal{L}$ to the torus $\mathbb{R}^2/2\pi\mathbb{Z}^2$ is constructed by stopping the process $X^\varepsilon(t)$ each time when it hits a separatrix after (i) exiting the boundary channel V^ε or (ii) going past a stagnation point. Next, the problem equivalent

to the study of the time-independent cell problem (5) is to consider the invariant distribution of $\tilde{X}^\varepsilon(\tau_n^\varepsilon)$ on $\tilde{\mathcal{L}}_0 = \tilde{\mathcal{L}} \setminus \cup\, x_{\rm st}^i$ ($x_{\rm st}^i$ are the stagnation points of the flow) and the invariant distribution of $\tau_n^\varepsilon - \tau_{n-1}^\varepsilon$ on $\mathbb{R}_{\geq 0}$.

The process $X^\varepsilon(\tau_n^\varepsilon)$ behaves like a random walk on the unbounded set $\mathcal{L}$ with variance d^ε. Thus, its mean square displacement is given by

$$\sigma(\varepsilon) = d^\varepsilon / \int_{\tilde{\mathcal{L}}_0} \mathbb{E}_x \tau_1^\varepsilon \, d\mu^\varepsilon(x). \tag{9}$$

Then is is shown that the asymptotics of d^ε are ε-independent, whereas for $\varepsilon \to 0$

$$\int_{\tilde{\mathcal{L}}_0} \mathbb{E}_x \tau_1^\varepsilon \, d\mu^\varepsilon = \frac{1}{\sqrt{\varepsilon}} \Big(\int_{\tilde{\mathcal{L}}_0} f^0(x)\, \mu^0(x) + o(1) \Big). \tag{10}$$

In the next section we are going to describe the asymptotics of $(X^\varepsilon(\tau_n^\varepsilon), \tau_n^\varepsilon - \tau_n^\varepsilon)$ in somewhat more details.

II. SCALING LIMIT AS A CONTINUOUS TIME MARKOV PROCESS

In this section we study for simplicity the case in which $H(x)$ is given by (3), see Fig. 1. To reveal the essential features of the small ε asympotitcs of $X^\varepsilon(t)$ it is appropriate to consider the scaling limit

$$(X_n^0, \tau_n^0) := \lim_{\varepsilon \to 0} (X^\varepsilon(\tau_n^\varepsilon), \sqrt{\varepsilon}(\tau_n^\varepsilon - \tau_{n-1}^\varepsilon)). \tag{11}$$

The state space of the Markov chain X_n^0 are the separatrices of the flow given by $H(x)$ (without the stagnation points $x_{\rm st}^i$). We now give an alternative discription of this state space: First, we construct a graph $G(V_H, E_H)$ associated with the set of separatrices of the flow given by $H(x)$. This graph is obtained by reducing each separatrix to a vertex and connecting by edges the separatrices which constitute the boundary of the same cell. For example, the separatrix $\gamma(1,2)$ in Fig. 1 is associated to the vertex $v(1,2)$ of the graph represented in Fig. 2. Furthermore, starting from the separatrix $\gamma(1,2)$ in Fig. 1 a particle can go to the cells e, f, g through the separatrices $v(2,3)$, $v(3,4)$, $v(4,1)$ by going into the interior of the cell a, and to the cells d, c, h through $v(2,5)$, $v(5,6)$, $v(6,1)$ by passing the cell b. Thus, $v(1,2)$ is connected by edges to six other vertices, $v(2,3)$, $v(3,4)$, $v(4,1)$ on the right and $v(2,5)$, $v(5,6)$, $v(6,1)$ on the left. For convenience, the set of vertices V_H is associated with the set $\mathbb{Z}^2$. Note that the graph $G(V_H, E_H)$ has a constant connectivity equal to six.

To complete the construction of the state space we assign to each vertex $v(i,j)$ an additional degree of freedom: the spin-space is the separatrix $\gamma(i,j)$ and the spin variable $\theta_{v(i,j)} \in \gamma(i,j)$ is determined using a suitable parametrization of $\gamma(i,j)$.

The process X_n^0 is specified by giving the transition probabilities $p(\theta_{v(i,j)}, \theta'_{v'(i',j')})$, where $v(i,j)$ and $v'(i',j')$ are two adjacent vertices of the graph $G(V_H, E_H)$ and

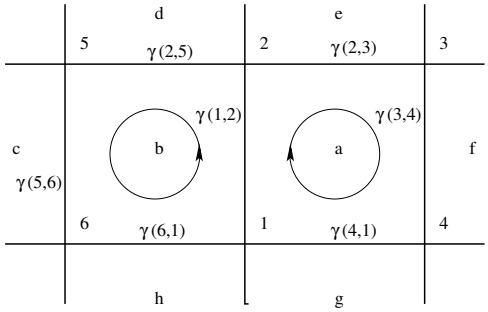

FIG. 1: Cells of the periodic flow $H(x_1, x_2) = \sin x_1 \sin x_2$. Stagnation point at $(0,0)$ is label by 1, the one at $(0,\pi)$ by 2, the one at (π,π) by 3 and so on. Starting at the separatrix $\gamma(1,2)$ a particle can excape to one of the six cells c, d, e, f, g or h.

$\theta_{v(i,j)} \in \gamma(i,j)$, $\theta'_{v'(i',j')} \in \gamma(i',j')$ are the corresponding points on the separatrices. According to the results in

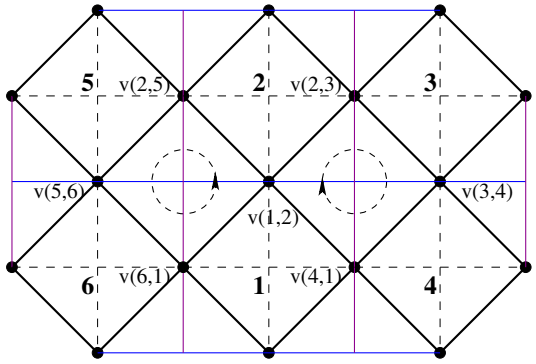

FIG. 2: Graph of for the random walk on separatrices. Vertices are denoted as $v(\cdot,\cdot)$, the separatrices themselves (which are also the boundaries of the flow cells) are indicated by dashed lines. The stagnation points are numbered from 1 to 6.

[6] these transition probabilities can be calculated from the kernel of a certain process which we now are going to consider in more detail.

A. Calculation of the transition probabilities

While the state space of the Markov chain X_n^0 is basically given by the set of the separatrices of the flow, it is the behavior of the process $\boldsymbol{X}^\varepsilon(t)$, $\varepsilon \to 0$ in the interior of the cells which determines the transition probabilities $p(\theta_{v(i,j)}, \theta'_{v'(i',j')})$. It turns out [6] that these probabilities can be calculated by using an auxiliary process which is an asymptotic representation of the process $X^\varepsilon(t)$ in the boundary layer at the separatrices.

Let us first make some technical remarks. Due to the symmetries of the flow (3) we can assume without any

restriction that we start at the vertex $v(1,2)$ which corresponds to the separatrix $\gamma(1,2)$. Thus, we parametrize the separatrices in cell a by the variable $\theta_a \in [0,8]$ in such a way that the separatrix $\gamma(1,2)$ corresponds to $\theta_a \in (0,2)$, separatrix $\gamma(2,3)$ to $\theta_a \in (2,4)$ etc. In the cell b the separatrices are parametrized as follows: $\gamma(1,2)$ corresponds to $\theta_b \in (0,2)$, $\gamma(1,6)$ to $\theta_b \in (2,4)$ and so on. Since the cells a and b have the separatrix $\gamma(1,2)$ in common, we identify $\theta_a = \theta_b$ for $\theta_a, \theta_b \in [0,2]$.

Now we specify the boundary layer process used for calculating the transition probabilities. The state space, represented on Fig. 3, is constructed by taking the two cells a and b, connected by the separatrix $\gamma(1,2)$ (see Fig. 1) and chosing a suitable parametrization h for the boundary layers of the corresponding cells. Note that while using the boundary layer coordinates the actual cell interior is mapped to infinity $h = \pm\infty$.

More precisely, the coordinates are defined as follows: (i) in the cell a we define the state space as (h, θ_a) where $h \geq 0$, $\theta_a \in [0,8]$. The domain (h, θ_a), $h > 0$ corresponds to the boundary layer in the cell a. (ii) The boundary layer of the cell b is given by (h, θ_b) where $h \leq 0$, $\theta_b \in [0,8]$. Since the both boundary layers are connected across the separatrix $\gamma(1,2)$, we identify $(0, \theta_a) = (0, \theta_b)$ for $\theta_a, \theta_b \in [0,2]$, see Fig. 3.

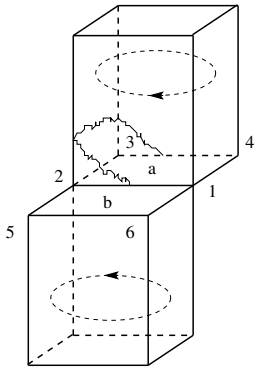

FIG. 3: Boundary layer of the cells a and b.

The auxiliary boundary layer process has the generator $\partial_\theta + \partial_h^2$ where θ actually plays the role of a time variable which is running backward. Furthermore we introduce absorbing boundary conditions at $h = 0$ for $\theta > 2$. These boundary conditions correspond to the condition that the partcile has to go past a stagnation point before it it hits one of the separatrices (which is condition (ii) in the definition of the Markov chain $\tilde{X}^\varepsilon(\tau_n^\varepsilon)$ quoted from [6] in Section I). Note that it is also possible for the particle to be absorbed at the separatrix $\gamma(1,2)$ after going one or several times around the cell a or b.

Because of the symmetry it is sufficient to determine the transition probabilities $p(\theta, \theta'_a)$ corresponding to the event that the particle starts at the separatrix $\gamma(1,2)$, that is $\theta \in (0,2)$ and hits one of the separatrices constituting the boundary of the cell a after passing the stagnation point 2, see Fig. 3. Since the particle hits the separatrix while coming from the boundary layer of the cell a, $h > 0$ for $\theta'' \in (2, \theta'_a)$.

Let us denote for simplicity $\theta' = \theta'_a$. Using the transition probability kernel $p((h,\theta),(h',\theta'))$ of the auxiliary process the transition probability $p(\theta, \theta')$ is given by

$$p(\theta, \theta') = p((0,\theta),(0,\theta')). \tag{12}$$

Now we proceed to determine the transition probabilities $p((0,\theta),(0,\theta'))$. We use the following notation:

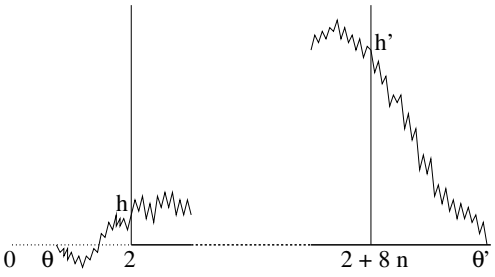

FIG. 4: Transition from θ to θ' after going n-times around the periodicity domain.

the probability kernels for the standard Brownian motion and the probability kernel for Brownian motion with absorbing boundary condition at $h = 0$ are

$$G_{\tilde{\theta}}(h,h') = \frac{1}{\sqrt{4\pi\tilde{\theta}}} \exp\left[-\frac{(h-h')^2}{4\theta}\right], \tag{13}$$

$$G^{\rm abs}_{\tilde{\theta}}(h,h') = \tag{14}$$
$$\frac{1}{\sqrt{4\pi\theta}}\left\{\exp\left[-\frac{(h-h')^2}{4\tilde{\theta}}\right] - \exp\left[-\frac{(h+h')^2}{4\tilde{\theta}}\right]\right\}.$$

The event that the particle starts at $(0,\theta)$, $\theta \in (0,2)$ and is absorbed at $(0,\theta')$ is composed of three events (see also Fig. 4): (i) the particle starting at $(0,\theta)$ goes past the stagnation point 2 into the boundary layer of the cell a and is stopped at $(2,h)$, $h > 0$. Since between θ and 2 the particle is allowed to cross the separatrix, the corresponding transition probability is given by (13) with $\tilde{\theta} = 2-\theta$. (ii) Starting at $(2,h)$ the particle goes a number of times around the periodicity domain and is stopped again at $(2,h')$, $h' > 0$ over the stagnation point 2. (iii) Starting at $(2,h')$ the particle is absorbed at $(0,\theta')$. The probability density $f_{\theta'-2}(h')$ of the event that starting at $(2,h')$ a Brownian particle will be absordeb at $(0,\theta')$ is given by

$$f_{\theta'-2}(h) = \frac{h}{\sqrt{4\pi(\theta'-2)^3}} e^{-\frac{h^2}{4(\theta'-2)}}. \tag{15}$$

Thus, using the Markov property the transition probability is determined as follows

$$p((0,\theta),(0,\theta')) = \int_0^\infty dh \int_0^\infty dh'\, G_{2-\theta}(0,h)\, K(h,h')\, f_{\theta'-2}(h'). \tag{16}$$

Here $K(h,h')$ is the probability density for the particle starting at $(h,2)$ to get to $(h',2)$ after going several times (or maybe not at all) around the periodicity domain without being absorbed. Actually, in order to evaluate the double integral in (16) we do not need to determine the kernel $K(h,h')$ directly. For this purpose it is suffucient to calculate the integral

$$g_{\theta'}(h) = \int_0^\infty dh'\, K(h,h')\, f_{\theta'-2}(h'). \tag{17}$$

As we shall see now, the evaluation of this integral can be reduced to solving an integral equation.

To study the event that a particle starting at $(h,2)$ is stopped at $(2,h')$ after making some numbers rounds of the periodic domain we introduce the integral operator T on $C([0,\infty))$ defined by

$$(Tf) = \int_0^\infty dh'\, G_8^{\rm abs}(h,h') f(h'). \tag{18}$$

Obviously, this operator T describes the particle going once around the periodicity domain without being absorbed.

Since the particle can be absorbed after making an arbitrary number of turns, we are led to consider the operator given by the absolutely convergent geoemtric series $\sum_{n=0}^\infty T^n$. Then the kernel $K(h,h')$ is defined by the relation

$$\int_0^\infty K(h,h')\, f(h')\, dh' = \Big((\sum_{n=0}^\infty T^n) f \Big)(h). \tag{19}$$

It follows immediately that $K(h,h')$ is the kernel of the operator $(1-T)^{-1}$ and

$$g_{\theta'}(h) = \big((1-T)^{-1} f_{\theta'-2} \big)(h). \tag{20}$$

In other words, function $g_{\theta'}(h)$ on the right-hand side of (20) is obtained by solving the integral equation

$$g_{\theta'}(h) - \int_0^\infty dh' G_8^{\rm abs}(h,h') g_{\theta'}(h') = f_{\theta'-2}(h). \tag{21}$$

We first note that $g_{\theta'}(h)$ is defined only for positive values of h. However, since $f_{\theta'-2}(-h) = -f_{\theta'-2}(h)$ and $G_8^{\rm abs}(h,h')$ is an odd function of h' we can define $g_{\theta'}(h)$ for arbitrary values of h by $g_{\theta'}(-h) = -g_{\theta'}(h)$.

Now, rewriting Equation (20) as

$$\begin{aligned} &g_{\theta'}(h) - \frac{1}{4}\frac{1}{\sqrt{2\pi}} \int_0^{+\infty} dh'\, e^{-(h-h')^2/32} g_{\theta'}(h') + \\ &\frac{1}{4}\frac{1}{\sqrt{2\pi}} \int_{-\infty}^0 dh'\, e^{-(h-h')^2/32} g_{\theta'}(-h') = f_{\theta'-2}(h) \end{aligned} \tag{22}$$

and using the above defined extension of $g_\theta(h)$ to negative values we obtain the equation

$$g_{\theta'}(h) - \frac{1}{4}\frac{1}{\sqrt{2\pi}} \int_{-\infty}^{+\infty} dh'\, e^{-(h-h')^2/32} g_{\theta'}(h') = f_{\theta'-2}(h), \tag{23}$$

which is solved using the Fourier transform

$$g_{\theta'}(h) = \frac{1}{\pi} \int_{-\infty}^{+\infty} dk\, e^{-ikh}\, \frac{ike^{-k^2(\theta'-2)}}{1 - \frac{1}{\sqrt{2\pi}} e^{-8k^2}} \tag{24}$$

By means of (16) the transition probability $p(\theta,\theta')$ can be expressed as

$$\begin{aligned} &p(\theta,\theta') = \\ &\frac{1}{\pi} \int_0^{+\infty} dh \int_{-\infty}^{+\infty} dk\, e^{-ikh}\, G_{2-\theta}(0,h)\, \frac{ike^{-k^2(\theta'-2)}}{1 - \frac{1}{\sqrt{2\pi}} e^{-8k^2}}. \end{aligned} \tag{25}$$

Both integrals being absolutely convergent we can interchange the order of integration and perform the integration with respect to h. This gives the following expression for the transtition probability density

$$p(\theta,\theta') = \frac{1}{2\pi} \int_{-\infty}^{+\infty} dk\, \frac{ike^{-k^2(\theta'-\theta)}}{1 - \frac{1}{\sqrt{2\pi}} e^{-8k^2}} \Big[1 - \mathrm{erf}(ik\sqrt{2-\theta}) \Big] \tag{26}$$

B. Transition times τ_n^0

The next step in specifying the process (X_n^0, τ_n^0) consists in determining the transition times τ_n^0. Here we can use directly the results of [6] for the probability $P_\theta^{\rm esc}$ of escape into the cell interior

$$P_\theta^{\rm esc} = \int_0^8 \int_0^\infty hp((0,\theta),(h,\theta'))\, dh d\theta' \tag{27}$$

The transition times τ_n^0 are directly related to $P_\theta^{\rm esc}$, whereas the sojourn times in the interior of the cell are asymptotically determined by the Wentzell–Freidlin type of analysis.

C. Childress cell problem

Actually, the process (X_n^0, τ_n^0) represents an asymptotique boundary layer approximation of the process $X^\varepsilon(t)$. It is well known that when we use the homogenization methods, the cell problem (5) for the flow (3) can be reduced to the so-called Childress cell problem:

$$\frac{\partial^2 \rho}{\partial h^2} + \frac{\partial \rho}{\partial \theta} = 0, \tag{28}$$

with boundary conditions

$$\begin{aligned} &\rho(0,\theta) = 0, \quad 0 < \theta < 2, \qquad \frac{\partial \rho}{\partial h}(0,\theta) = 0, \quad 2 < \theta < 4, \\ &\rho(0,\theta) = \pi, \quad 4 < \theta < 6, \qquad \frac{\partial \rho}{\partial h}(0,\theta) = 0, \quad 6 < \theta < 8. \end{aligned} \tag{29}$$

The constant c^* in (8) is then given by

$$c^* = \frac{1}{\pi^2}\int_0^\infty \int_0^8 \left(\frac{\partial \rho}{\partial h}\right)^2 dhd\theta, \tag{30}$$

and his been determined explicitly in [5] by solving an integral equation similar to (26).

III. DIFFUSION IN STEADY CELLULAR FLOWS

If the periodic cellular flow is replaced by a nonperiodic one the scaling of the diffusion coefficient changes. For example, for random flows considered in [8], the scaling law is ε^α where α depends on the geometry of the random flow.

However, the methods from the previous section can be applied to the case of diffusion in bounded cellular flows. Here, it is convenient to consider the following Dirichlet problem (see [7])

$$\varepsilon\Delta\phi^\varepsilon - \nabla^\perp \cdot \nabla\phi^\varepsilon = 0, \tag{31}$$

on Ω with Dirichlet boundary condition $\phi^\varepsilon(x) = T_0(x)$ for $x \in \partial\Omega$. We suppose that

$$\partial\Omega \subset \mathcal{L} = \{(x_1, x_2) \,:\, H(x_1, x_2) = 0\}, \tag{32}$$

where $\mathcal{L}$ is also the a set of separatrices containing a finite number of singular points of H.

Consider the process given by the solution of

$$dX_t^\varepsilon = \nabla^\perp H(X_t^\varepsilon)dt + \sqrt{2\varepsilon}dW_t, \tag{33}$$

with absorbing boundary conditions at $\partial\Omega$. Then the solutions of the Dirichlet problem is given by

$$\phi^\varepsilon(x) = \mathbb{E}_x\left[T_0(X^\varepsilon_{\tau^\varepsilon_\Omega})\right]. \tag{34}$$

Note that in order to exit through the boundary $\partial\Omega$ a particle has to arrive there through the system of boundary layers. Thus we first suppose that we have a process starting a some $x \in \mathcal{L}$, and $x \in \gamma(i,j)$ for some stagnation points i and j. Given $y \in \partial\Omega$ we have to calculate the transition probability kernel $p_{\text{exit}}(x,y)$ that the process starting at x will exit Ω at y.

If x and y lie on the connected edges (as in Fig. 5) then we can calculate $p_{\text{exit}}(x,y)$ just by considering a one cell problem, similar to the one-cell Childress problem. However, in general x and y will not lie on connected edges.

We introduce an auxiliary Markov chain as follows. First we will construct the state space. Consider the graph $G(V,E)$ whose vertices are identified with the separatrices $\gamma(i,j) \subset \mathcal{L}$ connecting the stagnation points (i,j). Two vertices $\gamma(i',j')$ and $\gamma(i'',j'')$ are connected iff starting from $\gamma(i',j')$ we can reach $\gamma(i'',j'')$ without crossing any separatrix, see Fig 5. The vertices which

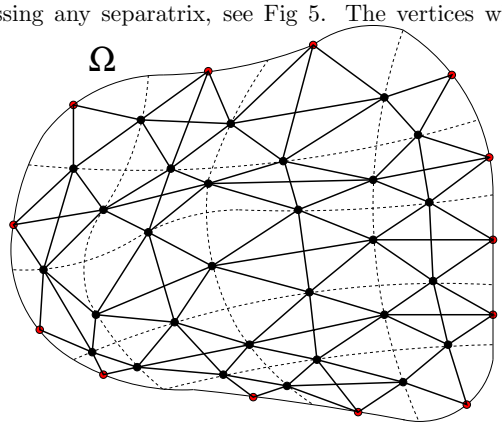

FIG. 5: Graph $G(V,E)$ of the state space Σ_H for a domain Ω and stream function $H(x_1,x_2)$.

correspond to the separatrices on the boundary $\partial\Omega$ will be called exterior vertices.

To each vertex of the graph we attach a spin space, an interval $I_{\gamma(i,j)} = [0, \Theta_{\gamma(i,j)}]$. Actually, $I_{\gamma(i,j)}$ is nothing else than the separatrix connecting the stagnation points i and j. The state space will be denoted Σ with elements $(\gamma(i,j),\theta)$

Given $x \in I_{\gamma(i,j)}$ and $x' \in I_{\gamma(i',j')}$ such that $\gamma(i,j) \sim \gamma(i',j')$ the transition probability $p_{\gamma(i,j)\gamma(i'j')}\left((\gamma(i,j),\theta_{\gamma(i,j)}),(\gamma(i',j'),\theta'_{\gamma(i',j')})\right)$ can be calculated using the two cell problem as on Fig **??**.

Now consider a path $\{\gamma(i_1,j_1),...,\gamma(i_n,j_n)\}$ on the graph $G(V,E)$. The transition probability from $(\gamma(i_1,j_1),\theta_1)$ to $\gamma(i_n,j_n)$ is calculated by the convolution of the kernels $p_{\gamma(i_1,j_1)\gamma(i_3,j_3)}\left((\gamma(i_1,j_1),\theta_1),(\gamma(i_2,j_2),\theta_2)\right)$,..., $p_{\gamma(i_{n-1},j_{n-1})\gamma(i_n,j_n)}\left((\gamma(i_{n-1},j_{n-1}),\theta_{n-1}),(\gamma(i_n,j_n),\theta_n)\right)$

$$p_{\gamma(i_1,j_1)\gamma(i_n,j_n)}\left((\gamma(i_1,j_1),\theta_1),(\gamma(i_n,j_n),\theta_n)\right) = \int_{I_{\gamma(i_2,j_2)}} ... \int_{I_{\gamma(i_{n-1},j_{n-1})}} p_{\gamma(i_1,j_1)\gamma(i_2,j_2)}\left((\gamma(i_1,j_1),\theta_1),(\gamma(i_2,j_2),\theta_2)\right)...$$
$$p_{\gamma(i_{n-1},j_{n-1})\gamma(i_n,j_n)}\left((\gamma(i_{n-1},j_{n-1}),\theta_{n-1}),(\gamma(i_n,j_n),\theta_n)\right)\, d\theta_2...\, d\theta_{n-1}. \tag{35}$$

Observe that the one step probability kernels can be calculated by solving a number of separated two-cells problems.

Using the process constructed above we can calculate the probability density $p_{\rm exit}(x,y)$ for the event that starting at $x \in I_{\gamma(i,j)}$ we will exit at point $y \in I_{\gamma(k,l)} \subset \partial\Omega$. Namely, we have to take the sum over all paths $\{\gamma(i,j),...,\gamma(k,l)\}$ on the graph $G(V,E)$ starting at the vertex $\gamma(i,j)$ and ending at $\gamma(k,l)$ such that $\gamma(k,l)$ is the only exterior vertex in the path. This means that the exterior vertices are absorbing. Thus

$$p_{\rm exit}(x,y) = \sum_{\{\gamma(i,j),...,\gamma(k,l)\}} p_{\gamma(i,j)\gamma(k,l)}\left((\gamma(i,j),x),(\gamma(k,l),y)\right) \quad (36)$$

IV. CONCLUSIONS

In this paper we have given a description of the process governing the behavior of solutions X^ε of the stochastic differential equations (2) in the limit of vanishing molecular viscosity $\varepsilon \to 0$. The limiting process is a continuous time Markov process with jumps on a graph corresponding to the flow given by the stream function $H(x_1,x_2)$. In between the jumps, the particles are trapped in a cell during the transition time τ_n^0. It is interesting to note that this process resembles the one considered in the so called trap model [9].

In the situation which we have considered the stream function is such that there exists a single unbounded level line, or, in the case of bounded flows, the level line connecting different cells coincides with the boundary of the flow. For flows with a different topology, for example such as the ones considered in [2, 8, 10] the limiting process may not even exist.

For flows with a topology such that every level line of the stream function is bounded (for example quasi-regular flows in [11]) the limiting process can be described by a process on the Reeb graph of the stream function [12]. The construction is similar to the limiting processes considered in [13, 14].

We finally note that recently dispersion of inertial particles in cellular flows of the type (3) has been studied by homogenization techniques [15]. It would be interesting to consider this problem from the probabilistic point of view.

Acknowledgments

Part of this work was done when the authors participated in the GFD summer school "Fast times and fine scales" at Woods Hole Oceanographic Institution and during a stay of one of the authors at Stanford University.

[1] A. Bensoussan, J. L. Lions and G. Papanicolaou, Asymptotic Analysis for Periodic Structures, Elsevier North-Holland (1978).

[2] A. Fannjiang and G. Papanicolaou, Convection enhanced diffusion for periodic flows, SIAM J. Appl. Math. 54 (1994) 333-408.

[3] M. I. Freidlin, Dirichlet's problem for an equation with periodic coefficients depending on a small parameter, Theory Prob. Appl. 9 (1964) 121–125.

[4] S. Childress, Alpha-effect in flux ropes and sheets, Phys. Earth Planet Inter. 20 (1979) 172–180.

[5] A. Soward, Fast dynamo action in fluid flow, J. Fluid Mech. 180 (1987) 267–295.

[6] L. Koralov, Random perturbations of 2-dimensional hamiltotnian flows, Probab. Theory Relat. Fields 129 (2004) 37–62.

[7] A. Novikov, G. Papanicolaou and L. Ryzhik, Boundary layers for cellular flows at high Péclet numbers, Commun. pure appl. math. 58 (2005) 867–922.

[8] A. Fannjiang and G. Papanicolaou, Convection enhanced diffusion for random flows, J. Stat. Phys. 88 (1997) 1033–1076.

[9] G. Ben Arous and J. Černý, Dynamics of trap models, Lecture Notes for Les Houches Summer School "Mathematical Statistical Physics" (2006).

[10] S. Childress and A. Soward, Scalar transport and alpha-effect for a family of cat's-eye flows, J. Fluid Mech. 250 (1989) 99–133.

[11] G. M. Zaslavskiĭ, R. .Z. Sagdeev and A. A. Chernikov, Stochastic nature of streamlines in steady-state flows, Zh. Eksp. Teor. Fiz. 94 (1988) 102–115.

[12] E. Vanden-Eijnden, Private communication.

[13] M. I. Freidlin and A. D. Wentzell, Diffusion processes on graphs and the averaging principle, Annals of Probability 21 (1993) 2215–2245.

[14] M. I. Freidlin and A. D. Wentzell, Random Perturbations of Dynamical Systems, Springer-Verlag (1998).

[15] G. A. Pavliotis and A. M. Stuart, Periodic homogenization for inertial particles, Physica D 204 (2005) 161–187.

Appendix A

Algebraic study of the two-dimensional Euler equation

Consider the two-dimensional Euler equation with the initial condition

$$\Psi_0(z_1, z_2) = \hat{F}(\mathfrak{p})\mathrm{e}^{-\mathrm{i}\,\mathfrak{p}\cdot z} + \hat{F}(\mathfrak{q})\mathrm{e}^{-\mathrm{i}\,\mathfrak{q}\cdot z} + \hat{F}^*(\mathfrak{p})\mathrm{e}^{\mathrm{i}\,\mathfrak{p}\cdot z} + \hat{F}^*(\mathfrak{q})\mathrm{e}^{\mathrm{i}\,\mathfrak{q}\cdot z}. \tag{A.1}$$

The solution can be written in a way which is analogous to the representation (5.11) used in the case of the Burgers equation

$$\begin{aligned}\psi(z,t) = \sum_{n=0}^{\infty} t^{2n-1} \Big[& F^{(n)}_{(\mathfrak{p},\mathfrak{q})}(t,z) + F^{(n)}_{(-\mathfrak{p},\mathfrak{q})}(t,z) + F^{(n)}_{(\mathfrak{p},-\mathfrak{q})}(t,z) + \\ & F^{(n)}_{(-\mathfrak{p},-\mathfrak{q})}(t,z) + F^{(n)}_{\mathfrak{p}}(t,z) + F^{(n)}_{-\mathfrak{p}}(t,z) + F^{(n)}_{\mathfrak{q}}(t,z) + F^{(n)}_{-\mathfrak{q}}(t,z) \Big],\end{aligned} \tag{A.2}$$

Here the functions $F^{(n)}_{(\mathfrak{p},\mathfrak{q})}(t,z)$ and $F^{(n)}_{\mathfrak{p}}(t,z)$ and $F^{(n)}_{\mathfrak{q}}(t,z)$ have the following representations: $F^{(n)}_{(\mathfrak{p},\mathfrak{q})}(t,z)$ is the function defined so that its Fourier coeffficients are inside the sector defined by the vectors $\mathfrak{p}$ and $\mathfrak{q}$

$$F^{(n)}_{(\mathfrak{p},\mathfrak{q})}(t,z) = \sum_{k_1=1}^{\infty}\sum_{k_2=1}^{\infty} \hat{F}^{(n)}_{(\mathfrak{p},\mathfrak{q})}(k_1,k_2) t^{k_1} t^{k_2} \mathrm{e}^{-\mathrm{i}\,k_1\,\mathfrak{p}\cdot z}\mathrm{e}^{-\mathrm{i}\,k_2\,\mathfrak{q}\cdot z}, \tag{A.3}$$

whereas $F^{(n)}_{\mathfrak{p}}(t,z)$ ($F^{(n)}_{\mathfrak{q}}(t,z)$) is supported by the border lines between the sectors defined by $\mathfrak{p}$, $\mathfrak{q}$ and $\mathfrak{p}$, $-\mathfrak{q}$ ($\mathfrak{p}$, $\mathfrak{q}$ and $-\mathfrak{p}$, $\mathfrak{q}$, respectively)

$$\begin{aligned} F^{(n)}_{\mathfrak{p}}(t,z) &= \sum_{k_1=1}^{\infty} \hat{F}^{(n)}_{\mathfrak{p}}(k_1)\, t^{k_1} \mathrm{e}^{-\mathrm{i}\,k_1\,\mathfrak{p}\cdot z}, \\ F^{(n)}_{\mathfrak{q}}(t,z) &= \sum_{k_2=1}^{\infty} \hat{F}^{(n)}_{\mathfrak{q}}(k_2)\, t^{k_2} \mathrm{e}^{-\mathrm{i}\,k_2\,\mathfrak{q}\cdot z}. \end{aligned} \tag{A.4}$$

For consistency the following must hold

$$\hat{F}^{(n)}_{(\mathfrak{p},\mathfrak{q})}(k_1,0) = \hat{F}^{(n)}_{\mathfrak{p}}(k_1) = \hat{F}^{(n)}_{(\mathfrak{p},-\mathfrak{q})}(k_1,0), \tag{A.5}$$

for $k_1 \geq 1$, and

$$\hat{F}^{(n)}_{(\mathfrak{p},\mathfrak{q})}(0,k_2) = \hat{F}^{(n)}_{\mathfrak{q}}(k_2) = \hat{F}^{(n)}_{(-\mathfrak{p},\mathfrak{q})}(0,k_2), \tag{A.6}$$

for $k_2 \geq 1$.

In the next step we insert representation (A.2) into the two-dimensional Euler equation. For $z \to \infty$ in the asymptotic direction given by $\mathfrak{p}$ and $\mathfrak{q}$ the terms containing negative powers of $\mathrm{e}^{-\mathrm{i}\,\mathfrak{p}\cdot z}$ and $\mathrm{e}^{-\mathrm{i}\,\mathfrak{q}\cdot z}$ vanish. Ordering the remaining terms with respect to t and $\mathrm{e}^{-\mathrm{i}\,\mathfrak{p}\cdot\tilde{z}}$, $\mathrm{e}^{-\mathrm{i}\,\mathfrak{q}\cdot\tilde{z}}$, where $\tilde{z}$ is defined through (6.3), we obtain an infinite sequence of recursion relations for $\hat{F}^{(n)}_{(\mathfrak{p},\mathfrak{q})}$, for $n = 0, 1, 2, \ldots$

$$
\begin{aligned}
&-\frac{1}{\mathfrak{p}\wedge\mathfrak{q}}\Big((2n-1)+k_1+k_2\Big)\Big(k_1\mathfrak{p}+k_2\mathfrak{q}\Big)^2\hat{F}^{(n)}_{(\mathfrak{p},\mathfrak{q})}(k_1,k_2) = \sum_{m=0}^{n}\sum_{k_1'=0}^{k_1}\sum_{k_2'=0}^{k_2}(k_1'k_2-k_1k_2')\Big((k_1-k_1')\mathfrak{p}+(k_2-k_2')\mathfrak{q}\Big)^2\\
&\hat{F}^{(m)}_{(\mathfrak{p},\mathfrak{q})}(k_1',k_2')\,\hat{F}^{(n-m)}_{(\mathfrak{p},\mathfrak{q})}(k_1-k_1',k_2-k_2') + \sum_{m=0}^{n-1}\sum_{l=0}^{m}\sum_{k_2'=0}^{k_2}\Bigg\{\Big((n-m)k_2+k_1(k_2-k_2')\Big)\Big(-(n-m)\mathfrak{p}+(k_2-k_2')\mathfrak{q}\Big)^2\\
&\hat{F}^{(l)}_{(\mathfrak{p},\mathfrak{q})}(n-m+k_1,k_2')\,\hat{F}^{(m-l)}_{(-\mathfrak{p},\mathfrak{q})}(n-m,k_2-k_2') - \Big((n-m)k_2+k_1k_2'\Big)\Big((n-m+k_1)\mathfrak{p}+(k_2-k_2')\mathfrak{q}\Big)^2\\
&\hat{F}^{(l)}_{(-\mathfrak{p},\mathfrak{q})}(n-m,k_2')\,\hat{F}^{(m-l)}_{(\mathfrak{p},\mathfrak{q})}(n-m+k_1,k_2-k_2')\Bigg\} - \sum_{m=0}^{n-1}\sum_{l=0}^{m}\sum_{k_1'=0}^{k_1}\Bigg\{\Big(k_1(n-m)+(k_1-k_1')k_2\Big)\Big((k_1-k_1')\mathfrak{p}-(n-m)\mathfrak{q}\\
&\hat{F}^{(l)}_{(\mathfrak{p},\mathfrak{q})}(k_1',n-m+k_2)\,\hat{F}^{(m-l)}_{(\mathfrak{p},-\mathfrak{q})}(k_1-k_1',n-m) - \Big(k_1(n-m)+k_1'k_2\Big)\Big((k_1-k_1')\mathfrak{p}+(n-m+k_2)\mathfrak{q}\Big)^2\\
&\hat{F}^{(l)}_{(\mathfrak{p},-\mathfrak{q})}(k_1',n-m)\,\hat{F}^{(m-l)}_{(\mathfrak{p},\mathfrak{q})}(k_1-k_1',n-m+k_2)\Bigg\} + \sum_{m=0}^{n-2}\sum_{l=0}^{m}\sum_{k=1}^{n-m-1}\Big(kk_2-k_1(n-m-k)\Big)\Bigg\{\Big(k\mathfrak{p}+(n-m-k)\mathfrak{q}\Big)^2\\
&\hat{F}^{(l)}_{(\mathfrak{p},\mathfrak{q})}(k+k_1,(n-m-k)+k_2)\hat{F}^{(m-l)}_{(-\mathfrak{p},-\mathfrak{q})}(k,n-m-k) - \Big((k+k_1)\mathfrak{p}+(n-m-k+k_2)\mathfrak{q}\Big)^2\hat{F}^{(l)}_{(-\mathfrak{p},-\mathfrak{q})}(k,n-m-k)\\
&\hat{F}^{(m-l)}_{(\mathfrak{p},\mathfrak{q})}(k+k_1,n-m-k+k_2)\Bigg\} + \sum_{m=0}^{n-2}\sum_{l=0}^{m}\sum_{k=1}^{n-m-1}\Big((k_1+k)k_2+k_1(n-m-k)\Big)\Bigg\{\Big(-k\mathfrak{p}+(n-m-k+k_2)\mathfrak{q}\Big)^2\\
&\hat{F}^{(l)}_{(\mathfrak{p},-\mathfrak{q})}(k+k_1,n-m-k)\hat{F}^{(m-l)}_{(-\mathfrak{p},\mathfrak{q})}(k_1,n-m-k+k_2) - \Big((k+k_1)\mathfrak{p}-(n-m-k)\mathfrak{q}\Big)^2\hat{F}^{(l)}_{(-\mathfrak{p},\mathfrak{q})}(k,n-m-k+k_2)\\
&\hat{F}^{(m-l)}_{(\mathfrak{p},-\mathfrak{q})}(k+k_1,n-m-k)\Bigg\}.
\end{aligned}
\tag{A.7}
$$

The initial conditions are as follows

$$
\begin{aligned}
\hat{F}^{(0)}_{(\mathfrak{p},\mathfrak{q})}(1,0) &= \hat{F}(\mathfrak{p}), \qquad & \hat{F}^{(0)}_{(\mathfrak{p},\mathfrak{q})}(0,1) &= \hat{F}(\mathfrak{q})\\
\hat{F}^{(0)}_{(-\mathfrak{p},\mathfrak{q})}(1,0) &= \hat{F}^*(\mathfrak{p}), \qquad & \hat{F}^{(0)}_{(-\mathfrak{p},\mathfrak{q})}(0,1) &= \hat{F}(\mathfrak{q})\\
\hat{F}^{(0)}_{(\mathfrak{p},-\mathfrak{q})}(1,0) &= \hat{F}(\mathfrak{p}), \qquad & \hat{F}^{(0)}_{(\mathfrak{p},-\mathfrak{q})}(0,1) &= \hat{F}^*(\mathfrak{q})\\
\hat{F}^{(0)}_{(-\mathfrak{p},-\mathfrak{q})}(1,0) &= \hat{F}^*(\mathfrak{p}), \qquad & \hat{F}^{(0)}_{(-\mathfrak{p},-\mathfrak{q})}(0,1) &= \hat{F}^*(\mathfrak{q})
\end{aligned}
$$

In the case $n = 0$ we obtain the well-known nonlinear recursion relation

$$
\begin{aligned}
&\frac{1}{\mathfrak{p}\wedge\mathfrak{q}}\Big(k_1+k_2-1\Big)\Big(k_1\mathfrak{p}+k_2\mathfrak{q}\Big)^2\hat{F}^{(0)}_{(\mathfrak{p},\mathfrak{q})}(k_1,k_2) = -\sum_{k_1'=0}^{k_1}\sum_{k_2'=0}^{k_2}(k_1'k_2-k_1k_2')\\
&\Big((k_1-k_1')\mathfrak{p}+(k_2-k_2')\mathfrak{q}\Big)^2\hat{F}^{(0)}_{(\mathfrak{p},\mathfrak{q})}(k_1',k_2')\,\hat{F}^{(0)}_{(\mathfrak{p},\mathfrak{q})}(k_1-k_1',k_2-k_2')
\end{aligned}
\tag{A.8}
$$

As noted in 6.1 the coefficients $\hat{F}^{(0)}_{(\mathfrak{p},\mathfrak{q})}(k_1,k_2)$ can be simplified by putting

$$
\hat{F}^{(0)}_{(\mathfrak{p},\mathfrak{q})}(k_1,k_2) = \Big(\mathfrak{p}\wedge\mathfrak{q}\Big)^{k_1+k_2-1}\Big(\hat{F}(\mathfrak{p})\Big)^{k_1}\Big(\hat{F}(\mathfrak{q})\Big)^{k_2}\hat{G}^{(0)}_{(\mathfrak{p},\mathfrak{q})}(k_1,k_2). \tag{A.9}
$$

The first few coefficients are

$$
\begin{aligned}
\hat{G}^{(1)}(1) &= -\frac{|\mathbf{q}|^2-|\mathbf{p}|^2}{|\mathbf{p}+\mathbf{q}|^2};\\
\hat{G}^{(2)}(1) &= \frac{1}{2}\,\frac{|\mathbf{q}|^2-|\mathbf{p}|^2}{|\mathbf{p}+\mathbf{q}|^2}\,\frac{|\mathbf{p}+\mathbf{q}|^2-|\mathbf{p}|^2}{|2\mathbf{p}+\mathbf{q}|^2};\\
\hat{G}^{(2)}(2) &= -\frac{1}{2}\,\frac{|\mathbf{q}|^2-|\mathbf{p}|^2}{|\mathbf{p}+\mathbf{q}|^2}\,\frac{|\mathbf{p}+\mathbf{q}|^2-|\mathbf{q}|^2}{|\mathbf{p}+2\mathbf{q}|^2};\\
\hat{G}^{(3)}(1) &= -\frac{1}{6}\,\frac{|\mathbf{q}|^2-|\mathbf{p}|^2}{|\mathbf{p}+\mathbf{q}|^2}\,\frac{|\mathbf{p}+\mathbf{q}|^2-|\mathbf{p}|^2}{|2\mathbf{p}+\mathbf{q}|^2}\,\frac{|2\mathbf{p}+\mathbf{q}|^2-|\mathbf{p}|^2}{|3\mathbf{p}+\mathbf{q}|^2};\\
\hat{G}^{(3)}(2) &= \frac{1}{3}\,\frac{|\mathbf{q}|^2-|\mathbf{p}|^2}{|\mathbf{p}+\mathbf{q}|^2}\left[\frac{|\mathbf{p}+\mathbf{q}|^2-|\mathbf{q}|^2}{|\mathbf{p}+2\mathbf{q}|^2}\,\frac{|\mathbf{p}+2\mathbf{q}|^2-|\mathbf{p}|^2}{|2\mathbf{p}+2\mathbf{q}|^2}+\frac{|\mathbf{p}+\mathbf{q}|^2-|\mathbf{p}|^2}{|2\mathbf{p}+\mathbf{q}|^2}\,\frac{|2\mathbf{p}+\mathbf{q}|^2-|\mathbf{q}|^2}{|2\mathbf{p}+2\mathbf{q}|^2}\right];\\
\hat{G}^{(3)}(3) &= -\frac{1}{6}\,\frac{|\mathbf{q}|^2-|\mathbf{p}|^2}{|\mathbf{p}+\mathbf{q}|^2}\,\frac{|\mathbf{p}+\mathbf{q}|^2-|\mathbf{q}|^2}{|\mathbf{p}+2\mathbf{q}|^2}\,\frac{|\mathbf{p}+2\mathbf{q}|^2-|\mathbf{q}|^2}{|\mathbf{p}+3\mathbf{q}|^2}.
\end{aligned}
\tag{A.10}
$$

The higher order coefficients quickly become quite involved. We list them here just for the sake of illustrating this point

$$
\begin{aligned}
\hat{G}^{(4)}(1) &= \frac{1}{24}\,\frac{|\mathbf{q}|^2-|\mathbf{p}|^2}{|\mathbf{p}+\mathbf{q}|^2}\,\frac{|\mathbf{p}+\mathbf{q}|^2-|\mathbf{p}|^2}{|2\mathbf{p}+\mathbf{q}|^2}\,\frac{|2\mathbf{p}+\mathbf{q}|^2-|\mathbf{p}|^2}{|3\mathbf{p}+\mathbf{q}|^2}\,\frac{|3\mathbf{p}+\mathbf{q}|^2-|\mathbf{p}|^2}{|4\mathbf{p}+\mathbf{q}|^2}.\\
\hat{G}^{(4)}(2) &= -\frac{1}{4}\,\frac{|\mathbf{q}|^2-|\mathbf{p}|^2}{|\mathbf{p}+\mathbf{q}|^2}\left[\frac{2}{3}\,\frac{|\mathbf{p}+\mathbf{q}|^2-|\mathbf{q}|^2}{|\mathbf{p}+2\mathbf{q}|^2}\,\frac{|\mathbf{p}+2\mathbf{q}|^2-|\mathbf{p}|^2}{|2\mathbf{p}+2\mathbf{q}|^2}\,\frac{|2\mathbf{p}+2\mathbf{q}|^2-|\mathbf{p}|^2}{|3\mathbf{p}+2\mathbf{q}|^2}+\right.\\
&\frac{2}{3}\,\frac{|\mathbf{p}+\mathbf{q}|^2-|\mathbf{p}|^2}{|2\mathbf{p}+\mathbf{q}|^2}\,\frac{|2\mathbf{p}+\mathbf{q}|^2-|\mathbf{q}|^2}{|2\mathbf{p}+2\mathbf{q}|^2}\,\frac{|2\mathbf{p}+2\mathbf{q}|^2-|\mathbf{p}|^2}{|3\mathbf{p}+2\mathbf{q}|^2}+\frac{1}{2}\,\frac{|\mathbf{p}+\mathbf{q}|^2-|\mathbf{p}|^2}{|2\mathbf{p}+\mathbf{q}|^2}\,\frac{|2\mathbf{p}+\mathbf{q}|^2-|\mathbf{p}|^2}{|3\mathbf{p}+\mathbf{q}|^2}\,\frac{3\mathbf{p}+\mathbf{q}|^2-|\mathbf{q}|^2}{|3\mathbf{p}+2\mathbf{q}|^2}\\
&\left.+\frac{1}{2}\,\frac{|\mathbf{q}|^2-|\mathbf{p}|^2}{|\mathbf{p}+\mathbf{q}|^2}\,\frac{|\mathbf{p}+\mathbf{q}|^2-|\mathbf{p}|^2}{|2\mathbf{p}+\mathbf{q}|^2}\,\frac{|2\mathbf{p}+\mathbf{q}|^2-|\mathbf{p}+\mathbf{q}|^2}{|3\mathbf{p}+2\mathbf{q}|^2}\right];\\
\hat{G}^{(4)}(3) &= \frac{1}{4}\,\frac{|\mathbf{q}|^2-|\mathbf{p}|^2}{|\mathbf{p}+\mathbf{q}|^2}\left[\frac{2}{3}\,\frac{|\mathbf{p}+\mathbf{q}|^2-|\mathbf{p}|^2}{2|\mathbf{p}+\mathbf{q}|^2}\,\frac{|2\mathbf{p}+\mathbf{q}|^2-|\mathbf{q}|^2}{|2\mathbf{p}+2\mathbf{q}|^2}\,\frac{|2\mathbf{p}+2\mathbf{q}|^2-|\mathbf{q}|^2}{|2\mathbf{p}+3\mathbf{q}|^2}+\right.\\
&\frac{2}{3}\,\frac{|\mathbf{p}+\mathbf{q}|^2-|\mathbf{q}|^2}{|\mathbf{p}+2\mathbf{q}|^2}\,\frac{|\mathbf{p}+2\mathbf{q}|^2-|\mathbf{p}|^2}{|2\mathbf{p}+2\mathbf{q}|^2}\,\frac{|2\mathbf{p}+2\mathbf{q}|^2-|\mathbf{q}|^2}{|2\mathbf{p}+3\mathbf{q}|^2}+\frac{1}{2}\,\frac{|\mathbf{p}+\mathbf{q}|^2-|\mathbf{q}|^2}{|\mathbf{p}+2\mathbf{q}|^2}\,\frac{|\mathbf{p}+2\mathbf{q}|^2-|\mathbf{q}|^2}{|\mathbf{p}+3\mathbf{q}|^2}\,\frac{\mathbf{p}+3\mathbf{q}|^2-|\mathbf{p}|^2}{|2\mathbf{p}+3\mathbf{q}|^2}\\
&\left.-\frac{1}{2}\,\frac{|\mathbf{q}|^2-|\mathbf{p}|^2}{|\mathbf{p}+\mathbf{q}|^2}\,\frac{|\mathbf{p}+\mathbf{q}|^2-|\mathbf{q}|^2}{|\mathbf{p}+2\mathbf{q}|^2}\,\frac{|\mathbf{p}+2\mathbf{q}|^2-|\mathbf{p}+\mathbf{q}|^2}{|2\mathbf{p}+3\mathbf{q}|^2}\right];
\end{aligned}
\tag{A.11}
$$

Actually, these formulae give us an impression of the algebraic complexity involved in solving recursion relation (A.8). We did calculate some still higher order terms, however, we do not list them here. For the moment it seems that there is no simple way of representing the algebraic solutions of (A.8)

The higher order recursion relations $n \geq 1$ are actually linear, corresponding to inhomogeneous linear partial differential equations. For example, the first order equation

has the form

$$
\begin{aligned}
&-\frac{1}{\mathfrak{p}\wedge\mathfrak{q}}(k_1+k_2+1)(k_1\mathfrak{p}+k_2\mathfrak{q})^2\hat{F}^{(1)}_{(\mathfrak{p},\mathfrak{q})}(k_1,k_2)=\sum_{k_1'=0}^{k_1}\sum_{k_2'=0}^{k_2}(k_1'k_2-k_1k_2')\\
&\Big((k_1-k_1')\mathfrak{p}+(k_2-k_2')\mathfrak{q}\Big)^2\Bigg\{\hat{F}^{(0)}_{(\mathfrak{p},\mathfrak{q})}(k_1',k_2')\hat{F}^{(1)}_{(\mathfrak{p},\mathfrak{q})}(k_1-k_1',k_2-k_2')+\hat{F}^{(1)}_{(\mathfrak{p},\mathfrak{q})}(k_1',k_2')\\
&\hat{F}^{(0)}_{(\mathfrak{p},\mathfrak{q})}(k_1-k_1',k_2-k_2')\Bigg\}+\sum_{k_2'=0}^{k_2}\Bigg\{\Big(k_2+k_1(k_2-k_2')\Big)\Big(-\mathfrak{p}+(k_2-k_2')\mathfrak{q}\Big)^2\\
&\hat{F}^{(0)}_{(\mathfrak{p},\mathfrak{q})}(k_1+1,k_2')\hat{F}^{(0)}_{(-\mathfrak{p},\mathfrak{q})}(1,k_2-k_2')-\Big(k_2+k_1k_2'\Big)\Big((k_1+1)\mathfrak{p}+(k_2-k_2')\mathfrak{q}\Big)^2\\
&\hat{F}^{(0)}_{(-\mathfrak{p},\mathfrak{q})}(1,k_2')\hat{F}^{(0)}_{(\mathfrak{p},\mathfrak{q})}(k_1+1,k_2-k_2')\Bigg\}-\sum_{k_1'=0}^{k_1}\Bigg\{\Big(k_1+(k_1-k_1')k_2\Big)\Big((k_1-k_1')\mathfrak{p}-\mathfrak{q}\Big)^2\\
&\hat{F}^{(0)}_{(\mathfrak{p},\mathfrak{q})}(k_1',k_2+1)\hat{F}^{(0)}_{(\mathfrak{p},-\mathfrak{q})}(k_1-k_1',1)-\Big(k_1+k_1'k_2\Big)\Big((k_1-k_1')\mathfrak{p}+(k_2+1)\mathfrak{q}\Big)^2\\
&\hat{F}^{(0)}_{(\mathfrak{p},-\mathfrak{q})}(k_1',1)\hat{F}^{(0)}_{(\mathfrak{p},\mathfrak{q})}(k_1-k_1',k_2+1)\Bigg\}.
\end{aligned}
\tag{A.12}
$$

Note that in the case $k_1=0$ or $k_2=0$ the contribution of the advection term is vanishing. Thus, in this case the coefficients are completely determined by the source terms (which are the second and the third term on the right-hand side of the equation above). The first few coefficients are

$$
\hat{F}^{(1)}_{(\mathfrak{p},\mathfrak{q})}(1,0)=\frac{1}{2}\frac{1}{|\mathfrak{p}|^2}\,(\mathfrak{p}\wedge\mathfrak{q})^2\,(|\mathfrak{q}|^2-|\mathfrak{p}|^2)\Big[2-\frac{|\mathfrak{q}|^2}{|\mathfrak{p}+\mathfrak{q}|^2}-\frac{|\mathfrak{q}|^2}{|\mathfrak{p}-\mathfrak{q}|^2}\Big]\,\hat{F}(\mathfrak{p})\,\hat{F}(\mathfrak{q})\,\hat{F}^*(\mathfrak{q}).
\tag{A.13}
$$

Appendix B

Perturbative expansion of the 2D similarity equation

We begin by writing the similarity equation for the short-time Euler flow in the form[1]

$$\big(\Delta_\phi(\zeta)H\big) = J\Big(H, \big(\Delta_\phi(\zeta)H\big)\Big), \tag{B.1}$$

with $\big(\Delta_\phi(\zeta)\big)$ given by

$$\big(\Delta_\phi(\zeta)\big) = \frac{1}{1+\zeta}\,\partial_1^2 + 2\cos\phi\,\partial_1\partial_2 + (1+\zeta)\,\partial_2^2. \tag{B.2}$$

The modified stream function $H(z_1, z_2; \zeta)$ can be represented by using the Taylor series expansion

$$H(z_1, z_2; \zeta) = \sum_{n=0}^{\infty} H_n(z_1, z_2)\,\zeta^n. \tag{B.3}$$

Upon inserting (B.3) into Equation (B.1) and arranging the terms according to the powers of ζ we obtain an infinite system of homogeneous linear partial differential equations for the functions $H_n(z_1, z_2)$. It has the following form: for $H_1(z_1, z_2)$ we get

$$(1-e^{z_2})\partial_1\Delta_\phi H_1 + (1+e^{z_1})\partial_2\Delta_\phi H_1 + e^{z_2}\partial_1 H_1 - e^{z_1}\partial_2 H_1 + 2e^{z_1+z_2} = \Delta_\phi H_1, \tag{B.4}$$

for $H_2(z_1, z_2)$

$$\begin{aligned}&\Delta_\phi H_2 + (\partial_2^2 - \partial_1^2)H_1 = (1-e^{z_2})\partial_1\Delta_\phi H_2 + (1+e^{z_1})\partial_2\Delta_\phi H_2 + e^{z_2}\partial_1 H_2 - \\ &e^{z_1}\partial_2 H_2 + J(H_1, \Delta_\phi H_1) + (1-e^{z_2})\partial_1(\partial_2^2 - \partial_1^2)H_1 + (1+e^{z_1})\partial_2(\partial_2^2 - \partial_1^2)H_1 + \\ &e^{z_2}\partial_1 H_1 + e^{z_1}\partial_2 H_1 - e^{z_1+z_2},\end{aligned} \tag{B.5}$$

for $H_3(\check{z}_1, \check{z}_2)$

$$\begin{aligned}&\Delta_\phi H_3 + (\partial_2^2 - \partial_1^2)H_2 + \partial_1^2 H_1 = (1-e^{z_2})\partial_1\Delta_\phi H_3 + (1+e^{z_1})\partial_2\Delta_\phi H_3 + e^{z_2}\partial_1 H_3 - \\ &e^{z_1}\partial_2 H_3 + J(H_1, \Delta_\phi H_2) + J(H_2, \Delta_\phi H_1) + (1-e^{z_2})\partial_1(\partial_2^2 - \partial_1^2)H_2 + \\ &(1+e^{z_1})\partial_2(\partial_2^2 - \partial_1^2)H_2 + e^{z_2}\partial_1 H_2 + e^{z_1}\partial_2 H_2 + J(H_1, (\partial_2^2 - \partial_1^2)H_1) + \\ &(1-e^{z_1})\partial_1^3 H_1 + (1+e^{z_1})\partial_1^2\partial_2 H_1 - e^{z_1}\partial_2 H_1 + e^{z_1+z_2},\end{aligned} \tag{B.6}$$

[1] For simplicity we denote the space variables $(\check{z}_1, \check{z}_2)$ as (z_1, z_2).

and for $H_n(\check{z}_1, \check{z}_2)$, $n \geq 4$

$$\Delta_\phi H_n + (\partial_2^2 - \partial_1^2)H_{n-1} + \sum_{n'=1}^{n-2}(-1)^{n-n'}\partial_1^2 H_{n'} = (1-e^{z_2})\partial_1\Delta_\phi H_n + (1+e^{z_1})\partial_2\Delta_\phi H_n +$$
$$e^{z_2}\partial_1 H_n - e^{z_1}\partial_2 H_n + \sum_{n'=1}^{n-1} J(H_{n-n'}, \Delta_\phi H_{n'}) + (1-e^{z_2})\partial_1(\partial_2^2 - \partial_1^2)H_{n-1} +$$
$$(1+e^{z_1})\partial_2(\partial_2^2 - \partial_1^2)H_{n-1} + e^{z_2}\partial_1 H_{n-1} + e^{z_1}\partial_2 H_{n-1} + \sum_{n'=2}^{n-1} J(H_{n-n'}, (\partial_2^2 - \partial_1^2)H_{n'-1}) +$$
$$\sum_{n'=1}^{n-2}(-1)^{n-n'}\Big[(1-e^{z_2})\partial_1^3 H_{n'} + (1+e^{z_1})\partial_1^2\partial_2 H_{n'}\Big] - \sum_{n'=2}^{n-1}(-1)^{n'}e^{z_1}\partial_2 H_{n-n'} +$$
$$\sum_{n'=3}^{n-1}\sum_{n''=1}^{n-2}(-1)^{n'-n''}J(H_{n-n'}, \partial_1^2 H_{n''}) + (-1)^{n-1}e^{z_1+z_2}. \tag{B.7}$$

For numerical purposes it is convenient to write $H(z_1, z_2; \zeta)$ as the triple series

$$H(z_1, z_2; \zeta) = z_1 - z_2 + \sum_{k_1=0}^{\infty}\sum_{k_2=0}^{\infty}\sum_{n=0}^{\infty}\hat{G}(k_1, k_2; n)\,\mathrm{e}^{k_1 z_1}\,\mathrm{e}^{k_2 z_2}\zeta^n. \tag{B.8}$$

The coefficients $\hat{G}(k_1, k_2; n)$ can be determined from an infinite system of linear recursion relations. The recursion relation for $\hat{G}(k_1, k_2; 1)$ is given by

$$(k_1+k_2-1)P(\phi)(k_1, k_2)G(k_1, k_2; 1) - k_1\Big[P(\phi)(k_1, k_2-1) - 1\Big]G(k_1, k_2-1; 1) +$$
$$k_2\Big[P(\phi)(k_1-1, k_2) - 1\Big]G(k_1-1, k_2; 1) + 2\delta_{k_1 1}\delta_{k_2 1} = 0; \tag{B.9}$$

for $\hat{G}(k_1, k_2; 2)$ we get

$$(k_1+k_2-1)P(\phi)(k_1, k_2)G(k_1, k_2; 2) - k_1\Big[P(\phi)(k_1, k_2-1) - 1\Big]G(k_1, k_2-1; 2) +$$
$$k_2\Big[P(\phi)(k_1-1, k_2) - 1\Big]G(k_1-1, k_2; 2) +$$
$$\sum_{k_1'=0}^{k_1}\sum_{k_2'=0}^{k_2}(k_1' k_2 - k_2' k_1)\,G(k_1', k_2'; 1)\,P(\phi)(k_1-k_1', k_2-k_2')\,G(k_1-k_1', k_2-k_2'; 1) +$$
$$(k_1+k_2-1)Q(k_1, k_2)G(k_1, k_2; 1) - k_1\Big[Q(k_1, k_2-1) - 1\Big]G(k_1, k_2-1; 1) +$$
$$k_2\Big[Q(k_1-1, k_2) + 1\Big]G(k_1-1, k_2; 1) - \delta_{k_1 1}\delta_{k_2 1} = 0, \tag{B.10}$$

for $\hat{G}(k_1,k_2;3)$

$$
\begin{aligned}
&(k_1+k_2-1)P(\phi)(k_1,k_2)G(k_1,k_2;3)-k_1\Big[P(\phi)(k_1,k_2-1)-1\Big]G(k_1,k_2-1;3)+\\
&k_2\Big[P(\phi)(k_1-1,k_2)-1\Big]G(k_1-1,k_2;3)+\\
&\sum_{k_1'=0}^{k_1}\sum_{k_2'=0}^{k_2}(k_1'k_2-k_2'k_1)\,G(k_1',k_2';1)\,P(\phi)(k_1-k_1',k_2-k_2')\,G(k_1-k_1',k_2-k_2';2)+\\
&\sum_{k_1'=0}^{k_1}\sum_{k_2'=0}^{k_2}(k_1'k_2-k_2'k_1)\,G(k_1',k_2';2)\,P(\phi)(k_1-k_1',k_2-k_2')\,G(k_1-k_1',k_2-k_2';1)+\\
&(k_1+k_2-1)Q(k_1,k_2)G(k_1,k_2;2)-k_1\Big[Q(k_1,k_2-1)-1\Big]G(k_1,k_2-1;2)+\\
&k_2\Big[Q(k_1-1,k_2)+1\Big]G(k_1-1,k_2;2)+\\
&\sum_{k_1'=0}^{k_1}\sum_{k_2'=0}^{k_2}(k_1'k_2-k_2'k_1)\,G(k_1',k_2';1)\,Q(k_1-k_1',k_2-k_2')\,G(k_1-k_1',k_2-k_2';1)+\\
&(k_1+k_2-1)k_1^2G(k_1,k_2;1)-k_1^3G(k_1,k_2-1;1)+\\
&k_2\Big[(k_1-1)^2-1\Big]G(k_1-1,k_2;1)+\delta_{k_11}\delta_{k_21}=0,
\end{aligned}
\tag{B.11}
$$

and for $\hat{G}(k_1,k_2;n)$, $n\geq 4$

$$
\begin{aligned}
&(k_1+k_2-1)P(\phi)(k_1,k_2)G(k_1,k_2;n)-k_1\Big[P(\phi)(k_1,k_2-1)-1\Big]G(k_1,k_2-1;n)+\\
&k_2\Big[P(\phi)(k_1-1,k_2)-1\Big]G(k_1-1,k_2;n)+\\
&\sum_{n'=1}^{n-1}\sum_{k_1'=0}^{k_1}\sum_{k_2'=0}^{k_2}(k_1'k_2-k_2'k_1)\,G(k_1',k_2';n-n')\,P(\phi)(k_1-k_1',k_2-k_2')\,G(k_1-k_1',k_2-k_2';n')+\\
&(k_1+k_2-1)Q(k_1,k_2)G(k_1,k_2;n-1)-k_1\Big[Q(k_1,k_2-1)-1\Big]G(k_1,k_2-1;n-1)+\\
&k_2\Big[Q(k_1-1,k_2)+1\Big]G(k_1-1,k_2;n-1)+\\
&\sum_{n'=2}^{n-1}\sum_{k_1'=0}^{k_1}\sum_{k_2'=0}^{k_2}(k_1'k_2-k_2'k_1)\,G(k_1',k_2';n-n')\,Q(k_1-k_1',k_2-k_2')\,G(k_1-k_1',k_2-k_2';n'-1)+\\
&\sum_{n'=1}^{n-2}(-1)^{n-n'}\Big[(k_1+k_2-1)k_1^2G(k_1,k_2;n')-k_1^3G(k_1,k_2-1;n')+\\
&k_2\big((k_1-1)^2-1\big)G(k_1-1,k_2;n')\Big]+\\
&\sum_{n'=3}^{n-1}\sum_{n''=1}^{n-2}(-1)^{n'-n''}\sum_{k_1'=0}^{k_1}\sum_{k_2'=0}^{k_2}(k_1'k_2-k_2'k_1)\,G(k_1',k_2';n-n')\,(k_1-k_1')^2\,G(k_1-k_1',k_2-k_2';n'')+\\
&(-1)^{n-1}\delta_{k_11}\delta_{k_21}=0.
\end{aligned}
\tag{B.12}
$$

Here we have used the following notation

$$
P(\phi)(k_1,k_2)=k_1^2+2\,\cos\phi\,k_1k_2+k_2^2,
\tag{B.13}
$$

and

$$Q(k_1, k_2) = k_2^2 - k_1^2. \tag{B.14}$$

Finally, the initialization of the recursion relations is given by

$$\begin{aligned}
&G(k_1, 0; n) = 0, \qquad k_1 > 1, \qquad n \geq 0, \\
&G(0, k_2; n) = 0, \qquad k_2 > 1, \qquad n \geq 0, \\
&G(0, 0; n) = 0, \qquad n \geq 0, \\
&G(0, 1; n) = 0, \qquad n \geq 1, \\
&G(1, 0; n) = 0, \qquad n \geq 1,
\end{aligned} \tag{B.15}$$

and, of course $G(0, 1; 0) = 1$, $G(1, 0; 0) = 1$.

Bibliography

[Ahl79] Lars V. Ahlfors, *Complex Analysis*, Mc. Graw-Hill (1979).

[Arn66] V. I. Arnold, Sur la géométrie diiférentielle des groupes de Lie de dimension infinie et ses applications à l'hydrodynamique des fluides parfaits, Annales de l'Institut Fourier 16 (1966) 316–361.

[Arn95] V. I. Arnold, Topological properties of Legendre projections in contact geometry of wave fronts, Saint Petersburg Mathematical Journal 6 (1995) 439–452.

[AT71] L. A. Aizenberg and V. M. Trutnev, A Borel summation method for n-tuple power series, Sibirsk. Matem. Zh. 12 (1971) 1895–1901.

[BBZ76] C. Bardos, S. Benachour and M. Zerner, Analycité des solutions périodiques de l'équation d'Euler en deux dimensions, C. R. Acad. Sci. Paris 282 (1976) 995–998.

[Ben76a] S. Benachour, Analycité des solutions de l'équation d'Euler en trois dimensions, C. R. Acad. Sci. Paris 283 (1976) 107–110.

[Ben76b] S. Benachour, Analycité des solutions des équations d'Euler, Arch. Ration. Mech. Anal. 71 (1976) 271–299.

[BF84] D. Bessis and J.-D. Fournier, Pole condensation and the Riemann surface associated with a shock in Burgers equation, J. Phys. Lett. 45 (1984) L833–L841.

[BMONMF83] M. E. Brachet, D. I. Meiron, S. A. Orszag, B. G. Nickel, R. H. Morf and U. Frisch, Small-scale structure of the Taylor–Green vortex, J. Fluid Mech. 167 (1983) 411–452.

[BT07] C. Bardos and E. Titi, Euler equations of incompressible ideal fluids, preprint (2007).

[Cal96] Julián Simón Calero, *La génesis de la mecánica de los fluidos (1640-1780)*, UNED (1996).

[CBDB05] C. Cichowlas, P. Bonaiti, F. Debasch and M. E. Brachet, Effective dissipation and turbulence in spectrally truncated Euler flows, Phys. Rev. Lett. 95 (2005) 264502.

[CGHJK96] R. M. Corless, G. H. Gonnet, D. E. G. Hare, D. J. Jeffrey and D. E. Knuth, On the Lambert W function, Advances in Computational Mathematics 5 (1996) 329–359.

[Cha07] D. Chae, Incompressible Euler equations: the blow-up problem and related results, preprint (2007).

[Con07] P. Constantin, On the Euler equations of incompressible fluids, preprint (2007).

[Dan40] P. J. Daniell, Ratio tests for double power series, Q. J. Math. 11 (1940) 183–192.

[Dar78] G. Darboux, Mémoire sur l'approximation des fonctions de très grands nombres, J. de Mathématiques Pures et Appliquées 4 (1878) 5–56 and 377–416

[Dar05] Olivier Darrigol, *Worlds of flow: A history of hydrodynamics from the Bernoullis to Prandtl*, Oxford University Press (2005).

[DF07] O. Darrigol and U. Frisch, From Newton's mechanics to Euler's equations, Physica D (2007) in press.

[Djo78] D. Z. Djoković, A property of the Taylor expansion of a class of rational functions in several variables, J. Math. Anal. Appl. 66 (1978) 679–685.

[Ego77] G. P. Egorychev, *Integral Representation and Calculation of Combinatorial Sums*, "Nauka", Sibirsk. Otdel. (1977); English transl., American Mathematical Society (1984).

[Ela05] S. Elaydi, *An Introduction to Difference Equations*, Springer (2005).

[Eul57] L. Euler, Principes généraux du mouvement des fluides, Mémoires de l'académie des sciences de Berlin 11 (1757) 274–315.

[Fey64] Richard P. Feynman, *The Feynman Lectures on Physics*, Volume 2, Addison Wesley (1964).

[FF83] J.-D. Fournier and U. Frisch, L'équation de Burgers déterministe et statistique, J. Méc. Th. Appl. 2 (1983) 699–750.

[FHKV05] B. Feng, Y.-H. He, K. D. Kennaway and C. Vafa, Dimer models from mirror symmetry and quivering amoebae, preprint (2005) arXiv:hep-th/0511287v1.

[FMB03] U. Frisch, T. Matsumoto and J. Bec, Singularities of the Euler equation? Not out of the blue!, J. Stat. Phys. 113 (2003) 761–781.

[FPTs00] M. Forsberg, M. Passare and A. K. Tsikh, Laurent polynomials and arrangements of hyperplane amoebas, Advances in Mathematics 151 (2000) 45–70.

[Fri83] U. Frisch, Fully developed turbulence and singularities, G. Ioos, R. Helleman and R. Stora (Eds.), *Chaotic Behaviour of Deterministic Systems, Les Houches 1981*, North-Holland (1983) 666–704.

[FW93] M. I. Freidlin and A. D. Wentzell, Diffusion processes on graphs and the averaging principle, Annals of Probability 21 (1993) 2215–2245.

[FW98] M. I. Freidlin and A. D. Wentzell, *Random Perturbations of Dynamical Systems*, Springer-Verlag (1998).

[GH65] R. Gilbert and H. C. Howard, Singularities of analytic functions having integral representations with a remark about the elastic, J. Math. Phys. 6 (1965) 1157–1162.

[GKZ94] I. Gelfand, M. Kapranov and A. Zelevinsky, *Discriminants, Resultants and Multidimensional Determinants*, Birkhäuser (1994).

[HK71] M. L. J. Hautus and D. A. Klarner, The diagonal of a double power series, Duke Math. J. 38 (1971) 229–335.

[Hoe02] J. van der Hoeven, Relax, but don't be too lazy, Journal of Symbolic Computation 34 (2002) 479–542.

[Hoe06] J. van der Hoeven, Algorithms for asymptotic interpolation, submitted to Journal of Symbolic Computation (2006).

[Kor04] L. Koralov, Random perturbations of 2-dimensional hamiltotnian flows, Probability Theory and Related Fields 129 (2004) 37–62.

[Lei04] E. K. Leinartas, Multiple Laurent series and difference equations Siberian Mathematical Journal 45 (2004) 321–326.

[LPTs05] E. K. Leinartas, M. Passare and A. K. Tsikh, Asymptotics of multidimensional difference equations, Communications of the Moscow Mathematical Society 60 (2005) 977–978.

[LS06] D. Li and Ya. Sinai, Blow Ups of Complex Solutions of the 3D-Navier-Stokes System, preprint (2006) arXiv:physics/0610101v1.

[MB02] Andrew J. Majda and Andrea L. Bertozzi, *Vorticity and Incompressible Flow*, Cambridge University Press (2002).

[MBF05] T. Matsumoto, J. Bec and U. Frisch, The analytic structure of 2D Euler flow at short times, Fluid Dynamics Research 36 (2005) 221–237.

[MBF07] T. Matsumoto, J. Bec and U. Frisch, Complex-space singularities of 2D Euler flow in Lagrangian coordinated, submitted to Physica D (2007).

[Mik00] G. Mikhalkin, Real algebaic curves, the moment map and amoebas, Annals of Mathematics 151 (2000) 309–326.

[Moo79] D. W. Moore, The spontaneous appearance of a singularity in the shape of an evolving vortex sheet, Proc. R. Soc. London A 365 (1979) 105–119.

[MP94] Carlo Marchioro and Mario Pulvirenti, *Mathematical Theory of Incompressible Nonviscous Fluids*, Springer–Verlag (1994).

[Mur97] D. J. Muraki, A simple illustration of a weak spectral cascade, SIAM J. Math. Anal. 28 (1997) 1457–1489.

[NPR] A. Novikov, G. Papanicolaou and L. Ryzhik, Boundary layers for cellular flows at high Péclet numbers, Communications on Pure and Applied Mathematics 58 (2004) 867–922.

[Orl93] A. G. Orlov, On asymptotics of Taylor coefficients of rational functions of two variables, Russian Mathematics (Iz. Vuz) 37 (1993) 23–30.

[Orl94] A. G. Orlov, About asymptotics of Taylor coefficients of algebraic functions, Siberian Math. J. 35 (1994) 1125–1137 (in Russian).

[Par62] O. S. Parasyuk, Hadamard's multiplication theorem and the analytic extension of the two-particle unitarity condition, Dokl. Akad. Nauk SSSR 145 (1962) 1247–1248; English transl. in Soviet Phys. Dokl. 7 (1963).

[PF07] W. Pauls and U. Frisch, A Borel Transform Method for Locating Singularities of Taylor and Fourier Series, J. Stat. Phys. 127 (2007) 1095–1119.

[PG97] R. B. Pelz and Y. Gulak, Evidence for a real-time singularity in hydrodynamics from time series, Phys. Rev. Lett. 79 (1997) 4998–5001.

[Pla64] G. W. Platzman, Am exact integral of complete spectral equations for unsteady one-dimensional flow, Tellus XVI (1964) 422–431.

[PM05a] W. Pauls and T. Matsumoto, Lagrangian singularities of steady two-dimensional flows, Geophys. Astrophys. Fluid Dyn. 99 (2005) 61–75.

[PM05b] W. Pauls and T. Matsumoto, Lagrangian singularities of steady two-dimensional flow, A. Litvak (Ed.), *Proceed. Frontiers of Nonlinear physics II*, Institute of Applied Physics RAS (2005) 236–242.

[PMFB06] W. Pauls, T. Matsumoto, U. Frisch and J. Bec, Nature of complex singuilarities for the 2D Euler equation, Physica D 219 (2006) 40–59.

[PO05] R. B. Pelz and K. Ohkitani, Linearly strained flows with and without boundaries – the regularizing effect of the pressure term, Fluid. Dyn. Res. 36 (2005) 193–210.

[Poi92] Henri Poincaré, *Les Méthodes Nouvelles de la Mécanique Céleste*, Gauthier-Villar (1892).

[Ron74] L. I. Ronkin, *Introduction to the Theory of Entire Functions of Several Variables*, American Mathematical Society (1974).

[SCE96] D. Senouf, R. Caflisch and N. Ercolani, Pole dynamics and oscillations for the complex Burgers equation in the small-dispersion limit, Nonlinearity 9 (1996) 1671–1702.

[Sch93] R. Schneider, Convex surfaces, curvature and surface area measures, P. M. Gruber and J. M. Wills (Eds.), *Handbook of Convex Geometry*, Volume A, North-Holland (1993) 273–299.

[Sen97a] D. Senouf, Dynamics and condensation of complex singularities for Burgers' equation I, SIAM J. Math. Anal. 28 (1997) 1457–1489.

[Sen97b] D. Senouf, Dynamics and condensation of complex singularities for Burgers' equation II, SIAM J. Math. Anal. 28 (1997) 1490–1513.

[Sha92] B. V. Shabat, *Introduction to Complex Analysis Part II. Functions of Several Variables*, American Mathematical Society (1992).

[SSF83] C. Sulem, P. L. Sulem and H. Frisch, Tracing complex singularities with spectral methods, Journal of Computational Physics 50 (1983) 138–161.

[STs84] K. V. Safonov and A. K. Tsikh, Singularities of the Grothendieck parameter residue and diagonals of double power series, Soviet. Math. (Iz. VUZ) 28 (1984).

[TG37] G.I. Taylor and A.E. Green, Mechanism of the production of small eddies from large ones, Proc. Roy. Soc. A 158 (1937) 499–521.

[The02] T. Theobald, Computing amoebas, Experiment. Math. 11 (2002) 513–526.

[Tru54] C. Truesdell, Rational fluid mechanics, 1657-1765, In Euler, *Opera Omnia* ser. 2 12 (1954) IX–CXXV.

[Tru72] V. M. Trutnev, The radial indicator in the theory of Borel summability with some applications, Sibirsk. Matem. Zh. 13 (1972) 659–664.

[Tsi92] A. K. Tsikh, *Multidimensional Residues and Their Applications*, American Mathematical Society (1992).

[Tsi93] A. K. Tsikh, Conditions for absolute convergence of series of Taylor coefficients of meromorphic functions of two variables, Math. USSR Sbornik 74 (1993) 336–360.

[Wei03] J. A. C. Weidemann, Computing the dynamics of complex singularities of nonlinear PDEs, SIAM J. Appl. Dyn. Syst. 2 (2003) 171–186.